Biochemical and Mass Spectrometric Characterization of Protein ADP-ribosylation

Dissertation

zur

Erlangung der naturwissenschaftlichen Doktorwürde

(Dr. sc. nat.)

vorgelegt der

Mathematisch-naturwissenschaftlichen Fakultät

der

Universität Zürich

von

Florian Nils Rosenthal

aus

Deutschland

Promotionskomitee

Prof. Dr. Dr. Michael O. Hottiger

(Vorsitz und Leitung der Dissertation)

Prof. Dr. Konrad Basler

Prof. Dr. Ruedi Aebersold

Prof. Dr. Robert Schneider

Zürich, 2013

SUMMARY

In the human cell, many processes are facilitated by proteins, which are regulated by the attachment of chemical groups, so called post-translational modifications (PTMs). ADP-ribosylation is an important PTM, which is involved in a variety of cellular processes and its misregulation or loss is implicated in a broad range of diseases. Many questions regarding ADP-ribosylation are still unanswered; especially which amino acids that serve as acceptors for ADP-ribosylation and which enzymes are able to revert the modification on a specific protein and residue.

The aim of this thesis was to shed light on these questions, to identify the acceptors of ADP-ribose and to analyze mono-ADP-ribosylhydrolases. Therefore, novel electron transfer dissociation (ETD) and higher-energy collisional dissociation (HCD) mass spectrometry (MS/MS) protocols were established and combined in order to optimize the challenging analysis of ADP-ribosylation by MS/MS. The optimized protocol led, for the first time, to the highly accurate identification of several ADP-ribosylation sites on proteins extracted from cells. The mapped sites included glutamic acid, arginine and lysine residues on known targets such as histone H1 and H2B. Many of these sites are also targets of other PTMs, suggesting a lively crosstalk between ADP-ribosylation and other PTMs.

Macrodomain containing proteins are known to bind ADP-ribose and were identified here as novel mono-ADP-ribosylhydrolases. The human proteins MacroD1, MacroD2 and C6orf130, as well as the archaeal enzyme Af1521, were able to hydrolyze glutamic acid linked mono-ADP-ribose, catalyzed by the mono-ADP-ribosyltransferase ARTD10 *in vitro* and *in vivo*. Structural modeling and mutagenesis identified a common core structure containing Asp102 and His106 of MacroD2 that is implicated in the hydrolytic reaction. Importantly, MacroD2 could revert the inhibitory ADP-ribosylation of the disease relevant kinase GSK3β and thereby restore its activity. Taken together, the establishment of a novel mass spectrometry workflow represented an important step towards the identification of the ADP-ribosylome. The identification of a variety of ADP-ribosylation acceptor sites in cellular proteins challenges the old dogma, which states that mainly glutamates serve as acceptors of poly-ADP-ribose in human cells. Furthermore, the identification of macrodomain containing proteins as novel mono-ADP-ribosylhydrolases closes a gap in the cellular ADP-ribosylation cycle and opens a new chapter in mono-ADP-ribosylation metabolism.

ZUSAMMENFASSUNG

In der menschlichen Zelle werden viele Vorgänge von Proteinen übernommen, welche durch chemische Modifikationen, die post-translationellen Modifikationen (PTM), reguliert werden. ADP-Ribosylierung ist eine wichtige PTM, die an vielen zellulären Prozessen beteiligt ist und deren Fehlregulierung oder Verlust mit Krankheiten assoziiert wird. Viele Fragen in Verbindung mit ADP-Ribosylierung sind bis heute unbeantwortet, besonders bezüglich der Aminosäure-Akzeptoren für ADP-Ribose und der Enzyme welche die Modifikationen wieder entfernen.

Das Ziel dieser Arbeit war es, diese Fragen zu beleuchten, Akzeptoren für ADP-Ribose zu identifizieren, sowie mono-ADP-Ribosylhydrolasen zu analysieren. Zu diesem Zweck wurden neue Massenspektrometrie Protokolle entwickelt, welche zum ersten Mal zur akkuraten Identifizierung von ADP-Ribosylierungsstellen auf extrahierten Proteinen führten. Unter anderem konnten Lysine und Arginine auf den bekannten Akzeptorproteinen Histon H1 und H2B lokalisiert werden. Viele dieser Modifikationsstellen sind auch Ziele anderer PTMs, was einen regen Austausch zwischen ADP-Ribosylierung und anderen PTMs suggeriert.

Proteine mit Makrodomänen binden ADP-Ribose und wurden hier als neue mono-ADP-ribosylhydrolasen identifiziert. Die menschlichen Proteine MacroD1, MacroD2 und C6orf130, sowie Af1521 aus Archaebakterien, waren in der Lage mono-ADP-Ribose von Glutamaten zu entfernen, welche von der mono-ADP-Ribosyltransferase ARTD10 *in vitro* und *in vivo* katalysiert wurde. Strukturmodelle und Mutagenese ermöglichten die Identifizierung einer Kernstruktur bestehend aus den Aminosäuren Asp102 und His106 von MacroD2, welche an der Hydrolasereaktion beteiligt ist. MacroD2 konnte auch die inhibierende ADP-Ribosylierung der krankheitsrelevanten Kinase GSK3β entfernen und dadurch deren Kinaseaktivität wieder herstellen.

Die Etablierung neuer Massenspektrometrie Protokolle war ein wichtiger Schritt zur Identifizierung des ADP-ribosyloms einer Zelle. Die Identifizierung verschiedener ADP-Ribosylierungsstellen steht in Kontrast zu einem alten Dogma, welches Glutamate als primäre ADP-Ribose Akzeptoren in menschlichen Zellen darstellt. Desweiteren schliesst die Identifizierung von Makrodomänen-proteinen als ADP-Ribosylhydrolasen eine grosse Lücke im ADP-Ribosylierungskreislauf und eröffnet ein neues Kapitel im mono-ADP-Ribosylierungsmetabolismus.

CONTENTS

1 INTRODUCTION

1.1 Post translational modifications

Post-translational protein modifications (PTMs) are defined as the attachment of chemical groups or peptides to specific amino acids of proteins or the processing of proteins by proteolytic cleavage (1). Until now, proteomic studies have identified more than 200 different PTMs that add a high level of complexity to the proteome, generating over 1 million different proteins from only 20,000 to 25,000 protein coding genes (Figure 1) (2,3).

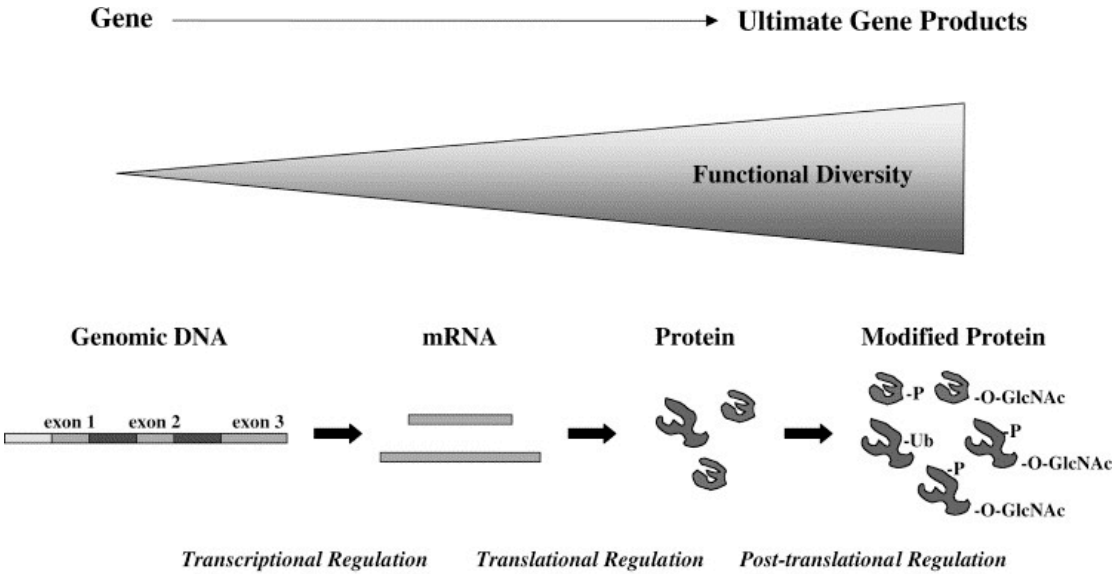

Figure 1: Post-translational modifications increase proteome complexity. Starting from a genome with 20-25'000 genes, the transcriptome represents a new level of complexity, which is further increased by the extremely high number and diversity of PTMs, resulting in over 1'000'000 different proteins. Modified from (4).

While changes or mutations in the genome are rather rare, PTMs allow cells to quickly regulate protein structure, function and interactions, as they can affect the overall chemical property of the modified amino acid (5). Furthermore, PTMs allow the cell to adapt and cope with stress conditions such as environmental stimuli, pathogens or diseases.

Well-studied post-translational modifications are the covalent modification of amino acids with small chemical groups such as phosphate, acetate or methyl. These PTMs are not only attached, but can also be removed to reverse a certain PTM in a fast

and dynamic way. Since several amino acids can be modified by different chemical groups, PTMs can influence each other; for example by competing for the same acceptor amino acid or by recruiting modifying enzymes (1). This phenomenon is well studied in the context of the so called `histone code`, where a variety of modifications of the histone tails orchestrate the recruitment of readers and additional writers of PTMs to influence DNA replication, transcription and repair (2,6).

Other types of PTMs comprise the addition of polypeptide groups instead of a small chemical group, such as ubiquitin and ubiquitin-like modifications (e.g., SUMO and NEDD) (1,7). Finally, also mechanisms that irreversibly alter amino acid properties (e.g., through the deamination of arginine to citrulline (8)) or the proteolytic cleavage of precursor proteins (9) are referred to as post-translational modifications.

1.2 ADP-ribosylation

ADP-ribosylation as a post-translational modification is known since 50 years, but nevertheless it is still poorly understood (10,11). It is an ancient modification that is conserved in all organisms from bacteria to humans, except in yeast, and is catalyzed by ADP-ribosyltransferases (ARTs) (12). ADP-ribosylation is the enzymatic attachment of ADP-ribose to proteins by ARTs using NAD^+ as a substrate. ARTs cleave the energetic bond between the nicotinamide and ADP-ribose moieties and transfer the latter to amino acids of themselves (i.e., auto-modification) or of target protein (13), while releasing nicotinamide as a side-product.

ADP-ribosylation can be divided into two subtypes (14): the first class defines a reaction in which only one ADP-ribose group is transferred to the target amino acid of proteins (mono-ADP-ribosylation) (15). The second class involves the elongation of the initial ADP-ribose moiety to generate long ADP-ribose chains (poly-ADP-ribosylation). In both types, the acceptor site is initially mono-ADP-ribosylated, which is in the case of poly-ADP-ribosylation followed by an elongation reaction (Figure 2). *In vitro,* this elongation step leads to the production of long polymers of ADP-ribose (PAR), reaching up to 200-400 ADP-ribose moieties, that are connected via ribose-ribose glycosidic bonds (13,16). PAR can be additionally branched, for which ADP-ribose chains are attached to the existing polymers in a non-linear manner (Figure 2) (16). The distance between branching points varies between 1 and 40 ADP-ribose units (17).

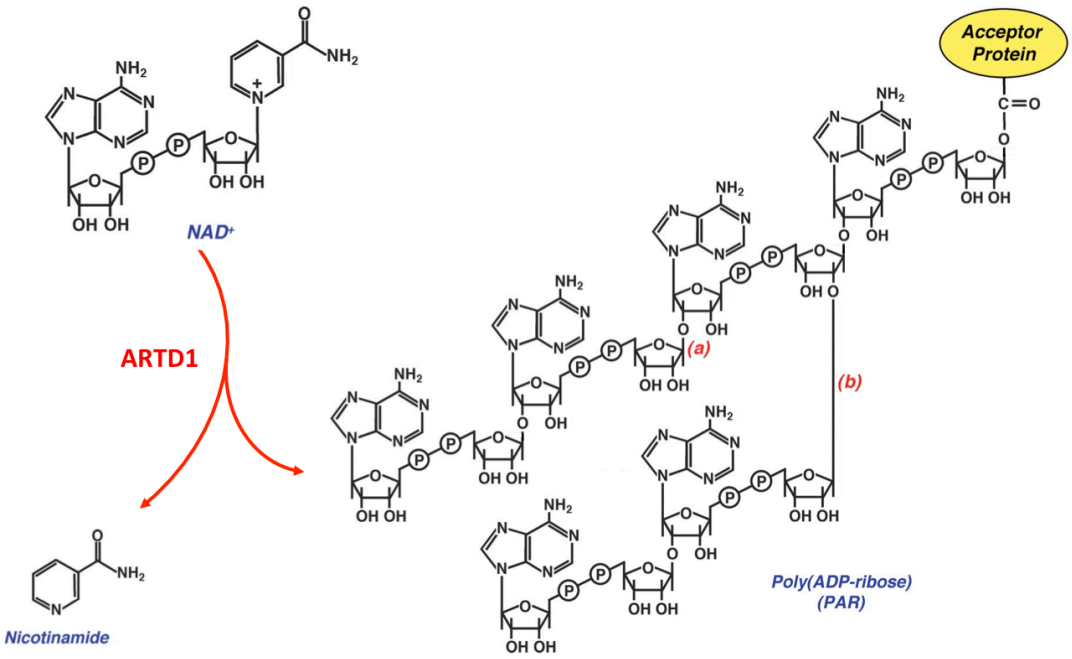

Figure 2: ADP-ribosylation metabolism. Poly-ADP-ribose (PAR) is for example synthesized by ARTD1 using NAD^+ as the ADP-ribose donor. The ADP-ribose moieties are linked via 1"-2' ribose-ribose glycosidic bonds (a) whereas PAR branching points are linked via 1"-2" ribose-ribose glycosidic bonds (b). Modified from (18).

1.2.1 Bacterial toxins as ADP-ribosyltransferases

During host invasion, bacterial pathogens make use of protein toxins that mono-ADP-ribosylate intracellular targets, which leads to the neutralization of the phagocytotic functions of immune cells, the disruption of the cytoskeleton or the inhibition of signal transduction (19,20). These toxic effects lead to apoptotic or necrotic cell death and causes diseases like diphteria, cholera and whooping cough. Bacterial toxins are well studied and the acceptor amino acids for ADP-ribosylation are defined in many cases (Table 1).

Based on structural aspects, bacterial toxins are divided into two main subclasses that harbor either a H-Y-E (found in the Diphteria toxins) or a R-S-E motif (found in the Cholera toxin) in their catalytic domain (12).

Exotoxin	Bacterium	Target	Role in pathogenesis	Target AA
Diphtheria toxin	*C. diphtheriae*	EF-2	Inhibition of protein synthesis	diphtamide
Exotoxin A	*P. aeruginosa*	EF-2	Inhibition of protein synthesis	diphtamide
Cholera toxin	*V. cholerae*	EF-2	Inhibition of protein synthesis	diphtamide
Heat-labile enterotoxin	*E. coli*	Gs	Inhibition of GTPase activity of Gs	arginine
Pertussis toxin	*B. pertussis*	Gi	Uncoupled Gi protein–mediated signal tansduction	cysteine
C2	*C. botulinum*	Actin	Actin depolymerization	arginine
C3stau2	*S. aureus*	Rho A	Traps Rho GTPase in GDP-bound state	asparagine

Table 1: Examples of bacterial ADP-ribosyltransferases. Shown are the transferases, their target proteins and amino acids, as well as the cellular reaction. Modified from (19) and (20).

1.2.2 The mammalian ARTD Family

Shortly after the identification of ADP-ribose as PTM, the first enzyme, which is able to synthesize PAR was discovered and named poly-ADP-ribose polymerase (PARP) (21). For nearly two decades, PARP was believed to be the only ADP-ribosyltransferase, capable of ADP-ribose polymer synthesis. In the late nineties with the sequencing of the human genome additional genes sharing the same catalytic domain were identified, suggesting that several other proteins might be able to synthesize PAR (22). Thanks to many studies providing information about protein structure and sequence, up to now 22 human proteins that harbor a catalytic domain similar to the one found in PARP have been identified (12). Based on available amino acid sequences and crystal structures, the mammalian ARTs can be grouped into two groups with different catalytic motifs (12). One group shares structural similarities with the bacterial cholera toxin and is therefore named ADP-ribosyltransferase Cholera toxin like (ARTC). Currently, the ARTCs comprise five members in human (ARTC1-5), which are all located at the cell membrane facing the extracellular space (12). The second group shares structural similarities to the bacterial diphteria toxin and is therefore named ADP-ribosyltransferase Diphteria toxin like (ARTD). Eighteen human ARTD members (ARTD1-18, ARTD1 representing the initial PARP protein) are currently distinguished and found in different compartments within the cell. The ARTD family can be further subdivided based on amino acid differences in the catalytic core domain. ARTDs that were though to synthesize PAR are characterized

by the presence of the conserved amino acid triad H-Y-E, whereas mono-ADP-ribosyltransferases lack the glutamate residue in position three of the triad (Figure 3) (12). This glutamate residue was described to be critical for the elongation step of the PAR formation. Interestingly, although ARTD3 harbors the H-Y-E triad, the enzyme was reported to catalyze only mono-ADP-ribosylation (23), suggesting that other amino acids or specific conditions are most likely important for PAR formation.

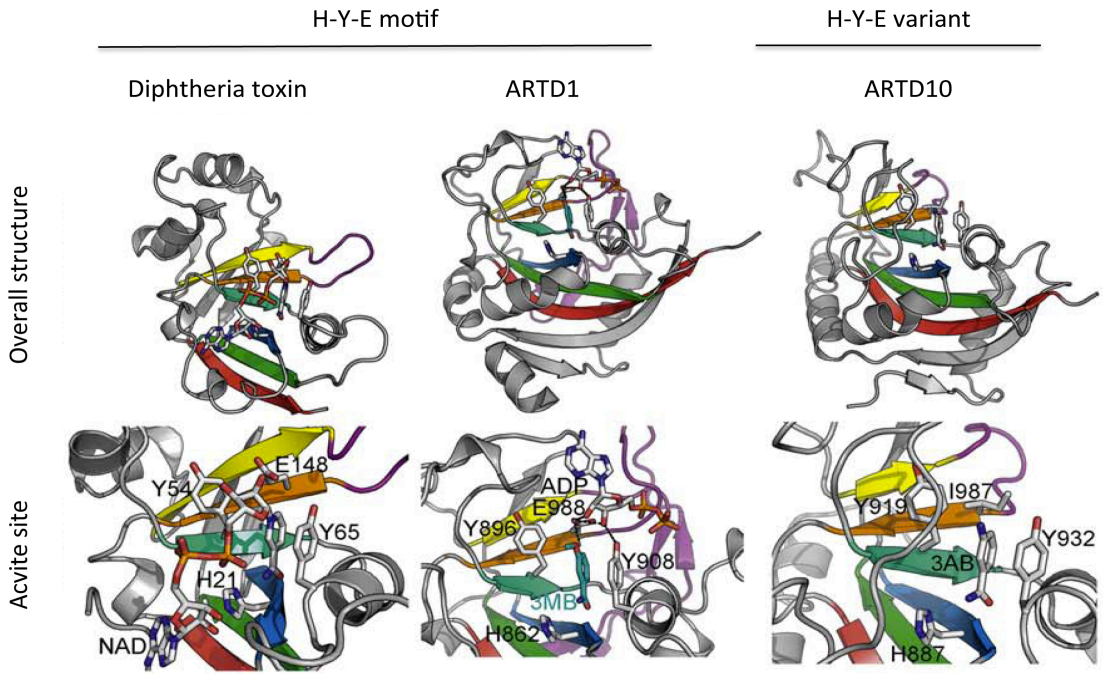

Figure 3: Structural comparison of H-Y-E motif containing ARTs. The overall structure and an enlargement of the active site are shown for the bacterial Diphtheria toxin, chicken ARTD1 and human ARTD10. The six β-sheets that form a scaffold for the catalytic domain are highlighted in rainbow colors. Ligands and conserved motif side chains are shown as sticks. Modified from (12).

Based on the biochemical characterization of the ARTD family, the members can be sub-divided into three groups: the family founding enzyme ARTD1 (PARP1) as well as ARTD2 (PARP2) generate branched PAR and are representative of the first group. In the cell, ARTD1 is the most abundant nuclear ARTD and accounts for approximately 90% of the PAR formation (24), whereas ARTD2 is less abundant, less active and responsible for the majority of the remaining PAR formation in mice lacking ARTD1 (24,25). The enzymatic property of ARTD3 is still under debate (see above), as both mono- and poly-ADP-ribosylation activity were reported (23,26). A

second group of enzymes consists of the telomere associated ARTD5 and ARTD6 (Tankyrase1 and 2), which are also able to modify themselves and several target proteins (27,28). In contrast to the first group, ARTD5 and ARTD6 are oligo-ADP-ribosyltransferases, which synthesize unbranched ADP-ribose chains with a maximum length of 20 units (28). The third group contains enzymes lacking the glutamate residue in the above-mentioned triad motif, limiting them to mono-ADP-ribosyltransferases, as shown for ARTD8 (PARP14) and ARTD10 (PARP10) (29). Moreover, although all identified ARTD family members share the catalytic domain, it is not clear whether all proteins are enzymatically active (12). Recent studies provided evidence, that ARTD9 and ARTD13 do not posses catalytic activity (29,30). For the other members of the ARTD family a catalytic activity was postulated but requires experimental validation (12).

1.2.3 Functions of cellular protein ADP-ribosylation

Cells are constantly exposed to a broad variety of stress situations caused by exogenous and endogenous sources. For example, the release of pathogen- or damage-associated molecular pattern molecules (DAMPs or PAMPs, respectively) induces cellular stress responses and often the formation of reactive oxygen species (31-33). A common mechanism, which is involved in the regulation of the cellular response to oxidative stress is the formation of nuclear PAR (13,34). In addition to its role in the cellular stress response, ADP-ribosylation was described to regulate important cellular processes such as replication, transcription, chromatin architecture, and telomere maintenance (10,34-36). These various processes are regulated through ADP-ribosylation, which is a rather large and negatively charged PTM. It affects the function of the modified proteins as well as the complex formation with other factors that are thus direct or indirectly influenced by mono- or poly-ADP-ribosylation (37). ADP-ribosylation was described to inhibit protein-protein or protein-nucleic acid interactions, leading for example to chromatin decondensation or the release of DNA binding proteins from chromatin (38,39). In contrast, ADP-ribose can also serve as a scaffold to recruit and build protein complexes, which is well documented by ADP-ribose binding motifs (see chapter 1.5). Additionally, ADP-ribosylation influences other PTMs such as ubiquitination, which results in the degradation of target proteins (40). Furthermore, *in vitro* studies showed, that the acetylation of K16 on histone H4

inhibits its ADP-ribosylation, suggesting that both PTMs are competing for histone H4K16 modification (41).

1.3 ADP-ribose degradation

The enzymatic activities that degrade PAR to ADP-ribose and reverse mono-ADP-ribosylation are currently poorly understood. This is partly due to the difficulty to analyze the different ADP-ribose structures (mono- and branched poly-ADP-ribose), to identify the different acceptor sites, and to define the chemical linkages within PAR and between the ADP-ribose and its acceptor site (42,43). The different linkage types, however, strongly suggest that different enzymes (ADP-ribosylhydrolases) likely exist.

1.3.1 Poly-ADP-ribose glycohydrolase (PARG)

PARG is the best-studied PAR degrading enzyme and comprises at least five isoforms: A nuclear 110-111 kDa isoform, three cytoplasmic isoforms with sizes of 102, 99 and 60 kDa, and a 55 kDa mitochondrial version (44,45). All isoforms result from alternative splicing or translation reinitiation of one single gene locus (13,46). PARG is the enzyme responsible for the majority of the PAR degrading activity in cells. It hydrolyses the 2'–1" glycosidic ribose-ribose bonds of PAR into free ADP-ribose moieties, which can function as second messenger in various compartments of the cell or can be recycled into ATP (13,46). Recent structural studies elucidated the enzymatic reaction mechanism and identified several moieties that are important for PAR binding and hydrolysis (47,48). The terminal ribose of the PAR chain is bound by PARG and the ribose-ribose O-glycosidic linkage forms an oxocarbenium intermediate with E115 in the catalytic core. Subsequently, a water molecule attacks the intermediate, resulting in the release of an ADP-β-ribose'' (47). The catalytic center of PARG was reported to have structural homology to macrodomains (47). Due to steric hindrance the protein bound ADP-ribose could not be hydrolyzed by PARG, resulting in a mono-ADP-ribosylated protein.

Although ARTD1 knockout mice are viable (49), a complete PARG knockout in mice (affecting all isoforms) is embryonic lethal, confirming that PAR is formed and highlighting crucial physiological and developmental functions (50). This also implies that PAR accumulation within the cell is deleterious and thus underlines the importance of counteracting PAR formation. In line with this, PARG or ARTD1 knockout mice show a genomic instability phenotype under genotoxic stress

conditions (51-53). In addition and similar to ARTD1 inactivation, inhibition of PARG also caused synthetic lethality in BRCA2 deficient tumors (54).

1.3.2 ADP-ribosylhydrolases (ARHs)

In the early nineties, a new hydrolase for mono-ADP-ribosylated arginine residues was purified and characterized (55). It was a 39 kDa protein that was identified as an ADP-ribosylarginine hydrolase in *in vitro* experiment and represented the founding member of the family of ADP-ribosylhydrolases (ARHs). Later, two more members of this family were identified by in silico sequence analysis, named ARH2 and 3 accordingly (56). Further studies revealed that ARH1 is indeed a mono-ADP-ribose hydrolase able to cleave ADP-ribose-arginine catalyzed by the bacterial cholera toxin (57). In contrast, no evidence for an enzymatic activity of ARH2 could be found so far (57). Interestingly, ARH3 has no activity towards mono-ADP-ribose modifications, but rather degrades PAR in a manner similar to PARG, although most PAR-hydrolyzing activity of the cell is assigned to PARG (57,58). As there is no structural similarity between the catalytic domains of ARH3 and PARG, but rather between ARH3 and ARH1 (56,58), the presence of two independent and different mechanisms of PAR degradation in human cells is possible. So far, ARH1 is the only enzyme able to revert mono-ADP-ribose of a modified arginine residue, which might be synthesized by ARTC family members (56,59,60). However, since ARH1 and the ARTC are not localized in the same cellular compartment, the ARH1 substrate might be synthesized by a so far unidentified arginine specific intracellular ART.

Very little is known about the biological function of the ARH protein family *in vivo,* but loss of ARH1 rendered mice more prone to tumor formation (61), indicating that the balance between ADP-ribose synthesis and degradation is a critical mechanism for proper cellular functions and survival.

1.3.3 The mysterious hydrolase/lyase

Early studies identified an additional protein in rat liver that was able to remove mono-ADP-ribose but not PAR from histone H2B and H1 (62,63). Even though the reaction product seemed to be slightly modified in comparison to ADP-ribose, this so-called lyase is a good candidate for an additional family of ADP-ribosylhydrolase. It had a size of 83 kDa and was reported to remove ADP-ribose from glutamic acid or lysine residues. Unfortunately, no further studies regarding this lyase were published and

therefore additional experimental evidence would be required to confirm the existence of this potential missing link in the ADP-ribose metabolism.

1.3.4 Nudix box hydrolases

In humans, an additional family of enzymes able to hydrolyze ADP-ribose exists. In contrast to the above mentioned enzymes, the nudix box containing enzymes do not remove protein bound ADP-ribose or PAR, but hydrolyze the pyrophosphate bond within ADP-ribose, generating AMP and ribose 5-phosphate (64). The nudix superfamily is conserved in all kingdoms of life and is defined by its characteristic 23 amino acid nudix box motif Gx_5Ex_5[UA]xREx_2EExGU, where U is a hydrophobic amino acid (64,65). Nudix proteins are pyrophosphohydrolases that act on a variety of substrates containing a nucleoside diphosphate linked to another moiety (64). In humans, NUDT5 and NUDT9 were shown to be ADP-ribose pyrophosphatases, however, NUDT5 is not specific for only ADP-ribose (66-68). Both enzymes were suggested to control the free ADP-ribose levels in the cell, thereby protecting proteins from non-enzymatic glycation by free ADP-ribose. In contrast, nudix proteins were also shown to be affected by cytotoxic agents, leading to an accumulation of free ADP-ribose in addition to the enhanced PAR formation under stress (68).

1.4 PARP inhibitors

The misregulation of ADP-ribosylation is implicated in a broad range of diseases such as acute and chronic inflammatory disorders, neurodegenerative and vascular diseases, diabetes, age-related diseases as well as several types of cancer (13,34,69). Since ARTD1 is by far the most active nuclear ARTD in the cell, many companies started to develop inhibitors against ARTD1 as single agents or to potentiate the cytotoxic effect of other drugs for cancer therapy (70,71). This class of molecules is known as PARP inhibitors, many of which are NAD^+ competitors and may thus not only inhibit ARTD1 but also other ARTD family members or enzymes using NAD^+ as a substrate. Most PARP inhibitors are therefore based on NAD^+ or nicotinamide analogues that are designed to enter the catalytic pocket and block the enzymatic activity. The first generation of inhibitors (e.g., 3-aminobenzamide (3-AB)) already proved to have therapeutic potential, but was too unspecific and not potent enough to be of medical value (72). Recent development of PARP inhibitors led to the chemical synthesis of a new inhibitor generation that reach Kd values in the nM range, strongly improving

their inhibitory potential. Currently, nine third-generation inhibitors are under evaluation and some have already entered phase three clinical trials with promising results (72,73). Nevertheless, the use of ADP-ribosylation inhibitors is still a matter of debate because different studies showed that many compounds are not specific for a certain ARTD family member or inhibit other NAD^+ consuming enzymes like Sirtuins. In addition, completely unrelated off target effects were observed (71,72).

The breakthrough for PARP inhibitors in cancer research occurred when two publications demonstrated synthetic lethality of Breast Cancer 1/2 (BRCA1/2) deficiency (resulting in cells with impaired homologous recombination (HR)) and PARP inhibitors in breast cancer cell lines (74,75). These reports suggested that PARP inhibitors could be used as single agents in cancer cell types with a defect in HR (69,71,76). The inhibition of ARTD1 on DNA-repair intermediates during DNA repair is believed to generate DNA single strand breaks that are converted into double strand breaks during replication. As these breaks are not repaired in HR deficient tumors, they would eventually lead to cell death (69). Recent reports indicate that also other mechanisms might account for the observed synthetic lethality (71,73).

Similar to BRCA1/2, also phosphatase and tensin homolog (PTEN) deficient tumours are sensitive to PARP inhibitors (77). Despite the early success in the treatment of BRCA-deficient cell lines *in vitro*, many of these tumours resist therapy by PARP inhibitors. Recent phase II trials of the PARP inhibitor Olaparib describe objective responses of 33% in BRCA-deficient ovarian cancer and 41% in BRCA-deficient breast cancers (78,79). Although these response rates were significantly higher than for cytotoxic chemotherapy, they are lower than observed with other targeted therapies, which have tumour response rates of 50-70% (80). Nevertheless, in contrast to other current cancer drugs, PARP inhibitors are well tolerated and have very low toxic side effects, what makes them a promising tool for future cancer therapy.

1.5 Readers of ADP-ribosylation

Mono- and poly-ADP-ribose modifications not only change the charge and enzymatic properties of target proteins, but also recruit a broad range of reader proteins (37). These proteins bind the ADP-ribose moieties with subnanomolar to micromolar affinities and can thereby be targeted to sites of ADP-ribosylation. So far, four different domains that bind mono- or poly-ADP-ribose could be identified (81). PAR-

binding zinc-fingers (PBZs), WWE domains and PAR-binding motifs (PBMs) are poly-ADP-ribose binding modules, whereas macrodomain-containing proteins can recognize mono- and/or poly-ADP-ribose (Fig. 4).

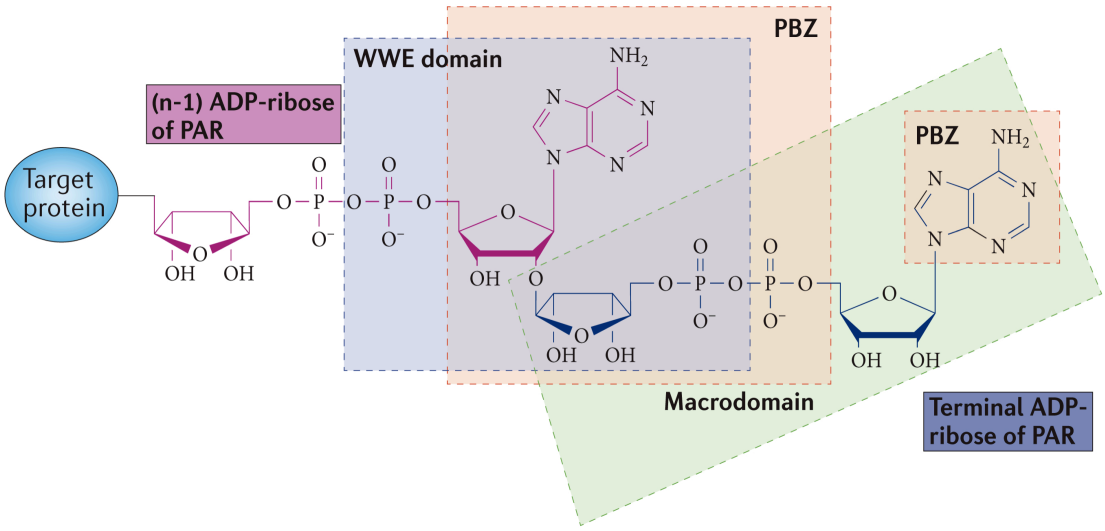

Figure 4: Binding behavior of ADP-ribose readers. A terminal ADP-ribose (blue), a (n-1) ADP-ribose (pink), and the structures recognized by ADP-ribose binding proteins are shown. WWE domains bind to the glycosidic bond and the surrounding parts of the two ADP-ribose units. PBZs recognize both phosphate groups within an ADP-ribose group as well as the adenosine of the proximal and the adenine ring of the distal ADP-ribose. Macrodomains in contrast interact with the whole terminal ADP-ribose moiety. Modified from (37).

1.5.1 The PAR-binding zinc finger (PBZ)

The PAR-binding zinc finger (PBZ) is a small unordered fold with a zinc-coordinated backbone that can interact with one or two ADP-ribose units in a PAR chain and the connecting pyrophosphate bond as well as with the α(1->2) O-glycosidic bond between the ADP-ribose moieties (Fig. 4) (37,82,83). PBZ domains were so far only identified in a few DNA-damage response proteins like aprataxin and PNK–like factor (APLF) or in checkpoint with forkhead-associated and RING domains (CHFR) (82,83). Both proteins are recruited to sites of DNA damage in a PBZ- and PAR-dependent manner. Misregulation of CHFR is implicated in tumor progression most probably due to its function in the antephase checkpoint, which is aberrant upon loss of the PBZ domain (82,84).

1.5.2 Macrodomain-containing proteins

The macrodomain is a protein domain consisting of 130-160 amino acids with a mixed α/β fold that is conserved from viruses and bacteria to humans and currently over 300 macrodomain-containing proteins are known (37,85). The first human macrodomain was identified in the histone variant called macroH2A (86). Up to now, ten genes encoding 14 macrodomain-containing proteins, which harbor one to three folds, were predicted by sequence homology in humans (87,88).

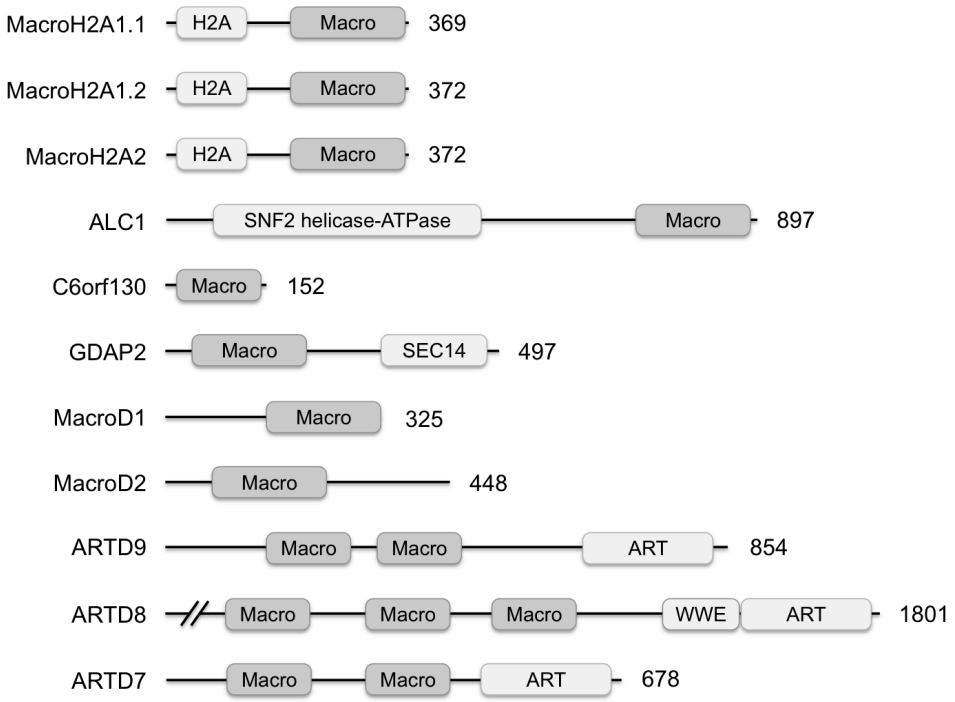

Figure 5: Human macrodomain containing proteins. A representative overview of the human macrodomain containing proteins and their domain structure. Modified from (89).

The so far best-studied macrodomain containing proteins are the histone variants macroH2A1 and macroH2A2, which are involved in X-chromosome inactivation, epigenetic silencing and chromatin rearrangement (86,90,91). Misregulation of macro H2A1 and macroH2A2 is implicated in melanoma progression and Huntington disease (92,93) . The Snf2-like helicase ALC1, which remodels chromatin upon DNA-damage, is another example (94). A second group consists of MacroD1, -D2 and -D3 (GDAP2), which are small proteins associated to different diseases such as breast cancer, Kabuki syndrome and neuroblastoma (95,96). A special group is formed by the macrodomains of ARTD7, -8 and -9 (B-aggressive lymphoma: BAL3, -2, -1), because these proteins

contain an ART domain as well as two or three macrodomains, which potentially enables them to bind to ADP-ribosylated proteins. They have been implicated in lymphoma aggressiveness and survival through inhibition of tumor suppressors via interferon and interleukin signaling (30,97,98).

A subgroup comprising human ARTD8, MacroD2, and viral SARS-CoV was shown to efficiently bind mono-ADP-ribosylated proteins (96,99-101). In contrast, PAR binding was observed for human macroH2A1.1 and the macrodomain of ARTD9 as well as for the viral SFV protein. A third group, able to bind both mono-ADP-ribose and PAR, contains human MacroD1, viral HEV, as well as archaeal Af1521 (96,100,102). Since it was suggested that macrodomains bind to the terminal ADP-ribose of PAR, it is likely that the differences in the binding of mono- and/or poly-ADP-ribose are due to steric reasons.

Interestingly, some macrodomain proteins also exhibit a catalytic function in addition to their ability to bind ADP-ribose. Human MacroD1, MacroD2 and orphan macrodomain (C6orf130) as well as *E.coli* YmdB are able to deacylate O-acetyl-ADP-ribose (OAADPr) (103,104). OAADPr is the product of a protein deacetylation reaction, catalyzed by the NAD^+ dependent Sirtuins (105). Macrodomains deacylate OAADPr, thereby producing ADP-ribose and acetate (104). Additional properties, which are poorly understood and investigated, include binding of OAADPr and poly(A) as well as ADPR-1''P phosphatase activity (87,96).

1.5.3 The WWE domain

The WWE domain is a globular domain that is defined by two conserved tryptophan (W) and a glutamic acid (E) residues and is usually found as single or double domain. So far, WWE domains were identified in two protein families; the E3 ubiquitin ligases (e.g., RNF146, DELTEX1 or Trip12) and the ARTDs (ARTD8 and ARTD11-14) (12,37,106). WWE domains have the ability to interact with iso-ADP-ribose within the PAR chain (Fig. 4) (40,106). Some WWE domains have mutations in their binding motif that abolish PAR binding, but which might turn them into mono-ADP-ribose binders (40,107). Examples are the WWE domains of DDHD2, of ARTD8 and, depending on the study, also of ARTD11 that are believed to bind the terminal ADP-ribose as well as a mono-ADP-ribose modification. The fact that all WWE domain containing proteins interact with ADP-ribose and either have ubiquitination activity or are members of the ARTD family suggests that both mechanisms are tightly linked

and influence each other. For example, ADP-ribosylation could be a signal or recruiting factor for E3 ubiquitin ligases that subsequently mark proteins for degradation or influence their properties (40).

1.5.4 PAR binding motifs (PBMs)

The first motif described to interact with PAR was the PAR binding motif (PBM), which is found in various proteins of the DNA damage signaling network and in DNA repair factors (e.g., p53, XRCC1, MRE11, ATM, Ku70/86 and DNA-PK) (22,108,109). The PBM consists of a stretch of amino acids with the sequence: $[HKR]_1$-X_2-X_3-$[AIQVY]_4$-$[KR]_5$-$[KR]_6$-$[AILV]_7$-$[FILPV]_8$ (37,109). The PBM non-covalently interacts with free PAR *in vitro,* which could act as a scaffold to recruit different DNA-repair proteins or functions as a signaling factor that is sensed by PBM domain containing proteins. This mechanism was so far only described *in vitro* and needs to be further validated *in vivo*.

1.6 ADP-ribose acceptor sites

In the case of bacterial ARTs, the acceptor amino acids were mapped successfully because most toxins modify exactly one protein or a class of proteins at one specific residue (19,20) (Table 1). Most sites were indirectly identified by chemical protection of potential acceptors, Edman-degradation, thin layer chromatography and other chemical methods and later confirmed by site directed mutagenesis (110-112). This led to the identification of several sites and the main acceptors are arginine, asparagine, diphtamine and cysteine (19). More recently, a study using mass spectrometry identified threonine 148 of actin and glutamine 61 and 63 of RhoA as ADP-ribose acceptors modified by *P. luminescens,* leading to actin clustering (113).

Despite substantial efforts, the identification of the amino acids that are modified in mammals by a distinct ARTD has not been possible. The acceptor sites for PAR in mammals were first characterized over thirty years ago based on the chemical properties and stability of the modification on ARTD1, the core histones and linker histone H1 (114-116). As the majority of the analyzed ADP-ribose modifications (over 70%) were sensitive to alkali and neutral NH_2OH, but stable to acid, a carboxylester linkage was suggested (Table 2) (116). Such a linkage points to glutamate and aspartate residues as acceptors, which was believed for many years without further

validation. The remaining 30% of the modifications were, however, NH_2OH resistant and 15% were even alkaline resistant, clearly indicating that other linkages must exist (115).

	Ketamine bond	Ester bond
Treatment		
Hydroxylamine	Resistant	Highly sensitive
Alkali	Partially resistant	Highly sensitive
Acid	Partially sensitive	Partially sensitive
Examples	ADP-ribose–lysine	ADP-ribose–glutamic acid ADP-ribose–aspartic acid

Table 2: Chemical stability of ADP-ribose bonds. ADP-ribose can be linked to acceptor amino acids via ketamine bonds (arginine) or ester bonds (glutamic and aspartic acid). The two linkages result in different stabilities towards certain chemicals. Modified from (35).

Indeed, a few years later, experiments with two mammalian ARTCs from avian erythrocytes confirmed that NH_2OH resistant and alkali stable fraction represent an ADP-ribose arginine linkage (116-118). Based on these findings, it was postulated that NH_2OH resistant mono-ADP-ribose on arginine residues is used for further elongation by ARTs that synthesize PAR (116).

More recent work using site directed mutagenesis studies of ARTD1 identified lysine residues as acceptors (119). In contrast, site directed mutagenesis for ARTD10 identified glutamates as acceptors sites (29). As these studies are either correlative or relying on mutagenesis experiments that can potentially alter protein structures and therefore introduce a bias, mass spectrometry methods were of need to pinpoint ADP-ribosylation on specific amino acids (see chapter 1.7.4).

Moreover, the linkages within PAR or between ADP-ribose and the acceptor residue can potentially be of different chemical nature and therefore exhibit different biochemical properties. The ribose 5-phosphate of ADP-ribose has three potential linkage acceptors, which are the OH-groups at C-1, C2 and C-3 (114). Preliminary studies suggested an attachment at C-1 in the case of modified glutamates, but these results were only indicative and not conclusively proven (114). In contrast, mono-ADP-ribosylation of arginines was analyzed by NMR and could be identified as C-1 linked (120). Furthermore, it was shown that the enzymatic reaction results in an

ribosyl-guanidinium linkage in α conformation, which undergoes anomerization to a β linkage in a 1:1 ratio under physiological conditions (120). All these results illustrate the high complexity of ADP-ribosylation. The specific types of linkages have potentially far reaching biological implications, since they may affect the interaction with other proteins as well as the removal of different modifications by ADP-ribosylhydrolases.

1.6.1 Non-enzymatic, covalent ADP-ribosylation

While research has focused on enzymatically catalyzed ADP-ribosylation, a covalent, non-enzymatic ADP-ribosylation has also been described (121,122). ADP-ribose is a potent histone glycation and glycoxidation agent *in vitro* (121). Glycation is the covalent binding of an ADP-ribose molecule through Schiff base formation to lysine residues, which is stable upon treatment with hydroxylamine. Incubation of ADP-ribose with histones H1, H2A, H2B, and H4 *in vitro* at pH 7.5 and 37°C over night resulted in the formation of ketoamines derived from a Schiff base by an Amadori rearrangement (121,123,124). In the case of an Amadori rearrangement the attached ADP-ribose would be linked via a C1 linkage (124). Based on the long incubation time, which is substantially longer than common incubation times of ADP-ribosylation reactions, glycation needs to be considered *in vivo* if very high concentrations of free ADP-ribose are generated from NAD^+ or PAR.

1.7 Toward identifying the ADP-ribosylome

The tools to study ADP-ribosylation are currently very limited. Especially the lack of suitable antibodies for mono-ADP-ribosylation or for site-specific modifications restricts the analysis of ADP-ribosylation. Until now, most studies that identified ADP-ribosylated proteins and their ADP-ribose acceptor sites were performed in a targeted manner, analyzing only a few candidate proteins. It is therefore of great importance to establish new methods for the analysis of ADP-ribosylated proteins and the identification of their modification acceptor sites. Advances in proteomics technologies, especially in mass spectrometry (MS), and the use of ADP-ribose readers as tools to purify or enrich ADP-ribosylated proteins recently opened new possibilities to study this complex protein modification and broaden our horizon in terms of the ADP-ribosylome.

1.7.1 Identification of ADP-ribosylated proteins by protein microarrays

Protein microarrays are a first option to study protein interactions and modifications in large scale and have been already successfully applied for the identification of kinase substrates (125). Recently, two studies utilized ProtoArrays® covering around 8'000 proteins immobilized on glass slides to identify target proteins for ARTD2, ARTD8 and ARTD10 (126,127). In both cases, recombinant ARTDs were used to *in vitro* modify the spotted proteins with biotinylated-NAD^+ and modified proteins were subsequently visualized by fluorescent labeling of the biotin moiety in NAD^+. Of the 8'000 spotted proteins, 51 were ARTD2 substrates, 142 were ARTD8 substrates and 78 proteins were modified by ARTD10. Among the identified proteins were already known targets, confirming the applicability of the protein microarray for ADP-ribosylation target identification. As protein microarrays are only applicable for *in vitro* approaches, alternative techniques such as mass spectrometry are key to obtain further insights in cellular ADP-ribosylation.

1.7.2 Enrichment strategies for ADP-ribosylated proteins

Since the fraction of modified proteins is usually in the low digit percentage range, researchers commonly use antibodies or enrichment strategies specific for certain PTMs. This reduces the complexity of the cell lysate, enables the purification of the modified proteins or peptides, and the subsequent identification of the proteins and modification sites by mass spectrometry. One prominent example is the well-studied phospho-proteome (128,129). Due to the availability of only one antibody against PAR and the lack of good antibodies against mono-ADP-ribosylated proteins, alternative methods for the identification of ADP-ribosylated proteins had to be established. Up to now, three studies employing different methods aimed to identify the 'ADP-ribosylome'. The first study made use of the above-described macrodomain Af1521 and its ability to bind ADP-ribosylated proteins, which were enriched, separated by SDS-PAGE, and analyzed by mass spectrometry (130). To reduce the background, a non-binding mutant of Af1521 was used in a pre-clearing step. This method led to the identification of ADP-ribosylated proteins, including previously known targets such as ARTD1, Elongation factor-1-α and GDH1. However, the fact that the binding occurred under native conditions allowed also an indirect enrichment of proteins by binding to PARylated proteins. This together with less than 20 identified proteins limits the relevance of this analysis.

A second, more elegant study used a clickable analogue of NAD^+ (6-alkyne-NAD) for the identification of ARTD1 substrate proteins (131). ARTD1 knockdown lysates were supplemented with ARTD1 and 6-alkyne-NAD, which was subsequently conjugated to Biotin-N3 in a click chemistry reaction and modified proteins were purified with streptavidin and analyzed by mass spectrometry. This assay identified over 70 proteins, with a partial overlap to the earlier described study. However, this procedure might be biased by the NAD analogue that is spiked into the lysate, which does not represent cellular conditions and might be prone to the identification of false positive hits.

A third study utilized the commonly used monoclonal PAR-binding antibody 10H (132) to enrich poly-ADP-ribosylated proteins from cellular extracts (109). To increase the amount of ADP-ribosylated proteins, PARG knockdown cells were additionally treated with 100 μM N-methyl-N'-nitro-N'-nitro-soguanidine (MNNG) to induce genotoxic stress. Modified proteins were enriched by immunoprecipitation using the 10H antibody, under conditions still allowing indirect complex formations, and afterwards separated by SDS-PAGE. This procedure led to the identification of over 300 PAR-associated proteins with various cellular functions. The majority comprised proteins involved in DNA damage response, DNA- and RNA metabolism and regulation as well as cell death and cell-cycle regulation (109). This study increased the number of identified PAR interacting proteins tremendously, but could unfortunately not fully distinguish between poly-ADP-ribosylated proteins and proteins that are forming a complex with modified proteins. Additionally, mono-ADP-ribosylated proteins could not be identified due to the fact that the 10H antibody binds only poly- and not oligo- and mono-ADP-ribose modifications (132).

1.7.3 Detecting ADP-ribosylated peptides by MS/MS

As PAR is very complex due to its length and the branched structure, the detection by MS/MS is very challenging. Especially as ADP-ribose is unstable upon conventional CID fragmentation, which results in undefined and variable modification masses, proper database searches are not possible. To overcome this drawback, the complexity of PAR can be reduced by different methods. The pre-treatment of the samples with PARG reduces the modification to one protein-bound ADP-ribose moiety. A second option is the use of mutant ARTD enzymes that are only able to catalyze mono-ADP-ribosylation, resulting in defined modification masses. A third possibility is the enzymatic reduction of ADP-ribose (e.g., phosphodiesterbond within ADP-ribose),

which would reduce the complexity further and generate a defined chemical group for identification by MS.

Recent studies reduced the complexity of PARylation by using a mutated ARTD1 carrying an E to Q mutation at position 988, which hinders PAR formation, making ARTD1 E988Q an inefficient mono-ADP-ribosyltransferase (133,134). With this approach D387, E488 and E491 within the automodification domain of the ARTD1 E988Q mutant could be identified as auto-ADP-ribosylation sites by CID mass spectrometry (135).

Another recent study analyzed the *in vitro* automodification of ARTD1 by cleaving the pyrophosphate bond of ADP-ribose by phosphodiesterase 1 (PDE1) *in vitro*. This reaction reduces the complexity of the modification and turns it into a chemically more stable group (i.e., phospho-ribose). The newly formed terminal phosphate group was used to enrich modified peptides with conventional phosphopeptide enrichment strategies. This study identified several glutamic acid as well as lysine residues in ARTD1 as potential acceptors, however, the unambiguous annotation of the exact modification site was not possible due to lacking sequence information in the CID spectra (136).

1.7.4 Identification of ADP-ribosylation acceptor sites by MS/MS

Earlier studies on ADP-ribosylated substrates revealed that the site identification with, at this time, state-of-the-art mass spectrometry techniques was not possible (137). Furthermore, detailed studies on the fragmentation behavior of ADP-ribose and modified peptides revealed that the modification is almost completely fragmented under conventional MS conditions using collision-induced dissociation (CID) (138). Although the fragmentation profile generates always the same fragments (Figure 6), with ions indicative for ADP-ribosylated peptides, the peptide backbone fragmentation with CID is too weak to gain enough information for peptide sequence and modification site determination. The identification of the acceptor site within a modified peptide by CID-MS remained therefore challenging.

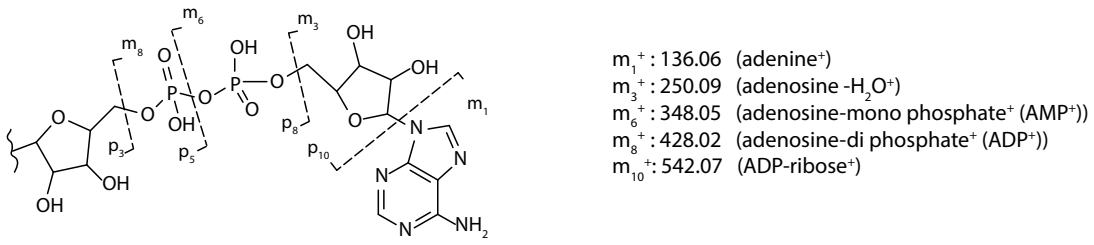

Figure 6: Nomenclature of ADP-ribose fragments. The fragments are defined as described by Hengel et al. (138). The ADP-ribose ions showing strong signals in the HCD MS/MS spectra are shown (m1, m3, m6, m8, m10). Modified from (139).

Recently, novel fragmentation techniques for the identification of ADP-ribosylated peptides by MS have been established. Electron capture dissociation (ECD) is a nonergonic process, leading to a high proportion of random peptide backbone cleavages during fragmentation (140). This process is especially suited for highly charged peptides since it leads to the stabilization of labile PTMs on the peptide and to a better *c* and *z* ion series, which allows better sequence assignments (141). When ECD was applied to a chemically ADP-ribosylated standard peptide containing only arginine as a potential acceptor, the modification as well as its site could be annotated, underlining the power of this method (138). A second fragmentation method that uses a comparable chemistry to ECD is electron transfer dissociation (ETD). The advantage of ETD is its better availability and accessibility due to lower machine costs (142). ETD was also successfully applied to chemically ADP-ribosylated peptides and more complex protein mixtures and enabled the identification of modified arginine as well as lysine residues (143,144). The first study that used ETD to detect ADP-ribosylation sites on histones that were enzymatically modified by ARTD1 *in vitro* identified lysine residues as acceptors and thereby showed the robustness of the ETD approach (41).

A third recently introduced fragmentation technique is higher energy collisional dissociation (HCD) (145). The advantage of HCD over CID is a better coverage of the whole mass range and the ability to acquire MS and MS/MS spectra at high resolution, thereby recording smaller fragment ions, which leads to better sequence and PTM assignment (146,147). Therefore, HCD could be a useful tool for ADP-ribosylation studies, but has not been yet evaluated.

2 AIM OF THE THESIS

ADP-ribosylation is an important post-translational modification with many cellular functions and implications in various human diseases. All above described studies revealed that the investigation of the ADP-ribosylome is still at an early development state. The two most aggravating limitations are the identification of ADP-ribose acceptor sites as well as the lack of enzymes that are able to reverse the mono-ADP-ribosylation.

It was therefore the aim of this thesis to define the ADP-ribose acceptor amino acids that are modified by ARTD1 and ARTD10 by mass spectrometry and to identify as well as biochemically characterize proteins that are able to remove protein-bound mono-ADP-ribose.

3 RESULTS

3.1 Overview of published manuscripts

3.1.1 Identification of distinct amino acids as ADP-ribose acceptor sites by mass spectrometry

Authors: **Florian Rosenthal**, Simon Messner, Bernd Roschitzki, Peter Gehrig, Paolo Nanni and Michael O. Hottiger

Journal: Methods Mol Biol. 2011;780:57-66.

Contributions: Planning, performing and evaluating the experiments. Preparation of the figures and drafting of the manuscript. PG and PN helped to plan and perform the MALDI and LC-MS/MS experiment respectively. SM and BR gave technical input.

3.1.2 Macrodomain-containing proteins are new mono-ADP-ribosylhydrolases

Authors: **Florian Rosenthal***, Karla L H Feijs*, Emilie Frugier, Mario Bonalli, Alexandra H Forst, Ralph Imhof, Hans C. Winkler, David Fischer, Amedeo Caflisch, Paul O. Hassa, Bernhard Lüscher and Michael O. Hottiger

* equal contribution

Journal: Nat Struct Mol Biol. 2013 Apr;20(4):502-7

Contributions: Performing and evaluating the experiments. In particular in vitro de-ADP-ribosylation experiments including kinetics and inhibition experiments (Figures 1b-f,i; 2a-c; 3c; Suppl. Figures 1b,c,e-f; 2c; 3b,c), product analysis by HPLC and LC-MS/MS (Figures 2f,g; Suppl. Figures 2b,d), preparation of the figures and revision of the manuscript.

3.1.3 Inheritance of silent rDNA chromatin is mediated by PARP1 via noncoding RNA

Authors: Claudio Guetg, Fabian Scheifele, **Florian Rosenthal**, Michael O. Hottiger and Raffaella Santoro

Journal: Mol Cell. 2012 Mar 30;45(6):790-800

Contributions: Enrichment of poly-ADP-ribosylated nucleolar proteins by aminophenyl boronate affinity chromatography (Figure 6d).

3.1.4 Crosstalk between SET7/9-dependent methylation and ARTD1-mediated ADP-ribosylation of histone H1.4

Authors: Ingrid Kassner, Marc Barandun, Monika Fey, **Florian Rosenthal** and Michael O. Hottiger

Journal: Epigenetics Chromatin. 2013 Jan 5;6(1):1

Contributions: *In vitro* poly-ADP-ribosylation time course of ARTD1 and histones (Suppl. Figure 1).

3.2 Overview of submitted manuscripts

3.2.1 Identification of ADP-ribosylation sites in cell extracts by higher energy collisional dissociation (HCD)-based mass spectrometry

Authors: **Florian Rosenthal***, Paolo Nanni*, Simon Barkow-Oesterreicher and Michael O. Hottiger

* equal contribution

Journal: Manuscript submitted

Contributions: Planning, performing and evaluating all experiments with input and technical support of PN and SBO.

3.2.2 Proteome-wide Identification of Poly(ADP-ribosyl)ation targets in different Genotoxic Stress Responses

Authors: Stephanie Jungmichel, **Florian Rosenthal**, Michael O. Hottiger and Michael L. Nielsen

Journal: Manuscript submitted

Contributions: In vitro poly-ADP-ribosylation assay with ARTD1 and ARTD1 on candidate proteins from the SILAC screen (Figure 6d).

Chapter 4

Identification of Distinct Amino Acids as ADP-Ribose Acceptor Sites by Mass Spectrometry

Florian Rosenthal, Simon Messner, Bernd Roschitzki, Peter Gehrig, Paolo Nanni, and Michael O. Hottiger

Abstract

ADP-ribosylation is a well-known post-translational protein modification, which regulates a variety of cellular processes. The proteins able to catalyze mono- or poly ADP-ribosylation of proteins belong to the family of ADP-ribosyltransferases. A variety of nuclear proteins has been described to be ADP-ribosylated, including ARTD1 itself and histone proteins. Despite intensive research during the last 40 years, the acceptor amino acids in ARTD1 or histone proteins could be identified and confirmed only recently by MS/MS and by site-directed mutagenesis. The establishment of a standardized protocol including the specific enrichment of ADP-ribosylated proteins and peptides and subsequent mass spectrometric analysis allows the identification of ADP-ribose acceptor sites of modified proteins and to address the functional contribution of ADP-ribosylation in vitro as well as in vivo.

Key words: ARTD1, ADP-Ribosylation, Electron transfer dissociation, Boronic acid, Enrichment

1. Introduction

ADP-ribosyltransferase diphtheria toxin-like 1 [ARTD1, formerly called poly(ADP-ribose) polymerase 1 (PARP1)) is a nuclear partially chromatin-associated protein that is present in most eukaryotes apart from yeast (1, 2). ARTD1 is responsible for the main formation of nuclear polymers of ADP-ribose (PAR) using NAD^+ as substrate. ARTD1 has been suggested to catalyze at least three different enzymatic reactions: the attachment of the first ADP-ribose moiety onto an acceptor amino acid (initiation reaction), the addition of further ADP-ribose units onto already existing ones (elongation reaction), and the generation of branching points

Alexei V. Tulin (ed.), *Poly(ADP-ribose) Polymerase: Methods and Protocols*, Methods in Molecular Biology, vol. 780,
DOI 10.1007/978-1-61779-270-0_4,

(branching reaction). PAR acceptor proteins include a variety of nuclear proteins, most prominently ARTD1 itself, as well as histone proteins (3).

In initial studies, glutamic acid residues of histone H1 and H2B were suggested to be acceptors of ADP-ribose in vivo due to the chemical properties of the linkage (4, 5). Despite intensive research during the last 40 years, the acceptor amino acids of ARTD1 or other proteins could not been identified by MS/MS or confirmed by site-directed mutagenesis. However, intensive site-directed mutagenesis studies of the automodification domain of ARTD1 and ARTD2 revealed recently that individual lysine residues of these domains function as acceptor sites for auto-ADP-ribosylation (6). Furthermore, studies utilizing novel protocols that involve electron transfer mass spectrometry, identified for the first time by MS/MS several lysine residues in peptides representing the core histone tails to be ADP-ribosylated in vitro by ARTD1 (7). The identification of acceptor sites of large proteins or protein complexes requires the enrichment of ADP-ribosylated polypeptides with boronic acid resins, to first reduce the complexity of the samples and second to facilitate the identification by mass spectrometry. Thus, the establishment of standardized protocols including the specific enrichment of ADP-ribosylated proteins and peptides and subsequent MS/MS analysis allows the identification of ADP-ribose acceptor sites of modified proteins and to address the functional contribution of ADP-ribosylation in vitro as well as in vivo.

2. Materials

2.1. ADP-Ribosylation Assays

1. hARTD1 is expressed and purified from insect cells as carboxyl-terminal His-tagged protein and stored in liquid nitrogen.
2. hPARG is expressed and purified from insect cells as carboxyl-terminal His-tagged protein and stored in liquid nitrogen.
3. β-Nicotinamide adenine dinucleotide hydrate (NAD^+), >99% (Sigma–Aldrich) is dissolved in Milli-Q water at 10 mM and aliquots are stored at −20°C.
4. Histone mix from calf thymus (Roche) is dissolved in Milli-Q water at 1 µg/µL and aliquots are stored at −80°C.
5. Biotinylated peptides representing histone tails; H2A (aa 3–23), H2B (aa 18–37), H3 (aa 23–42), H4 (aa 1–22), or H4K16ac (aa 1–22) are custom synthesized by PiProteomics and dissolved in Milli-Q water at 1 µg/µL and aliquots are stored at −80°C.
6. ARTD1 inhibitor 3-aminobenzamide (3AB), 97% (Sigma–Aldrich).

7. ADP-ribosylation buffer: 50 mM Tris–HCl pH 8.0, 4 mM $MgCl_2$, 250 μM DTT, 1 μg/mL protease inhibitors pepstatin, leupeptin, and bestatin. Always prepare fresh ADP-ribosylation buffer.

2.2. Protease Digestion

1. Sequencing grade, modified trypsin (Promega) is reconstituted to a final concentration of 0.1 μg/μL in 50 mM acetic acid and stored at −80°C.
2. Endoproteinase Glu-C sequencing grade (Roche) is reconstituted to a final concentration of 0.1 μg/μL in Milli-Q water and stored at −80°C.
3. Trypsin digestion buffer: 50 mM Tris–HCl pH 8.0, 1 mM $CaCl_2$, 5% acetonitrile.
4. Glu-C digestion buffer: 25 mM Ammonium bicarbonate, 5% acetonitrile.

2.3. Protein and Peptide Enrichment

1. Boronic acid resin: Prosep-PB affinity resin (Millipore).
2. Binding/wash buffer: 250 mM Ammonium acetate, 50 mM $MgCl_2$, 100 mM Tris–HCl, 500 mM NaCl (pH 8.8) (see Note 1).
3. Wash buffer: 250 mM Ammonium acetate, 50 mM $MgCl_2$ (pH 8.8).
4. Elution buffer: 0.1 M Acetic acid.

2.4. ZipTip Desalting

1. Reversed-phase μ-C18 ZipTips (for MALDI-MS) and C18 ZipTips (for LC-ESI-MS/MS) (Millipore).
2. Wetting solution: 80% acetonitrile in H_2O or 50% MeOH in H_2O.
3. Wash solution: 0.1% TFA in H_2O.
4. Elution solution: 50% MeOH, 0.1% TFA in H_2O (see Note 2).

2.5. MALDI TOF/TOF Mass Spectrometry

1. MALDI matrix solution 1: 4 mg α-cyano-4-hydroxycinnamic acid in 1 mL of 0.3 mM di-ammonium hydrogen citrate (Fluka), 60% acetonitrile in H_2O.
2. MALDI matrix solution 2: 10 mg of 2,5-dihydroxybenzoic acid in 1 mL of 70% acetonitrile in H_2O.
3. Instrumentation: 4800 MALDI TOF/TOF system (AB Sciex).

2.6. LC-MS/MS Analysis

1. HPLC solvent A: 1% acetonitrile, 0.2% formic acid in H_2O.
2. HPLC solvent B: 80% acetonitrile, 0.2% formic acid in H_2O.
3. Self-made capillary tip column (0.075 mm ID × 100 mm), column material: reverse phase Magic C18, AQ, 3 μm, 200 Å.
4. Instrumentation: LTQ-Orbitrap XL ETD (Thermo Scientific), Eksigent nanoHPLC 1D plus (Eksigent Technologies).

3. Methods

The generally low abundance of ADP-ribosylated proteins (estimated to be <1% for histones) is a drawback in the assignment of modification sites. We therefore recommend to enrich ADP-ribosylated proteins or peptides and optimized the usage of boronic acid-based resins (8). The protocol allows the accumulation of modified substrates and increases the possibilities of a successful analysis, including site determination.

The heterogenic nature of the modification, reaching from mono- to branched poly-ADP-ribose makes it particularly difficult to identify the ADP-ribose acceptor sites. It is thus necessary to reduce the complexity of different PAR chain lengths by treatment with poly(ADP-ribose) glycohydrolase (PARG) before subsequent analysis by mass spectrometry. Moreover, the predominantly used fragmentation method in mass spectrometry, collision induced dissociation (CID), is a useful tool for the detection of ADP-ribosylated peptides but lacks sufficient peptide backbone fragmentation to identify the acceptor amino acid (9). Recent advances in the field of mass spectrometry led to the utilization of electron capture dissociation (ECD) and electron transfer dissociation (ETD). These fragmentation methods preserve labile post-translational modifications on their targets (10) and therefore allow the identification of ADP-ribosylation and the determination of the modification site (9, 11).

3.1. ADP-Ribosylation Assays

1. For in vitro ADP-ribosylation of histones incubate 3 µg histone mix or 22 nmol biotinylated histone peptides with 10 pmol hARTD1 in the presence of 5 pmol annealed double-stranded oligomer (5′-GGAATTCC-3′) and 100 or 150 µM NAD^+ in ADP-ribosylation buffer (see Note 3).
2. Reaction volume: 25 µL, reaction conditions: 15 min, 30°C.
3. Terminate the reactions by the addition of 3AB to a final concentration of 20 mM.
4. To reduce the complexity of PAR, samples are incubated additionally with 1 µg hPARG, to generate mainly mono-ADP-ribosylated polypeptides. Adjust the concentrations of $MgCl_2$ to 10 mM, NaCl to 50 mM and incubate at 37°C for 1 h.
5. For the identification of acceptor sites in peptides proceed immediately with step 3 of Subheading 3 or ZipTip-desalting and mass spectrometry. Intact modified proteins need to be proteolytically cleaved prior to mass spectrometry either before or after enrichment.

3.2. Protease Digestion

1. Adjust the buffer conditions in the sample to the ones described for the relevant protease in the Subheading 2.

2. Reduce the disulphide bridges by adding DTT to a final concentration of 10 mM and incubate for 1 h at 65°C (see Note 4).
3. Alkylate cysteines by adding iodoacetamide to a final concentration of 50 mM and incubate for 1 h at room temperature in the dark.
4. To block the reaction, add DTT to a final concentration of 50 mM and incubate for 10 min at room temperature.
5. Add trypsin or Glu-C in a 1:50 ratio (w/w). Incubate the Glu-C digests at 25°C to avoid autolysis. Reaction time should be 4–12 h. The trypsin digests should be incubated at 37°C for 1–4 h (see Note 5).
6. Proceed either with peptide enrichment or ZipTip-desalting and mass spectrometry.

3.3. Enrichment of ADP-Ribosylated Peptides

1. Use 15 µL of a slurry of Prosep-PB resin per binding reaction and wash the beads in 1 mL binding/wash buffer (see Note 6).
2. Spin resins at 4°C for 1 min at 600×*g* and discard the supernatant.
3. Resuspend the equilibrated beads in 1 mL binding/wash buffer containing the ADP-ribosylated samples. Incubate at 4°C for 1 h under constant rolling.
4. Spin beads at 4°C for 1 min at 600×*g* and discard the supernatant.
5. Wash the beads twice in 1 mL binding/wash buffer at 4°C for 10 min.
6. Wash the beads once in 1 mL wash buffer at 4°C for 10 min.
7. Spin beads at 4°C for 1 min at 600×*g* and completely discard the supernatant.
8. Resuspend the beads in 200 µL elution buffer and incubate at 4°C for 15 min under constant rolling.
9. Spin at 4°C for 1 min at 600×*g* and save the supernatant containing the ADP-ribosylated peptides or proteins.
10. Repeat steps 8 and 9 once and pool the supernatants.
11. Spin the pooled supernatants in a vacuum concentrator till dryness (see Note 7). Store dried samples at –20°C or proceed with ZipTip-desalting and mass spectrometry. An example result of a peptide enrichment experiment is shown in Fig. 1.

3.4. ZipTip Desalting

1. Depress pipettor plunger to a dead stop. Using the maximum volume setting of 10 µL, aspirate wetting solution into the tip. Dispense to waste and repeat the procedure three times.
2. Aspirate the wash solution, dispense to waste, and repeat the step three times.

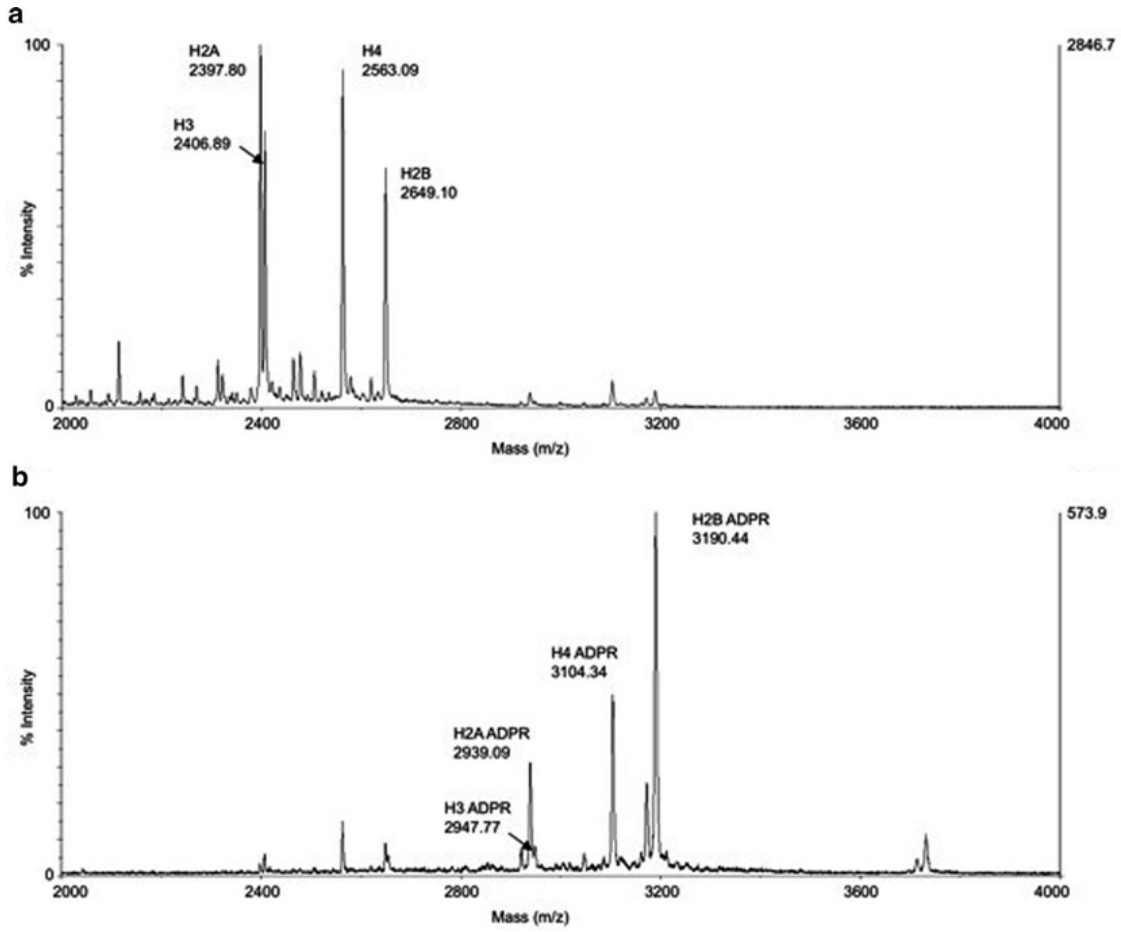

Fig. 1. MALDI-MS spectra of synthetic peptides that represent parts of the N-terminal tails of all four core histones. Peptides were modified according to Subheading 3.1. (**a**) Mass spectrum showing the masses of the input sample with mainly unmodified histone peptides. (**b**) Mass spectrum of the same sample after the procedure explained in Subheading 3.3. The enrichment generates a sample with highly abundant modified peptides. To increase the sensitivity, MALDI-MS was performed in linear mode. *ADPR* = ADP-ribose.

3. Bind peptides to ZipTip by fully depressing the pipette plunger to a dead stop. Aspirate and dispense the sample ten times for maximum binding of the peptides.
4. Aspirate wash solution into the tip and dispense to waste. Repeat once.
5. *For MALDI-analysis.* Elute the bound samples directly into matrix solution on the target plate. Pipette approximately 0.7 µL of MALDI matrix solution onto the target plate by using a regular pipette tip. Aspirate and dispense matrix solution through the ZipTip three times without introducing air into the sample (caution: acetonitrile evaporates rapidly).
6. *For LC-MS/MS-analysis.* Elute the bound samples in 20 µL elution solution. Aspirate and dispense the elution solution five times and save it in a new vial. Spin the eluted samples in a

vacuum concentrator till dryness. The dry samples can be stored at –20°C or proceed with mass spectrometry (see Note 7).

3.5. MALDI TOF/TOF Mass Spectrometry

1. MALDI analyses are performed on a 4800 MALDI TOF/TOF system equipped with a Nd:YAG laser operating at 200 Hz. Mass spectra are acquired in positive reflector mode or linear mode in the mass range from 500 to 4,000 Da and generated by accumulating data from 2,000 laser shots (see Note 8). In order to preserve the unstable bonds of ADP-ribosylated amino acid residues and to reach the optimal values for general peptide analyses the laser intensity is reduced by approximately 200 arbitrary units.
2. First, mass spectra are recorded from peptide standards and the default calibration parameters are updated. Subsequently, mass spectra are acquired for all sample spots on the MALDI target plate and calibrated using the default calibration parameters.

3.6. LC-MS/MS Acquisition

1. Peptide solutions are analyzed on a LTQ-Orbitrap XL ETD instrument connected to an Eksigent nanoHPLC 1D plus. 4 μL of peptide mixtures are injected by an autosampler on a self-made reverse phase tip column for 16 min with a flow rate of 500 nL/min. The peptide elution is performed with a flow rate of 200 nL/min and a linear gradient from 3 to 48% acetonitrile in 36 min. The acetonitrile concentration is raised to 80% in 4 min and the column is cleaned with 80% acetonitrile for 7 min.
2. The eluting peptides are analyzed on an Orbitrap with a resolution of 60,000 at m/z 400, at a target value of 5×10^5 and 1 micro scan. MS/MS is performed in the linear ion trap with a target value of 1×10^4 in data-dependent decision tree mode, using the following criteria to trigger ETD fragmentation (see Note 9): charge state is 3 and the m/z is less than 650, charge state is 4 and the m/z is less than 900, charge state is 5 and the m/z is less than 950. For higher charge states ETD is performed per default (see Note 10).
3. Fluoranthene is used as anion with target value of 1×10^5 (see Note 11) and reaction time is set to 100 ms (see Note 12) with additional supplemental activation. Maximum injection time for both MS and MS/MS was set to 300 ms.

3.7. Database Search

1. For database searches mgf-files with mascot generic format are created by the use of Mascot Distiller 2.3 with standard Orbitrap opt-file (see Note 13).
2. The search is done with a human database with common contaminants (117865 sequences) and a concatenated decoy database.

The peptide tolerance (see Note 14) is set to 5 ppm and the MSn tolerance to 0.6 Da. For the synthetic peptides, biotin is defined as fixed modification at the peptide N terminus. ADP-ribosylation on lysine, arginine, cysteine, and glutamic acid residues is defined as variable modification without neutral loss during fragmentation (see Note 15).

4. Notes

1. These buffer conditions are optimized for synthetic histone peptides. Therefore, the concentrations of Tris–HCl and NaCl might need further adjustments for given peptides.
2. Note that MALDI-MS samples can be directly eluted onto the MALDI sample plate in MALDI matrix solution (see Subheading 3.4, step 5).
3. Higher NAD^+ concentrations can trigger the generation of very long ADP-ribose polymers that might interfere with *trans*-ADP-ribosylation or subsequent analysis.
4. Subheading 3.2, steps 2–4 are not absolutely necessary for the proteolytic cleavage of histone proteins but might be crucial in case of other target proteins.
5. The trypsin/protein ratio and the incubation time result in an incomplete cleavage of the substrate proteins. Due to the high abundance of lysines and arginines in histone proteins, a complete cleavage would lead to very short peptides that are no longer suitable for ETD mass spectrometry.
6. The enrichment protocol with the Prosep-PB resin can also be adapted for the use in liquid chromatography.
7. Avoiding complete dryness increases peptide recovery.
8. Due to the labile nature of the modification, minor ADP-ribosylation is significantly better detectable in linear mode.
9. The use of supplemental activation largely decreases charge reduced precursor signals in the MS/MS and allows a better assignment of fragment masses.
10. If precursor signal intensity is very weak but the m/z ratio is known, MS/MS can be specifically acquired on that m/z value over the entire LC-MS run to achieve good data quality. It has to be assured, that the corresponding charge state for correct supplemental activation is selected.
11. In some cases it is beneficial to increase the anion population to 3×10^5 target value.

12. For precursor masses with known charge state it is beneficial to optimize the activation time for better fragmentation efficiency.
13. If CID and ETD data are saved in one LC-MS/MS RAW file it is necessary to choose the "no-merge" option in the Mascot Distiller option file. Otherwise the more intense CID fragment masses will cover all usually less intense ETD fragment masses.
14. If you choose to acquire MS/MS on a specific precursor signal over the complete LC-MS run, you have to modify the header of the extracted peak list (e.g., mgf file) manually with the correct monoisotopic precursor mass and the correct charge state.
15. In some cases for data-dependent acquisition of higher charge states the second isotope (^{13}C) is chosen as precursor. In that case it is advantageous to allow the Mascot search engine to use the second isotope by setting the isotope error to 1.

    It is important to note that, in contrast to other reports, we observed partial fragmentation of the ADP-ribose at the phosphodiester bond by application of ETD, as revealed by the presence of a m/z 348 ion, which corresponds to adenosine monophosphate. However, conventional collision induced dissociation (CID) mass spectrometry of ADP-ribosylated H4 peptide did not reveal any ADP-ribose acceptor sites, since the ADP-ribose was cleaved off from the peptide during fragmentation. The commonly used CID, instead of ETD, might thus explain why numerous efforts to identify ADP-ribosylated residues failed in the past. Consequently, we would strongly recommend ETD as standard technique for future investigations on ADP-ribosylated peptides, opening new opportunities to screen for modified residues in a systems-biology setup.

Acknowledgments

The authors would like to thank Dr. Dorothea Rutishauser (former member of the Functional Genomics Center Zurich, University of Zurich, Zurich, Switzerland) for advice and technical assistance. We also thank Felix R. Althaus (Institute of Pharmacology and Toxicology, University of Zurich-Vetsuisse) for providing hPARG expressing baculo virus. Work on ADP-ribosyltransferases in the laboratory of M.O.H is supported by the Swiss National Science Foundation (SNF 31-122421).

References

1. Hottiger MO, Hassa PO, Lüscher B et al (2010) Towards a unified nomenclature for mammalian ADP-ribosyltransferases. Trends Biochem Sci 35:208–219
2. Hassa PO, Haenni SS, Elser M, Hottiger MO (2006) Nuclear ADP-ribosylation reactions in mammalian cells: where are we today and where are we going? Microbiol Mol Biol Rev 70:789–829
3. Quenet D, El Ramy R, Schreiber V, Dantzer F (2009) The role of poly(ADP-ribosyl)ation in epigenetic events. Int J Biochem Cell Biol 41:60–65
4. Ogata N, Ueda K, Hayaishi O (1980) ADP-ribosylation of histone h2b. Identification of glutamic acid residue 2 as the modification site. J Biol Chem 255:7610–7615
5. Ogata N, Ueda K, Kagamiyama H, Hayaishi O (1980) ADP-ribosylation of histone h1. Identification of glutamic acid residues 2, 14, and the COOH-terminal lysine residue as modification sites. J Biol Chem 255:7616–7620
6. Altmeyer M, Messner S, Hassa PO et al (2009) Molecular mechanism of poly(ADP-ribosyl)ation by parp1 and identification of lysine residues as ADP-ribose acceptor sites. Nucleic Acids Res 37:3723–3738
7. Messner S, Altmeyer M, Zhao H et al (2010) PARP1 ADP-ribosylates lysine residues of the core histone tails. Nucleic Acids Res 38:6350–6362
8. Alvarez-Gonzales R, Juares-Salinas H, Jacobson EL, Jacobson MK (1983) Evaluation of immobilized boronates for studies of adenine and pyridine nucleotide metabolism. Anal Biochem 135:69–77
9. Hengel SM, Shaffer SA, Nunn BL, Goodlett DR (2009) Tandem mass spectrometry investigation of ADP-ribosylated kemptide. J Am Soc Mass Spectrom 20:477–483
10. Syka JEP, Coon JJ, Schroeder MJ et al (2004) Peptide and protein sequence analysis by electron transfer dissociation mass spectrometry. PNAS 26:9528–9533
11. Zee BM, Garcia BA (2010) Electron transfer dissociation facilitates sequencing of adenosine diphosphate-ribosylated peptides. Anal Chem 82:28–31

nature structural & molecular biology

Macrodomain-containing proteins are new mono-ADP-ribosylhydrolases

Florian Rosenthal[1,2,6], Karla L H Feijs[3,6], Emilie Frugier[4], Mario Bonalli[1], Alexandra H Forst[3], Ralph Imhof[1], Hans C Winkler[1], David Fischer[5], Amedeo Caflisch[4], Paul O Hassa[1], Bernhard Lüscher[3] & Michael O Hottiger[1]

ADP-ribosylation is an important post-translational protein modification (PTM) that regulates diverse biological processes. ADP-ribosyltransferase diphtheria toxin-like 10 (ARTD10, also known as PARP10) mono-ADP-ribosylates acidic side chains and is one of eighteen ADP-ribosyltransferases that catalyze mono- or poly-ADP-ribosylation of target proteins. Currently, no enzyme is known that reverses ARTD10-catalyzed mono-ADP-ribosylation. Here we report that ARTD10-modified targets are substrates for the macrodomain proteins MacroD1, MacroD2 and C6orf130 from *Homo sapiens* as well as for the macrodomain protein Af1521 from archaebacteria. Structural modeling and mutagenesis of MacroD1 and MacroD2 revealed a common core structure with Asp102 and His106 of MacroD2 implicated in the hydrolytic reaction. Notably, MacroD2 reversed the ARTD10-catalyzed, mono-ADP-ribose–mediated inhibition of glycogen synthase kinase 3β (GSK3β) *in vitro* and in cells, thus underlining the physiological and regulatory importance of mono-ADP-ribosylhydrolase activity. Our results establish macrodomain-containing proteins as mono-ADP-ribosylhydrolases and define a class of enzymes that renders mono-ADP-ribosylation a reversible modification.

ADP-ribosylation is a PTM involved in many biological processes including the regulation of chromatin structure, transcription and DNA repair[1–6]. ARTD10 is a mono-ADP-ribosyltransferase that transfers ADP-ribose to aspartate or glutamate residues by substrate-assisted catalysis[7]. Recently, GSK3β was identified as a new substrate of ARTD10. Mono-ADP-ribosylation noncompetitively inhibits GSK3β kinase activity[8].

Although many ADP-ribosyltransferases (including ARTDs and ADP-ribosyltransferases cholera toxin-like (ARTCs)) that ADP-ribosylate different amino acid acceptor sites have been identified[9], the enzymes able to reverse this modification are largely unknown. Irreversible ADP-ribosylation is highly detrimental and causes embryonic lethality[10,11]. In humans, the deficiency of an ADP-ribose hydrolase is the cause of fatal glutamyl ribose 5-phosphate storage disease[12]. Therefore, enzymes that remove ADP-ribose modifications must exist. The mammalian hydrolases characterized so far include the mono-ADP-ribosylarginine hydrolase 1 (ARH1) as well as poly-ADP-ribose glycohydrolases (PARG and ARH3). Whereas ARH1 is the only hydrolase that specifically removes mono-ADP-ribose from arginine residues, ARH3 and PARG hydrolyze the O-glycosidic ribose-ribose 1-2′ bonds within ADP-ribose polymers[13,14]. In contrast, enzymes catalyzing the removal of specific mono-ADP-ribose marks of modified aspartates or glutamates, such as those synthesized by ARTD10, are currently unknown (**Supplementary Fig. 1a**).

Macrodomains are a family of evolutionarily conserved proteins that bind mono- or poly-ADP-ribose (PAR), poly(A) or *O*-acetyl-ADP-ribose (OAADPr)[15–18]. Macrodomain proteins are involved in diverse cellular processes[15] and have been implicated in transcriptional regulation[19–22], chromatin remodeling[23,24] and developmental processes as well as in B-cell lymphomagenesis[25–27]. Macrodomain-containing proteins localize to the nucleus (for example, MacroD1v2) or to mitochondria (MacroD1v1) or are found in the cytoplasm (MacroD1v2, MacroD2 or C6orf130)[18]. In addition to the binding of ADP-ribose, the human MacroD1, MacroD2 and C6orf130 possess C2- or C3-specific OAADPr deacetylase activity[28,29] and weak C1-specific phosphatase activity toward ADP-ribose-1″-phosphate (Appr-1″-p), a product of ARTD18 (TPT1) and cyclic nucleotide phosphodiesterases[17,30,31]. On the basis of structural and functional analyses, several residues in the active centers of macrodomains were identified that participate in the catalytic mechanism[28,29]. Notably, the catalytically important residues of MacroD1 are not conserved in C6orf130, which indicates that sequence variation within the macrodomain family allows a different set of catalytic residues to perform OAADPr hydrolysis[29].

Here we test the hypothesis that macrodomain-containing proteins possess ADP-ribosylhydrolase activity and thereby to characterize the missing mono-ADP-ribosylhydrolases. We provide evidence that the human proteins MacroD1, MacroD2 and C6orf130 as well as the archaebacterial macrodomain Af1521 are able to hydrolyze ARTD10-catalyzed mono-ADP-ribosylation. Notably, MacroD2 rendered the inhibitory effect of GSK3β ADP-ribosylation reversible. Treatment with MacroD2 removed the ADP-ribose moiety from GSK3β, which was sufficient to restore kinase activity *in vitro* and in cells. These

[1]Institute of Veterinary Biochemistry and Molecular Biology, University of Zurich, Zurich, Switzerland. [2]Life Science Zurich Graduate School, University of Zurich, Zurich, Switzerland. [3]Institute of Biochemistry and Molecular Biology, Rheinisch-Westfälische Technische Hochschule Aachen, Aachen, Germany. [4]Department of Biochemistry, University of Zurich, Zurich, Switzerland. [5]Functional Genomics Center Zurich, University of Zurich, Zurich, Switzerland. [6]These authors contributed equally to this work. Correspondence should be addressed to B.L. (luescher@rwth-aachen.de) or M.O.H. (hottiger@vetbio.uzh.ch).

Received 12 September 2012; accepted 17 January 2013; published online 10 March 2013; doi:10.1038/nsmb.2521

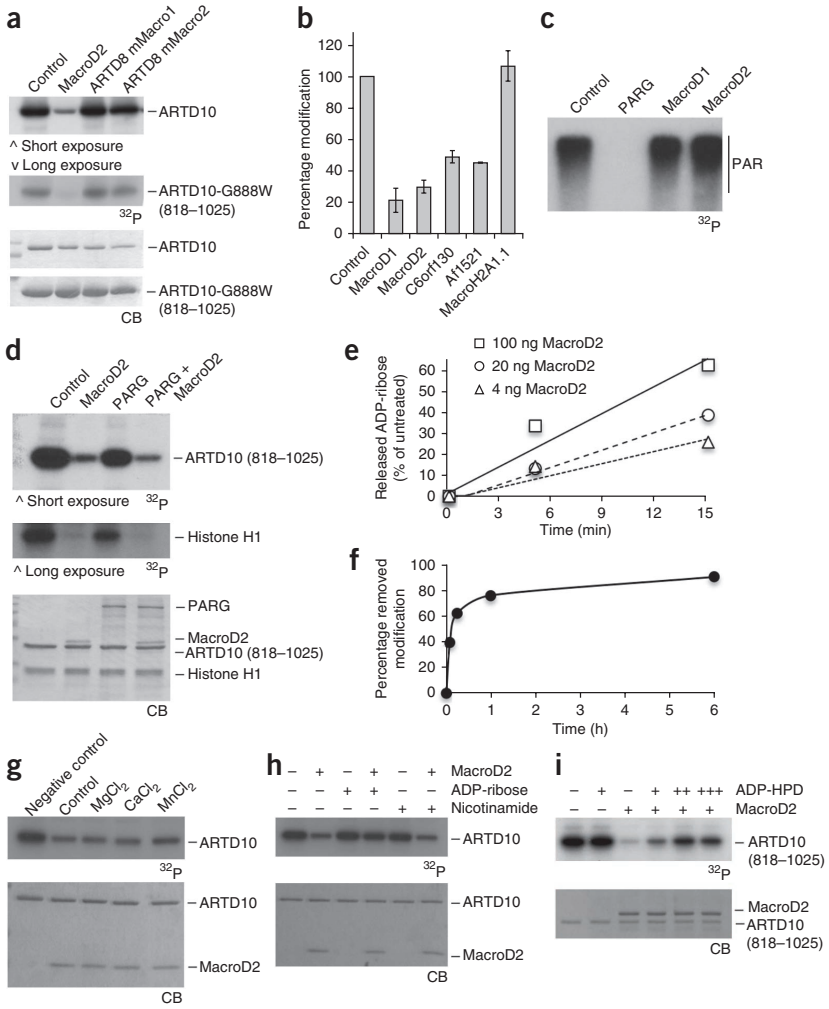

Figure 1 MacroD1, MacroD2, C6orf130 and Af1521 hydrolyze mono-ADP-ribose modifications. (**a**,**b**) Protein mono-ADP-ribosylhydrolase activity of MacroD1, MacroD2, C6orf130, mouse ARTD8 (mMacro1 and mMacro2), macroH2A1.1 and Af1521. Auto-ADP-ribosylated ARTD10 de-ADP-ribosylated by the indicated proteins is shown on SDS-PAGE with Coomassie blue (CB) staining or autoradiography (^{32}P). Shown are representative blots and quantification from two independent experiments, averaged and normalized to the untreated control ($n = 2$; mean ± range). (**c**) Hydrolase activity assays showing that MacroD-like macrodomains have no activity toward polymers of ADP-ribose, whereas PARG has strong activity. Auto-poly-ADP-ribosylated ARTD1 (with 160 μM radioactive NAD$^+$ to induce poly-ADP-ribosylation) was used with the indicated hydrolases. (**d**) Activity assays as in **a**, showing that PARG cannot hydrolyze ADP-ribose from mono-ADP-ribosylated ARTD10 or from histones. (**e**) Concentration-dependent removal of the mono-ADP-ribose from ARTD10 (818–1025) by MacroD2 under nonsaturating conditions. (**f**) Time course of MacroD2 activity toward mono-ADP-ribosylated ARTD10 catalytic domains. (**g**) Identification of cofactors (1 mM each) for ADP-ribose hydrolysis by MacroD2. (**h**) Effect of ADP-ribose and nicotinamide (40 μM each) on MacroD2-mediated de-ADP-ribosylation of ARTD10. (**i**) The ADP-ribose analog ADP-HPD inhibits MacroD2 in a concentration-dependent manner (4, 40 and 400 μM).

data highlight the important physiological function of endogenous mono-ADP-ribosylation for intracellular signaling and regulatory processes.

RESULTS

Macrodomain proteins are mono-ADP-ribosylhydrolases

To investigate whether macrodomain-containing proteins are able to release the mono-ADP-ribose moiety from ARTD10-modified target proteins, we incubated different macrodomains with *in vitro*–radiolabeled mono-ADP-ribosylated ARTD10 (full length or the catalytic domain, consisting of residues 818–1025) as a substrate (**Fig. 1a**,**b** and **Supplementary Fig. 1b**,**c**). Human MacroD1, MacroD2 and C6orf130 robustly hydrolyzed the mono-ADP-ribosyl linkage of modified full-length ARTD10 or the ARTD10 catalytic domain. Notably, the structurally related archaebacterial macrodomain protein Af1521 was also active, whereas neither the human histone variant MacroH2A1.1 nor the mouse macrodomains 1 or 2 of ARTD8 (PARP14) were able to remove mono-ADP-ribose under the tested conditions (**Fig. 1a**,**b** and **Supplementary Fig. 1b**,**c**). Pulldown experiments revealed that mono-ADP-ribosylhydrolase activity of the tested macrodomains correlated with the ability to bind mono-ADP-ribosylated ARTD10 (**Supplementary Fig. 1d**). In contrast to their activity toward mono-ADP-ribosylated substrates, MacroD1 and MacroD2 were each completely inactive toward PAR synthesized by ARTD1 (PARP1) in the presence of high NAD$^+$ concentrations, whereas the known PAR hydrolase PARG exhibited strong activity toward this substrate (**Fig. 1c**). However, PARG was not able to completely remove all ADP-ribose modifications from automodified ARTD1, even when tested under low NAD$^+$ concentrations (resulting in mono- and oligo-ADP-ribosylation; **Supplementary Fig. 1e** and as suggested in ref. 13). The nature of the modified protein did not affect PARG-dependent hydrolysis, because histones modified by ARTD1 under low NAD$^+$ concentrations were also not completely demodified (**Supplementary Fig. 1f**). Notably, prior PARG treatment rendered ARTD1, histone H1 and core histones at least partially susceptible to hydrolysis by MacroD2 (**Supplementary Fig. 1f**,**g**), which suggests that the acceptor residue and/or the linkage (C1 versus C2 or C3) between the ADP-ribose moiety and the acceptor residue are critical for the newly identified enzymatic activity. Consequently, PARG treatment probably generates mono-ADP-ribosylated residues that serve as substrates for hydrolysis by MacroD2. Comparably, PARG was inactive toward ARTD10-catalyzed mono-ADP-ribosylated histone H1, whereas MacroD2 demodified this substrate, irrespective of PARG treatment (**Fig. 1d**). These results suggested that MacroD2 is able to release mono-ADP-ribose from acceptor proteins but is inactive toward polymers or oligomers of ADP-ribose.

To biochemically characterize the enzymatic reaction catalyzed by MacroD2, we performed concentration- and time-dependent experiments. MacroD2 efficiently removed ADP-ribose modifications from

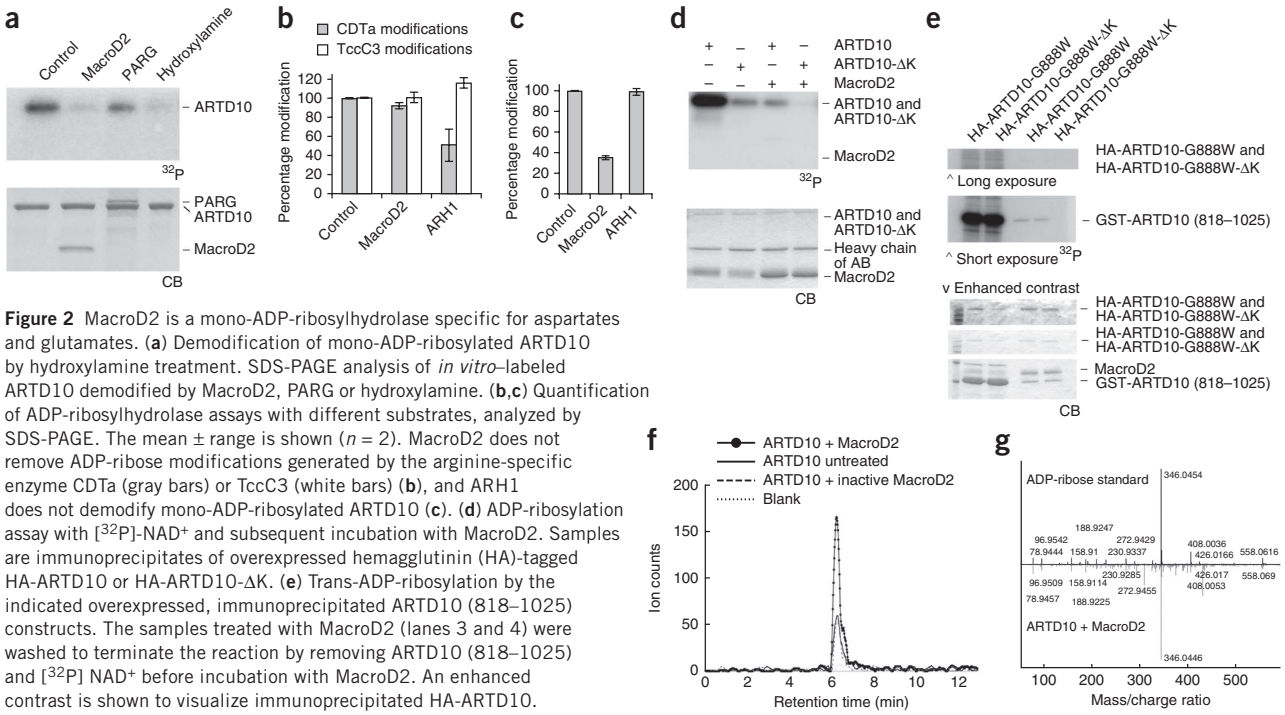

Figure 2 MacroD2 is a mono-ADP-ribosylhydrolase specific for aspartates and glutamates. (**a**) Demodification of mono-ADP-ribosylated ARTD10 by hydroxylamine treatment. SDS-PAGE analysis of *in vitro*–labeled ARTD10 demodified by MacroD2, PARG or hydroxylamine. (**b**,**c**) Quantification of ADP-ribosylhydrolase assays with different substrates, analyzed by SDS-PAGE. The mean ± range is shown ($n = 2$). MacroD2 does not remove ADP-ribose modifications generated by the arginine-specific enzyme CDTa (gray bars) or TccC3 (white bars) (**b**), and ARH1 does not demodify mono-ADP-ribosylated ARTD10 (**c**). (**d**) ADP-ribosylation assay with [^{32}P]-NAD$^+$ and subsequent incubation with MacroD2. Samples are immunoprecipitates of overexpressed hemagglutinin (HA)-tagged HA-ARTD10 or HA-ARTD10-ΔK. (**e**) Trans-ADP-ribosylation by the indicated overexpressed, immunoprecipitated ARTD10 (818–1025) constructs. The samples treated with MacroD2 (lanes 3 and 4) were washed to terminate the reaction by removing ARTD10 (818–1025) and [^{32}P] NAD$^+$ before incubation with MacroD2. An enhanced contrast is shown to visualize immunoprecipitated HA-ARTD10. (**f**) Extracted ion chromatograms of mass 558.064, the monoisotopic mass of the ADP-ribose [M-H] adduct. The elution time window of ADP-ribose was between 6 and 7 min. (**g**) MS-MS spectrum of mass 558.064. Typical mass fragments of ADP-ribose as seen in the ADP-ribose standard (top spectrum) are present in the MS-MS spectrum of ARTD10 + MacroD2 samples (bottom spectrum).

ARTD10 (818–1025) in a concentration-dependent manner (**Fig. 1e**). Furthermore, mono-ADP-ribose hydrolysis by MacroD2 was time dependent and removed >60% of the modifications within 15 min (**Fig. 1f**). Further characterization of the enzymatic activity revealed that MacroD2 activity was not markedly affected by the addition of magnesium, calcium or manganese as cofactor (**Fig. 1g**). Notably, MacroD2 activity was inhibited by the addition of the ADP-ribose analog adenosine 5′-diphosphate (hydroxymethyl) pyrrolidinediol (ADP-HPD) and by ADP-ribose itself in a concentration-dependent manner, whereas addition of nicotinamide did not influence the mono-ADP-ribosylhydrolase activity (**Fig. 1h**,**i**). These observations indicated that free ADP-ribose is able to inhibit the mono-ADP-ribose hydrolyzing activity by competing with protein-linked mono-ADP-ribose for binding to the active site. Together, these experiments thus defined MacroD1, MacroD2, C6orf130 and Af1521 as new specific mono-ADP-ribosylhydrolases.

MacroD2 is a mono-ADP-ribosylhydrolase for acidic residues

To define the specificity of MacroD2 mono-ADP-ribosylhydrolase activity, we characterized and analyzed different substrates. Hydroxylamine treatment was reported to remove ADP-ribose from glutamate and arginine residues[32]. Treatment of ARTD10 with hydroxylamine for 60 min at 37 °C released the modification of the enzyme, as already observed earlier (**Fig. 2a** and ref. 7), which suggests that MacroD2 is able to hydrolyze mono-ADP-ribose from acidic acceptor sites or arginine. To further investigate whether MacroD2 removed ADP-ribose from arginine acceptor amino acids, the arginine-specific ADP-ribosyltransferase CDTa was used[33]. MacroD2 showed no activity toward actin modified by CDTa (**Fig. 2b**), which indicates that modified arginine residues cannot be hydrolyzed by MacroD2. In contrast, the arginine-specific hydrolase ARH1 was able to remove the ADP-ribose from arginine-modified β- or γ-actin but was not able to remove ADP-ribose from ARTD10 (**Fig. 2c**), which confirms that ARTD10 is not modified at arginine residues. Actin modified at threonine residues by the threonine-specific transferase TccC3 (ref. 34) could not be demodified by either ARH1 or MacroD2 (**Fig. 2b**). To exclude that lysine residues were modified by ARTD10 and consecutively demodified by MacroD2, we mutated all ARTD10 lysine residues to arginines. This mutant (ARTD10-ΔK) showed reduced ADP-ribosylation activity toward both itself and GSK3β, a newly identified ARTD10 target (**Fig. 2d** and **Supplementary Fig. 2a**), which indicated that mutation of these lysine residues interferes with the enzymatic activity of ARTD10. However, the inactive mutant ARTD10-G888W-ΔK could be modified in *trans* by the catalytic domain of ARTD10 to a comparable extent as ARTD10-G888W (**Fig. 2e**), thus implying that lysines are not the acceptor sites. Of note, ARTD10-ΔK and ARTD10-G888W-ΔK were still demodified by MacroD2 to a comparable extent as were wild-type ARTD10 or ARTD10-G888W, respectively (**Fig. 2d**,**e**), which suggests that the same residues (for example, aspartates or glutamates) are automodified in ARTD10-ΔK and wild-type ARTD10 and consecutively demodified by MacroD2. In conclusion, these results suggested that MacroD2 probably releases ADP-ribose from ADP-ribosylated acidic residues.

To confirm that MacroD2 removes ADP-ribose from its target protein, the reaction products were analyzed by LC-MS and HPLC. Upon incubation of ARTD10 with MacroD2, a product that eluted at the same time as the ADP-ribose standard and had the expected mass of 558.064 Da was detected, thus showing that MacroD2 indeed removed ADP-ribose from ARTD10 (**Fig. 2f**,**g** and **Supplementary Fig. 2b**–**d**).

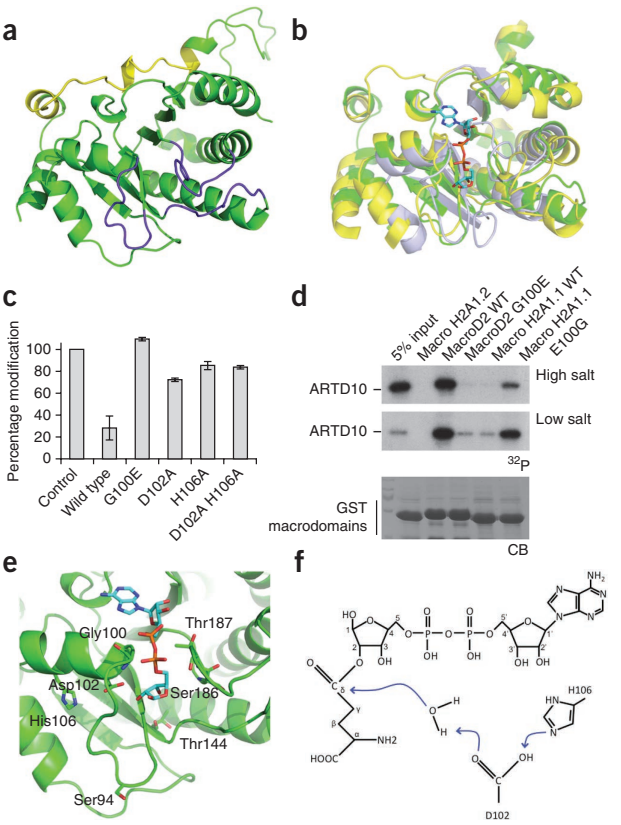

Figure 3 Structural and mutational analysis of the mono-ADP-ribosylhydrolase activity of MacroD2. (**a**) Structure of MacroD2 modeled on the basis of the PDB 2X47 crystal structure of MacroD1. Residues highlighted in yellow represent those having a low r.m.s. fluctuation value as compared to the crystal-structure *B* factors. The primary macrodomain binding-site loops are marked in violet. (**b**) Overlay of the MacroD1 (yellow), MacroD2 (green) and C6orf130 (violet) structures with the ADP-ribose product in the binding pocket. (**c**) Mutational analysis of MacroD2 highlights residues implicated in enzymatic activity toward mono-ADP-ribosylated ARTD10 (818–1025). Quantifications from blots of two independent experiments are shown normalized to the untreated control ($n = 2$; mean ± range). (**d**) ADP-ribose binding to wild-type (WT) and mutant macrodomain proteins, assessed with histidine- and glutathione-S-transferase (GST)-tagged, recombinantly expressed macrodomain proteins immobilized on glutathione or nickel Sepharose and incubated with automodified ARTD10. (**e**) Structural model of MacroD2 with the mutated residues highlighted. (**f**) Model for MacroD2 protein–catalyzed hydrolysis of mono-ADP-ribosylated glutamate residues.

Modeling of MacroD2 and of residues implicated in catalysis

Homology modeling and atomistic simulations were carried out to shed light on the hydrolysis reaction mechanism. First, the three-dimensional structure of MacroD2 was modeled by using the X-ray structure of MacroD1 as a template (**Fig. 3a**). Except for their flexible loops, the human MacroD1, MacroD2 and C6orf130 structures are highly similar, as emerges from their superposition (**Fig. 3b**). This structural likeness, along with their similar enzymatic activities, suggested a conserved mode of action.

Second, the ADP-ribose product of the hydrolysis reaction was automatically docked to MacroD2 and followed by multiple explicit solvent molecular dynamics simulations of the complex to validate the binding mode. The mono-ADP-ribosylhydrolase activity was then studied by mutational analysis of MacroD2 and by comparison with existing mutants of MacroD1 (ref. 29) because these two macrodomain-containing proteins are closely related.

To confirm that the hydrolase activity of MacroD2 is dependent specifically on the macrodomain, we mutated the conserved glycine at position 100 of MacroD2 (**Supplementary Fig. 3a**) to a glutamate, which is predicted to block the ADP-ribose–binding site in macrodomain proteins[35], or to an isoleucine. The resulting MacroD2 mutants lacked hydrolase and ADP-ribose–binding activity under the same assay conditions, which provided evidence that the macrodomain is responsible for the catalytic activity toward ARTD10-mediated mono-ADP-ribosylation and that the interaction with ADP-ribose is specific (**Fig. 3c**,**d** and data not shown). Notably, MacroH2A1.1 contains a glutamate at the corresponding position 225 instead of a glycine (**Supplementary Fig. 3a**), which possibly explains its inactivity due to its inability to bind mono-ADP-ribosylated ARTD10. However, although mutation of Glu225 of MacroH2A1.1 to a glycine resulted in a gain of binding, it did not restore its enzymatic activity (**Supplementary Fig. 3b**), thus indicating that additional residues are important for the activity.

Multiple explicit solvent molecular dynamics simulations of the MacroD2–ADP-ribose complex, together with defining conserved residues between MacroD1, MacroD2 and C6orf130, was used to propose site-specific mutants of MacroD2. Of particular note were Asp102 and its buried neighbor His106, which by modeling were predicted to be located near the 2- and 3-hydroxyl groups of the distal ribose (**Fig. 3e**). Mutational analysis, guided by the *in silico* predictions, indicated partial involvement in catalysis of Asp102 and His106 of MacroD2 as well as Asp184 and His188 of MacroD1 (**Fig. 3c** and **Supplementary Fig. 3c**). Pulldown experiments revealed that the MacroD2 mutants were still able to bind mono-ADP-ribosylated ARTD10 under the conditions tested for their enzymatic activity but that increasing the salt concentration to 500 mM reduced their affinity to the substrate to some extent (**Supplementary Fig. 3d**). On the basis of our findings, a model emerges for MacroD2-catalyzed hydrolysis of mono-ADP-ribosylated aspartate or glutamate residues (**Fig. 3f**). In this model, which is similar to the one previously suggested for the hydrolysis of OAADPr by MacroD1 (ref. 28), Asp102 or Asp184 acts as a general base that deprotonates a water molecule, which then acts as a nucleophile to attack the carbonyl carbon. We note that our mutagenesis data do not exclude participation of additional residues and/or transition-state stabilization due to induced fit.

MacroD2 regulates GSK3β function *in vitro* and in cells

GSK3β is a key regulator in processes ranging from cell structure and survival to diseases such as Alzheimer's disease, cancer and diabetes[36], and it was recently identified in a screen for ARTD10 target proteins (ref. 8 and **Supplementary Fig. 2a**). To address whether the ARTD10-catalyzed ADP-ribosylation of GSK3β is reversible (in addition to the observed ribosylation of ARTD10 and histones (**Figs. 1a**,**b**,**d** and **2e**)), the ADP-ribosylhydrolase activity of MacroD2 on GSK3β was analyzed. Notably, MacroD2 removed the ADP-ribosylation from both ARTD10 and GSK3β *in vitro* (**Fig. 4a**). These findings support the notion that ARTD10-mediated mono-ADP-ribosylation of target proteins in general is a reversible PTM. To test whether removal of the inhibitory mono-ADP-ribose by MacroD2 is sufficient to restore GSK3β kinase activity, mono-ADP-ribosylated GSK3β was demodified by MacroD2 and consecutively used in kinase assays with a primed peptide substrate. Although the ADP-ribosylated protein showed little *in vitro* kinase activity compared to the control, de-ADP-ribosylation restored the GSK3β activity (**Fig. 4b**).

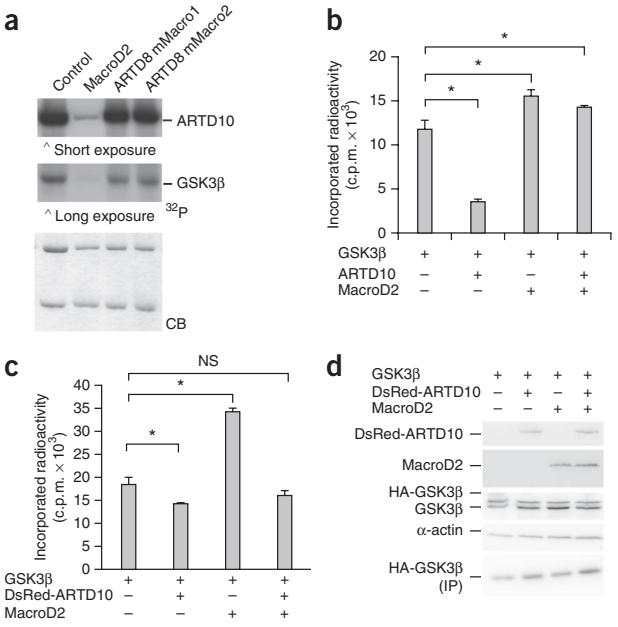

Figure 4 MacroD2 functionally and specifically regulates mono-ADP-ribosylation of GSK3β *in vitro* and in cells. MacroD2 but not the catalytically inactive macrodomains of ARTD8 removes mono-ADP-ribose from ARTD10 and GSK3β. (**a**) Coomassie blue (CB) staining and autoradiography (^{32}P) results of *in vitro* assays with tandem-affinity purification (TAP)-tagged ARTD10 and GST-GSK3β coupled to beads. (**b**) Scintillation counting of kinase assays using [γ-^{32}P]ATP and substrate peptide with modified or demodified GST-GSK3β. (**c**) Scintillation counting results as in **b** with HA-GSK3β from U2OS cells expressing DsRed-ARTD10, GFP-MacroD2 or both. (**d**) Input blot showing expression of DsRed-ARTD10, GFP-MacroD2 and HA-GSK3β in U2OS cells and immunoprecipitation efficiency of HA-GSK3β (lower blot). Data are represented as mean ± s.d. of at least triplicate measurements from representative experiments. $^{*}P < 0.05$; NS, not significant by two-tailed Student's *t* test.

To address whether MacroD2 also reversed ARTD10-mediated ADP-ribosylation in cells, HA-GSK3β was coexpressed with the fluorescently tagged DsRed-ARTD10 alone or together with GFP-MacroD2, and subsequently immunoprecipitated and included in a kinase assay (**Fig. 4c**). The presence of MacroD2 enhanced the kinase activity of GSK3β, which suggested that MacroD2 antagonized the ARTD10-mediated inactivation of GSK3β without affecting protein expression (**Fig. 4d**). These data indicated that MacroD2 hydrolyzes mono-ADP-ribosyl linkages in cells, thus rendering mono-ADP-ribosylation a dynamic modification that can regulate the activation or inactivation of proteins such as GSK3β.

DISCUSSION

The biochemical experiments, mutational analyses and structural predictions presented here suggest that certain macrodomain-containing proteins such as MacroD1, MacroD2, C6orf130 or Af1521, but neither the macrodomains 1 and 2 of ARTD8 nor macroH2A1.1, are bona fide protein mono-ADP-ribosylhydrolases. These results thus fill a major gap in understanding of the ADP-ribosylation cycle and define these proteins as new mono-ADP-ribosylhydrolases that reverse the PTM catalyzed by ARTD10.

The Appr-1″-p phosphatase activity and the OAADPr-hydrolyzing activity of macrodomain proteins have been previously described and studied[28–30]. OAADPr represents an ADP-ribose that is O-acetylated at the C2 or C3 atom, whereas the PAR chain features C1 linkages[37–39]. The OAADPr hydrolysis by MacroD-like macrodomains suggests that these proteins hydrolyze ADP-riboses with C2 or C3 linkages at the proximal ribose. In contrast, the lack of MacroD1 or MacroD2 and C6orf130 activity toward PAR suggests that the glycosidic (ribose-ribose 1′-2′) linkages at the C1 atom of ADP-ribose polymers are not attacked, whereas these bonds within PAR are efficiently degraded by PARG and ARH3. The inefficient hydrolysis of ADP-ribose from ARTD10 by PARG suggests that the C2 or C3 atoms form the glycosidic bond to a glutamate or aspartate (similar to the linkage in OAADPr) rather than to the C1 atom as in PAR. Alternatively, MacroDs might recognize not only the ADP-ribose but also parts of the modified target protein. Moreover, the inability of PARG and MacroD1 or MacroD2 to completely remove the protein-linked ADP-ribose unit from ARTD1 suggests that at least some of the modifications catalyzed by ARTD1 are linked to yet another acceptor site.

The MacroD2-mediated reaction seems to be very efficient because at a 1:10 ratio (MacroD2/ARTD10) more than 60% of the modification synthesized by ARTD10 was removed within 15 min *in vitro*. Owing to the low rates of enzymatic mono-ADP-ribosylation, it was not possible to generate sufficient amounts of mono-ADP-ribosylated MacroD2 substrate that would allow substrate-saturated conditions to exactly determine V_{max} and K_m. In addition, it has been previously shown that ARTD10 is ADP-ribosylated at multiple sites[7]. Because the MacroD2 affinity for these different acceptor sites probably varies, it is impossible to determine exact kinetics with such a substrate. However, chemical synthesis of defined mono-ADP-ribosylated peptides, which could serve as substrates, is currently not possible.

The activity of MacroD-like proteins toward other acceptor sites remains to be tested, but the different chemical nature of these linkages probably requires specific enzymes for the different acceptor sites (for example, ARH1). Furthermore, the specificity may additionally be determined by protein-protein interactions. However, as MacroD2 is expressed in the cytoplasm and MacroD1 exhibits nuclear and mitochondrial localization[18], these two proteins are likely to encounter different protein substrates but catalyze the same mono-ADP-ribosylhydrolysis reaction. ARTD10 and most of the other mono-ARTDs are mainly localized in the cytoplasm[40]. ARTD10-modified target proteins thus require cytoplasmic MacroD proteins for demodification.

On the basis of crystal structures, several residues in MacroD1 and C6orf130 were mutated in other studies to identify side chains involved in OAADPr hydrolysis[28,29]. Notably, we find that corresponding residues are implicated in MacroD1- and MacroD2-mediated hydrolysis of residues ADP-ribosylated by ARTD10. Mutating any of the putative catalytic residues (Asp102 and His106 of MacroD2) individually or together resulted in only a partial loss of activity, which indicates that other residues might compensate for the single mutations, to a certain extent. This observation is further supported by the fact that C6orf130 is active even though the residues identified in MacroD1 and MacroD2 are not conserved in C6orf130 (**Supplementary Fig. 2a**), which again points at sequence variation allowing different sets of residues to confer hydrolase activity. The residues Ser35 and Asp125, crucial for the hydrolysis of OAADPr by C6orf130, would indeed be strong candidates[28].

The removal of ADP-ribose from GSK3β is sufficient to restore kinase activity, which indicates that mono-ADP-ribosylation is a dynamic PTM that directly influences the catalytic activity of its substrates in a reversible manner. The hydrolases identified here represent the missing link in the regulatory network formed by mono-ADP-ribosylation, which may prove highly important for diverse signaling networks as implied by the diversity of ARTD10 substrates identified[8].

In summary, the findings presented here define the macrodomain-containing proteins MacroD1, MacroD2 and C6orf130 as protein mono-ADP-ribosylhydrolases and thus establish mono-ADP-ribosylation of acidic residues by ARTD10 as a reversible PTM. The MacroD-like proteins unite specific ADP-ribose binding with ADP-ribose degradation and thereby define new players in ADP-ribose metabolism and function. MacroD-like hydrolases form the functional antagonists of intracellular mono-ADP-ribosyltransferases. Notably, substrates of the mono-ADP-ribosyltransferase ARTD10 include many kinases, which may thus be activated and inactivated by the opposite activities of MacroD2 and ARTD10.

METHODS

Methods and any associated references are available in the online version of the paper.

Note: Supplementary information is available in the online version of the paper.

ACKNOWLEDGMENTS

We are grateful to I. Ahel (Paterson Institute for Cancer Research, Manchester, UK) and M. Neuvonen (Institute of Biotechnology, University of Helsinki, Helsinki, Finland) for MacroD1 and MacroD2 constructs and J. Moss (National Institutes of Health, Bethesda, Maryland, USA) for the ARH1 construct. F. Althaus (University of Zurich, Zurich, Switzerland) and K. Aktories (University of Freiburg, Freiburg, Germany) are acknowledged for generously providing a baculovirus expressing PARG and the CDTa and TccC3 enzymes together with purified actin, respectively. F. Freimoser (University of Zurich, Zurich, Switzerland) provided editorial assistance and critical input during the writing and M. Fey technical assistance. This work was supported by the Deutsche Forschungsgemeinschaft DFG (LU 466/15-1) to B.L. and in part by the University of Zurich (Forschungskredit 54041205 to E.F.), the Swiss National Science Foundation (SNF-31003A_125190 (to P.O.H.) and 31-122421 (to M.O.H.)) and the Kanton of Zurich (to M.O.H.).

AUTHOR CONTRIBUTIONS

F.R. and P.O.H. performed experiments with MacroD1, MacroD2 and other macrodomains, and MS analysis was done together with D.F.; K.L.H.F. analyzed the influence of MacroD2 on GSK3β; E.F. performed the computer modeling; E.F. and A.C. analyzed the modeling and simulation results; M.B. identified MacroD2 as an ADP-ribosylhydrolase; A.H.F. cloned and purified mMacro1 and mMacro2; R.I. performed the HPLC analysis; H.C.W. compared the macro sequences; A.C., P.O.H., B.L. and M.O.H. supervised the work. B.L. and M.O.H. wrote the manuscript.

COMPETING FINANCIAL INTERESTS

The authors declare no competing financial interests.

1. Erener, S. *et al.* ARTD1 deletion causes increased hepatic lipid accumulation in mice fed a high-fat diet and impairs adipocyte function and differentiation. *FASEB J.* **26**, 2631–2638 (2012).
2. Altmeyer, M. & Hottiger, M.O. Poly(ADP-ribose) polymerase 1 at the crossroad of metabolic stress and inflammation in aging. *Aging* **1**, 458–469 (2009).
3. Hassa, P.O., Haenni, S., Elser, M. & Hottiger, M.O. Nuclear ADP-ribosylation reactions in mammalian cells: where are we today and where are we going? *Microbiol. Mol. Biol. Rev.* **70**, 789–829 (2006).
4. Telli, M.L. PARP inhibitors in cancer: moving beyond BRCA. *Lancet Oncol.* **12**, 827–828 (2011).
5. Curtin, N.J. PARP inhibitors for cancer therapy. *Expert Rev. Mol. Med.* **7**, 1–20 (2005).
6. Schreiber, V., Dantzer, F., Ame, J.-C. & De Murcia, G. Poly(ADP-ribose): novel functions for an old molecule. *Nat. Rev. Mol. Cell Biol.* **7**, 517–528 (2006).
7. Kleine, H. *et al.* Substrate-assisted catalysis by PARP10 limits its activity to mono-ADP-ribosylation. *Mol. Cell* **32**, 57–69 (2008).
8. Feijs, K.L.H. *et al.* ARTD10 substrate identification on protein microarrays: regulation of GSK3β by mono-ADP-ribosylation. *Cell Commun. Signal* published online, doi:10.1186/1478-811X-11-5 (19 January 2013).
9. Hottiger, M.O., Hassa, P.O., Lüscher, B., Schüler, H. & Koch-Nolte, F. Toward a unified nomenclature for mammalian ADP-ribosyltransferases. *Trends Biochem. Sci.* **35**, 208–219 (2010).
10. Hanai, S. *et al.* Loss of poly(ADP-ribose) glycohydrolase causes progressive neurodegeneration in *Drosophila melanogaster*. *Proc. Natl. Acad. Sci. USA* **101**, 82–86 (2004).
11. Koh, D.W. *et al.* Failure to degrade poly(ADP-ribose) causes increased sensitivity to cytotoxicity and early embryonic lethality. *Proc. Natl. Acad. Sci. USA* **101**, 17699–17704 (2004).
12. Williams, J.C., Chambers, J.P. & Liehr, J.G. Glutamyl ribose 5-phosphate storage disease. A hereditary defect in the degradation of poly(ADP-ribosylated) proteins. *J. Biol. Chem.* **259**, 1037–1042 (1984).
13. Slade, D. *et al.* The structure and catalytic mechanism of a poly(ADP-ribose) glycohydrolase. *Nature* **477**, 616–620 (2011).
14. Dunstan, M.S. *et al.* Structure and mechanism of a canonical poly(ADP-ribose) glycohydrolase. *Nat. Commun.* **3**, 878 (2012).
15. Han, W., Li, X. & Fu, X. The macro domain protein family: structure, functions, and their potential therapeutic implications. *Mutat. Res.* **727**, 86–103 (2011).
16. Kim, I.K. *et al.* Structure of mammalian poly(ADP-ribose) glycohydrolase reveals a flexible tyrosine clasp as a substrate-binding element. *Nat. Struct. Mol. Biol.* **19**, 653–656 (2012).
17. Karras, G.I. *et al.* The macro domain is an ADP-ribose binding module. *EMBO J.* **24**, 1911–1920 (2005).
18. Neuvonen, M. & Ahola, T. Differential activities of cellular and viral macro domain proteins in binding of ADP-ribose metabolites. *J. Mol. Biol.* **385**, 212–225 (2009).
19. Angelov, D. *et al.* The histone variant macroH2A interferes with transcription factor binding and SWI/SNF nucleosome remodeling. *Mol. Cell* **11**, 1033–1041 (2003).
20. Buschbeck, M. *et al.* The histone variant macroH2A is an epigenetic regulator of key developmental genes. *Nat. Struct. Mol. Biol.* **16**, 1074–1079 (2009).
21. Changolkar, L.N. *et al.* Developmental changes in histone macroH2A1-mediated gene regulation. *Mol. Cell Biol.* **27**, 2758–2764 (2007).
22. Goenka, S., Cho, S.H. & Boothby, M. Collaborator of Stat6 (CoaSt6)-associated poly(ADP-ribose) polymerase activity modulates Stat6-dependent gene transcription. *J. Biol. Chem.* **282**, 18732–18739 (2007).
23. Ahel, D. *et al.* Poly(ADP-ribose)-dependent regulation of DNA repair by the chromatin remodeling enzyme ALC1. *Science* **325**, 1240–1243 (2009).
24. Gottschalk, A.J. *et al.* Poly(ADP-ribosyl)ation directs recruitment and activation of an ATP-dependent chromatin remodeler. *Proc. Natl. Acad. Sci. USA* **106**, 13770–13774 (2009).
25. Aguiar, R.C., Takeyama, K., He, C., Kreinbrink, K. & Shipp, M.A. B-aggressive lymphoma family proteins have unique domains that modulate transcription and exhibit poly(ADP-ribose) polymerase activity. *J. Biol. Chem.* **280**, 33756–33765 (2005).
26. Aguiar, R.C. *et al.* BAL is a novel risk-related gene in diffuse large B-cell lymphomas that enhances cellular migration. *Blood* **96**, 4328–4334 (2000).
27. Cho, S.H. *et al.* Glycolytic rate and lymphomagenesis depend on PARP14, an ADP ribosyltransferase of the B aggressive lymphoma (BAL) family. *Proc. Natl. Acad. Sci. USA* **108**, 15972–15977 (2011).
28. Chen, D. *et al.* Identification of macrodomain proteins as novel O-acetyl-ADP-ribose deacetylases. *J. Biol. Chem.* **286**, 13261–13271 (2011).
29. Peterson, F.C. *et al.* Orphan macrodomain protein (human C6orf130) is an O-acyl-ADP-ribose deacylase: solution structure and catalytic properties. *J. Biol. Chem.* **286**, 35955–35965 (2011).
30. Hofmann, A. *et al.* Structure and mechanism of activity of the cyclic phosphodiesterase of Appr>p, a product of the tRNA splicing reaction. *EMBO J.* **19**, 6207–6217 (2000).
31. Sawaya, R., Schwer, B. & Shuman, S. Structure-function analysis of the yeast NAD+-dependent tRNA 2′-phosphotransferase Tpt1. *RNA* **11**, 107–113 (2005).
32. Stone, P.R. & Hilz, H. Quantitation of hydroxylamine sensitive mono(adenosine diphosphate ribose) residues in different hepatic tissues. *FEBS Lett.* **57**, 209–212 (1975).
33. Barth, H., Aktories, K., Popoff, M.R. & Stiles, B.G. Binary bacterial toxins: biochemistry, biology, and applications of common *Clostridium* and *Bacillus* proteins. *Microbiol. Mol. Biol. Rev.* **68**, 373–402 (2004).
34. Lang, A.E. *et al. Photorhabdus luminescens* toxins ADP-ribosylate actin and RhoA to force actin clustering. *Science* **327**, 1139–1142 (2010).
35. Timinszky, G. *et al.* A macrodomain-containing histone rearranges chromatin upon sensing PARP1 activation. *Nat. Struct. Mol. Biol.* **16**, 923–929 (2009).
36. Jope, R.S. & Johnson, G.V. The glamour and gloom of glycogen synthase kinase-3. *Trends Biochem. Sci.* **29**, 95–102 (2004).
37. Jackson, M.D. & Denu, J.M. Structural identification of 2′- and 3′-O-acetyl-ADP-ribose as novel metabolites derived from the Sir2 family of β-NAD+-dependent histone/protein deacetylases. *J. Biol. Chem.* **277**, 18535–18544 (2002).
38. Sauve, A.A. *et al.* Chemistry of gene silencing: the mechanism of NAD+-dependent deacetylation reactions. *Biochemistry* **40**, 15456–15463 (2001).
39. Jackson, M.D., Schmidt, M.T., Oppenheimer, N.J. & Denu, J.M. Mechanism of nicotinamide inhibition and transglycosidation by Sir2 histone/protein deacetylases. *J. Biol. Chem.* **278**, 50985–50998 (2003).
40. Kleine, H. *et al.* Dynamic subcellular localization of the mono-ADP-ribosyltransferase ARTD10 and interaction with the ubiquitin receptor p62. *Cell Commun. Signal.* **10**, 28 (2012).

ONLINE METHODS

Purification of recombinant proteins. Macrodomain cDNAs were amplified by PCR, cloned into a pET28-GST vector according to standard protocols, recombinantly expressed in *E. coli* BL21 and purified by using Ni Sepharose High Performance beads (Amersham Biosciences) according to the manufacturer's protocol. GSK3β was purified from SF9 cells[8]. Bound MacroD2 was cleaved from the beads with PreScission protease 3C (GE Healthcare) or eluted with 200 mM imidazole. Protein concentration was determined with a spectrophotometer ND-1000 (Nanodrop), and cleavage was verified by SDS-PAGE. ARTD10 was purified by using the TAP-tagging method as described before[7]. Cloning and purification of mMacro1 and mMacro2 of ARTD8 has been described[41].

De-ADP-ribosylation assay with recombinant proteins. Unless otherwise stated, 50 pmol recombinant purified GST-ARTD10 or His-ARTD1 were incubated with 100 nM [^{32}P]nicotinamide adenine dinucleotide ([^{32}P]NAD$^+$, PerkinElmer) for 15 min at 30 °C in reaction buffer (10 mM potassium phosphate, pH 7.2, 10 mM $MgCl_2$, 1.25 mM DTT, 1 μg/ml pepstatin, 1 μg/ml bestatin, 1 μg/ml leupeptin) and in the case of His-ARTD1 supplemented with 5 pmol annealed double-stranded oligomer (5′-GGAATTCC-3′). The reaction was stopped by filtration through a G50 column (GE Healthcare). De-ADP-ribosylation reactions were performed with 10 pmol MacroD2 protein at 30 °C for 15 min and stopped by the addition of SDS-PAGE loading buffer and boiling (5 min, 95 °C). De-ADP-ribosylation of automodified proteins was visualized by SDS-PAGE and autoradiography. Bands were quantified by using GelEval (http://www.frogdance.dundee.ac.uk).

ADP-ribosylation assays with immunoprecipitated proteins. ADP-ribosylation assays were carried out at 30 °C for 30 min. The reaction mixture (50 mM Tris-HCl, pH 8.0, 0.2 mM DTT, 5 mM $MgCl_2$ and 50 μM β-NAD$^+$ (Sigma) and 1 μCi [^{32}P]β-NAD$^+$ (Amersham Biosciences)) was added to IgG beads with immunoprecipitated HA-ARTD10 or HA-ARTD10-ΔK and optionally 0.5 μg substrate protein in a total reaction volume of 30 μl. Reactions were stopped by adding SDS sample buffer and were subsequently boiled and run on SDS-PAGE. Incorporated radioactivity was analyzed by autoradiography.

ADP-ribosylation of actin by bacterial toxins. *In vitro* ADP-ribosylation of actin was performed as reported[42]. Briefly, 2 μg β/γactin was incubated with either 100 ng recombinant TccC3hvr or 50 ng CDTa in the presence of 100 nM [^{32}P]NAD$^+$, 150 μM cold NAD$^+$ and reaction buffer (5 mM HEPES, pH 7.5, 0.1 mM CaCl2, 0.5 mM NaAc, 0.1 mM ATP). TccC3hvr and CDT1 reactions were incubated for 30 min at room temperature or 37 °C, respectively.

De-ADP-ribosylation assays with immunoprecipitated proteins. ADP-ribosylation assays were terminated by placing on ice and washing with high-salt buffer (50 mM Tris-HCl, pH 8.0, 0.2 mM DTT, 5 mM $MgCl_2$, 200 mM NaCl). MacroD2 (500 ng) was added to the beads in 30 μl high-salt buffer. After incubation (30 °C, 20 min), the reaction was stopped by addition of SDS sample buffer and boiling for analysis by SDS-PAGE and autoradiography. For subsequent kinase assays, beads with coupled GST-GSK3β were cooled and washed after incubation with MacroD2.

Chemical de-ADP-ribosylation. For chemical de-ADP-ribosylation with hydroxylamine, automodified ARTD10 was supplemented with 0.8 M hydroxylamine in a 1:1 ratio (v/v). The reactions were incubated at 37 °C for 1 h and subsequently stopped by the addition of SDS loading buffer.

GST-macro pulldown assays with ARTD10 proteins. GST- or His-tagged macrodomains were immobilized on glutathione or Ni Sepharose (Amersham Biosciences) at 4 °C (wild type and mutants) and incubated with automodified ARTD10 (full length; 100 ng) or GST-ARTD10 (818–1025; 50 ng) proteins for 2 h at 4 °C in 1,200 μl of binding buffer (100 mM Tris, pH 7.6, 250 mM NaCl, 125 mM KCl, 50 mM KAc, 1.5% NP-40 (high salt) or 75 mM NaCl, 25 mM KCl, 15 mM KAc, 1% NP-40 (low salt), 10% glycerol and protease inhibitors) and washed 5× with binding buffer (1,200 μl) for 25 min at 4 °C. Bound proteins were dissolved by boiling and were loaded on an SDS-PAGE gel for subsequent autoradiography.

Kinase assays. [γ^{32}P]ATP was diluted to 0.16 μCi/μl in 250 μM ATP in 3× kinase assay buffer (5 mM MOPS, pH 7.2, 2.5 mM β-glycerophosphate, 1 mM EGTA, 0.4 mM EDTA, 4 mM $MgCl_2$, 50 μM DTT and 40 ng/μl BSA). GST-GSK3β (25 ng) or precipitate was incubated in a reaction volume of 25 μl (5 μl 0.16 μCi/μl [^{32}P]ATP solution, 5 μg substrate peptide RRRPASVPPSPSLSRHS(pS)HQRR (Millipore)). After incubating (30 °C, 15 min), the reaction was stopped by placing on ice. Aliquots of 10 μl were spotted on P81 paper in duplicate, washed with 0.5% phosphoric acid and air dried before scintillation counting. Data are presented as mean ± s.d. of at least triplicate measurements from representative experiments. Statistical significance was determined by employing two-tailed Student's *t* test.

LC-MS and HPLC analysis of ADP-ribose. For HPLC analysis, released ADP-ribose or ADP-ribose standards were purified over Microcon Ultracel YM-3 columns and subjected to reversed-phase liquid chromatography on an Accucore C18 2.7 μm, 150 × 2.1 mm ID Column. A water-methanol gradient from 0% to 20% MeOH at a flow rate of 200 μl/min was applied. Free ADP-ribose was monitored by UV absorbance at 260 nm. For LC-MS analysis, 10 μM ADP-ribose standard and samples were analyzed by using hydrophilic interaction chromatography (HILIC) coupled to accurate MS. The chromatographic separation of ADP-ribose was performed on a 0.2 μm × 150 mm BEH amide column, using a linear gradient of acetonitrile to water, 0.5 mM ammonium acetate, pH 9. For MS, we used negative mode with a capillary voltage of 1.2 kV. Data were acquired in MS and MS-MS mode. Extracted ion chromatograms from the MS data were generated by using the monoisotopic mass of ADP-ribose adduct [M-H] 558.064 and a mass window of 10 mDa. For relative quantification of ADP-ribose, MS scans in the elution time range of ADP-ribose were combined, and the ion abundance of mass 558.064 was calculated.

Homology modeling of MacroD2. The MacroD2 homology model (obtained by Modeller[43–46]; **Supplementary Note**) with the lowest discrete optimized protein energy assessment score[47] was selected for minimization and molecular-dynamics refinement. Following 0.5 ns of NVT and subsequent 0.5 ns of NPT equilibration during which the protein heavy atoms and protein Cα atoms were, respectively, positionally restrained, two 100-ns trajectories were generated by using different random seeds (MD runs I and II). Trajectory analyses (**Supplementary Fig. 4a–c**) were performed with the MD-analysis tool WORDOM[48,49].

Docking and molecular-dynamics simulations of ADP-ribose in MacroD2. From the MD simulations of the apo-MacroD2 homology model, a trajectory frame was selected that maximized the solvent-accessible surface area of putative binding-site residues within the mixed α/β macrodomain fold[35], and which maintained similar Asp78 χ1 and χ2 angles relative to the corresponding residue of Af1521 (PDB 2BFQ).

Water molecules and ions were removed from this frame. AutoDock Vina[50] was employed to dock the ADP-ribose ligand to the mixed α/β fold. The 20 top-ranking poses were minimized with CHARMM by using the CHARMM27 force field for the protein atoms and the CHARMM general force field[51,52] for ADP-ribose. Upon structural superposition of MacroD2 and Af1521, the minimized pose of ADP-ribose having the lowest r.m.s. deviation value relative to the one in Af1521 (PDB 2BFQ) was immersed in a box of TIP3P water molecules and subjected to ten explicit water MD runs of 10 ns each at 300 K.

For each run, the distance between the center of mass of the putative binding site of MacroD2 and that of ADP-ribose was calculated by using WORDOM[48,49]. Residues forming the putative binding site were those having at least one atom within 5 Å of any ligand atom following equilibration.

A total of 65% of the obtained MD trajectory frames presented a binding-site ligand center-of-mass distance of <6 Å; above this distance, the distal ribose of the ligand rarely re-entered the binding site. Unbinding of ADP-ribose within 10 ns in almost half of the runs is consistent with its high μM inhibition of human MacroD1 activity[28].

Residues participating in hydrogen-bonding to ADP-ribose among trajectory frames in which the ligand remained bound were identified by using WORDOM with a distance cutoff of 4.0 Å between donor (D) and acceptor (A) atoms and a D-H··A angle larger than 130°. Predicted interactions of the distal ribose of ADP-ribose are predominantly with the carboxylate of Asp102 and with protein backbone atoms (**Supplementary Fig. 4d,e**).

MacroD2 residues forming stable hydrogen bonds to structural water molecules were identified by using the GROMACS g_hbond function. The most stable water molecules in the vicinity of the distal ribose are shown (**Supplementary Fig. 4f**) along with their interaction partners in MacroD2.

Figures were created with Pymol (http://pymol.sourceforge.net/).

41. Forst, A.H. *et al.* Recognition of mono-ADP-ribosylated ARTD10 substrates by ART8 macrodomains. *Structure* (in the press).
42. Gülke, I. *et al.* Characterization of the enzymatic component of the ADP-ribosyltransferase toxin CDTa from *Clostridium difficile*. *Infect. Immun.* **69**, 6004–6011 (2001).
43. Eswar, N. *et al.* Comparative protein structure modeling using Modeller. in *Curr. Protoc. Bioinformatics* **15**, 5.6 (2006).
44. Martí-Renom, M.A. *et al.* Comparative protein structure modeling of genes and genomes. *Annu. Rev. Biophys. Biomol. Struct.* **29**, 291–325 (2000).
45. Sali, A. & Blundell, T.L. Comparative protein modelling by satisfaction of spatial restraints. *J. Mol. Biol.* **234**, 779–815 (1993).
46. Fiser, A., Do, R.K. & Sali, A. Modeling of loops in protein structures. *Protein Sci.* **9**, 1753–1773 (2000).
47. Shen, M.Y. & Sali, A. Statistical potential for assessment and prediction of protein structures. *Protein Sci.* **15**, 2507–2524 (2006).
48. Seeber, M., Cecchini, M., Rao, F., Settanni, G. & Caflisch, A. Wordom: a program for efficient analysis of molecular dynamics simulations. *Bioinformatics* **23**, 2625–2627 (2007).
49. Seeber, M. *et al.* Wordom: a user-friendly program for the analysis of molecular structures, trajectories, and free energy surfaces. *J. Comput. Chem.* **32**, 1183–1194 (2011).
50. Trott, O. & Olson, A.J. AutoDock Vina: improving the speed and accuracy of docking with a new scoring function, efficient optimization, and multithreading. *J. Comput. Chem.* **31**, 455–461 (2010).
51. Vanommeslaeghe, K. *et al.* CHARMM general force field: A force field for drug-like molecules compatible with the CHARMM all-atom additive biological force fields. *J. Comput. Chem.* **31**, 671–690 (2010).
52. Brooks, B.R. *et al.* CHARMM: the biomolecular simulation program. *J. Comput. Chem.* **30**, 1545–1614 (2009).

Molecular Cell
Article

Inheritance of Silent rDNA Chromatin Is Mediated by PARP1 via Noncoding RNA

Claudio Guetg,[1,2] Fabian Scheifele,[1] Florian Rosenthal,[1,2] Michael O. Hottiger,[1] and Raffaella Santoro[1,*]
[1]Institute of Veterinary Biochemistry and Molecular Biology
[2]Molecular Life Science Program, Life Science Zurich Graduate School
University of Zurich, Winterthurerstrasse 190, 8057 Zurich, Switzerland
*Correspondence: raffaella.santoro@vetbio.uzh.ch
DOI 10.1016/j.molcel.2012.01.024

SUMMARY

Faithful propagation of specific chromatin states requires re-establishment of epigenetic marks after every cell division. How the original epigenetic signature is inherited after disruption during DNA replication is still poorly understood. Here, we show that the poly(ADP-ribose)-polymerase-1 (PARP1/ARTD1) is implicated in the maintenance of silent rDNA chromatin during cell division. We demonstrate that PARP1 associates with TIP5, a subunit of the NoRC complex, via the noncoding pRNA and binds to silent rRNA genes after their replication in mid-late S phase. PARP1 represses rRNA transcription and is implicated in the formation of silent rDNA chromatin. Silent rDNA chromatin is a specific substrate for ADP-ribosylation and the enzymatic activity of PARP1 is necessary to establish rDNA silencing. The data unravel a function of PARP1 and ADP-ribosylation that serves to allow for the inheritance of silent chromatin structures, shedding light on how epigenetic marks are transmitted during each cell cycle.

INTRODUCTION

Maintenance and transmission of proper chromatin organization is fundamental for genome stability and function in eukaryotes. During DNA replication, both heterochromatin and euchromatin are disrupted ahead of the replication fork and are then reassembled into their original epigenetic states behind the fork. How chromatin domains are restored on new DNA and transmitted through mitotic cell division remains a fundamental question in biology, with implications for development and complex diseases like cancer (Jasencakova and Groth, 2011). In higher eukaryotes, the repeated ribosomal RNA (rRNA) genes represent a striking example of how specific chromatin states are propagated during the cell cycle. In each cell, a fraction of rRNA genes is transcriptionally silent, replicates in late S phase, and is organized in heterochromatic structures by epigenetic mechanisms, including silent histone marks and CpG methylation (Li et al., 2005; Santoro, 2005, 2011; Santoro and Grummt, 2001; Santoro et al., 2002). By contrast, the "active" euchromatic rDNA fraction that replicates in early S phase represents rRNA genes competent for transcription whose activity is modulated according to the requirement of cell metabolism (Moss et al., 2007). Inheritance of silent rDNA chromatin is controlled by NoRC, the nucleolar remodeling complex comprising TIP5 and the ATPase SNF2h (Guetg et al., 2010; Santoro and Grummt, 2005; Santoro et al., 2002; Zhou et al., 2002). In mid-late S phase, TIP5 binds to silent rRNA genes after the passage of the replication fork and recruits DNA methyltransferases and histone modifier enzymes to re-establish silent rDNA chromatin (Li et al., 2005; Santoro et al., 2002; Zhou et al., 2002). Knockdown of TIP5 impairs rDNA silencing and induces genome instability at the rDNA locus and at the nearby centric and pericentric sequences (Guetg et al., 2010; Santoro et al., 2009). NoRC function requires the association of TIP5 with the noncoding RNA pRNA, a transcript originating from an RNA polymerase I (Pol I) promoter located 2 kb upstream of the pre-rRNA transcription start site (Mayer et al., 2006; Santoro et al., 2010). pRNA is synthesized by active rRNA genes during early S phase and then processed during mid S phase into a 250–300 nt fragment that matches the rDNA promoter sequences from −220 to +1 (Mayer et al., 2006; Santoro et al., 2010). Nucleolar retention of TIP5, rDNA methylation, and silent histone modifications at rDNA depend on pRNA (Mayer et al., 2006). Importantly, a TIP5 mutant with impaired RNA-binding activity (W531G,Y532A; $TIP5_{\Delta RNA}$) failed to establish rDNA heterochromatin (Mayer et al., 2006). pRNA sequences from nucleotides −127 to −49 in mouse forms a conserved hairpin structure that is specifically recognized by the TIP5-TAM domain. Upon pRNA binding, TIP5 undergoes a conformational change that was proposed to facilitate the interaction with other proteins required for rDNA silencing (Mayer et al., 2008). We have now examined the mechanism of NoRC-pRNA interaction that modulates recruitment of chromatin modifier enzymes to propagate rDNA heterochromatin during cell division.

RESULTS

PARP1 Associates with TIP5 and Binds to Silent rRNA Genes

To dissect the mechanisms of NoRC function in rDNA heterochromatin formation, we identified TIP5 interaction partners in HEK293T cells expressing HA-FLAG-TIP5 in association with proteomics and immunoblot analyses. As shown in Figure 1A, we identified the poly(ADP-ribose)-polymerase-1 (PARP1, also known as ARTD1) (Hottiger et al., 2010) as a TIP5-interacting protein. PARP1 is an enzyme possessing NAD^+-dependent

Kassner et al. Epigenetics & Chromatin 2013, 6:1
http://www.epigeneticsandchromatin.com/content/6/1/1

Epigenetics & Chromatin

RESEARCH Open Access

Crosstalk between SET7/9-dependent methylation and ARTD1-mediated ADP-ribosylation of histone H1.4

Ingrid Kassner[1,2], Marc Barandun[1], Monika Fey[1], Florian Rosenthal[1,2] and Michael O Hottiger[1*]

Abstract

Background: Different histone post-translational modifications (PTMs) fine-tune and integrate different cellular signaling pathways at the chromatin level. ADP-ribose modification of histones by cellular ADP-ribosyltransferases such as ARTD1 (PARP1) is one of the many elements of the histone code. All 5 histone proteins were described to be ADP-ribosylated *in vitro* and *in vivo*. However, the crosstalk between ADP-ribosylation and other modifications is little understood.

Results: In experiments with isolated histones, it was found that ADP-ribosylation of H3 by ARTD1 prevents H3 methylation by SET7/9. However, poly(ADP-ribosyl)ation (PARylation) of histone H3 surprisingly allowed subsequent methylation of H1 by SET7/9. Histone H1 was thus identified as a new target for SET7/9. The SET7/9 methylation sites in H1.4 were pinpointed to the last lysine residues of the six KAK motifs in the C-terminal domain (K121, K129, K159, K171,
K177 and K192). Interestingly, H1 and the known SET7/9 target protein H3 competed with each other for SET7/9-dependent methylation.

Conclusions: The results presented here identify H1.4 as a novel SET7/9 target protein, and document an intricate crosstalk between H3 and H1 methylation and PARylation, thus implying substrate competition as a regulatory mechanism. Thereby, these results underline the role of ADP-ribosylation as an element of the histone code.

Keywords: PARP-1, SET7/9, Lysine methylation, Poly-ADP-ribosylation, Post-translational modification

Background

Histones are nuclear proteins that package and order the DNA into nucleosomes [1]. Five major families of histones exist: H1 (H5), H2A, H2B, H3, and H4. Two copies of the core histones H2A, H2B, H3 and H4 form the octameric nucleosome core particles [2]. Unlike the other histones, only one copy of the linker histone H1 is present and stabilizes the DNA, which is wrapped around the core nucleosome [3]. Linker histones bind to both the nucleosome and the linker DNA region (approximately 20 to 80 nucleotides in length) between nucleosomes. The interaction of H1 with the nucleosome and additional DNA stretches at the entry/exit of the nucleosome forms the chromatosome and leads to higher order chromatin structure [4]. Many experiments addressing H1 function have been performed with purified, processed chromatin under low-salt conditions, but the *in vivo* role of H1 is less clear. Cellular studies have shown that overexpression of H1 can cause aberrant nuclear morphology and chromatin structure and, depending on the gene, H1 can serve as either a positive or a negative regulator of transcription [5]. Similar to the core histones, H1 is composed of three domains [6]. The N-terminus is a short, flexible segment rich in basic amino acids, the central domain exhibits a globular structure composed of a winged helix motif [6] and the C-terminus is predominantly composed of lysine, alanine and proline residues and is the main determinant for H1 binding to chromatin [7]. Among the five histone families of the chromatosome, the linker histone H1 is the least conserved. In the human genome, 11 genes encoding H1 variants have been identified and

* Correspondence: hottiger@vetbio.uzh.ch
[1]Institute of Veterinary Biochemistry and Molecular Biology, University of Zurich, Winterthurerstrasse 190, Zurich 8057, Switzerland
Full list of author information is available at the end of the article

Identification of ADP-ribosylation sites in cell extracts by higher energy collisional dissociation (HCD)-based mass spectrometry

Florian Rosenthal[1,2,4], Paolo Nanni[3,4], Simon Barkow-Oesterreicher[3] and Michael O. Hottiger[1*]

[1]Institute of Veterinary Biochemistry and Molecular Biology, University of Zurich, Zurich, Switzerland.

[2]Life Science Zurich Graduate School, University of Zurich, Zurich, Switzerland.

[3]Functional Genomics Center Zurich, University of Zurich, Zurich, Switzerland.

[4]These authors contributed equally to this work.

* Correspondence should be addressed to M.O.H. (hottiger@vetbio.uzh.ch).

RUNNING TITLE:

Identification of ADP-ribosylation sites by HCD-based MS

Abbreviations

Accumulation gain control (AGC)

Adenosine di-phosphate (ADP)

Adenosine mono-phosphate (AMP)

ADP-ribosyl transferase (ART)

ART cholera toxin like (ARTC)

ART diphtheria toxin like (ARTD)

Bestatin (B)

Electron capture dissociation (ECD)

Electron transfer dissociation (ETD)

Higher energy collisional dissociation (HCD)

Ioadoacetamide (IAM)

Ion trap (IT)

Leupeptin (L)

NCE (normalized collision energy)

Neutral loss (NL)

Nicotinamide adenine dinucleotide (NAD^+)

Orbitrap (FT)

Pepstatin (P)

Phosphorus-32 (^{32}P)

Poly-ADP-ribosyl glycohydrolase PARG

Post-translational modification (PTM)

Product dependent (PD)

Trichloroacetic acid (TCA)

Wildtype (WT)

Summary

ADP-ribosylation is an important post-translational modification, which is catalyzed by the family of ADP-ribosyl transferases (ARTs) and can occur as mono- and poly-ADP-ribosylation. Due to the limited availability of antibodies and mass spectrometry (MS) tools for the study of ADP-ribosylation, our knowledge of its acceptor amino acids and the function of ADP-ribosylation is very limited. Here, we describe a new higher energy collisional dissociation (HCD)-based liquid chromatography mass spectrometry (LC-MS/MS) approach for the detection of ADP-ribosylated peptides and the identification of ADP-ribose acceptor sites. The presence of diagnostic ions of ADP-ribose in the HCD spectra allowed us to detect putative ADP-ribosylated peptides to target in a second LC-MS/MS analysis. The combination with electron transfer dissociation (ETD) fragmentation did only slightly improve the results obtained with HCD alone. However, a two-stage HCD-ETD approach proofed most robust for the analysis of a variety of samples.

The herein described new approach led to the identification of ADP-ribosylated peptides and their specific modification sites in *in vitro* modified samples as well as in complex cell extracts. With these methods it was possible to identify for the first time several ADP-ribose acceptor sites (glutamates, lysines and arginies) on different proteins in cell extracts without prior enrichment of ADP-ribosylated proteins or peptides. Histones were identified as the most prominent ADP-ribosylated proteins in the nucleus and glutamates as well as lysines were discovered as the main ADP-ribose acceptor sites. Interestingly, several ADP-ribosylation sites correspond to residues that are also subject to acetylation or methylation and therefore suggest lively crosstalk between these different PTMs. This protocol can thus be applied to various

proteins of interest and opens the possibility to identify ADP-ribose acceptor sites in cellular extracts and eventually even tissue samples.

Introduction

ADP-ribosylation is a post-translational protein modification (PTM) that is synthesized by ADP-ribosyltransferases (ARTs) (1). Based on sequence similarity to bacterial diphtheria toxin or cholera C2 and C3 toxin, respectively, the ARTD and ARTC subfamilies are distinguished (2). The proteins of the ARTD subfamily comprise the main intracellular ADP-ribosyltransferases that are implicated in many regulatory processes and linked to various diseases and pathological conditions (3-5). These enzymes use nicotinamide adenine dinucleotide (NAD^+) as a substrate to transfer the ADP-ribose moiety onto specific acceptor sites of target proteins or existing ADP-ribose units, thereby synthesizing mono- or poly-ADP-ribosylated proteins (1). In cells, the ADP-ribose modification is short-lived because of the hydrolytic action of poly-ADP-ribose glycohydrolase (PARG) which degrades polymers of ADP-ribose as well as macrodomain proteins that remove mono-ADP-ribose from certain proteins (6).

ADP-ribosylation is an important protein modification, which is considered an element of the histone code and which co-regulates gene transcription, protein function, differentiation processes, stress responses, as well as the onset and progression of diseases (6-10). Although research on ADP-ribosylation has a long history, many inherent and technological difficulties are the reason for large gaps in the understanding of the cellular and molecular functions of this PTM. For example, ADP-ribose modifications can be synthesized during the sample preparation, because ARTD1 (PARP1) is activated by fragmented DNA. On the other hand, the modification is also easily lost during extraction or sample preparation. The variable length of the poly-ADP-ribose chain is a further complication due to its high charge and the unpredictable mass shift of an undefined and potentially branched polymer. This problem can be addressed by enzymatically degrading all ADP-ribose modifications post sample preparation to the mono-ADP-ribose form

with PARG (6). One of the most limiting factors for the functional analysis of ADP-ribosylation is the lack of suitable methods to identify and quantify specific ADP-ribosylation sites and their modification status. Without such tools it is impossible to link physiological and cellular readouts to the activity of a particular ARTD or the modification status of a specific amino acid.

Until now, only few acceptor sites for ADP-ribosyltransferases of the ARTD family have been identified. The acceptor sites for mono-ADP-ribose are side chains of specific amino acid residues and so far the following acceptor amino acids in eukaryotic cells were reported to covalently bind ADP-ribose: lysine, arginine, glutamate, aspartate, cysteine, diphthamide, phospho-serine and asparagine residues (2). Early work predicted ADP-ribosylated glutamic acid residues for ARTD1 (11). More recently, Tao et al. described weak mono-ADP-ribosylation activity of the E988Q ARTD1 mutant enzyme and identified modified aspartic and glutamic acid residues by liquid chromatography mass spectrometry (LC-MS) with collision induced dissociation (CID) fragmentation (12). This is in contrast to site directed mutagenesis studies that identified lysines to be modified on ARTD1 (13). A recent analysis of wildtype (WT) ARTD1 pretreated with phosphodiesterase and subsequent CID MS/MS analysis identified glutamic acid and lysine residues as acceptor sites (14). Finally, LC-MS/MS with electron transfer dissociation (ETD) analysis of histone tails, modified by WT ARTD1 *in vitro*, predominantly identified lysines as acceptor sites (13, 15).

LC-MS/MS strategies are frequently used to identify specific PTMs and the most commonly employed fragmentation method is CID. However, labile PTMs such as ADP-ribosylation are instable during CID fragmentation. Indeed, a typical CID MS/MS spectrum of an ADP-ribosylated peptide is dominated by fragment ions originating from the ADP-ribose backbone, but lacks sufficient peptide backbone fragment ions to identify the amino acid sequence (16, 17).

In particular, fragment ions corresponding to adenine, adenosine and water, adenosine mono-phosphate (AMP), adenosine di-phosphate (ADP) and ADP-ribose are commonly observed.

In contrast to CID, during ETD or electron capture dissociation (ECD) the ADP-ribose modification is maintained on the peptide, allowing the identification of the peptide sequence and the localization of the modification site. For this reason, these fragmentation techniques are so far considered the best choices for the identification of ADP-ribosylation sites (16, 18). Recently, a marker ion approach was proposed that circumvents the difficulties in peptide identification and takes advantage of the altered fragmentation pattern of ADP-ribosylated peptides (18). In a first LC-MS/MS run, putative ADP-ribosylated peptides are detected (based on the presence of marker ions in the CID spectra), which are then targeted for ETD fragmentation and subsequent peptide identification in a second LC-MS/MS analysis (16, 18). Although this strategy requires twice as much sample and instrument time and could be affected by the loss of low mass ions during ion trap CID fragmentation (with consequent loss of marker ion information), it can lead to the characterization of ADP-ribosylated peptides.

Interestingly, the use of higher energy collision dissociation (HCD) has never been tested with ADP-ribosylated proteins up to now, even though the results are expected to be similar to QTOF-like CID (with detection of low mass ions). Here, we describe for the first time the analysis of ADP-ribosylated peptides using HCD fragmentation, which provides a new and powerful method for the identification of modified peptides and their ADP-ribose modification site. The benefits of HCD as an alternative to or in combination with ETD fragmentation of standard peptides, enzymatically modified histones and nuclear extracts are discussed. Together, HCD-based approaches identified novel ADP-ribose acceptor sites from *in vitro* and *in vivo* ADP-ribosylated proteins.

Experimental Procedures

In vitro modification of standard peptide and histone mix

The peptide Biotin-KAARKSAPATGGVKKPHRYR (H3) or histones were modified as described earlier (6). Briefly, 1 µg of peptide or 3 µg of histone mix were incubated with 10 pmol GST-ARTD10 (818-1025) or HIS-ARTD1 for 15 min at 30°C in reaction buffer (50 mM Tris-HCL pH 8.0, 4 mM $MgCl_2$, 250 µM DTT) in the presence of 160 µM NAD^+. Reactions with HIS-ARTD1 were supplemented with 5 pmol annealed double-stranded oligomer (5`-GGAATTCC-3`). The reactions were stopped by the addition of PJ34 (ARTD inhibitor) and further processed or frozen until desalting.

PARG treatment

To shorten ADP-ribose polymers, the buffer conditions of *in vitro* modified HIS-ARTD1 were adjusted to 50 mM Tris-HCL pH 8.0, 10 mM $MgCl_2$, 50 mM NaCl, 250 µM DTT. Subsequently, 5 pmol HIS-PARG were added and the reactions were incubated at 30°C for 1h. The reactions were frozen until ZipTip C18 (Millipore, Billerica (MA), USA) desalting according to the suppliers guidelines.

Extraction of nuclear / chromatin fraction

To obtain ADP-ribosylated proteins, HEK293T cells were treated with 10 mM H_2O_2 in PBS with 1 mM $MgCl_2$ for 10 min at 37°C. Nuclear and chromatin fractions were extracted as described earlier (19). Briefly, cells were resuspended in hypotonic lysis buffer (supplemented with Roche inhibitor cocktail (Roche, Mannheim, Germany), 10 µM Pj34 (Enzo, Lausen, Switzerland) and 0.5 µM ADP-HPD (Santa Cruz, Santa Cruz (CA), USA)), incubated at 4°C for 30 min, and

centrifuged at 10000 g for 10 min. The pelleted nuclei were lysed in high salt buffer (supplemented with Roche inhibitor cocktail, 10 μM Pj34 and 0.5 μM ADP-HPD), sonicated 3 times for 10 sec, and incubated on a roller shaker for 2 h at 4°C. Separation of the nucleoplasm and chromatin fraction was achieved by centrifugation at 4000 rpm for 20 min.

Protein denaturation and Trypsin digestion

Proteins were precipitated using trichloroacetic acid (TCA) and resuspended in 50 mM Tris-HCl, 1 mM $CaCl_2$ (pH 7.6). Nucleoplasm and chromatin fractions were pooled. Disulfide bridges were reduced by the addition of 10 mM DTT (in 50 mM Tris-HCl) at 50°C for 45 min. Cysteins were alkylated with 50 mM ioadoacetamide (IAM, in 50 mM Tris-HCl) for 1 h at RT in the dark, the reactions were blocked by the addition of Dithiothreitol (DTT) to a final concentration of 50 mM and an incubation for 10 min at RT. Sequencing grade modified trypsin (Promega, Madison (WI), USA) was added in a 1:100 w/w ratio and the reactions were incubated at 37°C over night.

High-pH reversed-phase HPLC pre-fractionation

Tryptic peptides were fractionated on a YMC-Triart reverse phase C18 column (150-4,8 mm i.d., S-5 μm, 12 nm, YMC Europe) using an Agilent 1100 series HPLC (Agilent, Waldbronn, Germany) at a flow rate of 850 nl/min. The buffer composition at the two channels was 5% acetonitrile, 25 mM K_2HPO_4 pH11 (buffer A) and 95% acetonitrile, 25 mM K_2HPO_4 pH 11 (buffer B). Peptides were diluted with buffer A and adjusted to pH 11. Peptides were eluted with a linear gradient from 5 to 48% Acetonitrile over 70 min. Fractions were collected in 2 min intervals and dried to near completion in a SpeedVac.

Nano-Liquid Chromatography-Tandem Mass spectrometry

Mass spectrometry analysis was performed on a LTQ-Orbitrap Velos ETD mass spectrometer (Thermo Fisher Scientific, Bremen, Germany) coupled to an Eksigent-Nano-HPLC system (Eksigent Technologies, Dublin (CA), USA). Solvent composition at the two channels was 0.1% formic acid for channel A and 0.1% formic acid, 99.9% acetonitrile for channel B. Peptides were loaded on a self-made tip column (75 μm × 80 mm) packed with reverse phase C18 material (AQ, 3 μm 200 Å, Bischoff GmbH, Leonberg, Germany) and eluted with a flow rate of 250 nl per min by a gradient from 2 to 35% of B in 30 minutes (for standard peptides) or 60 minutes (for complex histone samples).

Full-scan MS spectra (300–1700 *m/z*) were acquired at a resolution of 30 000 at 400 *m/z*, an accumulation gain control (AGC) of $1x10^6$ and a maximum injection time of 250 ms. The AGC values for MS/MS analysis were set to $1x10^4$ for ETD experiments with ion trap detection (IT, 100 ms injection time) and to $1x10^5$ for HCD and ETD experiments with detection in the Orbitrap (FT, 200 ms injection time) respectively. The HCD normalized collision energy was set to 40%, enabling the stepped collision energy (width 15%, 3 steps), and detecting the ions at a resolution of 7500 at 400 m/z. In all the experiments only 1 microscan was used for detection. The isolation width was set to 2 amu and 4 amu for HCD and ETD experiments, respectively. Full scans and Orbitrap MS/MS scans were acquired in profile mode, whereas ion trap mass spectra were acquired in centroid mode

All the experiments were recorded in data dependent manner from signals above a threshold of 2000.

Charge state screening was enabled and singly charge states were rejected. For ETD experiments, the ETD anion target value was set to 1e5 and the activation time to 100 ms. Charge-state dependent ETD reaction times were enabled, setting a reference value of 100 ms for doubly charged peptides. A supplemental activation with 25% normalized collision energy was always enabled.

For the analysis of standard peptides, precursor masses already selected three times for MS/MS were excluded for further selection for 45s. For the analysis of complex histone samples, the dynamic exclusion was set to 1. The exclusion window was set to 10 ppm and the exclusion size was limited to a maximum of 500 entries.

The following LC-MS/MS acquisition methods were performed: *(a)* Orbitrap full MS scan followed by top 10 data-dependent Orbitrap HCD MS/MS; (*b*) Orbitrap full MS scan followed by top 10 data-dependent ion trap ETD MS/MS, or (*c*) top 8 data-dependent Orbitrap ETD MS/MS; (*d*) Orbitrap full MS scan followed by top 10 double-play data-dependent HCD MS/MS and ion trap ETD MS/MS (or, (*e*), Orbitrap ETD MS/MS); (*f*) Orbitrap full MS scan followed by top 10 data-dependent HCD and an additional ETD ion trap event when a peak at 136.0623 (ADP-ribose fragment ion) was observed among the top 10 most abundant peaks of the HCD scan (HCD-PD1-ETD); (*g*) Orbitrap full MS scan followed by top 10 data-dependent HCD and an additional ETD ion trap event when the peaks at 136.0623, 250.0940 and 348.0709 (were observed among the top 10 most abundant peaks of the HCD scan (HCD-PD3-ETD); (*h*) Two-steps, consisting of HCD and an additional ETD ion trap MS/MS acquisition on the top 10 precursors where the marker ions 136.0623, 250.0940 and 348.07091 were observed in a previous HCD run. A complete description of all tandem MS experiments employed in this study can be found in Table 1.

Database analysis and configuration of Mascot modifications

MS and MS/MS spectra were converted into Mascot generic format (mgf) using Proteowizard (version 3 (20)). When both HCD and ETD scans were presents in the same raw files, separate mgfs for the two fragmentation techniques were created. All high-resolution HCD and ETD MS/MS spectra were deconvoluted using the H-score algorithm (21). The mgfs were searched against the UniProtKB human database (taxonomy 9606, version 20120914), including 35787 Swiss-Prot, 37802 TrEMBL entries, 73589 decoy hits, and 260 common contaminants. In order to speed up the searches relative to the standard peptide, the peptide sequence KAARKSAPATGGVKKPHRYR was added to the database as the separate entry "ZZ_FGCZCont0260". Mascot 2.4.1 (Matrix Science) was used for the identification with the following search settings: the combined HCD and Orbitrap ETD mgfs were searched with a peptide tolerance of 10 ppm and MS/MS tolerance of 0.05 Da, while the MS/MS tolerance for the ion trap ETD spectra was set to 0.6 Da. For the HCD runs, singly charged *b* and *y* ion series, immonium ions, water and ammonia loss ion series were searched. For ETD, multiply charged *c*, *y*, *z*, *z+1*, *z+2* series were considered. In the case of histone samples, enzyme specificity was set to trypsin, allowing up to 3 missed cleavages. For the standard peptide, a 'non cutting' enzyme named NoCleave was defined and N-Term biotin was set as fixed modification. Decoy hits were used to control the false discovery rate on peptide and protein level.

The ADP-ribose variable modification was set up differently for the searches of HCD or ETD spectra. For HCD mgfs the following modification settings were tested: (*i*) ADP-rib, corresponding to a mass shift of 541.0611; (*ii*) ADP-rib-HCDm, that additionally ignores for scoring the marker ions at m/z 428.0372, 348.0709, 250.0940, 136.0623; (*iii*) ADP-rib-HCDm-

NL541/347, equal to ADP-rib-HCDm with additional scoring of the neutral losses (NL) equal to 541.0611 and 347.0631 (coming from b and y series); (*iv*) ADP-rib-HCDm-NL347/249, with scoring of the neutral losses equal to 347.0631 and 249.0862; (*v*) ADP-rib-HCDm-NL347, with scoring of a single neutral losses equal to 347.063. Unfortunately, Mascot allowed only the screening for neutral losses and not for losses carrying different number of charges.

For the identification of ADP-ribosylation from ETD spectra, only the mass shift of 541.0611 was used (setting *i*, ADP-rib). A detailed description of the Mascot modification settings can be found in figure 2 and in the supplementary figure S1.

An ADP-ribosylated peptide was considered as correctly identified when a Mascot score higher than 20 and an expectation value lower than 0.05 was obtained. To assess the location of the ADP-ribosylation sites, we used the site localization analysis provided by Mascot, which is based on the work by Savitski et al. (22) and was developed especially for phosphorylations. This method is not optimized for ADP-ribosyl modification, due to the lack of standard peptides having known modification sites. For this reason, even if Mascot states a correctness of 95% for the site localization, this value is arbitrary and cannot be experimentally validated. Due to the lack of a better estimate, in the following we define correctness as having a confidence of at least 95% in the Mascot site localization analysis.

PTM MarkerFinder

For LC-MS/MS experiments where HCD fragmentation has been used, the Mascot output *.dat* files have been further analyzed using PTM MarkerFinder (23). Briefly, PTM MarkerFinder screens the Mascot outputs for HCD spectra containing the ADP-ribose marker ions at m/z 136.0623, 250.0940, 348.0709 and 428.0372. The spectra containing at least two marker ions

and where the sum of the marker ion intensities covers at least 5 % of the total ion intensities are considered as spectra from putative ADP-ribosylated peptides. Finally, PTM MarkerFinder summarizes information about the presence and the intensity of marker ions and annotates the spectra with the corresponding peptide sequence.

Results and Discussion

Preparation of ADP-ribosylated peptides for the subsequent identification of the modification site(s)

The currently available MS/MS protocols for ADP-ribosylated peptides do not allow the accurate and reliable detection of ADP-ribosylated peptides in a complex sample. To develop a novel MS-based approach, three samples with different complexities were prepared. The sample with the lowest complexity was a biotinylated peptide with the sequence KAARKSAPATGGVKKPHRYR, representing a part of the N-terminal histone H3 tail, which was previously described to be ADP-ribosylated by ARTD1 (15). The second sample was a mixture containing the ADP-ribosylated four core histones as well as the H1 linker histone as full-length proteins. The most complex sample was a nuclear extract of H_2O_2 treated HEK 293T cells. The H3 standard peptide and the histone mix were modified *in* either by recombinant ARTD1 stimulated with a 8mer double stranded DNA oligo or by the recombinant GST-tagged catalytic domain (amino acids 818-1025) of ARTD10. The modification by ARTD1 resulted in poly-ADP-ribosylation of the peptide or proteins, whereas ARTD10 (818-1025) catalyzed mono-ADP-ribosylation (data now shown). Poly-ADP-ribosylated samples modified by ARTD1 were optionally treated with PARG to reduce the resulting ADP-ribose polymers to a single moiety (see below).

Optimal HCD fragmentation of the ADP-ribosylated standard peptide using ramped CE

In order to evaluate the behavior of ADP-ribosylated peptides during HCD fragmentation and to detect the diagnostic ions characteristic for ADP-ribose modification, the standard peptide was

fragmented using HCD with NCE (normalized collision energy) values ranging from 23% to 60% (Fig. 1a,b and as described by (16)). The analysis revealed that the standard peptides either modified by ARTD1 or ARTD10 (poly- or mono-ADP-ribosylated), showed high intensity signals for the expected ADP-ribose marker ions, but low intensity signals for the peptide fragment at higher NCE values (Fig. S2). A good balance between the intensity of ADP-ribose marker ions and peptide backbone fragments was achieved by using ramped NCE (width 15%, 3 steps centered around 40%). The HCD spectra acquired with such parameters were dominated by the marker ions originating from the internal fragmentation of ADP-ribose (with the ion at 136 being the most abundant one), as well as by additional fragments corresponding to the peptide plus a residual mass from ADP-ribose fragmentation (Fig. 1c). These ADP-ribose fragments are often not caused by neutral losses and may thus exhibit charge states different from the one of the precursor. Based on these results, ramped NCE was defined as the optimal setting and used for all following analyses.

Implementing ADP-ribose neutral losses improves identification of ADP-ribose acceptor sites by Mascot

Considering the simple attachment of ADP-ribose as a variable modification for the Mascot analyses resulted in poor identification of modified peptides. In order to optimize the computational analysis of the generated mass spectrometry data with the modified standard peptide, different settings were tested. In particular, different ADP-ribose modification settings (described in the Experimental Procedures and as summarized in Fig. 2a) were generated to take advantage of the ADP-ribose marker ions and neutral losses for the Mascot searches. The criteria

used for the evaluation of the different settings included the overall number of identifications (considering a peptide identified when the Mascot score is higher than 20 and the expectation value lower than 0.05) and the percentage of assigned spectra for each peptide species. The search for ADP-ribose modifications (Fig. 2a, setting *i*) based on mass shift allowed the identification of only 20 to 40% of the spectra corresponding to the ADP-ribosylated standard peptide. To improve the identification, we first tested whether ignoring the ADP-ribose marker ions for scoring purposes increases the number of identifications or the percentage of assigned spectra (setting *ii*, ADP-rib-HCDm). As no improvement was observed (Fig. 2b), the main neutral losses (NL) of ADP-ribose (249, 347 and 541) were included into the search settings *iii* - *v*. Including the two NL 541 and 347 (setting *iii*) doubled the number of identified ADP-ribosylated peptides and allowed the assignment of up to 91% of the spectra. In contrast, searching for the NL 347 and 249 (setting *iv*) or only 347 (setting *v*) resulted in fewer assigned spectra, indicating that the side NL reaction due to the loss of 249 does not provide any benefit for the scoring. Although the search for NL 541 and 347 lead to the reliable identification of modified peptides, it did not allow the exact localization of the modification (Fig. S3). We therefore selected the setting *iv* (ADP-rib-HCDm-NL347/249) as variable modification in Mascot for the rest of the study because it represents the best compromise between the rates of modified peptide identification and site-localization.

These optimization steps led to the identification of different acceptor sites in the standard peptide modified by ARTD1 or ARTD10 (Fig. 2b). Predominantly arginine 20 and lysine 14 of the peptide were modified by both ARTDs, but arginine 20 most probably represents an in vitro artifact because it is the terminal amino acid (data not shown). The modification catalyzed by ARTD1 mainly resulted in the detection of mono-, di- and tri-ADP-ribosylations, which are

either derived from ADP-ribose polymers or different modified sites on the same peptide. The ARTD10 modified peptide on the other hand revealed mainly mono-ADP-ribose as well as a few di-modifications (approximately 10%). The latter can be either due to oligo-ADP-ribose synthesized by ARTD10 or can be caused by the modification of different sites on the same peptide. As the peptide contained multiple modification sites in close proximity, it was not possible to distinguish between these two possibilities. In general, the peptides were more efficiently modified by ARTD10 than by ARTD1, due to the higher efficiency and lower specificity of the catalytic ARTD10 domain *in vitro* (data not shown).

The combination of HCD and ETD approaches increases the identifications of ADP-ribosylation sites

ETD fragmentation is considered the method of choice for ADP-ribosylated peptides and was therefore compared to HCD fragmentation (Table 1 / Fig. 3). In a first step, the mono- and poly-ADP-ribosylated peptides were analyzed by HCD (as described above) or by ETD fragmentation acquired in the ion trap (IT) or Orbitrap (FT). Since the average charge state of the identified modified peptides was relatively high (more than 4, Fig. S4a), the *c* and *z* fragmentation series often consisted of multiple charged ions. Consequently, even if the acquisition of the spectra in the IT allowed a higher throughput compared to the FT detection (due to the shorter length of the scan cycles), the identification of the correct charge states of the fragment ions could only be achieved by acquiring the MS/MS spectra in the FT. More spectra were acquired via ETD (IT) analysis, but the number of identifications was similar for ETD (IT) and ETD (FT) (Fig. 4). Interestingly, these results were similar to those obtained with HCD alone, strongly suggesting

that the HCD fragmentation alone provides enough information for the identification of ADP-ribosylated peptides.

However, combination of ETD and HCD may improve the identification of ADP-ribosylated peptides and modification sites, as it takes advantage of the information generated by both approaches. Subjecting the entire sample to both, HCD-ETD (IT) and HCD-ETD (FT), resulted in increased cycle times, but did not significantly influence the number of identifications or assigned spectra (Fig. 4). This strategy is particularly inefficient for complex samples, because all peptides, also those that are not modified, are fragmented and analyzed twice. An alternative method is a previously suggested two-stage ("marker ion") approach (16), which has not yet been considered and tested with HCD and ETD. To evaluate this method, samples were first analyzed using HCD fragmentation as described above. Subsequently, the Mascot output was screened for spectra containing ADP-ribose marker ions using PTM MarkerFinder (23), to obtain a list of precursor ions corresponding to putative ADP-ribosylated peptides. Only these precursor ions were targeted for HCD and ETD (IT) fragmentation in a second LC-MS/MS experiment. Although this method resulted in a higher number of ADP-ribosylated peptide identifications (Fig 4a) compared to single HCD runs, the throughput of the process was substantially reduced, because it required twice as much LC-MS analysis time and more computational steps.

In order to overcome the shortcomings of these combinations, HCD was followed by ETD on the same precursors only when one or more marker ions were present in the HCD spectra (product dependent approach, HCD-PD-ETD) (16). To our knowledge, this method was never applied to ADP-ribosylated peptides, while it was already successfully used for glycopeptide studies (24-26). The ETD (IT) was either triggered upon the detection of only one marker ion: 136.0623 (HCD-PD1-ETD (IT)) or the detection of three marker ions 136.0623, 250.0940, 348.0709

(HCD-PD3-ETD (IT)). In general, the marker ion 136.0623 proved specific enough for the triggering of ETD fragmentation, while the inclusion of 3 marker ions increased the number of missed PD-ETD activations. Moreover, one single marker ion triggered more ETD events when the standard peptide was poly-ADP-ribosylated (i.e., ARTD1-modified sample, Fig 4a). For this ARTD1 modified peptide the HCD-PD1-ETD (IT) method proved less efficient than the two-stage HCD-ETD (IT) combination in identifying spectra from the ADP-ribosylated peptide, but allowed a much higher throughput. In all samples the localization of the ADP-ribosylation site could be achieved only for few peptides, with the best results obtained for HCD and ETD (FT) spectra (supplementary Fig. S5). Due to the characteristics of the sample analyzed (one single highly charged peptide; Fig. S4a) and the different results from ARTD1 or ARTD10, a final conclusion could not be achieved after this series of analysis. HCD-PD1-ETD (IT) or two-stage HCD-ETD (IT) performed in general better than the other tested combination

An HCD-ETD approach identifies ADP-ribosylation sites from in vitro modified full-length histone proteins

Next, we applied our novel protocols to a more complex sample that reflects a typical experiment for the identification of *in vitro* modified full-length proteins (Fig. 3). A mixture of all four core histones and linker histone H1 was *in vitro* modified by ARTD10 (818-1025). ARTD10 was chosen, because it *in vitro* modified peptides more efficiently than ARTD1 (compare Fig. 4a upper and lower panel) and hence resulted in a larger diversity of ADP-ribose modifications. The performance of the different methods (HCD, ETD (IT), ETD (FT), HCD-ETD (IT), HCD-PD-ETD (IT) or two-stage HCD-ETD (IT)) was validated by the overall number of ADP-ribosylated peptides and the number of differentially modified peptides. Modification sites with a Mascot

Site Analysis confidence of ≥ 95% were considered as localized, whereas all other hits were considered as modified peptides however, without accurately mapped modification site (Fig. 5).

When ADP-ribosylated samples were analyzed either by HCD or ETD fragmentation alone, HCD resulted in nearly 3 times more identified spectra than ETD (Fig 5a). The application of ETD (IT) or ETD (FT) analysis led to comparable results, which was most probably due to lower charge states of the analyzed peptides in comparison to the highly charged peptide used in the first part of this study (Fig. S4b). Moreover, HCD fragmentation of the modified samples allowed the validation of modifications by screening for marker ions using PTM MarkerFinder. Screening with this software allowed the association of 1561 spectra to putative ADP-ribosylated peptides. A summary of the behavior of marker ions in these spectra is shown in Fig. S6. When marker ions were included into the LC-MS methods, the HCD-PD1-ETD (IT) approach identified approximately the same number of peptides as the two single HCD and ETD (IT) runs together, indicating that all modified peptides with a clear ion pattern were already picked and identified by the two single runs. In comparison, the two-stage HCD-ETD (IT) identified approximately 30% more modified peptides, which was most probably due to a repeated measurement of potentially modified precursors, increasing the chance for high-quality spectra and high identification scores in comparison to single HCD. The comparison of the number of total identified peptides to the number of different identified peptides correlated strongly throughout all runs (Fig. 5a,b). Interestingly, the two-stage HCD-ETD (IT) run identified fewer differentially modified peptides than the HCD-PD1-ETD (IT) approach, indicating that the more abundant modified peptides most probably suppressed the detection of less abundant ones, since we used different settings in dynamic exclusions between single HCD and marker ion dependent runs. To validate the potential benefits of the ETD fragmentation in these approaches, the

contributions from HCD and ETD spectra to the identified peptides from the combined HCD-ETD (IT) runs were compared. 83 – 94% of all identified ADP-ribosylated peptides in HCD-ETD (IT) were already present in the HCD covered fraction, suggesting that the additional ETD fragmentation provided only little additional information compared to HCD alone (Fig. 5c).

Taken together, the identification and mapping of the ADP-ribosylation sites in a more complex sample was best achieved by the application of HCD-PD1-ETD (IT) or the two-stage HCD-ETD (IT) approach. Both methods identified a high number of acceptor sites and record the additional ETD-information. However, in most cases a single HCD run might be sufficient to capture the majority of ADP-ribosylated peptides and their acceptor sites.

The different MS/MS protocols described above led to the identification of 150 ADP-ribosylated peptides and 41 modification sites of *in vitro* modified ARTD10 and histones (Table S1 and S2). Several sites or areas of ADP-ribosylation were covered by different overlapping peptides, underlining the robustness of this new approach. Interestingly, ADP-ribosylation of histones was not limited to a single amino acid residue, but found on glutamates as well as lysine and arginine residues. In contrast, for ARTD10 mainly glutamate residues were identified as auto-modification sites. This implies that ARTD10 is able to modify more than one type of amino acid and/or that ARTD10 auto-modification is mainly directed towards one residue (e.g., glutamate), from where the modification may be transferred to other sites (e.g., lysine or arginine).

Two-stage HCD-ETD (IT) improves the identification of ADP-ribosylation acceptor sites in proteins from nuclear extracts

After the identification of ADP-ribosylation sites in *in vitro* modified proteins, the next step is the analysis of ADP-ribosylated proteins in cell extracts. Therefore, nuclear lysates of H_2O_2 treated HEK293T cells were digested with trypsin and analyzed (Fig. 6a). The high complexity of these samples as well as a high number of non-ADP-ribosylated peptides both contribute to a massive background and make the analysis far more challenging. To reduce this complexity, samples were fractioned by high-pH reversed-phase chromatography after trypsin digestion. The fractionated samples were subsequently analyzed with a single-HCD run to confirm the presence of putative ADP-ribosylated peptides. Due to the low abundance of ADP-ribosylated peptides in the analyzed extracts, the HCD run resulted only in a very small number of Mascot-identified ADP-ribosylated peptides (Fig. 6a,b). The obtained data were thus further screened with the PTM-MarkerFinder software, which identified 120 to 140 putative ADP-ribosylated peptides (Fig. S7), although some ADP-ribose maker ions had low intensities. We therefore assumed that in complex extracts, a single HCD run is not sufficient to properly identify ADP-ribosylated peptides. This observation together with the putative 120-140 modified peptides, made a two-stage HCD-ETD (IT) run the method of choice for a further analysis. The application of the two-stage approach allowed the identification of 10 times more ADP-ribosylated peptides (Fig 6b) as well as 5-7 times more different peptides (Fig. 6c, Table 2 and 3). This was true for both site localization confidence scores over and under 95%. As already previously observed, also in this case the majority (85%) of the different identified peptides were, identified by the HCD runs (Fig. 6d). All the spectra corresponding to correctly identified and localized ADP-ribosylated peptides are shown in the supplementary figure S8. Taken together, the two-stage HCD-ETD

(IT) approach with HPLC pre-fractionation is a powerful tool for the identification of cellular ADP-ribosylation sites, which can be applied to a complex cell extracts.

Pre-treatment of samples with PARG provides additional information for the analysis by HCD

The complexity of a sample is not only defined by the presence of differently modified proteins, but also by the complexity added by the different chain length of the ADP-ribose polymer. To define and address this aspect, the ARTD1-modified standard peptide, as well as the nuclear lysates were pre-treated with PARG to remove the ADP-ribose chain except the proximal ADP-ribose moiety (6). As expected, only one ADP-ribose group was identified on PARG treated peptides modified by ARTD1 using HCD fragmentation (Fig. 2c), suggesting that only one site per peptide was ADP-ribosylated. The use of PARG increased the number of identified modification sites in all combined HCD-ETD runs (Fig. 4b). The same holds true for the nuclear lysates, where PARG treatment led to an increased identification (Fig. 6b,c). Here 85% of the HCD identifications were covered by the PARG untreated nuclear sample, which was also not altered using ETD fragmentation (85.7% were covered (Fig. 6d)). Therefore, PARG treatment (i.e., shortening of the ADP-ribose chains) resulted in a 25% benefit in terms of modification localization. Together, theses measurements suggest that PARG treatment is an optional step that increases the number of identified ADP-ribose acceptor sites by around 25%.

Glutamate and lysine residues are ADP-ribose acceptor sites in vivo

Over all, the optimization of especially HCD-MS/MS and the application of two-stage HCD-ETD (IT) allowed for the first time the identification of several ADP-ribosylation sites of proteins in a complex cell extract without enrichment of modified proteins (Table 2). Interestingly the ADP-ribosylation sites comprised both lysine and glutamate residues to the same extent, indicating that there is not only one general acceptor amino acid for ADP-ribose in cells. This could either be due to different ARTDs catalyzing the modification through different mechanisms or to the above mentioned possibility of a common mechanism which modifies only one residue (e.g., glutamate) with a very unstable linkage that allows the ADP-ribose moiety to be transferred on close by residues with a more stable linkage (e.g., lysines).

Histone proteins comprised the major part of the identified ADP-ribosylated protein, which is in accordance to previous studies, reporting histones as the main acceptors for ADP-ribose in cells (9). The fact that we could not identify modification sites of ARTD1 (neither modified *in vitro* nor *in vivo*) could be explained by the underrepresentation of ARTD1 peptides in the analyzed mixture. Interestingly, we were able to identify ADP-ribose acceptor residues on histone proteins that are identical or in close proximity to known sites of other PTMs. We could localize ADP-ribosylation to H2B K5, which is also acetylated (27), to H3 K14 which is acetylated (28) and to H1.2 at either K184 or 187 (K187 is methylated (29)). This shows that ADP-ribosylation acceptor sites are also targets of other PTM's and suggest a lively crosstalk (e.g., between ADP-ribosylation, acetylation and methylation of lysine residues).

Conclusions

The herein described approach for the identification of ADP-ribosylated proteins and their specific modification sites comprises new methods for the preparation of samples of modified proteins, data acquisition and data analysis (Fig. 1a, 3a, 6a). The improvements and innovations in this HCD-based protocol, enables the identification of ADP-ribosylation sites with high reliability and confidence of *in vitro* modified proteins by preferably HCD-PD1-ETD (IT) or two-stage HCD-ETD (IT) and from cellular extracts. For the first time we could identify several ADP-ribose acceptor sites (glutamates, lysines and arginies) on different proteins. This approach does not require the enrichment of ADP-ribosylated proteins or peptides, although this might further enhance the number of identified peptides. Taken together, we present a robust method for the exact identification of ADP-ribosylation sites that can be applied to various proteins of interest and which opens the possibility to identify ADP-ribose acceptor sites in cellular extracts and eventually even tissue samples.

References

1. Hassa, P. O., Haenni, S., Elser, M., and Hottiger, M. O. (2006) Nuclear ADP-ribosylation reactions in mammalian cells: where are we today and where are we going? *Microbiol Mol Biol Rev* 70, 789-829
2. Hottiger, M. O., Hassa, P. O., Lüscher, B., Schüler, H., and Koch-Nolte, F. (2010) Toward a unified nomenclature for mammalian ADP-ribosyltransferases. *Trends Biochem Sci* 35, 208-219
3. Gagne, J. P., Hendzel, M. J., Droit, A., and Poirier, G. G. (2006) The expanding role of poly(ADP-ribose) metabolism: current challenges and new perspectives. *Curr Opin Cell Biol* 18, 145-151
4. Hassa, P. O., and Hottiger, M. O. (2008) The diverse biological roles of mammalian PARPs, a small but powerful family of poly-ADP-ribose polymerases. *Front Biosci* 13, 3046-3082
5. Krishnakumar, R., and Kraus, W. (2010) The PARP Side of the Nucleus: Molecular Actions, Physiological Outcomes, and Clinical Targets. *Mol Cell* 39, 8-24
6. Rosenthal, F., Feijs, K. L. H., Frugier, E., Bonalli, M., Forst, A. H., Imhof, R., Winkler, H. C., Fischer, D., Caflisch, A., Hassa, P. O., Lüscher, B., and Hottiger, M. O. (2013) Macrodomain-containing proteins are novel mono-ADP-ribosylhydrolases. *Nat Struct Mol Biol*, accepted for publication
7. Hottiger, M. O., and Kraus, W. L. (2013) PARP-1 and gene regulation: progress and puzzles. *Mol Aspects Med*, accepted for publication
8. Luo, X., and Kraus, W. L. (2012) On PAR with PARP: cellular stress signaling through poly(ADP-ribose) and PARP-1. *Genes Dev* 26, 417-432
9. Hottiger, M. O. (2011) ADP-ribosylation of histones by ARTD1: An additional module of the histone code? *FEBS Lett* 585, 1595-1599
10. Messner, S., and Hottiger, M. O. (2011) Histone ADP-ribosylation in DNA repair, replication and transcription. *Trends Cell Biol* 21, 534-542
11. Schreiber, V., Dantzer, F., Ame, J. C., and de Murcia, G. (2006) Poly(ADP-ribose): novel functions for an old molecule. *Nat Rev Mol Cell Biol* 7, 517-528
12. Tao, Z., Gao, P., and Liu, H. (2009) Identification of the ADP-ribosylation sites in the PARP-1 automodification domain: analysis and implications. *J Am Chem Soc* 131, 14258-14260
13. Altmeyer, M., Messner, S., Hassa, P. O., Fey, M., and Hottiger, M. O. (2009) Molecular mechanism of poly(ADP-ribosyl)ation by PARP1 and identification of lysine residues as ADP-ribose acceptor sites. *Nucleic Acids Res* 37, 3723-3738
14. Chapman, J. D., Gagne, J. P., Poirier, G. G., and Goodlett, D. R. (2013) Mapping PARP-1 Auto-ADP-ribosylation Sites by Liquid Chromatography-Tandem Mass Spectrometry. *Journal of proteome research*
15. Messner, S., Altmeyer, M., Zhao, H., Pozivil, A., Roschitzki, B., Gehrig, P., Rutishauser, D., Huang, D., Caflisch, A., and Hottiger, M. O. (2010) PARP1 ADP-ribosylates lysine residues of the core histone tails. *Nucleic Acids Res* 38, 6350-6362
16. Hengel, S. M., Shaffer, S. A., Nunn, B. L., and Goodlett, D. R. (2009) Tandem mass spectrometry investigation of ADP-ribosylated kemptide. *J Am Soc Mass Spectrom* 20, 477-483

17. Rosenthal, F., Messner, S., Roschitzki, B., Gehrig, P., Nanni, P., and Hottiger, M. O. (2011) Identification of distinct amino acids as ADP-ribose acceptor sites by mass spectrometry. *Methods Mol Biol* 780, 57-66
18. Hengel, S. M., and Goodlett, D. R. (2012) A Review of Tandem Mass Spectrometry Characterization of Adenosine Diphosphate-Ribosylated Peptides. *Int J Mass Spectrom* 312, 114-121
19. Torrente, M. P., Zee, B. M., Young, N. L., Baliban, R. C., LeRoy, G., Floudas, C. A., Hake, S. B., and Garcia, B. A. (2011) Proteomic interrogation of human chromatin. *PLoS One* 6, e24747
20. Chambers, M. C., Maclean, B., Burke, R., Amodei, D., Ruderman, D. L., Neumann, S., Gatto, L., Fischer, B., Pratt, B., Egertson, J., Hoff, K., Kessner, D., Tasman, N., Shulman, N., Frewen, B., Baker, T. A., Brusniak, M. Y., Paulse, C., Creasy, D., Flashner, L., Kani, K., Moulding, C., Seymour, S. L., Nuwaysir, L. M., Lefebvre, B., Kuhlmann, F., Roark, J., Rainer, P., Detlev, S., Hemenway, T., Huhmer, A., Langridge, J., Connolly, B., Chadick, T., Holly, K., Eckels, J., Deutsch, E. W., Moritz, R. L., Katz, J. E., Agus, D. B., MacCoss, M., Tabb, D. L., and Mallick, P. (2012) A cross-platform toolkit for mass spectrometry and proteomics. *Nat Biotechnol* 30, 918-920
21. Savitski, M. M., Mathieson, T., Becher, I., and Bantscheff, M. (2010) H-score, a mass accuracy driven rescoring approach for improved peptide identification in modification rich samples. *J Proteome Res* 9, 5511-5516
22. Savitski, M. M., Lemeer, S., Boesche, M., Lang, M., Mathieson, T., Bantscheff, M., and Kuster, B. (2011) Confident phosphorylation site localization using the Mascot Delta Score. *Mol Cell Proteomics* 10, M110 003830
23. Nanni, P., Panse, C., Gehrig, P., Mueller, S., Grossmann, J., Schlapbach, R., (2013) PTM MarkerFinder, a software tool to detect and validate spectra from peptides carrying post-translational modifications. . *proteomics* revision submitted
24. Zhao, P., Viner, R., Teo, C. F., Boons, G. J., Horn, D., and Wells, L. (2011) Combining high-energy C-trap dissociation and electron transfer dissociation for protein O-GlcNAc modification site assignment. *Journal of proteome research* 10, 4088-4104
25. Singh, C., Zampronio, C. G., Creese, A. J., and Cooper, H. J. (2012) Higher energy collision dissociation (HCD) product ion-triggered electron transfer dissociation (ETD) mass spectrometry for the analysis of N-linked glycoproteins. *Journal of proteome research* 11, 4517-4525
26. Mayampurath, A. M., Wu, Y., Segu, Z. M., Mechref, Y., and Tang, H. (2011) Improving confidence in detection and characterization of protein N-glycosylation sites and microheterogeneity. *Rapid Commun Mass Spectrom* 25, 2007-2019
27. Wyrick, J. J., and Parra, M. A. (2009) The role of histone H2A and H2B post-translational modifications in transcription: a genomic perspective. *Biochim Biophys Acta* 1789, 37-44
28. Jenuwein, T., and Allis, C. D. (2001) Translating the histone code. *Science* 293, 1074-1080
29. Weiss, T., Hergeth, S., Zeissler, U., Izzo, A., Tropberger, P., Zee, B. M., Dundr, M., Garcia, B. A., Daujat, S., and Schneider, R. (2010) Histone H1 variant-specific lysine methylation by G9a/KMT1C and Glp1/KMT1D. *Epigenetics Chromatin* 3, 7

Acknowledgements

F. Freimoser (University of Zurich, Switzerland) provided editorial assistance and critical input during the writing. We thank Peter Gehrig and Christian Panse from the FGCZ critical input and help with the PTM MarkerFinder respectively. This work was supported in part by the Swiss National Science Foundation Grant 31-122421 and the Kanton of Zurich (to M.O.H.).

Figure Legends

Figure 1: Optimal HCD fragmentation of the ADP-ribosylated standard peptide using ramped CE. *A*. Overview of the sample preparation, liquid chromatography mass spectrometry and data analysis workflow employed for the evaluation of HCD fragmentation behavior of the biotin-KAARKSAPATGGVKKPHRYR (H3) ADP-ribosylated peptide; *B*. Nomenclature of ADP-ribose fragments as described by Hengel et al. (16). The ADP-ribose fragment ions showing strong signals in the HCD MS/MS spectra are shown (m1, m3, m6, m8, m10); *C*. HCD spectrum of the biotin-KAARKSAPATGGVKKPHRYR (H3) ADP-ribosylated peptide. The loss of adenine, adenosine and water, adenosine mono-phosphate (AMP), adenosine di-phosphate (ADP) and ADP-ribose can be observed in the zoomed panel. The arrows mark the three most abundant ADP-ribose fragment ions.

Figure 2: **Implementing ADP-ribose neutral losses improves identification of ADP-ribose acceptor sites by Mascot.** *A*. Details of the ADP-ribose modification settings defined in the Mascot Server. The marker ions ignored were not considered for scoring. *B*. Summary of the results obtained by HCD analysis of the biotin-KAARKSAPATGGVKKPHRYR (H3) peptide treated with ARTD1 and ARTD10, using the modification settings defined in panel *A*. The bars represent the number of HCD spectra identified as peptide carrying 1 (white), 2 (grey) or 3 (black) ADP-ribosylations. The black line shows the percentage of spectra corresponding to ADP-ribosylated peptides that has been correctly identified. *C*. Summary of the results obtained by HCD analysis of the biotin-KAARKSAPATGGVKKPHRYR (H3) peptide treated with ARTD1 and PARG.

Figure 3: Analysis of ADP-ribosylated peptides using combination of HCD and ETD fragmentation techniques. Schematic overview of the mass spectrometry methods employed in the present study. Both the biotin-KAARKSAPATGGVKKPHRYR (H3) peptide and a histone mixture are ADP-ribosylated and analyzed using various combination of HCD and ETD fragmentation techniques. ETD spectra can be acquired in the ion trap (IT) or in the orbitrap (FT). The black circles represent ADP-ribose marker ions present in the HCD spectra, that trigger an ETD fragmentation event. PTM MarkerFinder is a software that screens for ADP-ribose marker ions and creates an inclusion list containing putative ADP-ribosylated peptides to be targeted in a second LC-MS/MS analysis.

Figure 4: Analysis of the ADP-ribosylated H3 peptide KAARKSAPATGGVKKPHRYR using a combination of HCD and ETD fragmentation techniques. Every pie-chart shows for each combination of HCD and ETD fragmentation the number of spectra unassigned (white) and assigned to ADP-ribosylated peptides (colored). *A.:* results obtained by the analysis of the peptide treated with ARTD1 and ARTD10. The bars report the number of spectra identified as

peptides carrying 1 (blue), 2 (red) or 3 (green) ADP-ribose moieties. *B.*: results for the peptide treated with ARTD1/PARG.

Figure 5: Analysis of histones *in vitro* modified by ARTD10 using combinations of HCD and ETD fragmentation techniques. Histones *in vitro* modified by ARTD10 were analyzed by MS/MS usind six different combinations of HCD and/or ETD fragmentation techniques. Both the ADP-ribosylated peptides where the site localization confidence score is higher than 95% (black bars) and lower than 95% (grey bar) are plotted. *A.:* number of spectra assigned to ADP-ribosylated peptides. *B.*: number of different ADP-ribosylated peptides identifications (different modification sites on the same peptide are considered as different peptides). *C.*: Venn diagrams showing the differences and overlaps between HCD and ETD identifications. The diagrams refer only to the peptides having a site localization score higher than 95%.

Figure 6: Results of the analysis of HEK 293T nuclear lysates using combinations of HCD and ETD fragmentation techniques. *A.*: identification of ADP-ribosylated peptides in nuclear lysate of HEK 293T cells by LC-MS/MS analysis using a two-stage HCD-ETD (IT) approach. Panel *B.* and *C.* show the identified ADP-ribosylated peptides having a site localization confidence score both higher (black bars) and lower (grey bar) than 95%. *B.:* number of spectra assigned to ADP-ribosylated peptides. *C.*: number of different ADP-ribosylated peptides identifications (different modification sites on the same peptide are considered as different peptides). *D.*: Venn diagrams showing the differences and overlaps between HCD and ETD identifications as well as untreated and PARG treated samples. The diagrams refer only to the peptides having a site localization score higher than 95%.

Table Legends

Table 1: Overview of evaluated tandem mass spectrometry methods

Table 2: Identification of ADP-ribosylated peptides from nuclear lysates having unambiguous site localization. Newly identified ADP-ribosylation sites are highlighted in bold red. All ADP-ribosylated peptides with a Mascot localization score over 95% are listed. The number of identifications represents, how often the peptide was independently identified.

Table 3: Identification of ADP-ribosylated peptides from nuclear lysates having ambiguous site localization. Newly identified ADP-ribosylation sites are highlighted in bold red. All ADP-ribosylated peptides with a Mascot localization score under 95% are listed. The number of identifications represents, how often the peptide was independently identified.

Figure 1

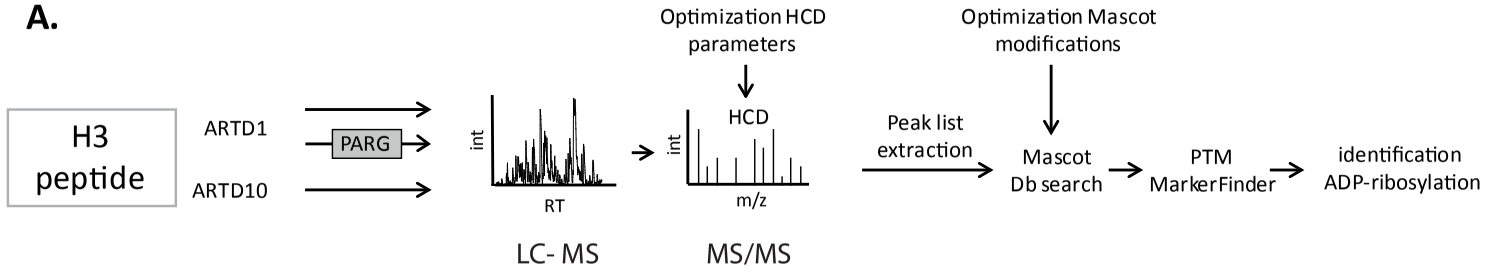

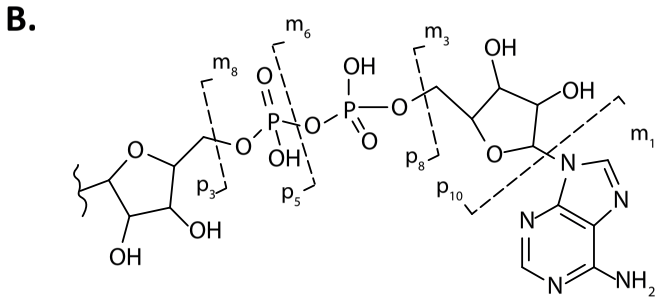

m_1^+ : 136.06 (adenine$^+$)
m_3^+ : 250.09 (adenosine -H_2O^+)
m_6^+ : 348.05 (adenosine-mono phosphate$^+$ (AMP$^+$))
m_8^+ : 428.02 (adenosine-di phosphate$^+$ (ADP$^+$))
m_{10}^+: 542.07 (ADP-ribose$^+$)

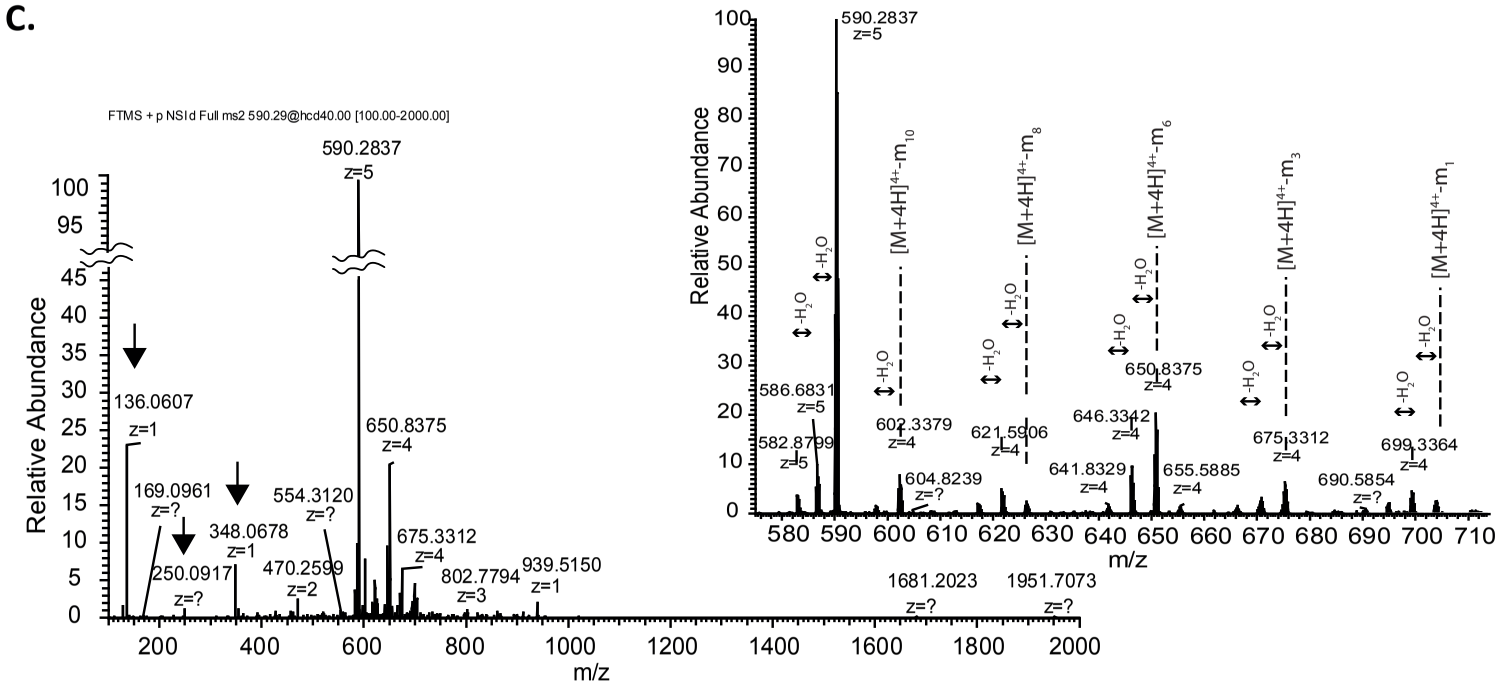

Figure 2

A.

	Modification name	Mass shift (Da)	Marker ion ignored (m/z)	Neutral losses (NL)
i	ADP-rib	541.0611	-	-
ii	ADP-rib-HCDm	541.0611	428.0372, 348.0709, 250.0940, 136.0623	-
iii	ADP-rib-HCDm-NL541/347	541.0611	428.0372, 348.0709, 250.0940, 136.0623	541.0611 347.0631
iv	ADP-rib-HCDm-NL347/249	541.0611	428.0372, 348.0709, 250.0940, 136.0623	347.0631 249.0862
v	ADP-rib-HCDm-NL347	541.0611	428.0372, 348.0709, 250.0940, 136.0623	347.0631

B.

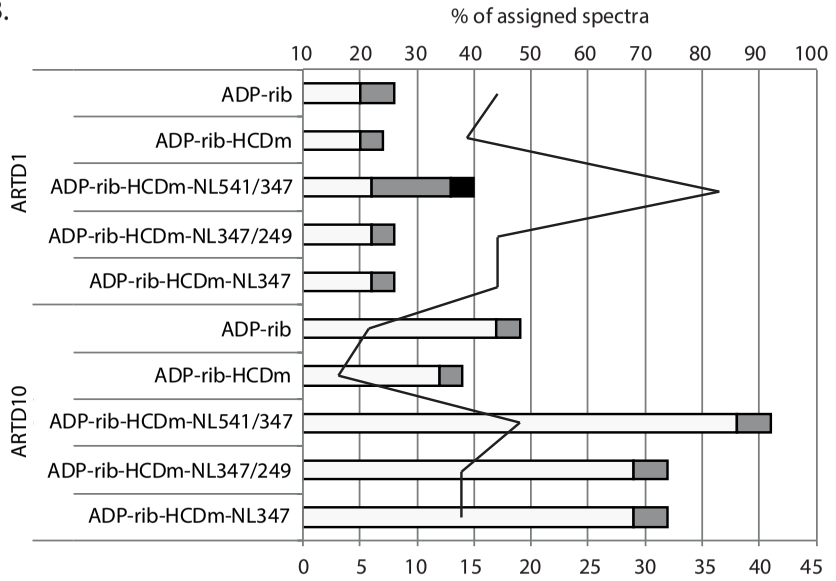

C.

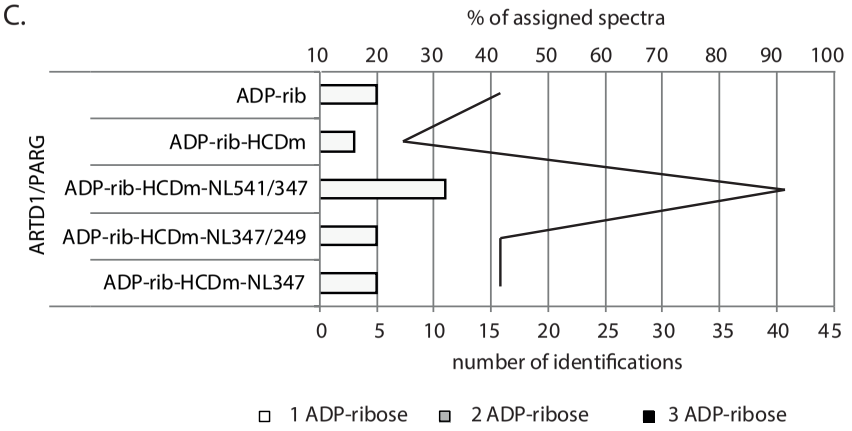

Figure 3

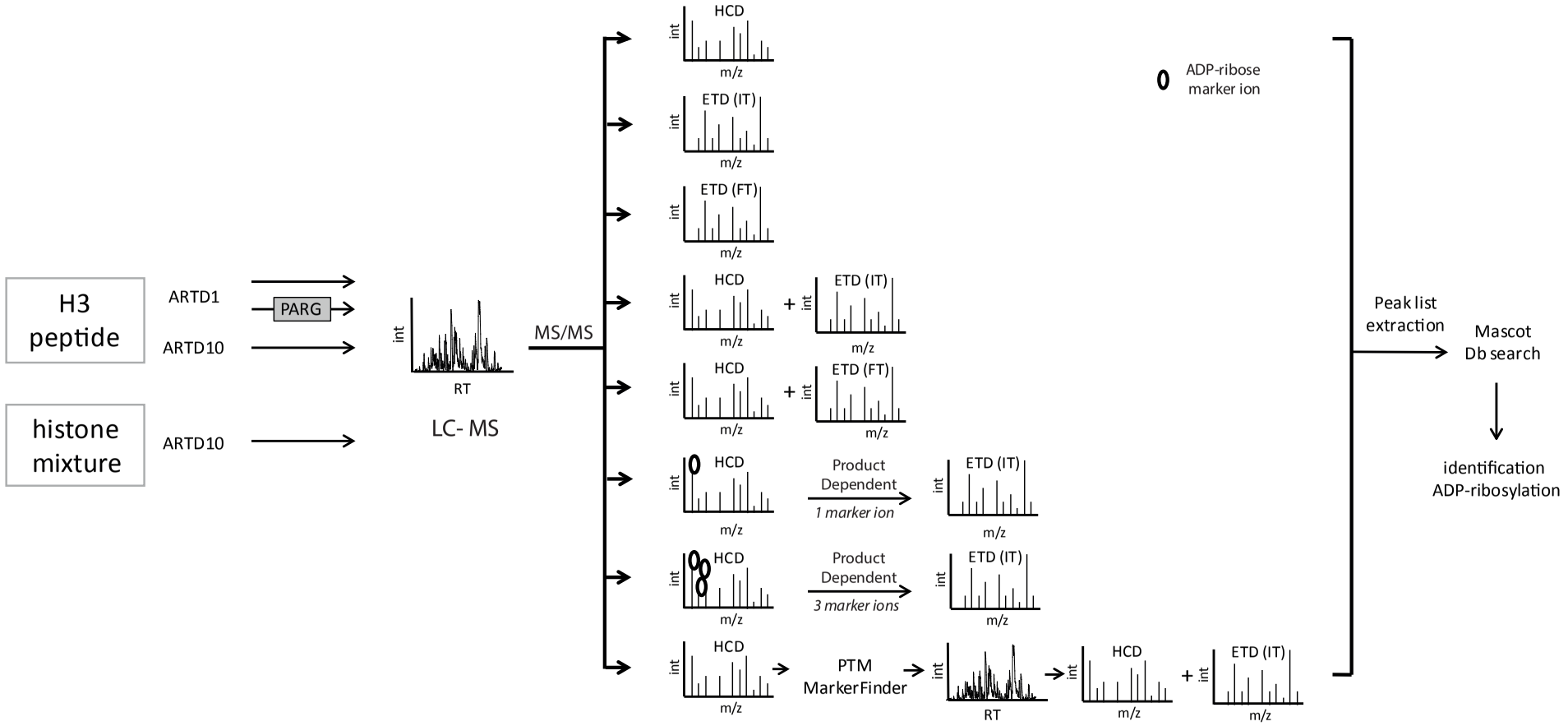
H3 peptide
histone mixture
ARTD1
PARG
ARTD10
ARTD10
int
RT
LC- MS
MS/MS
HCD
ETD (IT)
ETD (FT)
m/z
ADP-ribose marker ion
Product Dependent
1 marker ion
3 marker ions
PTM MarkerFinder
Peak list extraction
Mascot Db search
identification ADP-ribosylation

Figure 4

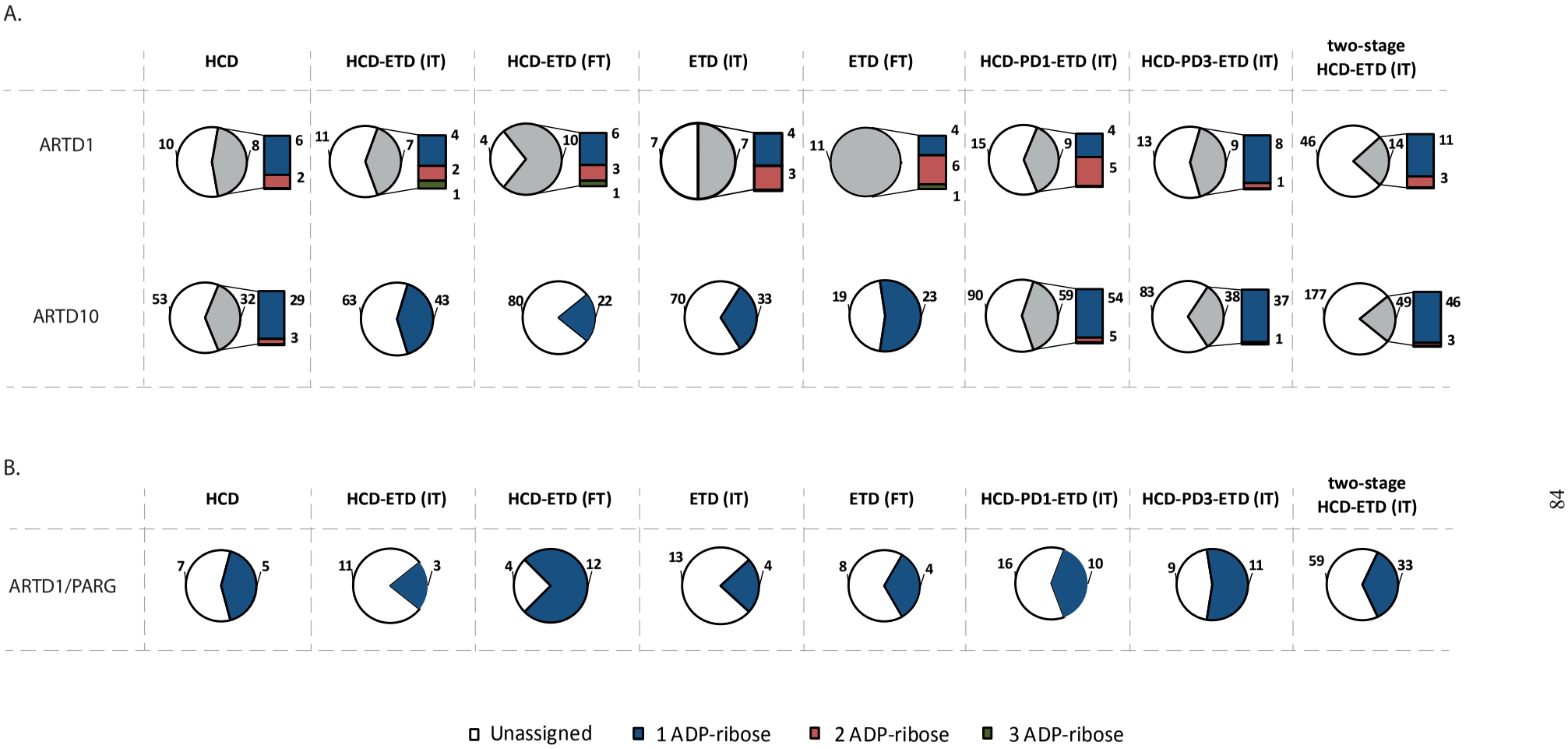
A.
HCD
HCD-ETD (IT)
HCD-ETD (FT)
ETD (IT)
ETD (FT)
HCD-PD1-ETD (IT)
HCD-PD3-ETD (IT)
two-stage HCD-ETD (IT)
ARTD1
ARTD10
B.
ARTD1/PARG
Unassigned
1 ADP-ribose
2 ADP-ribose
3 ADP-ribose

Figure 5

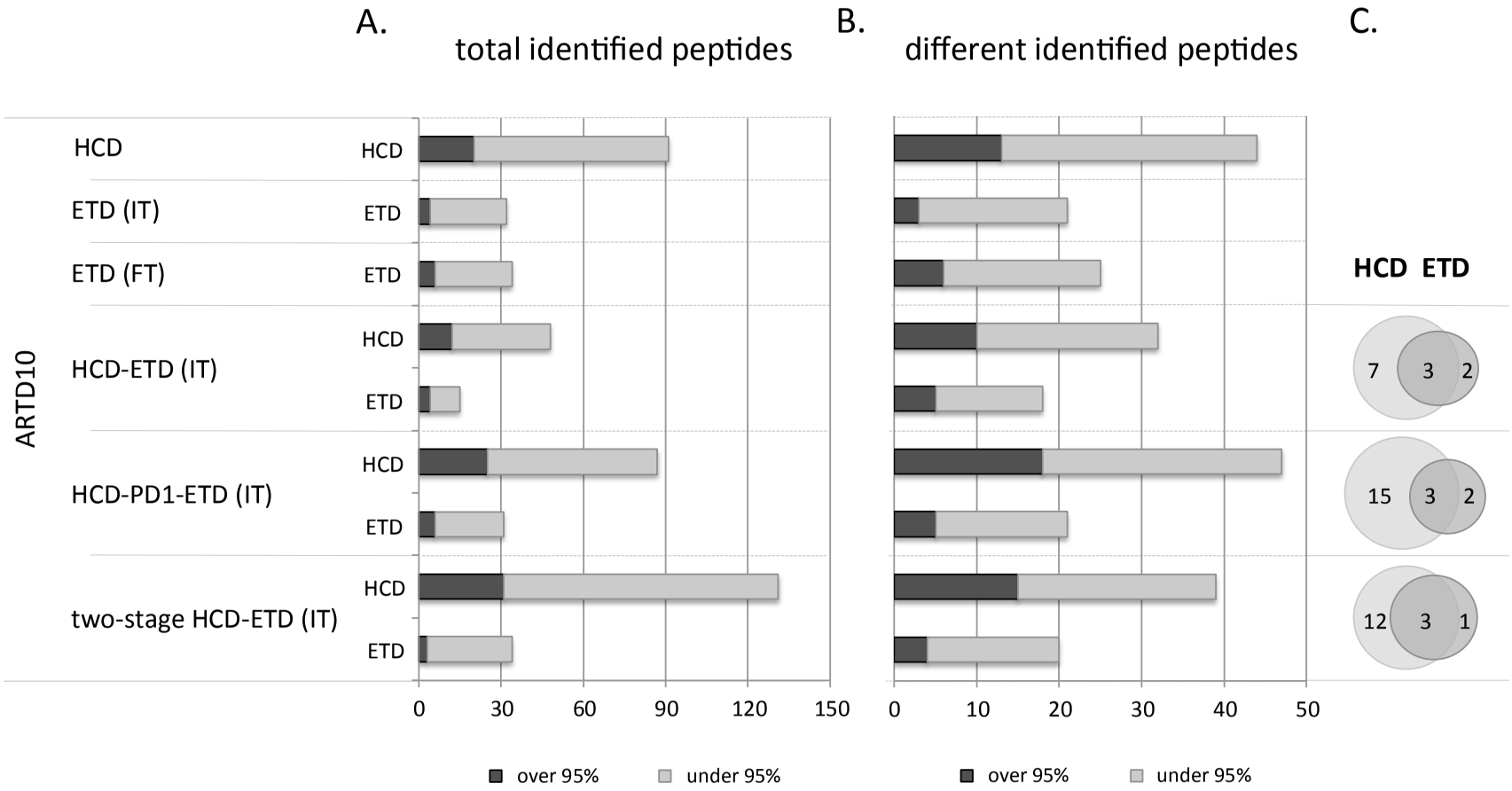
A.
total identified peptides
B.
different identified peptides
C.
ARTD10
HCD
ETD (IT)
ETD (FT)
HCD-ETD (IT)
HCD-PD1-ETD (IT)
two-stage HCD-ETD (IT)
HCD
ETD
0
30
60
90
120
150
0
10
20
30
40
50
over 95%
under 95%
HCD ETD
7
3
2
15
3
2
12
3
1

Figure 6

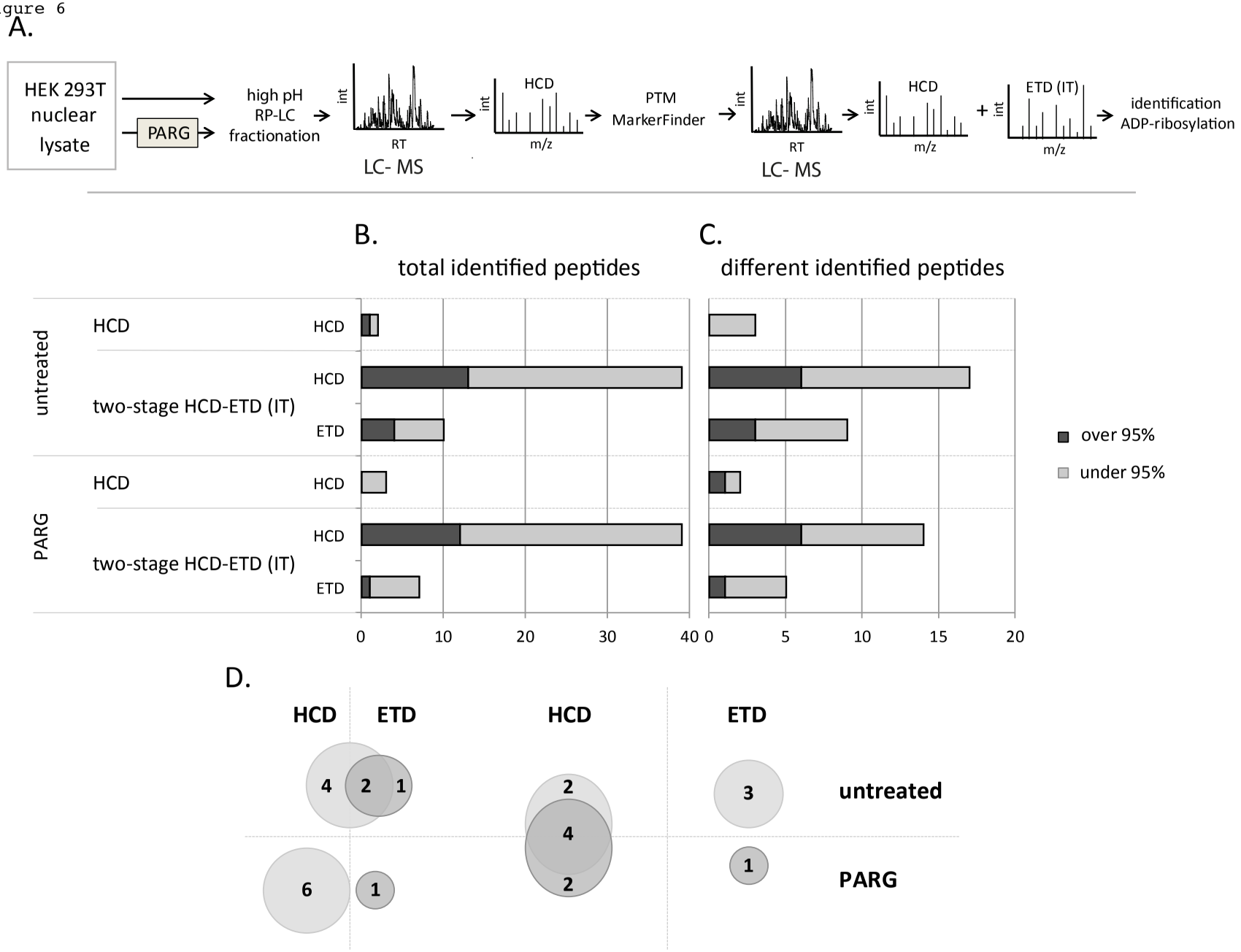
A.
HEK 293T nuclear lysate
PARG
high pH RP-LC fractionation
int
RT
LC- MS
HCD
m/z
PTM MarkerFinder
ETD (IT)
identification ADP-ribosylation
B.
total identified peptides
C.
different identified peptides
untreated
PARG
HCD
two-stage HCD-ETD (IT)
ETD
over 95%
under 95%
0
10
20
30
40
5
15
D.
HCD
ETD
4
2
1
6
untreated
PARG
3

Table 1

	MS Method	Full MS scan range (m/z)	MS2 events		Data collection		MS2 AGC target			MS2 max injection time (ms)			Product ions
			HCD	ETD	Orbitrap	Ion Trap	Orbitrap	Ion Trap	Anion	Orbitrap	ion Trap	Reagent	
a.	HCD	300-1700	10	-	Profile	-	1e5	-	-	200	50	-	-
b.	ETD (IT)	300-1700	-	10	-	Centroid	-	1e4	1e5	-	50	100	-
c.	ETD (FT)	300-1700	-	8	Profile	-	1e5	-	1e5	200	-	100	-
d.	HCD-ETD (IT)	300-1700	10	10	Profile	Centroid	1e5	1e4	1e5	200	-	100	-
e.	HCD-ETD (FT)	300-1700	8	8	Profile	-	1e5	-	1e5	200	50	100	-
f.	HCD-PD1-ETD (IT)	300-1700	10	10	Profile	Centroid	1e5	1e4	1e5	200	50	100	136.0623
g.	HCD-PD3-ETD (IT)	300-1700	10	10	Profile	Centroid	1e5	1e4	1e5	200	50	100	136.0623, 250.0940, 348.0709
h.	two-stage HCD-ETD (IT)	300-1700	10	10	Profile	Centroid	1e5	1e4	1e5	200	50	100	-

Table 2: List of ADP-ribosylated peptides identified in HEK 293T cells with unambiguous site localization (>95%)

protein description	peptide sequence	peptide mz	charge	peptide mr	peptide score	expect value	confidence	protein accession	No. of identifications
Histone H1.2	**K**AAKSAAKAVKPK	460.4799	4+	1837.8906	60.22	0.0000035	99.88%	sp|P16403|H12_HUMAN	3
Histone H2B	P**E**PAKSAPAPKKGSK	678.6409	3+	2032.901	41.75	0.0096	99.60%	sp|P06899|H2B1J_HUMAN	9
Histone H2B	PDPA**K**SAPAPKKGSK	673.9697	3+	2018.8872	20.78	0.012	100.00%	sp|P23527|H2B1O_HUMAN	5
Histone H2B	PDPA**K**SAPAPKKGSKK	537.7525	4+	2146.9809	36.85	0.027	99.61%	sp|P23527|H2B1O_HUMAN	2
Histone H2B	P**E**PTKSAPAPKKGSK	688.6427	3+	2062.9063	43.54	0.000092	97.73%	sp|P58876|H2B1D_HUMAN	4
Histone H2B	PEPT**K**SAPAPKKGSK	688.6418	3+	2062.9035	27.23	0.023	96.11%	sp|P58876|H2B1D_HUMAN	1
Histone H2B	P**E**LAKSAPAPKKGSK	683.9858	3+	2048.9357	42.67	0.00011	97.95%	sp|Q99880|H2B1L_HUMAN	2
Histone H2B	P**E**PSKSAPAPKKGSK	683.9722	3+	2048.8949	44.82	0.005	99.38%	sp|P33778|H2B1B_HUMAN	1
KHDR1	SSG**R**SGSMDPSGAHPSVR	771.626	3+	2311.8561	60.88	0.00018	100.00%	sp|Q07666-2|KHDR1_HUMAN	2
Histone H3	STGG**K**APRKQLATK	661.973	3+	1982.8972	28.53	0.0068	95.44%	sp|Q71DI3|H32_HUMAN	1

Table 3: List of ADP-ribosylated peptides identified in HEK 293T cells with ambiguous site localization (<95%)

protein description	peptide sequence	peptide mz	charge	peptide mr	peptide score	expect value	confidence	protein accession	No. of identifications
Histone H1.2	SAAKAVKPKAAKPKVVKPK	498.2706	5+	2486.3166	26.14	0.0036	92.52%	sp|P16403|H12_HUMAN	22
Histone H1.2	SAAKAVKPKAAKPKVVKPK	622.5881	4+	2486.3234	26.15	0.0052	71.77%	sp|P16403|H12_HUMAN	7
Histone H1.2	KAAKSAAKAVKPK	613.6371	3+	1837.8896	23.13	0.016	89.91%	sp|P16403|H12_HUMAN	2
Histone H1.2	KAAKSAAKAVKPK	613.637	3+	1837.8892	30.51	0.0018	69.15%	sp|P16403|H12_HUMAN	2
Histone H1.2	KAAKSAAKAVKPK	460.4793	4+	1837.888	22.91	0.029	48.81%	sp|P16403|H12_HUMAN	1
Histone H1.2	VAKPKKAAKSAAK	613.6376	3+	1837.8909	39.46	0.00021	91.08%	sp|P16403|H12_HUMAN	2
Histone H1.2	VAKPKKAAKSAAK	613.6376	3+	1837.8909	26.91	0.0057	93.51%	sp|P16403|H12_HUMAN	2
Histone H1.3	SAKKVKTPQPK	584.9381	3+	1751.7925	25.19	0.0051	90.41%	sp|P16402|H13_HUMAN	2
Histone H1.0	SDEPKKSVAFKK	635.6108	3+	1903.8105	23.94	0.0058	66.97%	sp|P07305|H10_HUMAN	1
Histone H2B	PELAKSAPAPKKGSK	683.9849	3+	2048.9328	41.02	0.00018	94.50%	sp|Q99880|H2B1L_HUMAN	4
Histone H2B	PELAKSAPAPK	825.3514	2+	1648.6883	36.77	0.029	86.92%	sp|Q99880|H2B1L_HUMAN	1
Histone H2B	PEPAKSAPAPKKGSKK	541.2557	4+	2160.9936	35.69	0.03	94.05%	sp|O60814|H2B1K_HUMAN	4
Histone H2B	PEPAKSAPAPKKGSK	678.6393	3+	2032.8962	27.1	0.0039	93.60%	sp|O60814|H2B1K_HUMAN	1
Histone H2B	PEPAKSAPAPKKGSK	678.6393	3+	2032.8962	25.35	0.038	84.30%	sp|O60814|H2B1K_HUMAN	2
Histone H2B	PEPTKSAPAPKKGSK	688.6427	3+	2062.9063	39.43	0.02	94.92%	sp|P58876|H2B1D_HUMAN	4
Histone H2B	PEPTKSAPAPKKGSK	688.6425	3+	2062.9055	24.01	0.035	91.98%	sp|P58876|H2B1D_HUMAN	1
Histone H2B	PDPAKSAPAPKKGSK	673.9677	3+	2018.8813	26.39	0.0067	94.96%	sp|P58876|H2B1D_HUMAN	3
Histone H2B	PDPAKSAPAPKKGSKK	716.6663	3+	2146.977	22.57	0.0093	93.94%	sp|Q99880|H2B1L_HUMAN	2
Histone H2B	PEPSKSAPAPKKGSK	683.9718	3+	2048.8936	36.72	0.033	92.53%	sp|P33778|H2B1B_HUMAN	2

Legend supplementary figures / tables

Fig. S1: Mascot modification settings used for the configuration of ADP-ribose modification. *Page 1*: ADP-rib, corresponding to a mass shift of 541.0611; *Page 2*: ADP-rib-HCDm, that additionally ignores for scoring the marker ions at m/z 428.0372, 348.0709, 250.0940, 136.0623; *Page 3*: ADP-rib-HCDm-NL541/347, equal to ADP-rib-HCDm with additional scoring of the neutral losses (NL) equal to 541.0611 and 347.0631 (coming from b and y series); *Page 4*: ADP-rib-HCDm-NL347/249, with scoring of the neutral losses equal to 347.0631 and 249.0862; *Page 5*: ADP-rib-HCDm-NL347, with scoring of a single neutral losses equal to 347.063.

Fig. S2: HCD spectra of peptide Biotin-KAARKSAPATGGVKKPHRYR + 1 ADP-ribose. HCD spectra of the ADP-ribosylated Biotin-KAARKSAPATGGVKKPHRYR peptide using different normalized collision energies (NCE). *A.*: NCE 23%; *B.*: NCE 30%; *C.*: NCE 38%; *D.*: NCE 45%; *E.*: NCE 52%; *F.*: NCE 60%; *G.*: NCE 40% using stepped NCE (3 steps, step width 15%)

Fig. S3: Results of the Mascot Site Localization Analysis of HCD spectra of peptide Biotin-KAARKSAPATGGVKKPHRYR + 1 ADP-ribose. Results of the Mascot Site Localization Analysis using different configuration of ADP-ribose modifications for the analysis of HCD spectra.

Fig. S4: Average charge state of the identified ADP-ribosylated peptides. *A.*: Biotin-KAARKSAPATGGVKKPHRYR peptide carrying 1 ADP-ribose modification; *B.*: histone mixture, digested with trypsin at 30ºC, overnight; *C.*: HEK 293T nuclear lysate

Fig. S5: Localization of ADP-ribosylation sites in standard peptide sample using multiple fragmentation techniques. Results of the Mascot Site Localization analysis for the peptide Biotin- KAARKSAPATGGVKKPHRYR + 1 ADP-ribose using different combinations of HCD and ETD fragmentation. The figure shows both the sites localized with a score higher (black) and lower (grey) than 95%.

Fig. S6: Behaviour of ADP-ribose marker ions during HCD fragmentation. The PTM MarkerFinder analysis of all the LC-MS/MS analysis of histone mixtures detected 1561 HCD spectra containing ADP-ribose marker ions. The box plot shows the log[10] intensities of the ADP-ribose marker ions at m/z 136.0623, 250.0940, 348.0709 and 428.0372.

Fig. S7: PTM MarkerFinder analysis of HEK 293T nuclear lysate. Number of putative ADP-ribosylated peptides detected by PTM MarkerFinder analysis of HCD spectra from HEK 293T nuclear lysate.

Fig. S8: Spectra of ADP-ribosylated peptides identified in HEK 293T nuclear lysates, having modification site correctly localized. The panels show the spectrum, Mascot results, fragment ion annotation and marker ion information for all the ADP-ribosylated peptides identified in HEK 293T nuclear lysates with a Mascot score higher than 20, Expect value lower than 0.05 and Mascot Site Localization analysis higher than 95%.

Table S1: Identification of ADP-ribosylated histone peptides having unambiguous site localization. Newly identified ADP-ribosylation sites from histones in vitro modified by ARTD10. The modification sites are presented in brackets. All ADP-ribosylated peptides with a Mascot localization score over 95% are listed. The number of identifications represents, how often the peptide was independently identified.

Table S2: Identification of ADP-ribosylated histone peptides having ambiguous site localization. Newly identified ADP-ribosylation sites from histones in vitro modified by ARTD10. The modification sites are presented in brackets. All ADP-ribosylated peptides with a Mascot localization score under 95% are listed. The number of identifications represents, how often the peptide was independently identified.

Supplementary Figure S1

(*i*) *ADP-Rib*
(mass shift of 541.0611 Da)

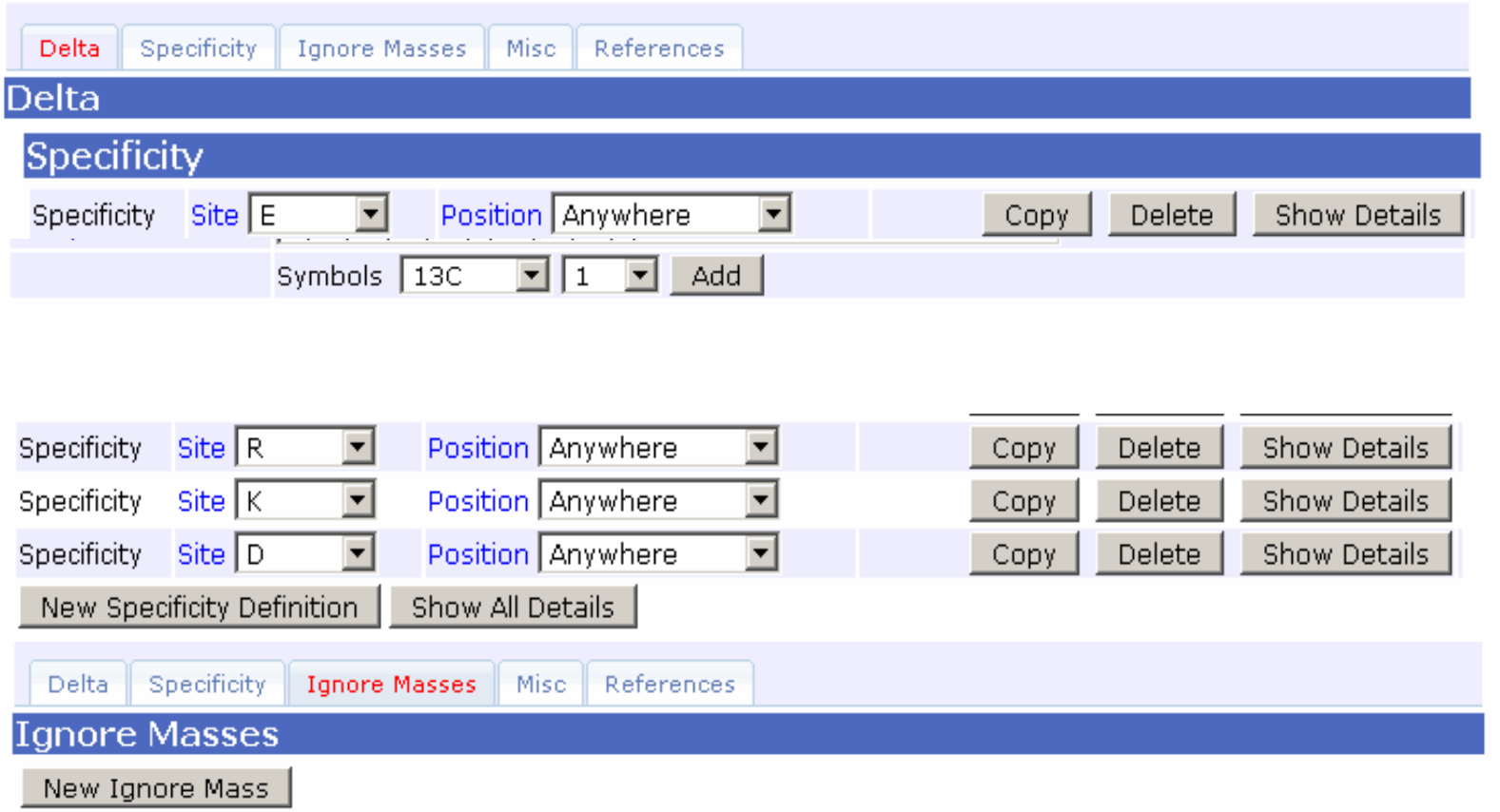

(*ii*) *ADP-Rib-HCDm*

(mass shift of 541.0611 Da, ignored the marker masses at m/z 428.0372, 348.0709, 250.0940, 136.0623)

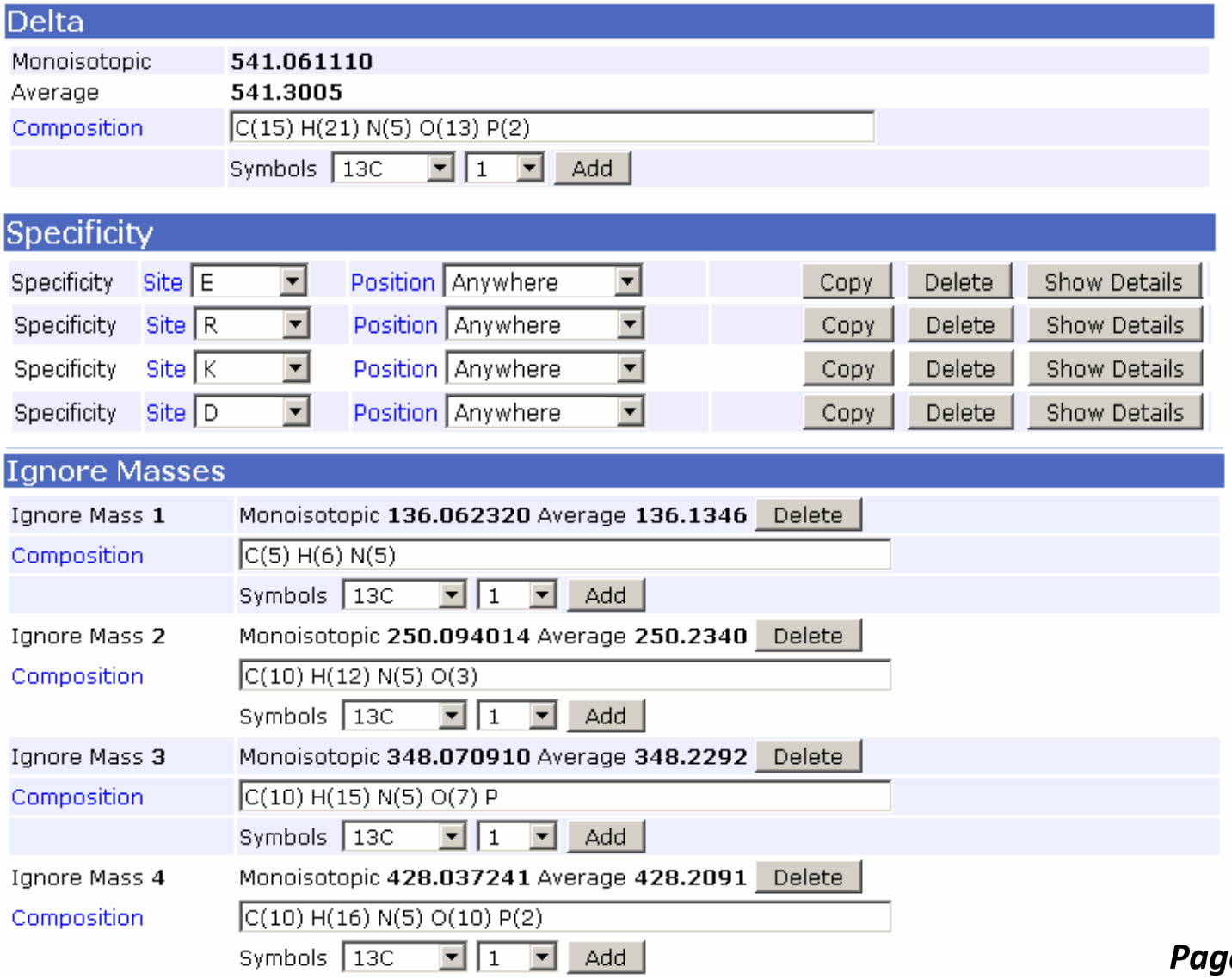

(*iii*) *ADP-Rib-HCDm-NL347/249*

(mass shift of 541.0611 Da, ignored the marker masses at m/z 428.0372, 348.0709, 250.0940, 136.0623, neutral losses (NL) equal to 347.0631 and 249.0862 from b and y ion series)

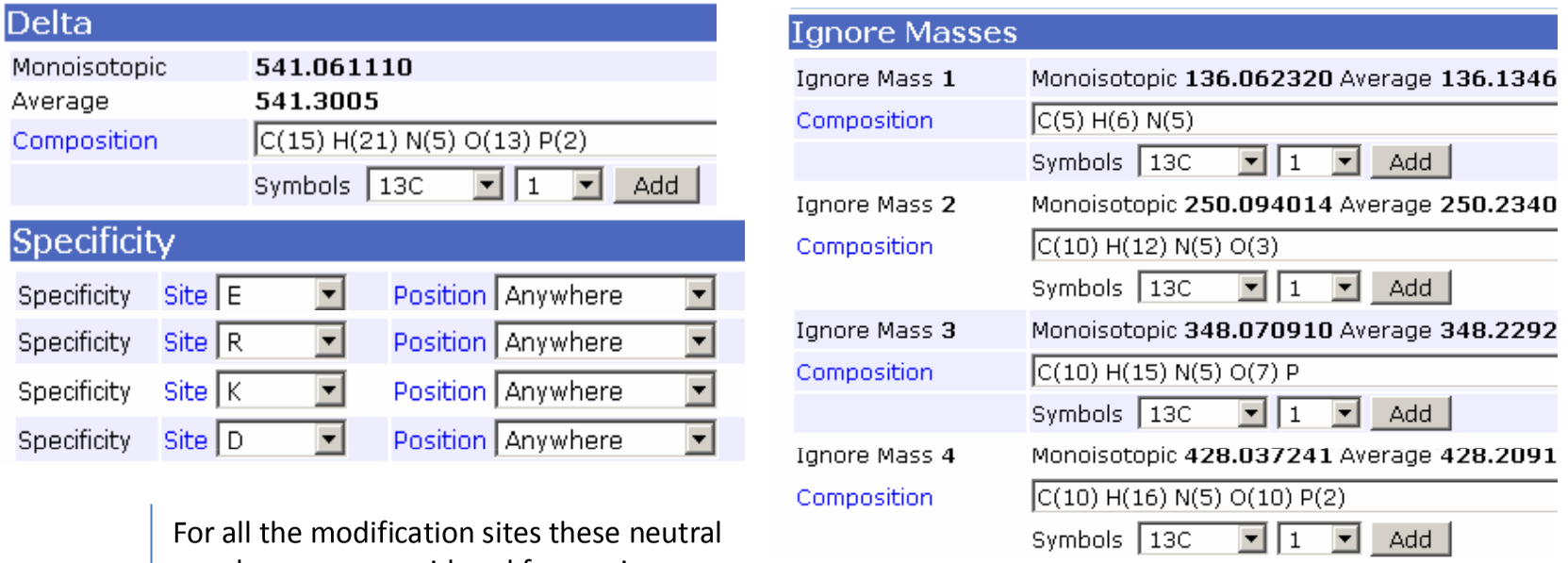

For all the modification sites these neutral losses are considered for scoring

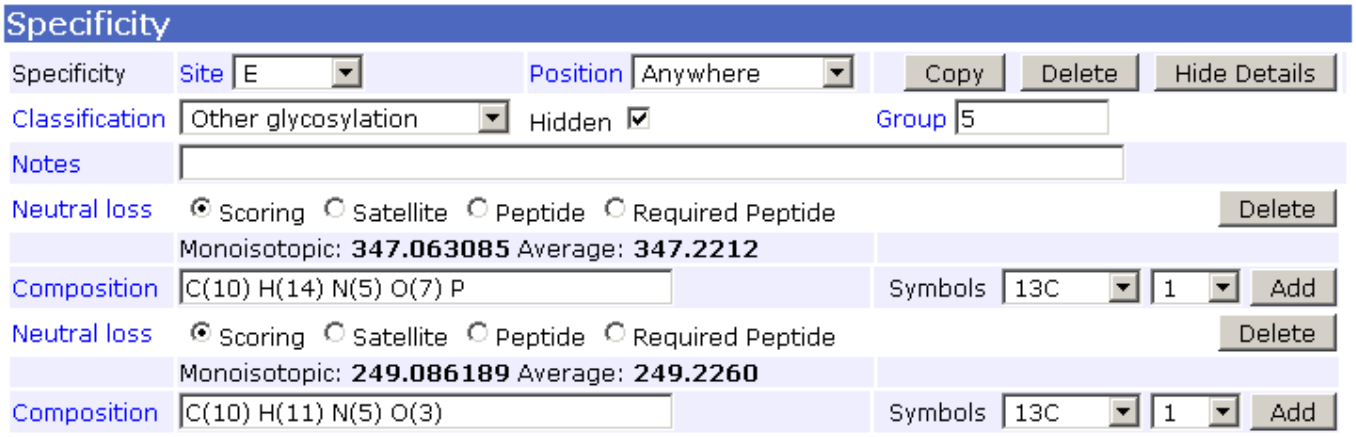

(*iv*) *ADP-Rib-HCDm-NL541/347*

(mass shift of 541.0611 Da, ignored the marker masses at m/z 428.0372, 348.0709, 250.0940, 136.0623, neutral losses (NL) equal to 541.0611 and 347.0631 from b and y ion series)

Delta

Monoisotopic	**541.061110**
Average	**541.3005**
Composition	C(15) H(21) N(5) O(13) P(2)
	Symbols 13C 1 Add

Specificity

Specificity	Site	E	Position	Anywhere
Specificity	Site	R	Position	Anywhere
Specificity	Site	K	Position	Anywhere
Specificity	Site	D	Position	Anywhere

Ignore Masses

Ignore Mass **1**	Monoisotopic **136.062320** Average **136.1346**
Composition	C(5) H(6) N(5)
	Symbols 13C 1 Add
Ignore Mass **2**	Monoisotopic **250.094014** Average **250.2340**
Composition	C(10) H(12) N(5) O(3)
	Symbols 13C 1 Add
Ignore Mass **3**	Monoisotopic **348.070910** Average **348.2292**
Composition	C(10) H(15) N(5) O(7) P
	Symbols 13C 1 Add
Ignore Mass **4**	Monoisotopic **428.037241** Average **428.2091**
Composition	C(10) H(16) N(5) O(10) P(2)
	Symbols 13C 1 Add

For all the modification sites these neutral losses are considered for scoring

Specificity

Specificity	Site	E	Position	Anywhere	Copy Delete	Hide Details
Classification	Other glycosylation		Hidden ☑		Group 5	
Notes						
Neutral loss	◉ Scoring ○ Satellite ○ Peptide ○ Required Peptide					Delete
	Monoisotopic: **541.061110** Average: **541.3005**					
Composition	C(15) H(21) N(5) O(13) P(2)			Symbols	13C 1	Add
Neutral loss	◉ Scoring ○ Satellite ○ Peptide ○ Required Peptide					Delete
	Monoisotopic: **347.063085** Average: **347.2212**					
Composition	C(10) H(14) N(5) O(7) P			Symbols	13C 1	Add

(*v*) *ADP-Rib-HCDm-NL347*

(mass shift of 541.0611 Da, ignored the marker masses at m/z 428.0372, 348.0709, 250.0940, 136.0623, neutral losses (NL) equal to 347.0631 from b and y ion series)

Delta

Monoisotopic	**541.061110**
Average	**541.3005**
Composition	C(15) H(21) N(5) O(13) P(2)
	Symbols 13C 1 Add

Specificity

Specificity	Site	E	Position	Anywhere
Specificity	Site	R	Position	Anywhere
Specificity	Site	K	Position	Anywhere
Specificity	Site	D	Position	Anywhere

Ignore Masses

Ignore Mass **1**	Monoisotopic **136.062320** Average **136.1346**
Composition	C(5) H(6) N(5)
	Symbols 13C 1 Add
Ignore Mass **2**	Monoisotopic **250.094014** Average **250.2340**
Composition	C(10) H(12) N(5) O(3)
	Symbols 13C 1 Add
Ignore Mass **3**	Monoisotopic **348.070910** Average **348.2292**
Composition	C(10) H(15) N(5) O(7) P
	Symbols 13C 1 Add
Ignore Mass **4**	Monoisotopic **428.037241** Average **428.2091**
Composition	C(10) H(16) N(5) O(10) P(2)
	Symbols 13C 1 Add

For all the modification sites these neutral losses are considered for scoring

Specificity

Specificity	Site	E	Position	Anywhere	Copy	Delete	Hide Details
Classification	Other glycosylation		Hidden ☑		Group	5	
Notes						
Neutral loss	◉ Scoring	○ Satellite	○ Peptide	○ Required Peptide		Delete
	Monoisotopic: **347.063085** Average: **347.2212**					
Composition	C(10) H(14) N(5) O(7) P				Symbols 13C 1 Add	

Supplementary Figure S2

HCD spectra of Biotin-KAARKSAPATGGVKKPHRYR + 1 ADP-ribose

A.

NCE 23%

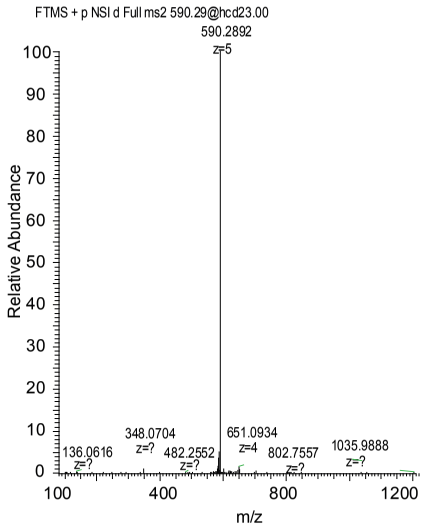

B.

NCE 30%

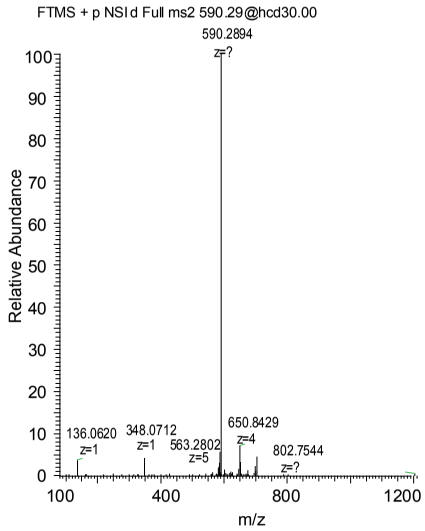

C.

NCE 38%

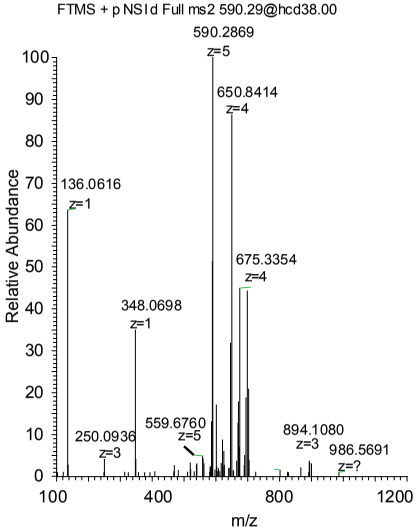

D.

NCE 45%

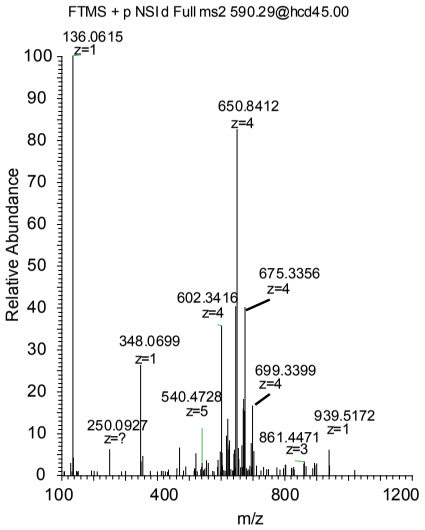

E.

NCE 52%

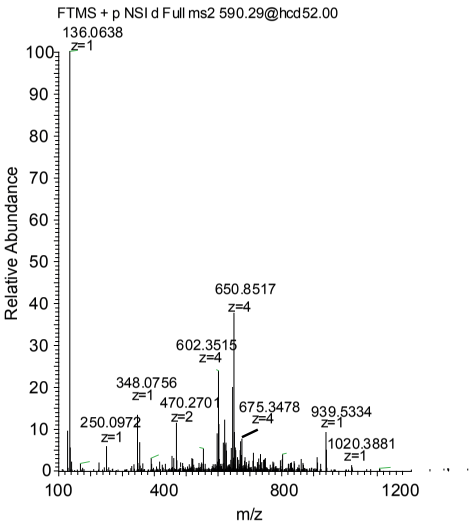

F.

NCE 60%

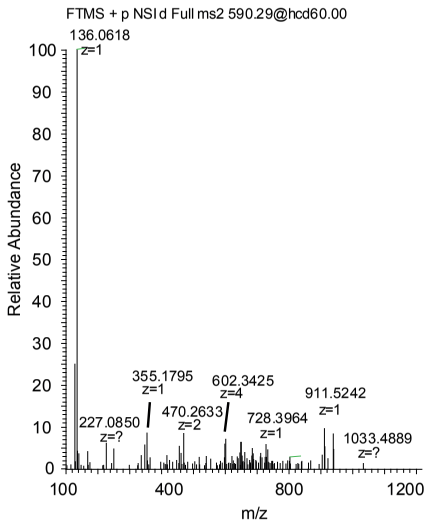

G.

NCE 40% (step width: 15%, 3 steps)

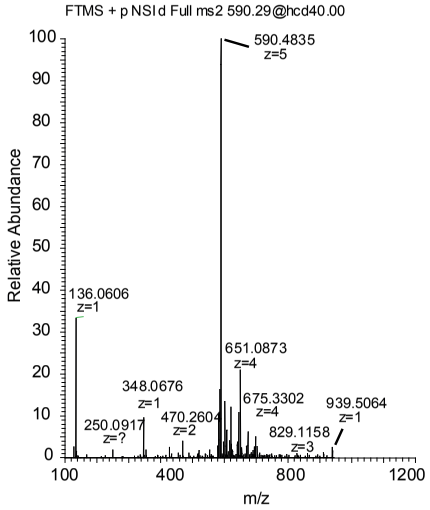

Supplementary Figure S3

Mascot Site Localization Analysis

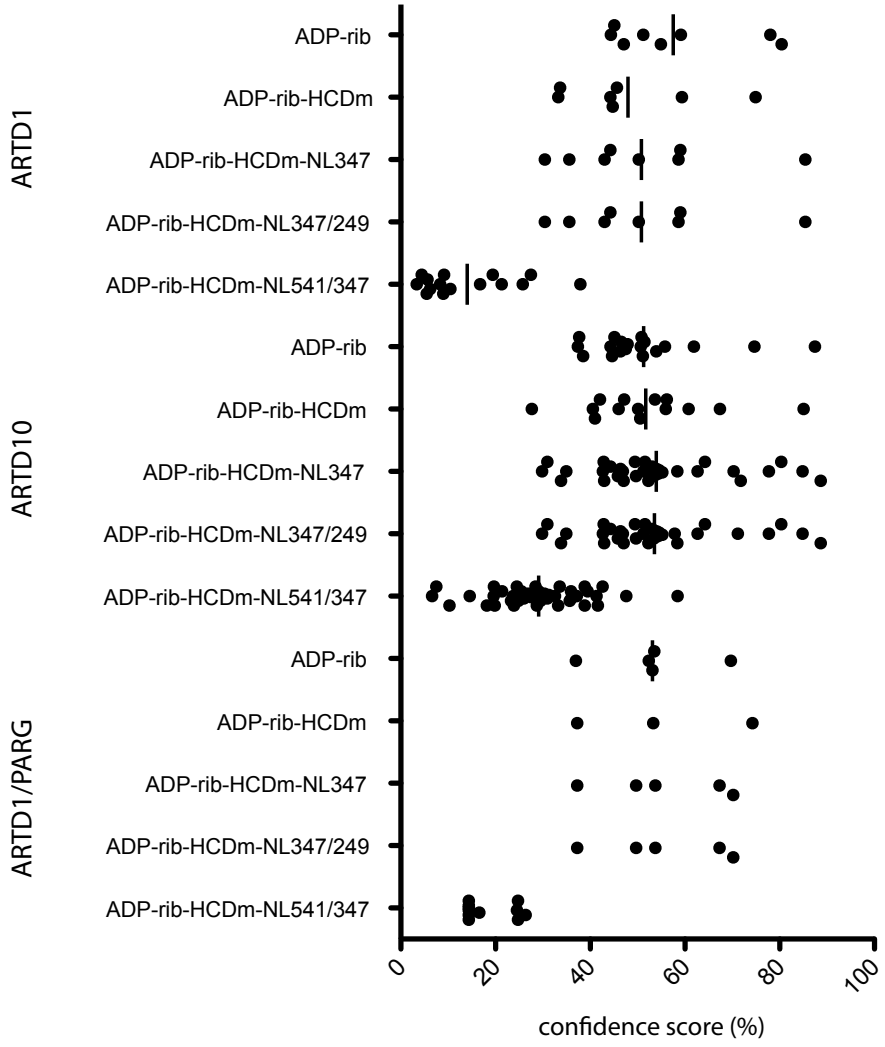

Supplementary Figure S4

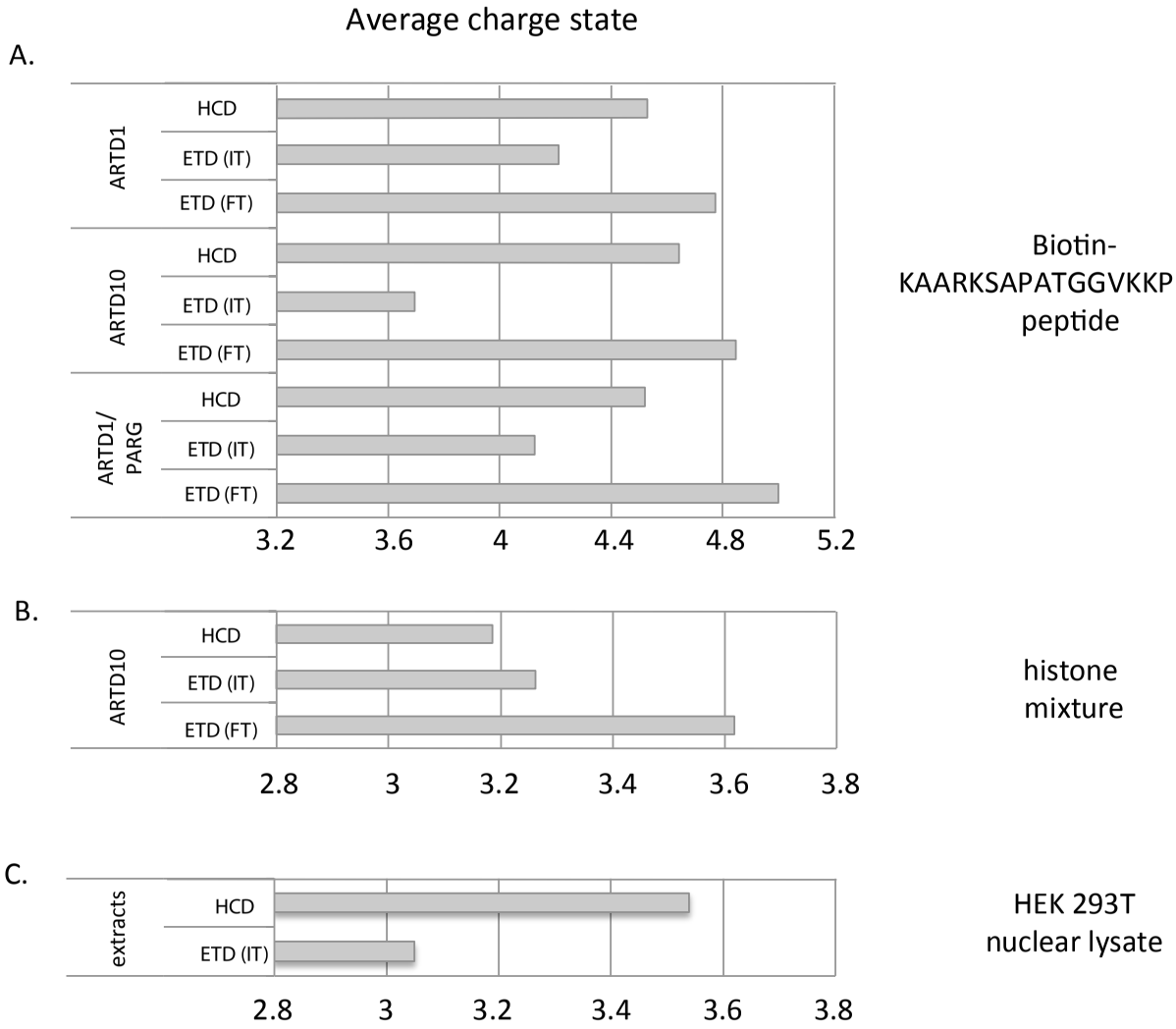

Supplementary Figure S5

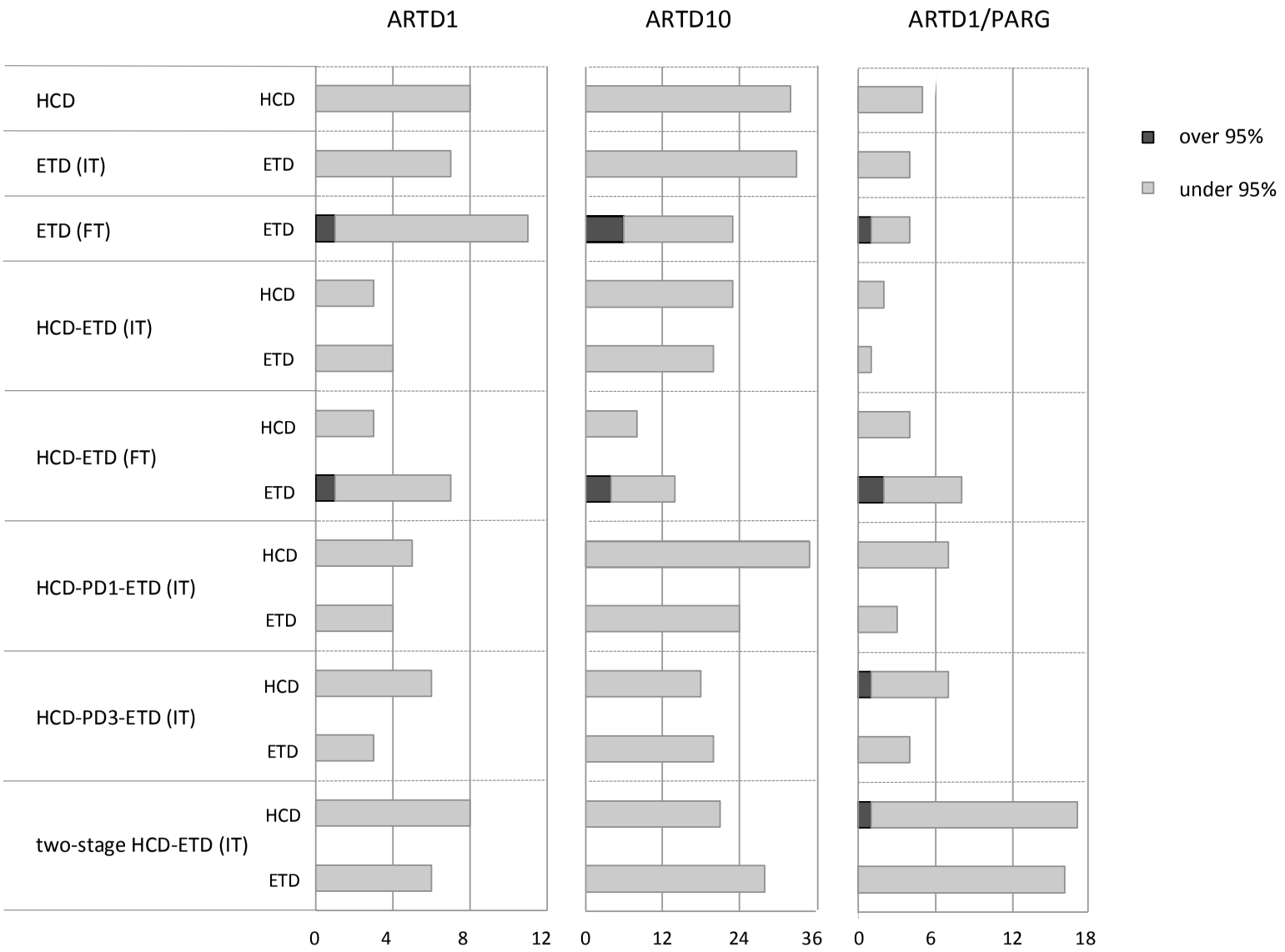

Supplementary Figure S6

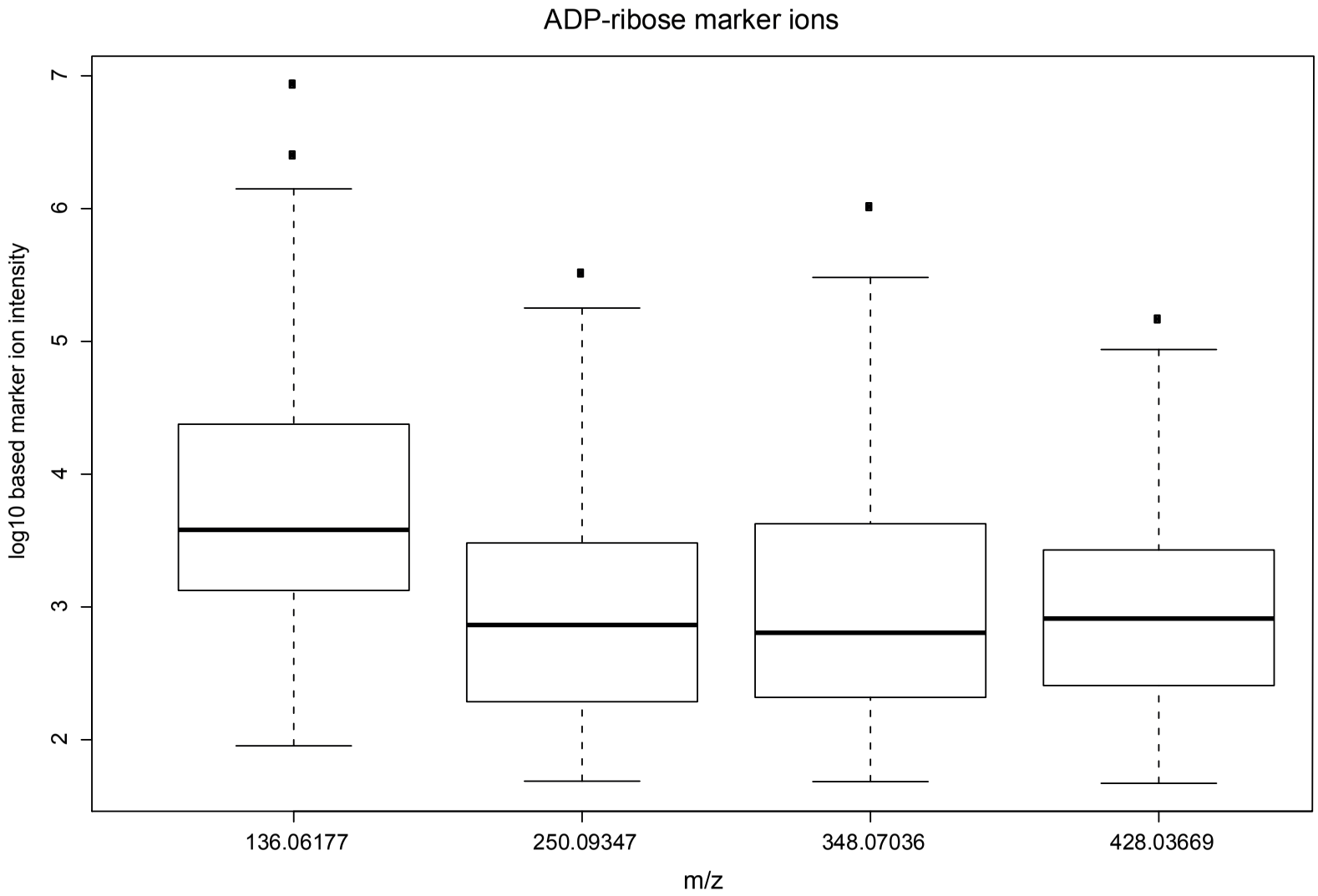

Supplementary Figure S7

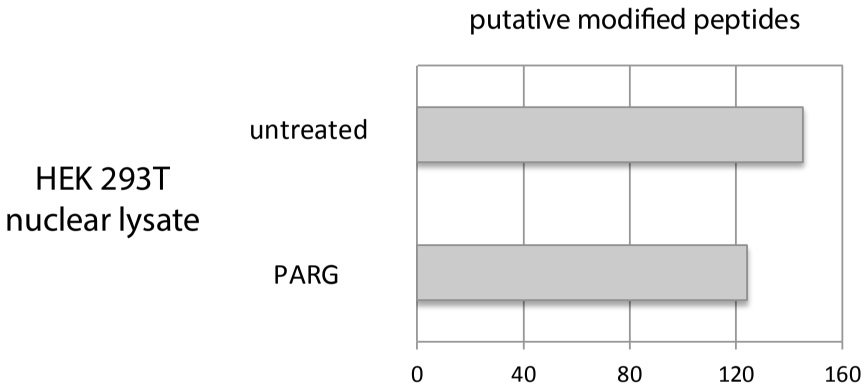

Supplementary figure S8

Spectra of ADP-ribosylated peptides identified in HEK 293T nuclear lysate

(score >20, Expect <0.05, Site localization confidence >95%)

Histone H1.2

K.K$_{[ADP\text{-}ribose]}$AAKSAAKAVKPK.A

20120817_13_frac6_PARG_HCD_ETD_inclusion #2091 RT: 20.47 AV: 1 NL: 4.85E4
T: FTMS + p NSI d Full ms2 460.48@hcd40.00 [100.00-1855.00]

m/z 460.4799, 4+

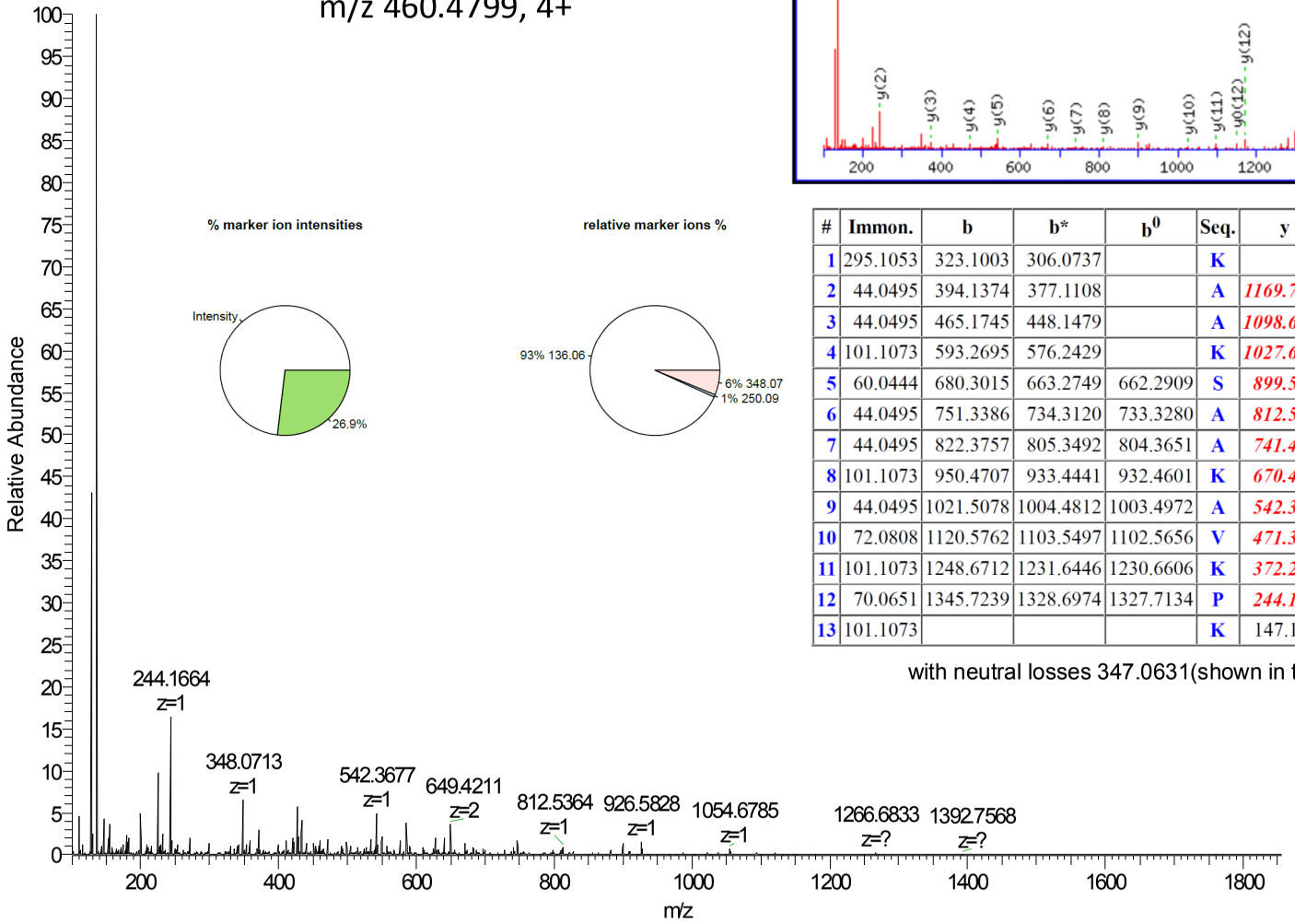

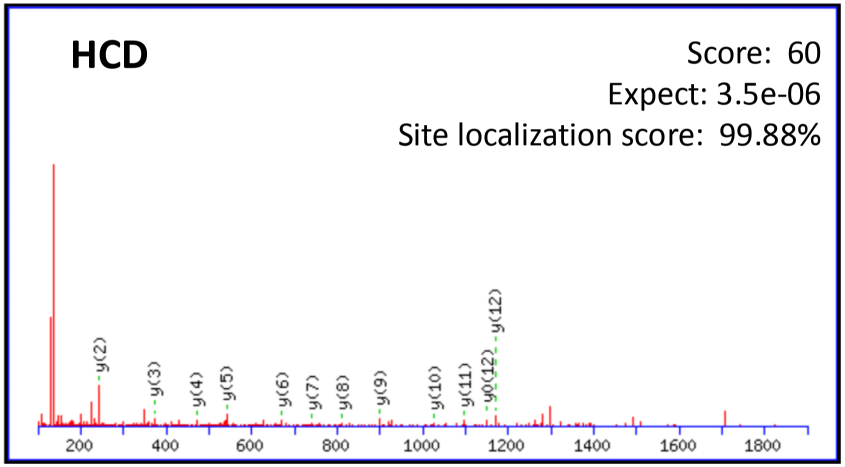

#	Immon.	b	b*	b^0	Seq.	y	y*	y^0	#
1	295.1053	323.1003	306.0737		K				13
2	44.0495	394.1374	377.1108		A	*1169.7365*	1152.7099	1151.7259	12
3	44.0495	465.1745	448.1479		A	*1098.6994*	1081.6728	1080.6888	11
4	101.1073	593.2695	576.2429		K	*1027.6622*	1010.6357	1009.6517	10
5	60.0444	680.3015	663.2749	662.2909	S	*899.5673*	882.5407	881.5567	9
6	44.0495	751.3386	734.3120	733.3280	A	*812.5353*	795.5087		8
7	44.0495	822.3757	805.3492	804.3651	A	*741.4981*	724.4716		7
8	101.1073	950.4707	933.4441	932.4601	K	*670.4610*	653.4345		6
9	44.0495	1021.5078	1004.4812	1003.4972	A	*542.3661*	525.3395		5
10	72.0808	1120.5762	1103.5497	1102.5656	V	*471.3289*	454.3024		4
11	101.1073	1248.6712	1231.6446	1230.6606	K	*372.2605*	355.2340		3
12	70.0651	1345.7239	1328.6974	1327.7134	P	*244.1656*	227.1390		2
13	101.1073				K	147.1128	130.0863		1

with neutral losses 347.0631(shown in table), 249.0862

Histone H2B

M.PE[ADP-ribose]PAKSAPAPKKGSK.K

20120817_02_frac3_PARG_HCD_ETD_inclusion #2183 RT: 21.10 AV: 1 NL: 3.00E4
T: FTMS + p NSI d Full ms2 678.64@hcd40.00 [100.00-2000.00]

m/z 678.6409,3+

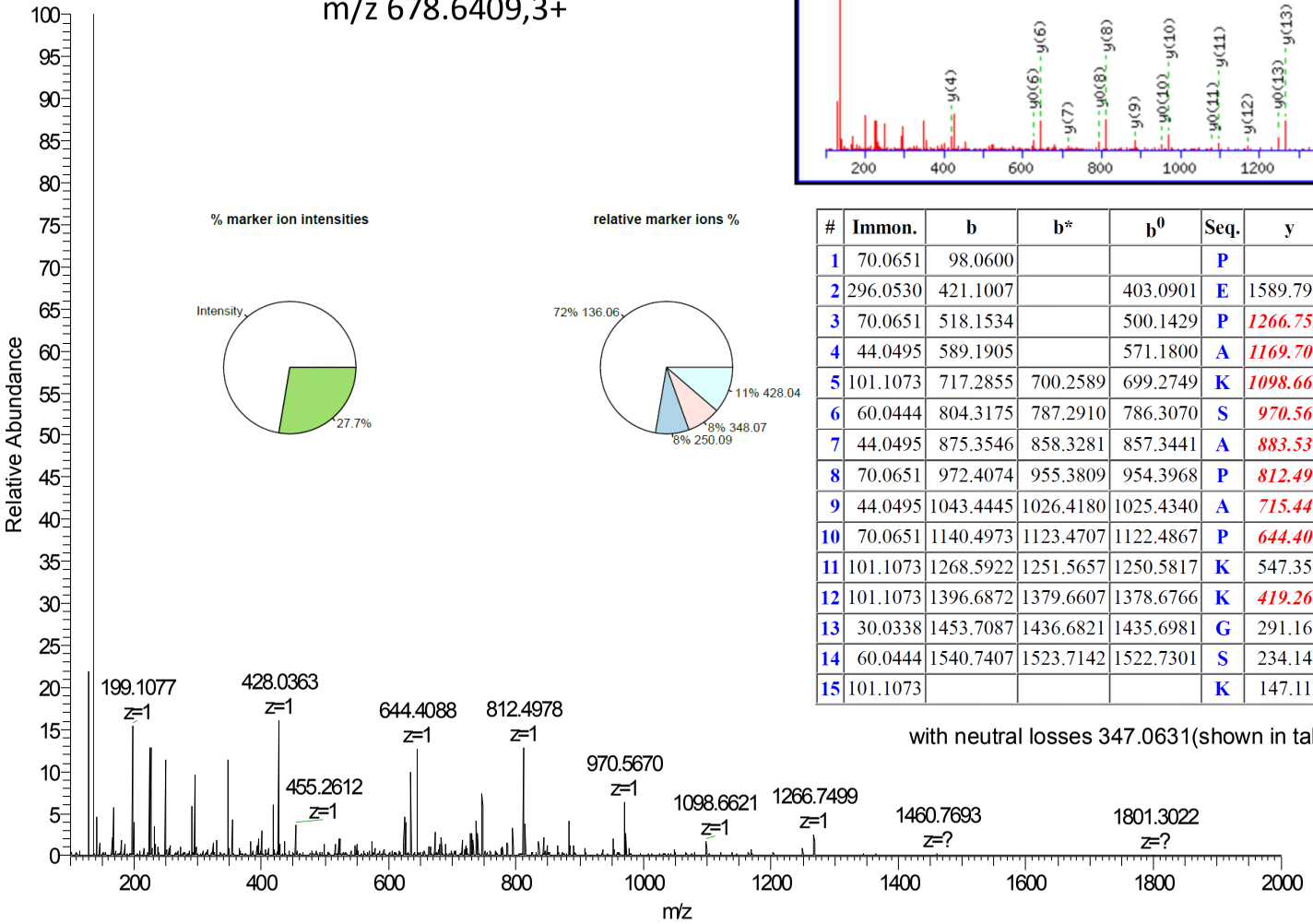

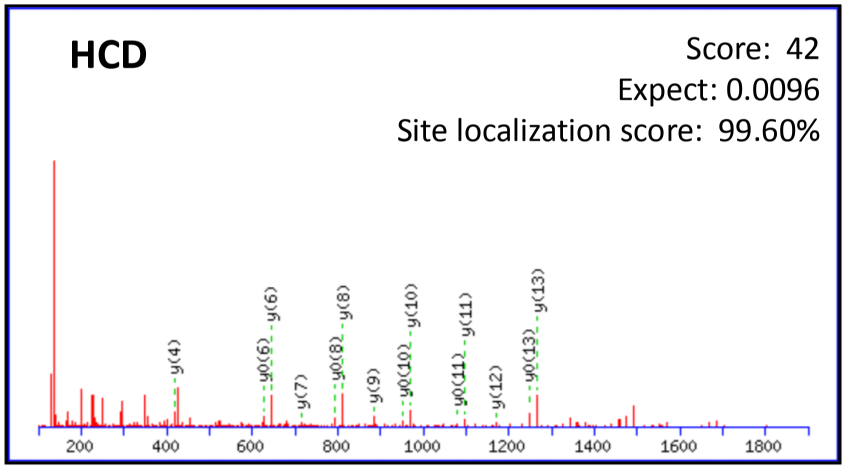

#	Immon.	b	b*	b^0	Seq.	y	y*	y^0	#
1	70.0651	98.0600			P				15
2	296.0530	421.1007		403.0901	E	1589.7935	1572.7669	1571.7829	14
3	70.0651	518.1534		500.1429	P	*1266.7528*	1249.7263	1248.7423	13
4	44.0495	589.1905		571.1800	A	*1169.7001*	1152.6735	1151.6895	12
5	101.1073	717.2855	700.2589	699.2749	K	*1098.6630*	1081.6364	1080.6524	11
6	60.0444	804.3175	787.2910	786.3070	S	*970.5680*	953.5415	952.5574	10
7	44.0495	875.3546	858.3281	857.3441	A	*883.5360*	866.5094	865.5254	9
8	70.0651	972.4074	955.3809	954.3968	P	*812.4989*	795.4723	794.4883	8
9	44.0495	1043.4445	1026.4180	1025.4340	A	*715.4461*	698.4196	697.4355	7
10	70.0651	1140.4973	1123.4707	1122.4867	P	*644.4090*	627.3824	626.3984	6
11	101.1073	1268.5922	1251.5657	1250.5817	K	547.3562	530.3297	529.3457	5
12	101.1073	1396.6872	1379.6607	1378.6766	K	*419.2613*	402.2347	401.2507	4
13	30.0338	1453.7087	1436.6821	1435.6981	G	291.1663	274.1397	273.1557	3
14	60.0444	1540.7407	1523.7142	1522.7301	S	234.1448	217.1183	216.1343	2
15	101.1073				K	147.1128	130.0863		1

with neutral losses 347.0631(shown in table), 249.0862

Histone H2B

M.PDPAK[ADP-ribose]SAPAPKKGSK.K

20120817_04_frac4_PARG_HCD_ETD_inclusion #2911 RT: 27.76 AV: 1 NL: 4.58E3
T: FTMS + p NSI d Full ms2 673.97@hcd40.00 [100.00-2000.00]

m/z 673.9697,3+

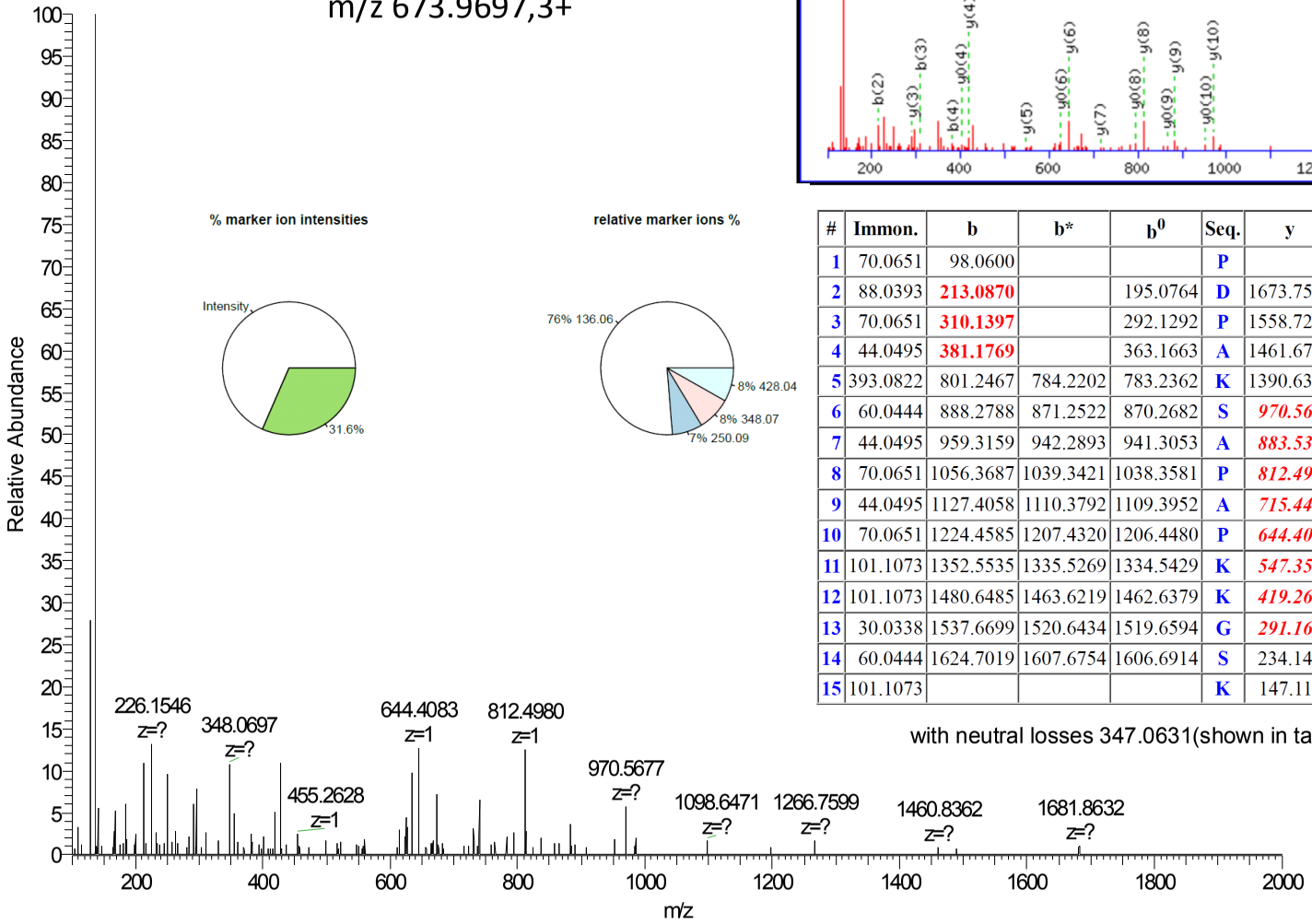

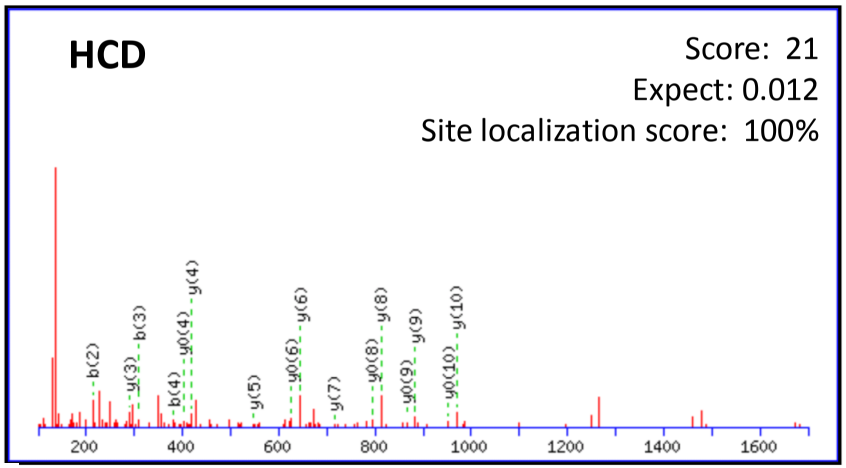

#	Immon.	b	b*	b^0	Seq.	y	y*	y^0	#
1	70.0651	98.0600			P				15
2	88.0393	**213.0870**		195.0764	D	1673.7547	1656.7282	1655.7441	14
3	70.0651	**310.1397**		292.1292	P	1558.7278	1541.7012	1540.7172	13
4	44.0495	**381.1769**		363.1663	A	1461.6750	1444.6485	1443.6644	12
5	393.0822	801.2467	784.2202	783.2362	K	1390.6379	1373.6113	1372.6273	11
6	60.0444	888.2788	871.2522	870.2682	S	***970.5680***	953.5415	952.5574	10
7	44.0495	959.3159	942.2893	941.3053	A	***883.5360***	866.5094	865.5254	9
8	70.0651	1056.3687	1039.3421	1038.3581	P	***812.4989***	795.4723	794.4883	8
9	44.0495	1127.4058	1110.3792	1109.3952	A	***715.4461***	698.4196	697.4355	7
10	70.0651	1224.4585	1207.4320	1206.4480	P	***644.4090***	627.3824	626.3984	6
11	101.1073	1352.5535	1335.5269	1334.5429	K	***547.3562***	530.3297	529.3457	5
12	101.1073	1480.6485	1463.6219	1462.6379	K	***419.2613***	402.2347	401.2507	4
13	30.0338	1537.6699	1520.6434	1519.6594	G	***291.1663***	274.1397	273.1557	3
14	60.0444	1624.7019	1607.6754	1606.6914	S	234.1448	217.1183	216.1343	2
15	101.1073				K	147.1128	130.0863		1

with neutral losses 347.0631(shown in table), 249.0862

Histone H2B

M.PDPAK$_{[ADP\text{-}ribose]}$SAPAPKKGSKK.A

20120817_03_frac4_HCD_ETD_inclusion #2181 RT: 21.04 AV: 1 NL: 4.54E5
T: FTMS + p NSI d Full ms2 537.76@hcd40.00 [100.00-2000.00]

m/z 537.7525,4+

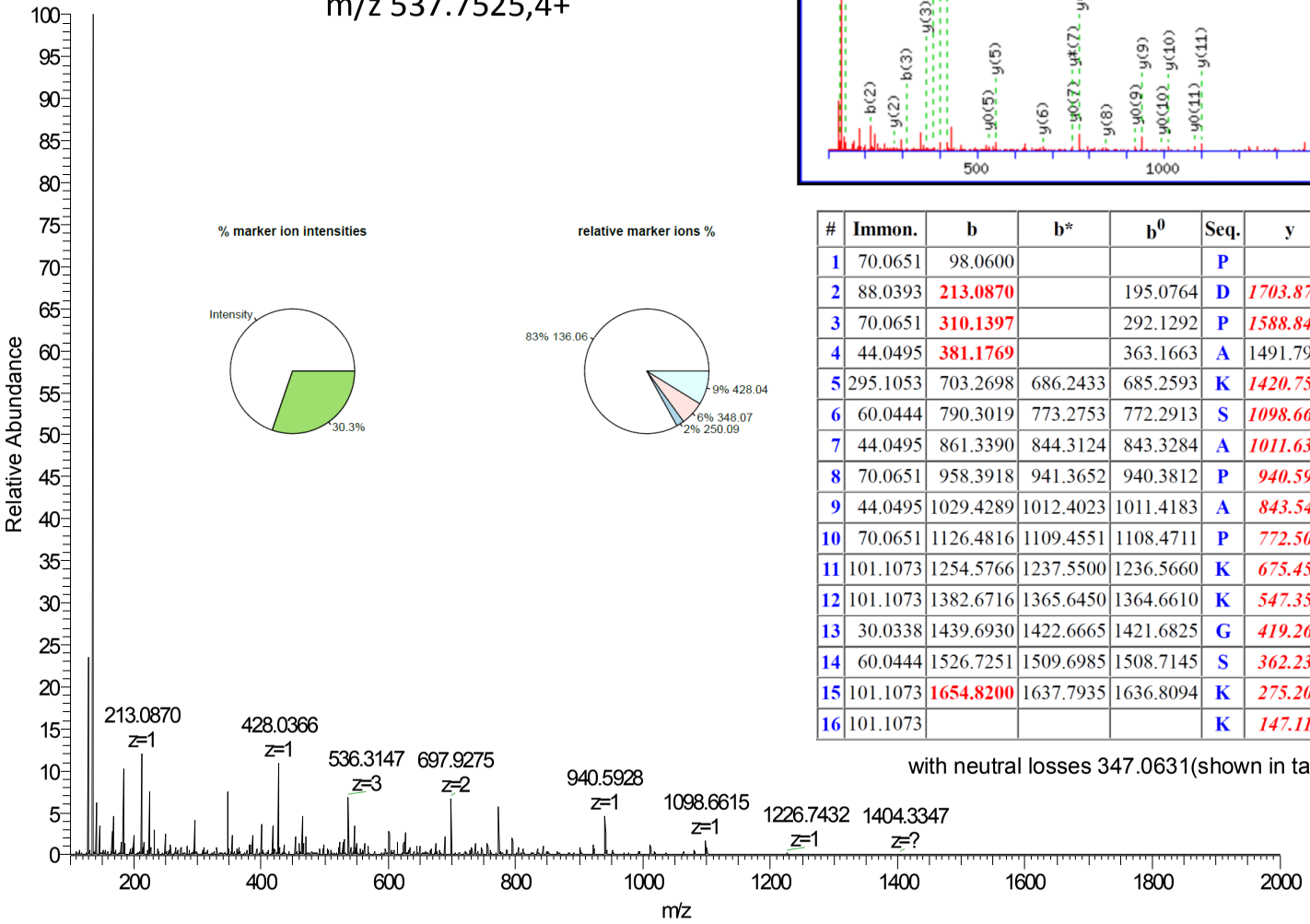

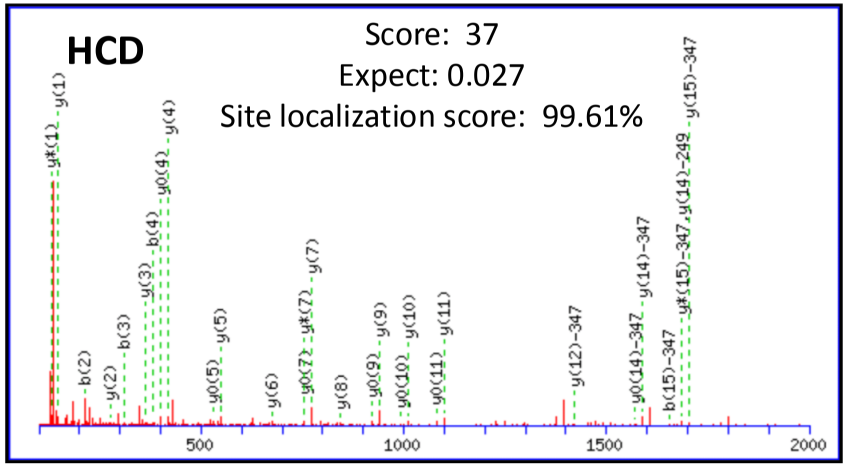

#	Immon.	b	b*	b^0	Seq.	y	y*	y^0	#
1	70.0651	98.0600			P				16
2	88.0393	**213.0870**		195.0764	D	*1703.8728*	1686.8462	1685.8622	15
3	70.0651	**310.1397**		292.1292	P	*1588.8458*	1571.8193	1570.8353	14
4	44.0495	**381.1769**		363.1663	A	1491.7931	1474.7665	1473.7825	13
5	295.1053	703.2698	686.2433	685.2593	K	*1420.7560*	1403.7294	1402.7454	12
6	60.0444	790.3019	773.2753	772.2913	S	*1098.6630*	1081.6364	1080.6524	11
7	44.0495	861.3390	844.3124	843.3284	A	*1011.6309*	994.6044	993.6204	10
8	70.0651	958.3918	941.3652	940.3812	P	*940.5938*	923.5673	922.5833	9
9	44.0495	1029.4289	1012.4023	1011.4183	A	*843.5411*	826.5145	825.5305	8
10	70.0651	1126.4816	1109.4551	1108.4711	P	*772.5039*	755.4774	754.4934	7
11	101.1073	1254.5766	1237.5500	1236.5660	K	*675.4512*	658.4246	657.4406	6
12	101.1073	1382.6716	1365.6450	1364.6610	K	*547.3562*	530.3297	529.3457	5
13	30.0338	1439.6930	1422.6665	1421.6825	G	*419.2613*	402.2347	401.2507	4
14	60.0444	1526.7251	1509.6985	1508.7145	S	*362.2398*	345.2132	344.2292	3
15	101.1073	**1654.8200**	1637.7935	1636.8094	K	*275.2078*	258.1812		2
16	101.1073				K	*147.1128*	130.0863		1

with neutral losses 347.0631(shown in table), 249.0862

Histone H2B

M.PE[ADP-ribose]PTKSAPAPKKGSK.K

20120817_01_frac3_HCD_ETD_inclusion #2198 RT: 21.09 AV: 1 NL: 3.53E5
T: FTMS + p NSI d Full ms2 688.64@hcd40.00 [100.00-2000.00]

m/z 688.6425,3+

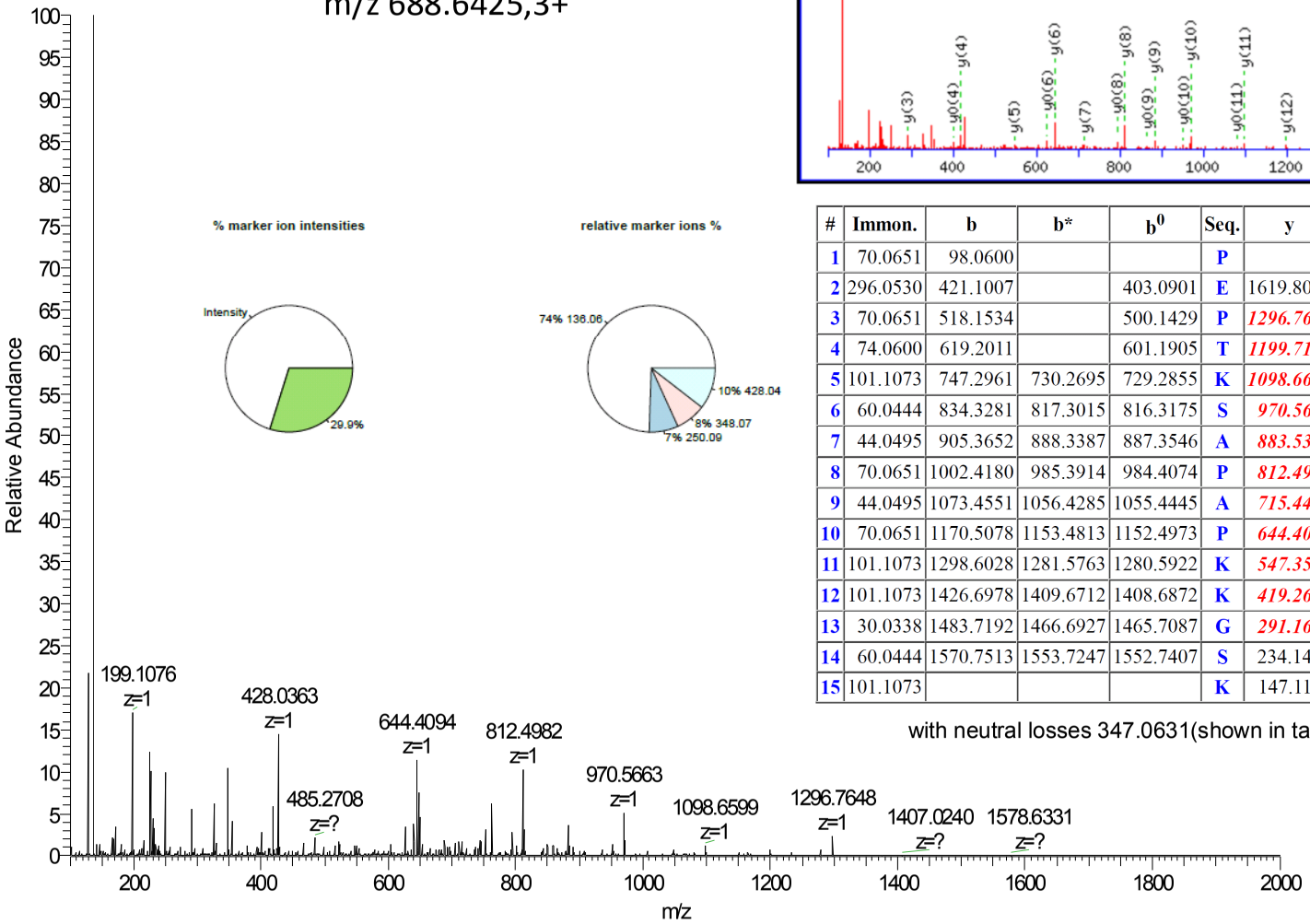

HCD

Score: 50
Expect: 0.0018
Site localization score: 96.98%

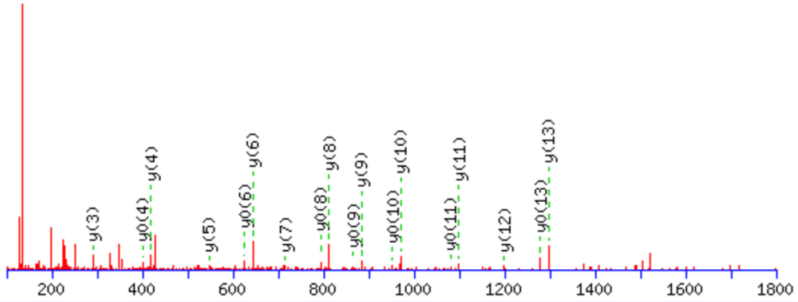

#	Immon.	b	b*	b^0	Seq.	y	y*	y^0	#
1	70.0651	98.0600			P				15
2	296.0530	421.1007		403.0901	E	1619.8040	1602.7775	1601.7935	14
3	70.0651	518.1534		500.1429	P	*1296.7634*	1279.7369	1278.7528	13
4	74.0600	619.2011		601.1905	T	*1199.7106*	1182.6841	1181.7001	12
5	101.1073	747.2961	730.2695	729.2855	K	*1098.6630*	1081.6364	1080.6524	11
6	60.0444	834.3281	817.3015	816.3175	S	*970.5680*	953.5415	952.5574	10
7	44.0495	905.3652	888.3387	887.3546	A	*883.5360*	866.5094	865.5254	9
8	70.0651	1002.4180	985.3914	984.4074	P	*812.4989*	795.4723	794.4883	8
9	44.0495	1073.4551	1056.4285	1055.4445	A	*715.4461*	698.4196	697.4355	7
10	70.0651	1170.5078	1153.4813	1152.4973	P	*644.4090*	627.3824	626.3984	6
11	101.1073	1298.6028	1281.5763	1280.5922	K	*547.3562*	530.3297	529.3457	5
12	101.1073	1426.6978	1409.6712	1408.6872	K	*419.2613*	402.2347	401.2507	4
13	30.0338	1483.7192	1466.6927	1465.7087	G	*291.1663*	274.1397	273.1557	3
14	60.0444	1570.7513	1553.7247	1552.7407	S	234.1448	217.1183	216.1343	2
15	101.1073				K	147.1128	130.0863		1

with neutral losses 347.0631(shown in table), 249.0862

Histone H2B

M.PEPTK[ADP-ribose]SAPAPKKGSK.K

20120817_02_frac3_PARG_HCD_ETD_inclusion #2199 RT: 21.27 AV: 1 NL: 5.75E4
T: ITMS + c NSI d sa Full ms2 688.64@etd66.67 [50.00-2000.00]

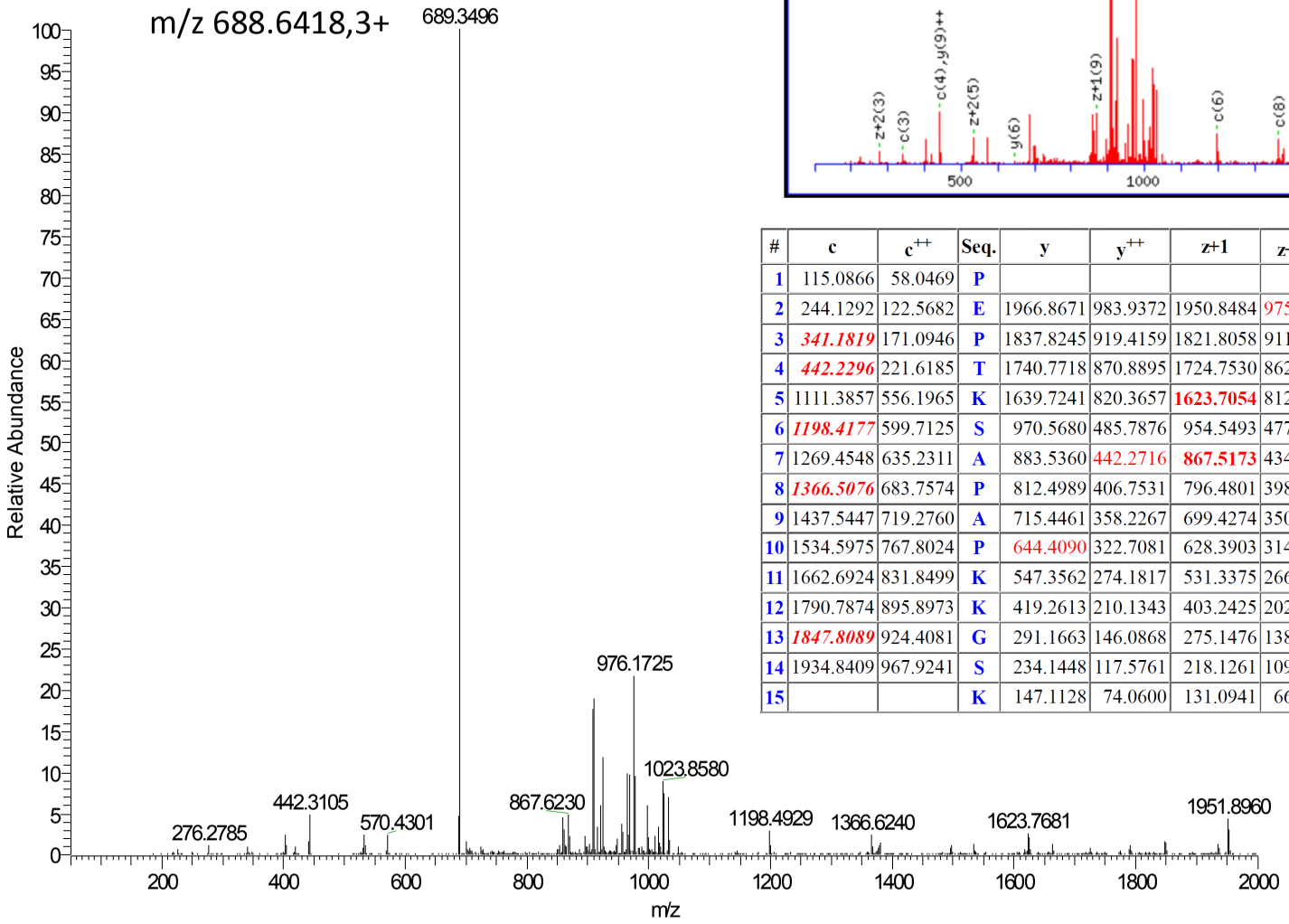

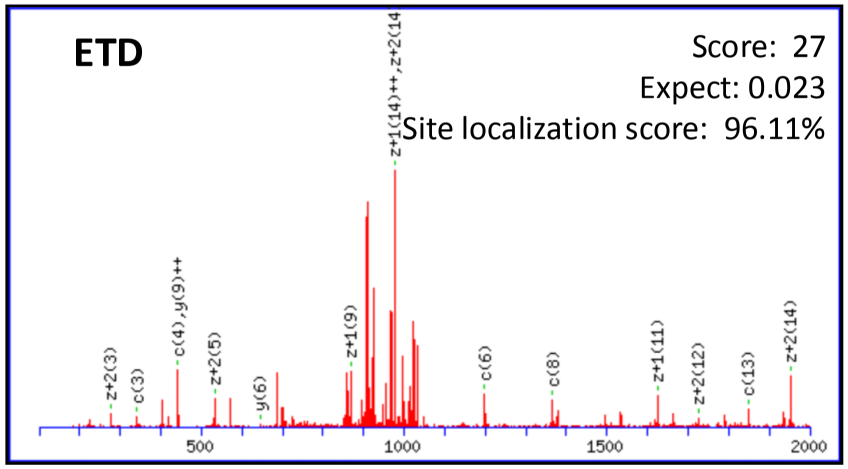

#	c	c^{++}	Seq.	y	y^{++}	z+1	$z+1^{++}$	z+2	$z+2^{++}$	#
1	115.0866	58.0469	P							15
2	244.1292	122.5682	E	1966.8671	983.9372	1950.8484	975.9278	***1951.8562***	976.4317	14
3	***341.1819***	171.0946	P	1837.8245	919.4159	1821.8058	911.4065	1822.8136	911.9104	13
4	***442.2296***	221.6185	T	1740.7718	870.8895	1724.7530	862.8802	***1725.7609***	863.3841	12
5	1111.3857	556.1965	K	1639.7241	820.3657	**1623.7054**	812.3563	1624.7132	812.8602	11
6	***1198.4177***	599.7125	S	970.5680	485.7876	954.5493	477.7783	955.5571	478.2822	10
7	1269.4548	635.2311	A	883.5360	442.2716	**867.5173**	434.2623	868.5251	434.7662	9
8	***1366.5076***	683.7574	P	812.4989	406.7531	796.4801	398.7437	797.4880	399.2476	8
9	1437.5447	719.2760	A	715.4461	358.2267	699.4274	350.2173	700.4352	350.7212	7
10	1534.5975	767.8024	P	644.4090	322.7081	628.3903	314.6988	629.3981	315.2027	6
11	1662.6924	831.8499	K	547.3562	274.1817	531.3375	266.1724	***532.3453***	266.6763	5
12	1790.7874	895.8973	K	419.2613	210.1343	403.2425	202.1249	404.2504	202.6288	4
13	***1847.8089***	924.4081	G	291.1663	146.0868	275.1476	138.0774	***276.1554***	138.5813	3
14	1934.8409	967.9241	S	234.1448	117.5761	218.1261	109.5667	219.1339	110.0706	2
15			K	147.1128	74.0600	131.0941	66.0507	132.1019	66.5546	1

Corresponding HCD scan

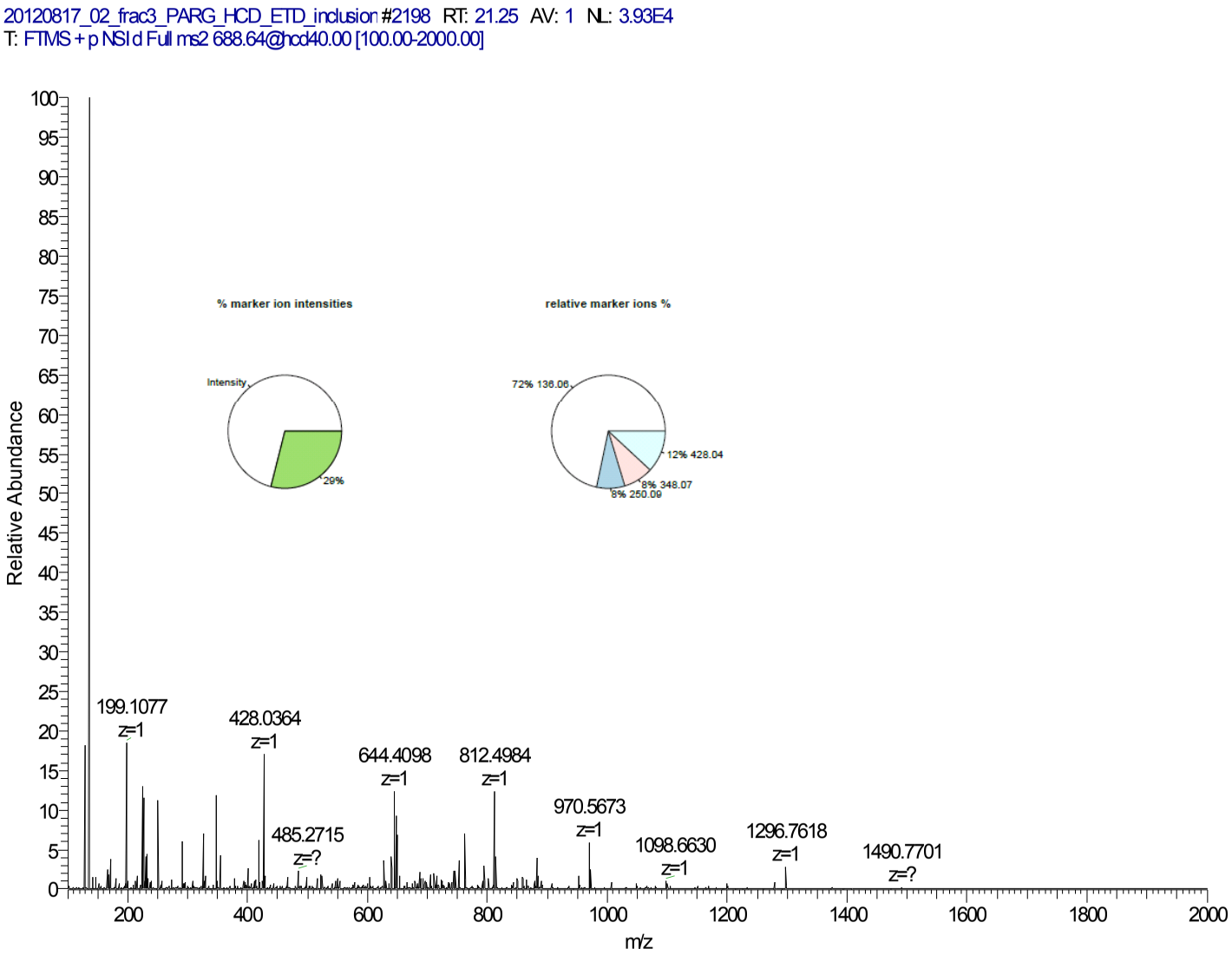

Histone H2B

M.PE$_{[ADP\text{-}ribose]}$LAKSAPAPKKGSK.K

20120817_07_frac5_PARG_HCD_ETD_inclusion #3123 RT: 29.81 AV: 1 NL: 1.23E4
T: FTMS + p NSI d Full ms2 683.98@hcd40.00 [100.00-2000.00]

m/z 683.9858,3+

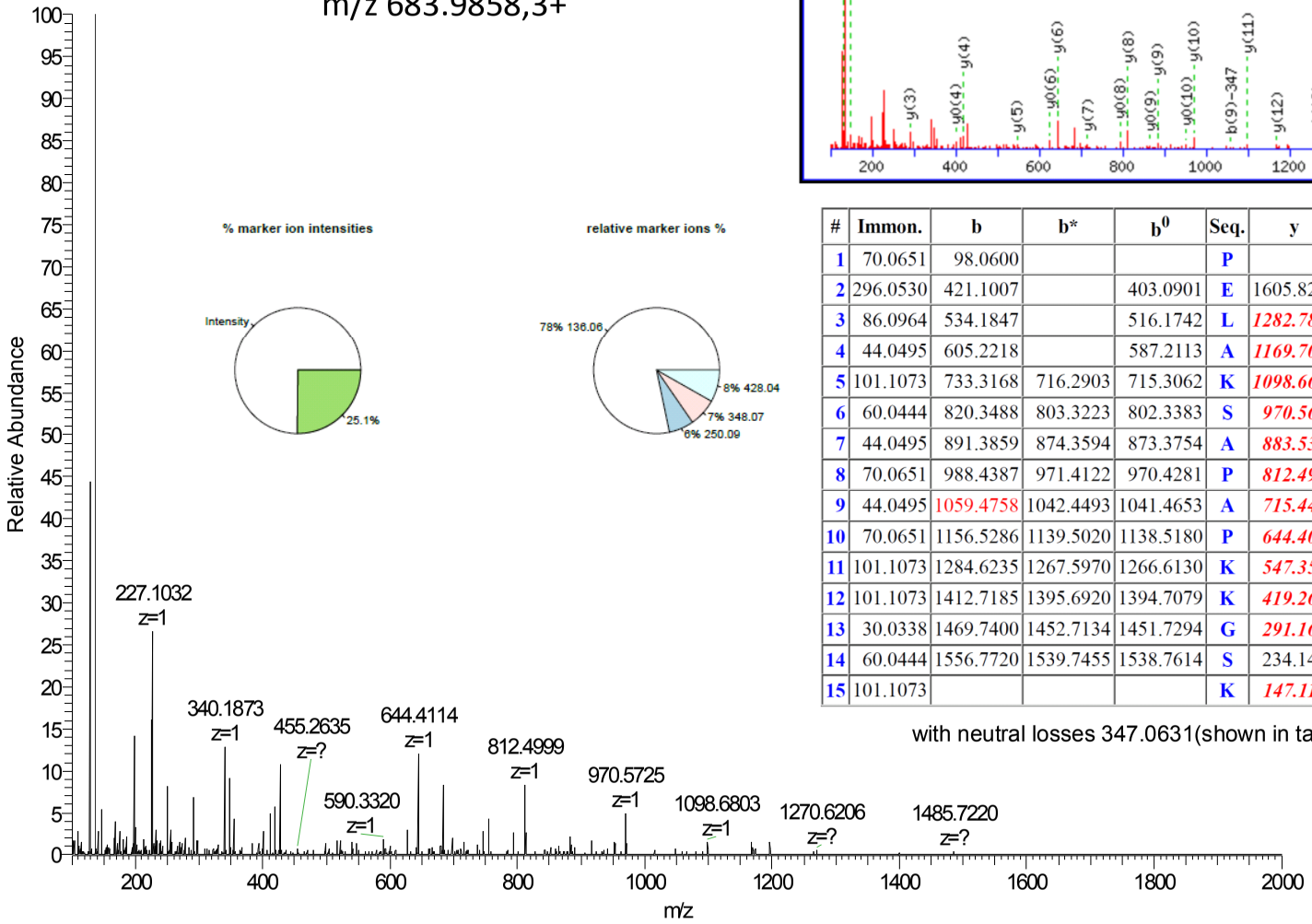

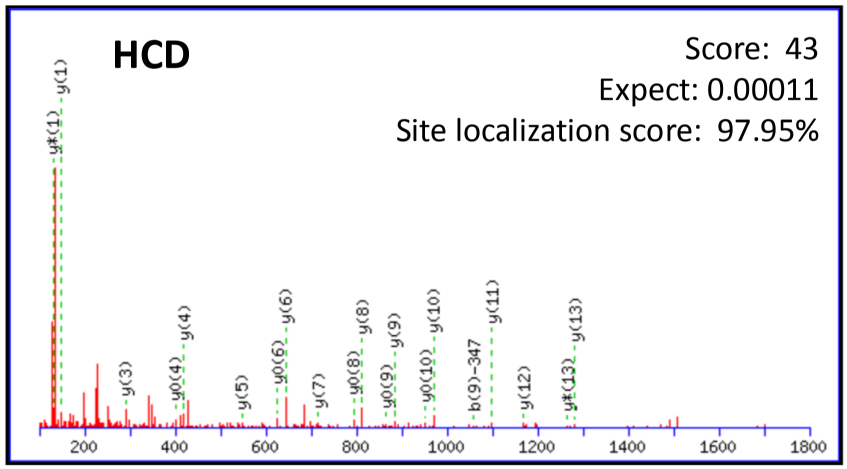

#	Immon.	b	b*	b^0	Seq.	y	y*	y^0	#
1	70.0651	98.0600			P				15
2	296.0530	421.1007		403.0901	E	1605.8248	1588.7982	1587.8142	14
3	86.0964	534.1847		516.1742	L	*1282.7841*	1265.7576	1264.7736	13
4	44.0495	605.2218		587.2113	A	*1169.7001*	1152.6735	1151.6895	12
5	101.1073	733.3168	716.2903	715.3062	K	*1098.6630*	1081.6364	1080.6524	11
6	60.0444	820.3488	803.3223	802.3383	S	*970.5680*	953.5415	952.5574	10
7	44.0495	891.3859	874.3594	873.3754	A	*883.5360*	866.5094	865.5254	9
8	70.0651	988.4387	971.4122	970.4281	P	*812.4989*	795.4723	794.4883	8
9	44.0495	1059.4758	1042.4493	1041.4653	A	*715.4461*	698.4196	697.4355	7
10	70.0651	1156.5286	1139.5020	1138.5180	P	*644.4090*	627.3824	626.3984	6
11	101.1073	1284.6235	1267.5970	1266.6130	K	*547.3562*	530.3297	529.3457	5
12	101.1073	1412.7185	1395.6920	1394.7079	K	*419.2613*	402.2347	401.2507	4
13	30.0338	1469.7400	1452.7134	1451.7294	G	*291.1663*	274.1397	273.1557	3
14	60.0444	1556.7720	1539.7455	1538.7614	S	234.1448	217.1183	216.1343	2
15	101.1073				K	*147.1128*	130.0863		1

with neutral losses 347.0631(shown in table), 249.0862

Histone H2B

M.PE$_{[ADP\text{-}ribose]}$PSKSAPAPKKGSK.K

20120817_02_frac3_PARG_HCD_ETD_inclusion #2178 RT: 21.05 AV: 1 NL: 3.96E4
T: FTMS + p NSI d Full ms2 683.97@hcd40.00 [100.00-2000.00]

m/z 683.9722,3+

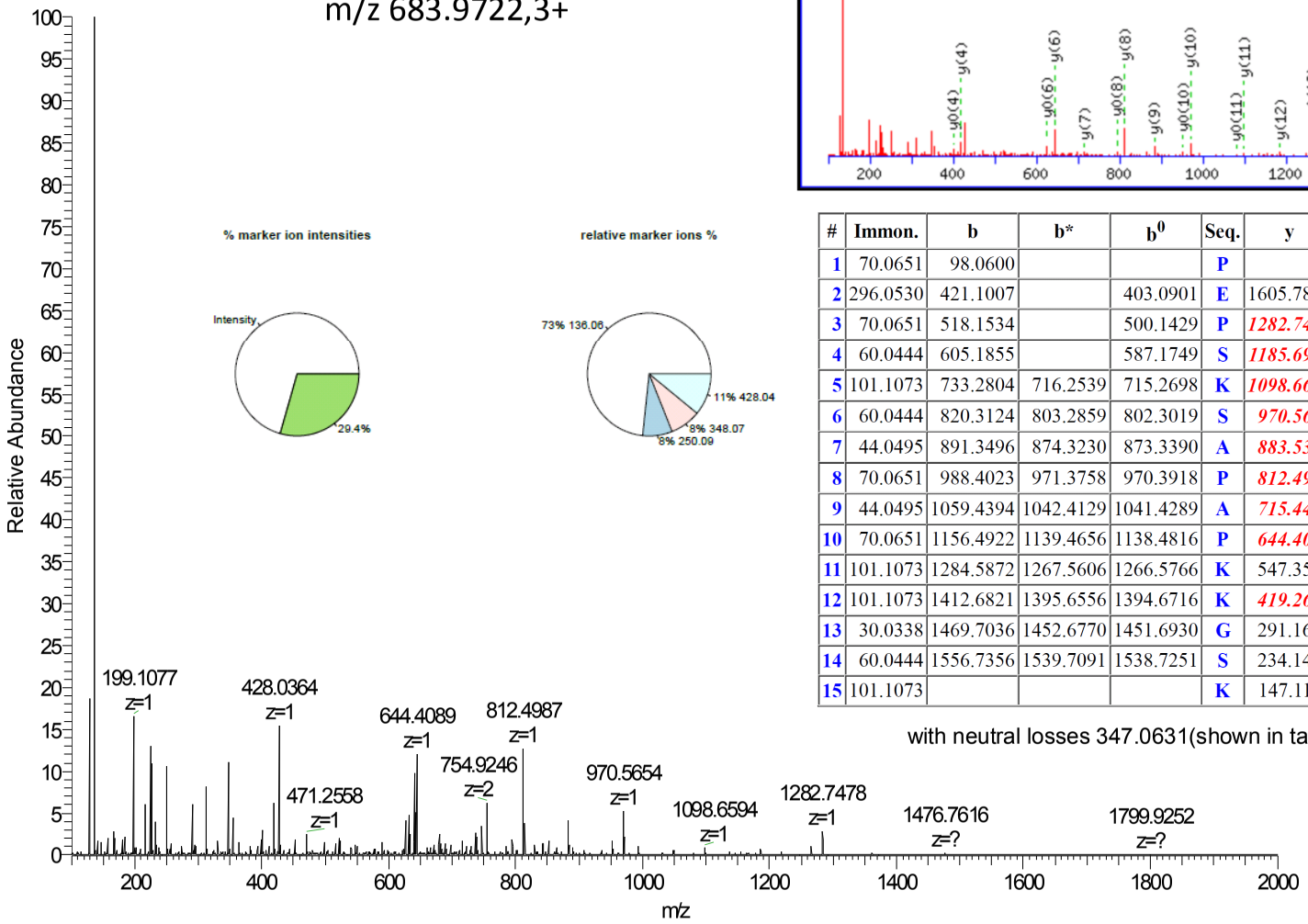

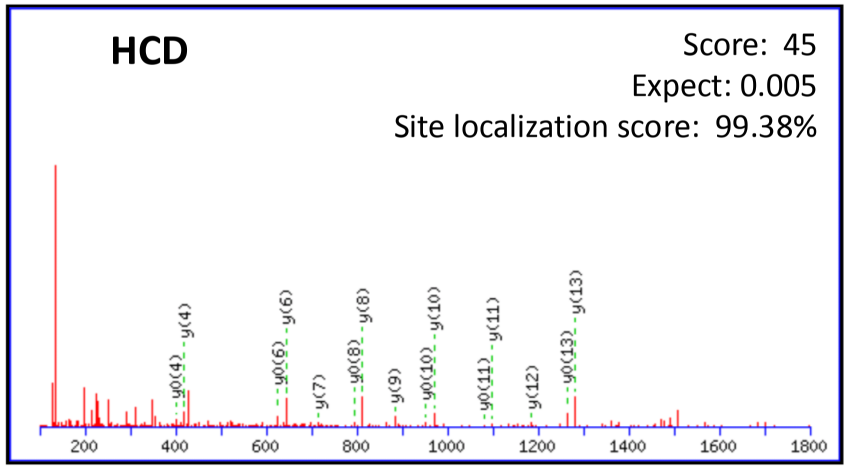

#	Immon.	b	b*	b^0	Seq.	y	y*	y^0	#
1	70.0651	98.0600			P				15
2	296.0530	421.1007		403.0901	E	1605.7884	1588.7618	1587.7778	14
3	70.0651	518.1534		500.1429	P	*1282.7478*	1265.7212	1264.7372	13
4	60.0444	605.1855		587.1749	S	*1185.6950*	1168.6684	1167.6844	12
5	101.1073	733.2804	716.2539	715.2698	K	*1098.6630*	1081.6364	1080.6524	11
6	60.0444	820.3124	803.2859	802.3019	S	*970.5680*	953.5415	952.5574	10
7	44.0495	891.3496	874.3230	873.3390	A	*883.5360*	866.5094	865.5254	9
8	70.0651	988.4023	971.3758	970.3918	P	*812.4989*	795.4723	794.4883	8
9	44.0495	1059.4394	1042.4129	1041.4289	A	*715.4461*	698.4196	697.4355	7
10	70.0651	1156.4922	1139.4656	1138.4816	P	*644.4090*	627.3824	626.3984	6
11	101.1073	1284.5872	1267.5606	1266.5766	K	547.3562	530.3297	529.3457	5
12	101.1073	1412.6821	1395.6556	1394.6716	K	*419.2613*	402.2347	401.2507	4
13	30.0338	1469.7036	1452.6770	1451.6930	G	291.1663	274.1397	273.1557	3
14	60.0444	1556.7356	1539.7091	1538.7251	S	234.1448	217.1183	216.1343	2
15	101.1073				K	147.1128	130.0863		1

with neutral losses 347.0631(shown in table), 249.0862

KHDR1

R.SSGR$_{[ADP\text{-}ribose]}$SGSMDPSGAHPSVR.Q

20120817_01_frac3_HCD_ETD_inclusion #3894 RT: 37.26 AV: 1 NL: 5.31E4
T: FTMS + p NSI d Full ms2 771.63@hcd40.00 [100.00-2000.00]

m/z 771.6260,3+

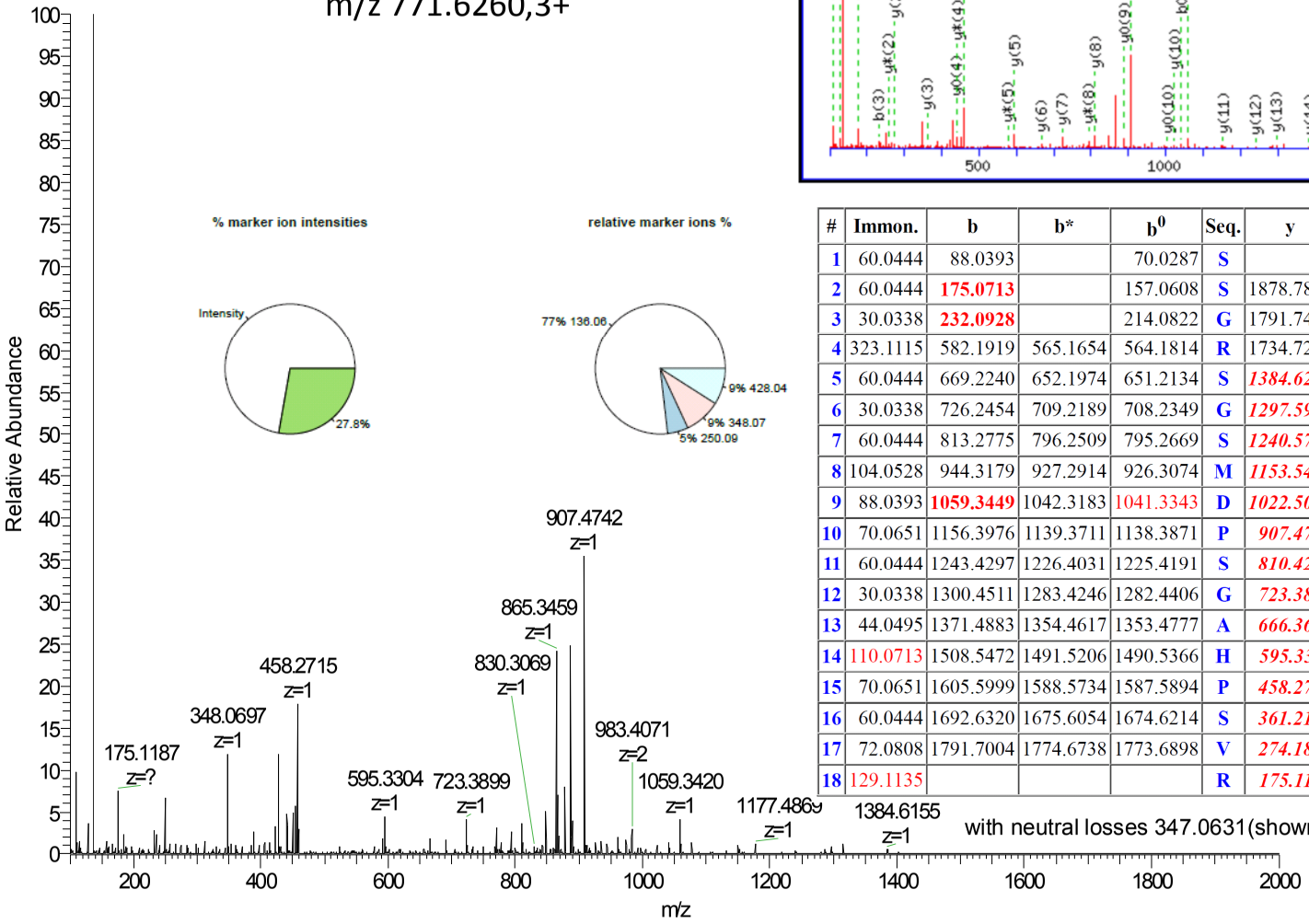

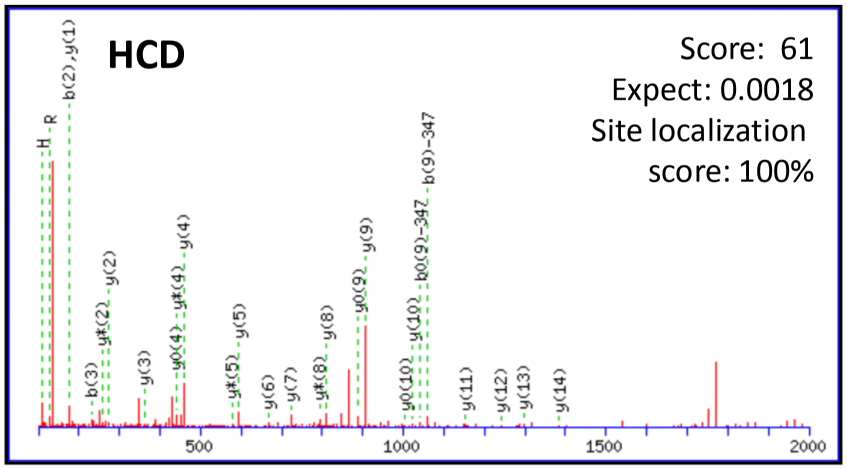

#	Immon.	b	b*	b^0	Seq.	y	y*	y^0	#
1	60.0444	88.0393		70.0287	S				18
2	60.0444	**175.0713**		157.0608	S	1878.7800	1861.7535	1860.7695	17
3	30.0338	**232.0928**		214.0822	G	1791.7480	1774.7214	1773.7374	16
4	323.1115	582.1919	565.1654	564.1814	R	1734.7265	1717.7000	1716.7160	15
5	60.0444	669.2240	652.1974	651.2134	S	***1384.6274***	1367.6008	1366.6168	14
6	30.0338	726.2454	709.2189	708.2349	G	***1297.5954***	1280.5688	1279.5848	13
7	60.0444	813.2775	796.2509	795.2669	S	***1240.5739***	1223.5473	1222.5633	12
8	104.0528	944.3179	927.2914	926.3074	M	***1153.5419***	1136.5153	1135.5313	11
9	88.0393	**1059.3449**	1042.3183	1041.3343	D	***1022.5014***	1005.4748	1004.4908	10
10	70.0651	1156.3976	1139.3711	1138.3871	P	***907.4744***	890.4479	889.4639	9
11	60.0444	1243.4297	1226.4031	1225.4191	S	***810.4217***	793.3951	792.4111	8
12	30.0338	1300.4511	1283.4246	1282.4406	G	***723.3896***	706.3631	705.3791	7
13	44.0495	1371.4883	1354.4617	1353.4777	A	***666.3682***	649.3416	648.3576	6
14	110.0713	1508.5472	1491.5206	1490.5366	H	***595.3311***	578.3045	577.3205	5
15	70.0651	1605.5999	1588.5734	1587.5894	P	***458.2722***	441.2456	440.2616	4
16	60.0444	1692.6320	1675.6054	1674.6214	S	***361.2194***	344.1928	343.2088	3
17	72.0808	1791.7004	1774.6738	1773.6898	V	***274.1874***	257.1608		2
18	129.1135				R	***175.1190***	158.0924		1

with neutral losses 347.0631(shown in table), 249.0862

Histone 3

K.STGGK$_{[ADP\text{-}ribose]}$APRKQLATK.A

20120817_05_frac5_HCD_ETD_inclusion #2360 RT: 22.57 AV: 1 NL: 1.05E4
T: ITMS + c NSI d sa Full ms2 661.98@etd66.67 [50.00-2000.00]

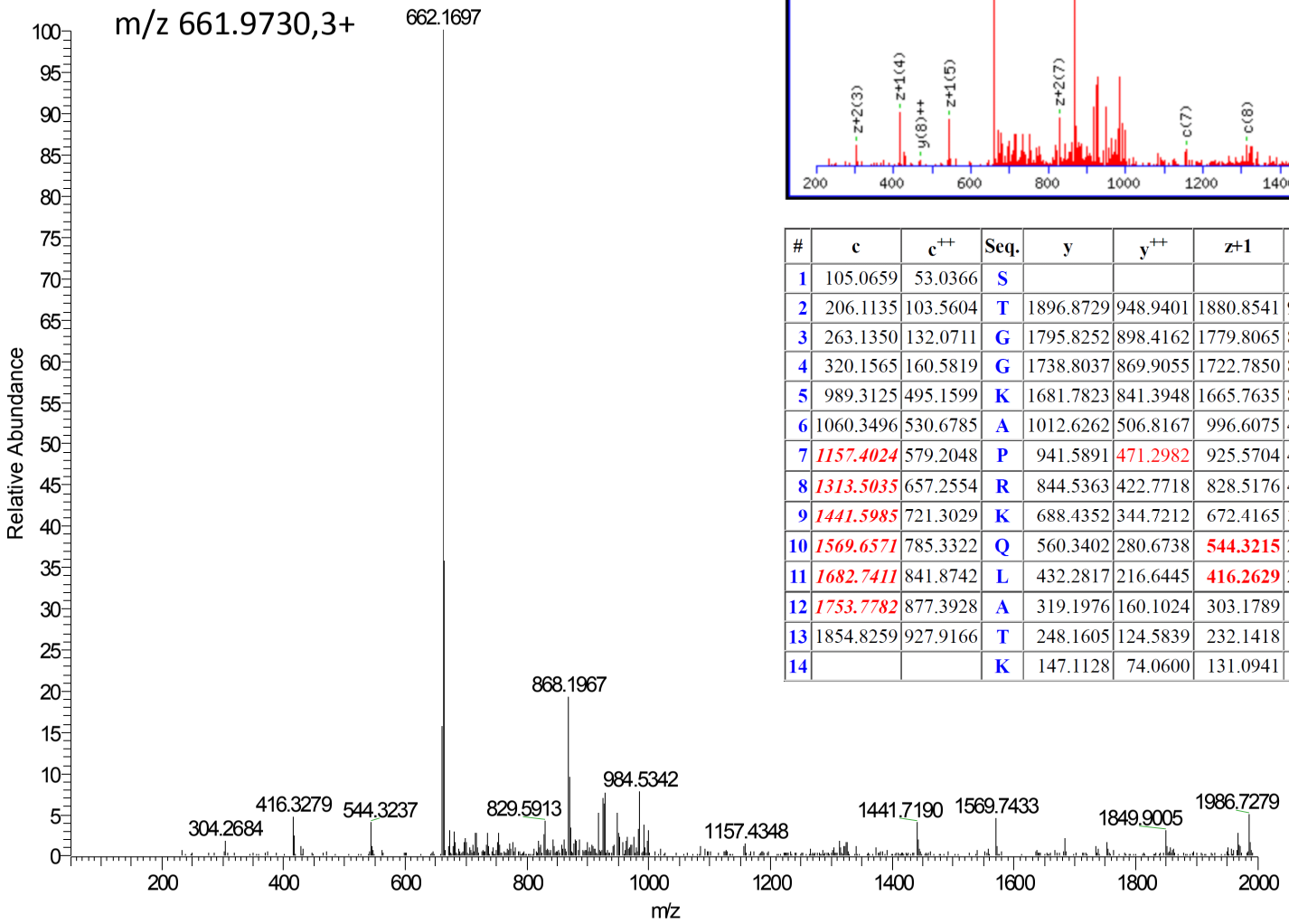

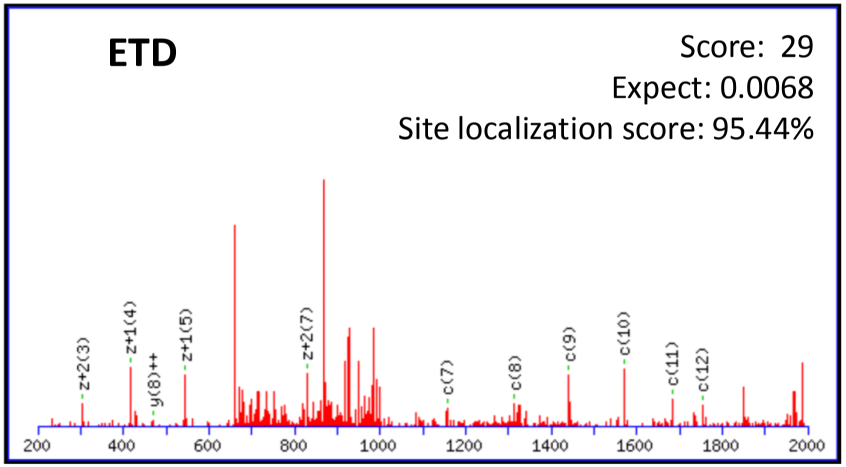

#	c	c^{++}	Seq.	y	y^{++}	z+1	$z+1^{++}$	z+2	$z+2^{++}$	#
1	105.0659	53.0366	S							14
2	206.1135	103.5604	T	1896.8729	948.9401	1880.8541	940.9307	1881.8620	941.4346	13
3	263.1350	132.0711	G	1795.8252	898.4162	1779.8065	890.4069	1780.8143	890.9108	12
4	320.1565	160.5819	G	1738.8037	869.9055	1722.7850	861.8961	1723.7928	862.4001	11
5	989.3125	495.1599	K	1681.7823	841.3948	1665.7635	833.3854	1666.7714	833.8893	10
6	1060.3496	530.6785	A	1012.6262	506.8167	996.6075	498.8074	997.6153	499.3113	9
7	*1157.4024*	579.2048	P	941.5891	471.2982	925.5704	463.2888	926.5782	463.7927	8
8	*1313.5035*	657.2554	R	844.5363	422.7718	828.5176	414.7624	**829.5254**	415.2663	7
9	*1441.5985*	721.3029	K	688.4352	344.7212	672.4165	336.7119	673.4243	337.2158	6
10	*1569.6571*	785.3322	Q	560.3402	280.6738	**544.3215**	272.6644	545.3293	273.1683	5
11	*1682.7411*	841.8742	L	432.2817	216.6445	**416.2629**	208.6351	417.2708	209.1390	4
12	*1753.7782*	877.3928	A	319.1976	160.1024	303.1789	152.0931	**304.1867**	152.5970	3
13	1854.8259	927.9166	T	248.1605	124.5839	232.1418	116.5745	233.1496	117.0784	2
14			K	147.1128	74.0600	131.0941	66.0507	132.1019	66.5546	1

Corresponding HCD scan

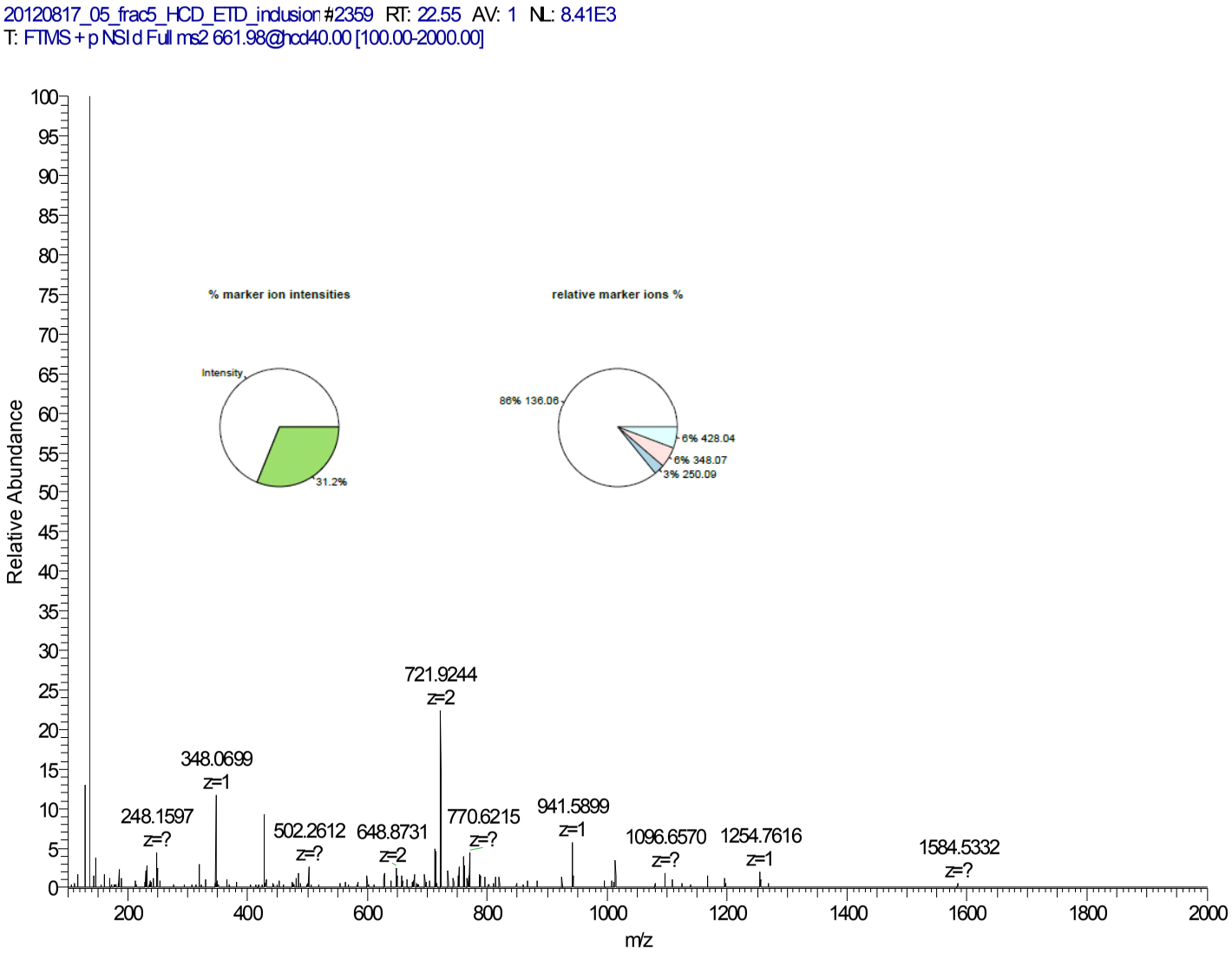

Table S1: List of ADP-ribosylated peptides with unambiguous site localization (>95%)

protein description	peptide sequence	pep mz	charge	peptide mr	pep score	expect value	confidence	protein accession	No. of identif.
ARTD10	ASLSVQD(R)YSPPNADGHKAVFVAR	782.3515	4+	3125.3769	24.84	0.016	98.00%	tr|F5H462|F5H462_HUMAN	1
ARTD10	LAENTGEFQ(E)VVR	1016.9038	2+	2031.7931	63.04	0.0000016	97.25%	tr|F5H462|F5H462_HUMAN	2
ARTD10	RASLSVQDRYSPPNADGH(K)AVFVAR	657.3004	5+	3281.4657	68.12	0.00000041	99.91%	tr|F5H462|F5H462_HUMAN	1
ARTD10	RPV(E)QVLYHGTTAPAVPDICAHGFNR	780.1174	4+	3116.4406	132.4	3.9E-13	99.92%	tr|F5H462|F5H462_HUMAN	3
Histone H1.4	GTGASGSF(K)LNKK	502.9108	3+	1505.7105	26.6	0.024	100.00%	sp|P10412|H14_HUMAN	1
Histone H1.4	IKLGL(K)SLVSK	466.6051	3+	1396.7934	49.02	0.00024	99.83%	sp|P10412|H14_HUMAN	1
Histone H2A type 1	ND(E)ELNKLLGK	605.2515	3+	1812.7326	55.21	0.000017	97.52%	sp|P0C0S8|H2A1_HUMAN	8
Histone H2A type 1	VGAGAPVYLAAVL(E)YLTAEILELAGNAAR	1152.8849	3+	3455.6328	59.51	0.0000026	100.00%	sp|P0C0S8|H2A1_HUMAN	6
Histone H2A type 1-B/E	VGAGAPVYLAAVL(E)YLTAEILELAGNAARDNKK	789.1868	5+	3940.8978	58.73	0.0000031	99.87%	sp|P04908|H2A1B_HUMAN	5
Histone H2A type 2-A	AGLQFPVG(R)VHR	516.9292	3+	1547.7658	44.59	0.0016	99.75%	sp|Q6FI13|H2A2A_HUMAN	1
Histone H2A type 2-A	HLQLAIRND(E)ELNK	635.6425	3+	1903.9055	64.76	0.000004	96.04%	sp|Q6FI13|H2A2A_HUMAN	1
Histone H2A type 2-A	HLQLAIRND(E)ELNKLLGK	579.8024	4+	2315.1804	118.5	1.8E-11	98.17%	sp|Q6FI13|H2A2A_HUMAN	3
Histone H2A type 2-A	HLQLAIRNDE(E)LNKLLGK	662.068	4+	2644.2429	78.07	0.000000078	95.31%	sp|Q6FI13|H2A2A_HUMAN	1
Histone H2A type 2-A	HLQLAIRNDEELNKLLG(K)VTIAQGGVLPNIQAVLLPK	1140.1075	4+	4556.4011	55.5	0.0006	98.55%	sp|Q6FI13|H2A2A_HUMAN	1
Histone H2A type 2-A	SS(R)AGLQFPVGR	496.24	3+	1485.6981	39.93	0.0028	100.00%	sp|Q6FI13|H2A2A_HUMAN	3
Histone H2A type 2-A	VGAGAPVYMAAVL(E)YLTAEILELAGNAAR	787.1387	4+	3144.5258	80.45	0.00000011	99.50%	sp|Q6FI13|H2A2A_HUMAN	1
Histone H2A type 2-A	VH(R)LLRK	488.2288	3+	1461.6645	20.19	0.016	100.00%	sp|Q6FI13|H2A2A_HUMAN	1
Histone H2A.Z	HLQLAIRGDE(E)LDSLIK	831.0441	3+	2490.1104	83.63	0.000000017	96.39%	sp|P0C0S5|H2AZ_HUMAN	1
Histone H2A.Z	VGATAAVYSAAIL(E)YLTAEVLELAGNASK	1146.1967	3+	3435.5681	40.12	0.00017	98.99%	sp|P0C0S5|H2AZ_HUMAN	2
Histone H2B	SRKESYSVYVY(K)	683.9482	3+	2048.8227	21.66	0.011	96.67%	tr|B4DLA9|B4DLA9_HUMAN	1
Histone H2B type 1-K	EIQTAV(R)LLLPGELAK	764.7081	3+	2291.1026	27.09	0.0047	99.21%	sp|O60814|H2B1K_HUMAN	1
Histone H2B type 1-K	IAGEAS(R)LAHYNKR	450.2217	4+	1796.8577	78.93	0.0000036	99.54%	sp|O60814|H2B1K_HUMAN	2
Histone H2B type 1-K	LLLPG(E)LAK	498.8919	3+	1493.6538	20.76	0.014	95.85%	sp|O60814|H2B1K_HUMAN	1
Histone H2B type 1-K	QVHPDTGISS(K)AMGIMNSFVNDIFER	859.371	4+	3433.4548	31.52	0.0011	100.00%	sp|O60814|H2B1K_HUMAN	13
Histone H2B type 1-K	VL(K)QVHPDTGISSK	574.288	3+	1719.8421	36.91	0.004	100.00%	sp|O60814|H2B1K_HUMAN	9
Histone H2B type 3-B	AMGIMNSFVNDIF(E)R	1142.9469	2+	2283.8792	85.79	0.000000009	97.57%	sp|Q8N257|H2B3B_HUMAN	6
Histone H2B type F-S	(E)IQTAVRLLLPGELAK	764.7075	3+	2291.1007	43.21	0.000089	97.64%	sp|P57053|H2BFS_HUMAN	1
Histone H2B type F-S	K(E)SYSVYVYK	602.9035	3+	1805.6887	60.56	0.0000075	97.89%	sp|P57053|H2BFS_HUMAN	2
Histone H2B type F-S	LLLPG(E)LAK	498.8943	3+	1493.661	22.09	0.013	96.55%	sp|P57053|H2BFS_HUMAN	1
Histone H3.1	(E)IAQDFKTDLR	626.2538	3+	1875.7397	33.82	0.0016	99.68%	sp|P68431|H31_HUMAN	7
Histone H3.1	EIAQDF(K)TDLR	626.2534	3+	1875.7382	37.47	0.036	96.17%	sp|P68431|H31_HUMAN	3
Histone H3.1	FQSSAV(M)ALQE(A)CEAYLVGLFEDTNLCAIHAKR	1075.7166	4+	4298.8371	85.94	8.8E-09	97.25%	sp|P68431|H31_HUMAN	1
Histone H3.1	FQSSAV(M)ALQEACEAYLVG(L)FEDTNLCAIHAK	1272.2459	3+	3813.7157	27.24	0.012	97.04%	sp|P68431|H31_HUMAN	1
Histone H3.1	FQSSAVMALQEACEAYLVGLF(E)DTNLCAIHAK	950.431	4+	3797.6948	55.98	0.00001	99.59%	sp|P68431|H31_HUMAN	1
Histone H3.1	KLPFQ(R)LVR	456.9174	3+	1367.7304	35.94	0.0055	98.90%	sp|P68431|H31_HUMAN	1
Histone H3.1	KPH(R)YRPGTVALR	523.7462	4+	2090.9555	45.37	0.004	95.83%	sp|P68431|H31_HUMAN	1
Histone H3.1	LVREIAQDFKTDL(R)	749.0035	3+	2243.9888	60.75	0.00021	99.94%	sp|P68431|H31_HUMAN	2
Histone H3.1	RVTIMP(K)DIQLAR	584.9741	3+	1751.9004	48.56	0.001	99.86%	sp|P68431|H31_HUMAN	4
Histone H3.1	YRPGTVAL(R)EIRR	450.486	4+	1797.9147	66.27	0.000046	96.81%	sp|P68431|H31_HUMAN	1
Histone H4	DAVTYT(E)HAK	449.5215	3+	1345.5425	23.32	0.01	100.00%	sp|P62805|H4_HUMAN	11
Histone H4	DAVTYT(E)HAKR	611.2385	3+	1830.6936	27.09	0.0029	97.94%	sp|P62805|H4_HUMAN	3
Histone H4	GVL(K)VFLENVIRDAVTYTEHAK	761.6132	4+	3042.4235	46.03	0.002	99.88%	sp|P62805|H4_HUMAN	1
Histone H4	ISGLIY(E)ETRGVLK	706.9858	3+	2117.9355	67.05	0.0000055	98.29%	sp|P62805|H4_HUMAN	3
Histone H4	ISGLIYE(E)TRGVLK	597.3026	3+	1788.886	64.43	0.000012	97.68%	sp|P62805|H4_HUMAN	1
Histone H4	RKTVTAMDVVYAL(K)R	491.5071	4+	1961.9992	52.38	0.00027	95.18%	sp|P62805|H4_HUMAN	1
Histone H4	VFL(E)NVIR	765.8229	2+	1529.6312	24.53	0.005	100.00%	sp|P62805|H4_HUMAN	19
Histone H4	VFL(E)NVIRDAVTYTEHAK	662.2984	4+	2645.1645	26.3	0.0035	95.56%	sp|P62805|H4_HUMAN	1
Histone H4	VFLENVIRDAVTYT(E)HAK	580.0341	4+	2316.1074	54.82	0.000034	99.28%	sp|P62805|H4_HUMAN	1
Histone H4	VFLENVIRDAVTYTEHA(K)	882.7233	3+	2645.1482	65.94	0.000081	99.35%	sp|P62805|H4_HUMAN	2

Table S2: List of ADP-ribosylated peptides with ambiguous site localization (<95%)

protein description	peptide sequence	peptide mz	charge	peptide mr	peptide score	expect value	confidence	protein accession	No. of identif.
ARTD10	C(E)RRPVEQVLYHGTTAPAVPDICAHGFNR	713.3304	5+	3561.6155	61.43	0.0000028	86.49%	tr|F5H462|F5H462_HUMAN	4
ARTD10	CERRPV(E)QVLYHGTTAPAVPDICAHGFNR	973.6728	4+	3890.6621	44.04	0.000074	49.47%	tr|F5H462|F5H462_HUMAN	1
ARTD10	CERRPVEQVLYHGTTAPAVPDICAHGFN(R)	713.3317	5+	3561.6222	20.3	0.012	20.00%	tr|F5H462|F5H462_HUMAN	1
ARTD10	LAENTG(E)FQEVVR	678.2683	3+	2031.7831	54.81	0.0000073	63.30%	tr|F5H462|F5H462_HUMAN	1
ARTD10	LAENTGEFQ(E)VVR	1016.9024	2+	2031.7903	47.62	0.000034	93.24%	tr|F5H462|F5H462_HUMAN	4
ARTD10	LAENTGEFQEVV(R)	852.3806	2+	1702.7466	41.55	0.00025	25.00%	tr|F5H462|F5H462_HUMAN	2
ARTD10	RASLSVQDRYSPPNADGH(K)AVFVAR	657.3004	5+	3281.4657	74.69	0.000000099	94.84%	tr|F5H462|F5H462_HUMAN	4
ARTD10	RPV(E)QVLYHGTTAPAVPDICAHGFNR	862.3829	4+	3445.5026	70.14	0.00000027	94.24%	tr|F5H462|F5H462_HUMAN	3
ARTD10	RPVEQVLYHGTTAPAVPDICAHGFN(R)	780.1152	4+	3116.4318	27.59	0.0026	33.33%	tr|F5H462|F5H462_HUMAN	1
ARTD10	VSHPLLQQQYELYR(E)R	867.3785	3+	2599.1138	41.62	0.00013	69.94%	tr|F5H462|F5H462_HUMAN	1
ARTD10	VSHPLLQQQYELYRE(R)	757.6953	3+	2270.0639	38.67	0.00052	46.17%	tr|F5H462|F5H462_HUMAN	5
Histone H2A type 1	HLQLAIRND(E)ELNKLLGK	882.4185	3+	2644.2337	42.54	0.00019	90.17%	sp|P0C0S8|H2A1_HUMAN	43
Histone H2A type 1	HLQLAIRNDE(E)LNKLLGK	882.416	3+	2644.226	65.51	0.0000011	92.56%	sp|P0C0S8|H2A1_HUMAN	50
Histone H2A type 1	HLQLAIRNDEELN(K)	745.3234	3+	2232.9484	55.34	0.00068	84.42%	sp|P0C0S8|H2A1_HUMAN	4
Histone H2A type 1	HLQLAIRNDEELNKLLG(K)VTIAQGGVLPNIQAVLLPK	912.2802	5+	4556.3644	26.9	0.028	86.81%	sp|P0C0S8|H2A1_HUMAN	8
Histone H2A type 1	ND(E)ELNKLLGKVTIAQGGVLPNIQAVLLPK	932.2258	4+	3724.874	20.49	0.012	23.17%	sp|P0C0S8|H2A1_HUMAN	1
Histone H2A type 1-A	HLQLAIRNDE(E)LNKLLGGVTIAQGGVLPNIQAVLLPK	1122.3306	4+	4485.2932	29.33	0.0056	57.44%	sp|Q96QV6|H2A1A_HUMAN	3
Histone H2A type 1-A	HLQLAIRNDEELN(K)LLGGVTIAQGGVLPNIQAVLLPK	1122.3407	4+	4485.3337	25.5	0.0041	35.45%	sp|Q96QV6|H2A1A_HUMAN	1
Histone H2A type 1-A	ND(E)ELNKLLGGVTIAQGGVLPNIQAVLLPK	914.4592	4+	3653.8076	24.25	0.0053	42.92%	sp|Q96QV6|H2A1A_HUMAN	1
Histone H2A type 1-B/E	HLQLAI(R)NDEELNKLLGR	669.066	4+	2672.2351	38.14	0.03	78.40%	sp|P04908|H2A1B_HUMAN	5
Histone H2A type 1-B/E	HLQLAIRNDE(E)LNKLLGR	586.8063	4+	2343.196	70.72	0.0000025	89.85%	sp|P04908|H2A1B_HUMAN	29
Histone H2A type 1-B/E	HLQLAIRNDEELN(K)LLGR	669.0717	4+	2672.2575	64.75	0.000063	91.81%	sp|P04908|H2A1B_HUMAN	3
Histone H2A type 1-B/E	HLQLAIRNDEELNKLLG(R)	782.0748	3+	2343.2027	24.42	0.019	24.92%	sp|P04908|H2A1B_HUMAN	10
Histone H2A type 1-B/E	VGAGAPVYLAAVL(E)YLTAEILELAGNAAR	782.6557	4+	3126.5937	27.4	0.0044	93.67%	sp|P04908|H2A1B_HUMAN	6
Histone H2A type 1-B/E	VGAGAPVYLAAVLEYLTA(E)ILELAGNAARDNKK	903.9695	4+	3611.8488	21.97	0.021	36.55%	sp|P04908|H2A1B_HUMAN	1
Histone H2A type 1-B/E	VGAGAPVYLAAVLEYLTAEIL(E)LAGNAAR	864.9166	4+	3455.6374	32.42	0.00096	70.64%	sp|P04908|H2A1B_HUMAN	2
Histone H2A type 1-C	VGAGAPVYLAAVL(E)YLTAEILELAGNAARDNKK	903.9685	4+	3611.8449	53.29	0.000034	91.08%	sp|Q93077|H2A1C_HUMAN	1
Histone H2A type 1-C	VGAGAPVYLAAVLEYLTA(E)ILELAGNAAR	864.917	4+	3455.6389	36.47	0.00074	88.00%	sp|Q93077|H2A1C_HUMAN	5
Histone H2A type 1-C	VGAGAPVYLAAVLEYLTAEILELAGNAA(R)	1043.2123	3+	3126.615	92.56	2.9E-09	25.00%	sp|Q93077|H2A1C_HUMAN	4
Histone H2A type 1-C	VGAGAPVYLAAVLEYLTAEILELAGNAA(R)DNKK	903.9659	4+	3611.8344	56.9	0.00066	87.19%	sp|Q93077|H2A1C_HUMAN	1
Histone H2A type 1-C	VGAGAPVYLAAVLEYLTAEILELAGNAARDNK(K)	903.9767	4+	3611.8776	98.08	6.4E-10	16.67%	sp|Q93077|H2A1C_HUMAN	2
Histone H2A type 2-A	AGLQFPVGRVH(R)	516.9285	3+	1547.7636	27.64	0.0064	50.00%	sp|Q6FI13|H2A2A_HUMAN	2
Histone H2A type 2-A	HLQLAIRND(E)ELNK	635.642	3+	1903.9041	53.67	0.000054	92.90%	sp|Q6FI13|H2A2A_HUMAN	7
Histone H2A type 2-A	HLQLAIRNDE(E)LNK	745.3264	3+	2232.9572	48.77	0.000027	63.02%	sp|Q6FI13|H2A2A_HUMAN	2
Histone H2A type 2-A	HLQLAIRNDE(E)LNKLLGKVTIAQGGVLPNIQAVLLPK	1140.103	4+	4556.383	28.03	0.0024	51.83%	sp|Q6FI13|H2A2A_HUMAN	5
Histone H2A type 2-A	HLQLAIRNDEELN(K)LLGK	772.7357	3+	2315.1853	49.41	0.0026	54.76%	sp|Q6FI13|H2A2A_HUMAN	3
Histone H2A type 2-A	HLQLAIRNDEELN(K)LLGKVTIAQGGVLPNIQAVLLPK	1140.1074	4+	4556.4006	63.38	0.00023	93.67%	sp|Q6FI13|H2A2A_HUMAN	5
Histone H2A type 2-A	HLQLAIRNDEELNKLLG(K)	882.4178	3+	2644.2315	51.53	0.0013	92.07%	sp|Q6FI13|H2A2A_HUMAN	14
Histone H2A type 2-A	HLQLAIRNDEELNKLLGKVTIAQGGVLPNIQAVLLP(K)	912.2861	5+	4556.3943	39.13	0.0024	49.68%	sp|Q6FI13|H2A2A_HUMAN	2
Histone H2A type 2-A	IIP(R)HLQLAIRNDEELNKLLGK	781.8942	4+	3123.5476	20.4	0.013	92.97%	sp|Q6FI13|H2A2A_HUMAN	3
Histone H2A type 2-A	LLR(K)GNYAER	477.9042	3+	1430.6908	26.47	0.025	93.91%	sp|Q6FI13|H2A2A_HUMAN	1
Histone H2A type 2-A	LLRKGNYA(E)R	477.9044	3+	1430.6912	38.94	0.0023	90.68%	sp|Q6FI13|H2A2A_HUMAN	1
Histone H2A type 2-A	LLRKGNYAE(R)	477.9053	3+	1430.6941	55.77	0.000037	25.00%	sp|Q6FI13|H2A2A_HUMAN	2
Histone H2A type 2-A	ND(E)ELNKLLGK	605.2505	3+	1812.7298	29.97	0.0031	94.68%	sp|Q6FI13|H2A2A_HUMAN	8
Histone H2A type 2-A	NDE(E)LNKLLGK	605.2506	3+	1812.73	22.09	0.0085	83.52%	sp|Q6FI13|H2A2A_HUMAN	2
Histone H2A type 2-A	NDE(E)LNKLLGKVTIAQGGVLPNIQAVLLPK	932.2241	4+	3724.8674	22.98	0.022	46.91%	sp|Q6FI13|H2A2A_HUMAN	2
Histone H2A type 2-A	NDEELNKLLG(K)VTIAQGGVLPNIQAVLLPK	932.2267	4+	3724.8776	46.08	0.0038	70.05%	sp|Q6FI13|H2A2A_HUMAN	2
Histone H2A type 2-A	SSRAGLQFPVG(R)	496.2404	3+	1485.6995	38.99	0.00091	50.00%	sp|Q6FI13|H2A2A_HUMAN	1
Histone H2A type 2-A	VGAGAPVYMAAVL(E)YLTAEILELAGNAAR	1049.1802	3+	3144.5187	45.78	0.00024	86.91%	sp|Q6FI13|H2A2A_HUMAN	1
Histone H2A type 2-A	VGAGAPVYMAAVLEYLTAEIL(E)LAGNAAR	1049.1887	3+	3144.5443	28.37	0.0063	47.72%	sp|Q6FI13|H2A2A_HUMAN	1
Histone H2A type 2-A	VGAGAPVYMAAVLEYLTAEILELAGNAA(R)	1049.1968	3+	3144.5685	80.37	0.00000006	25.00%	sp|Q6FI13|H2A2A_HUMAN	1
Histone H2A type 2-A	VTIAQGGVLPNIQAVLLPKKT(E)SHHK	598.9269	5+	2989.5983	54.04	0.0000095	83.41%	sp|Q6FI13|H2A2A_HUMAN	1
Histone H2A type 2-B	HLQLAVRNDE(E)LNKLLGGVTIAQGGVLPNIQAVLLPK	895.2673	5+	4471.3	27.06	0.0029	37.89%	sp|Q8IUE6|H2A2B_HUMAN	1
Histone H2A.x	HLQLAIRND(E)ELNKLLGGVTIAQGGVLPNIQAVLLPK	1122.3407	4+	4485.3337	33.95	0.0024	56.35%	sp|P16104|H2AX_HUMAN	2
Histone H2A.Z	HLQLAIRGD(E)ELDSLIK	831.0446	3+	2490.112	65.48	0.00000072	91.95%	sp|P0C0S5|H2AZ_HUMAN	8
Histone H2A.Z	HLQLAIRGDE(E)LDSLIK	831.046	3+	2490.1162	65.41	0.00000088	94.68%	sp|P0C0S5|H2AZ_HUMAN	10
Histone H2A.Z	VGATAAVYSAAIL(E)YLTAEVLELAGNASK	1146.2009	3+	3435.581	25.06	0.0045	89.76%	sp|P0C0S5|H2AZ_HUMAN	1
Histone H2B type 1-K	IAGEAS(R)LAHYNKR	450.2213	4+	1796.8563	37.67	0.048	94.59%	sp|O60814|H2B1K_HUMAN	1
Histone H2B type 1-K	KESYSVVYKVL(K)	606.6368	3+	1816.8887	41.32	0.0012	62.34%	sp|O60814|H2B1K_HUMAN	2
Histone H2B type 1-K	KRS(R)KESYSVYVYK	584.2629	4+	2333.0224	73.94	0.0000097	82.68%	sp|O60814|H2B1K_HUMAN	1
Histone H2B type 1-K	LAHYNK(R)STITSR	440.4686	4+	1757.8453	50.66	0.0021	93.55%	sp|O60814|H2B1K_HUMAN	1
Histone H2B type 1-K	LLLPG(E)LAK	498.8942	3+	1493.6608	20.33	0.013	94.94%	sp|O60814|H2B1K_HUMAN	1
Histone H2B type 1-K	S(R)KESYSVYVYK	574.2611	3+	1719.7615	48.88	0.0039	86.41%	sp|O60814|H2B1K_HUMAN	1
Histone H2B type 1-K	SR(K)ESYSVYVYK	683.9484	3+	2048.8234	41.34	0.018	47.90%	sp|O60814|H2B1K_HUMAN	1
Histone H2B type 1-K	SRK(E)SYSVYVYK	683.9459	3+	2048.8158	34.33	0.0011	86.63%	sp|O60814|H2B1K_HUMAN	3
Histone H2B type 2-C	IAGEASRLAHYNK(R)	450.2214	4+	1796.8565	32.85	0.00083	25.00%	sp|Q6DN03|H2B2C_HUMAN	2
Histone H2B type 3-B	A(M)GIMNSFVNDI(F)ER	767.6317	3+	2299.8733	88.1	5.5E-09	49.99%	sp|Q8N257|H2B3B_HUMAN	2
Histone H2B type 3-B	AMGIMNSFVNDIF(E)R	762.3013	3+	2283.882	60.76	0.000002	94.40%	sp|Q8N257|H2B3B_HUMAN	9
Histone H2B type 3-B	AMGIMNSFVNDIFE(R)	762.2984	3+	2283.8734	76.45	0.000000068	50.00%	sp|Q8N257|H2B3B_HUMAN	6
Histone H2B type 3-B	LAHYNKRSTITS(R)	440.4683	4+	1757.8441	51.91	0.000021	33.33%	sp|Q8N257|H2B3B_HUMAN	1
Histone H2B type 3-B	LLLPG(E)LAKHAVSEGTK	768.6908	3+	2303.0506	24.55	0.005	81.64%	sp|Q8N257|H2B3B_HUMAN	3
Histone H2B type 3-B	LLLPGELAKHAVSEGT(K)	659.0093	3+	1974.0062	83.39	0.000000015	25.00%	sp|Q8N257|H2B3B_HUMAN	1
Histone H2B type 3-B	QVHPDTGISSKAMGIMNSFVNDIFE(R)	1035.8105	3+	3104.4098	94.77	1.3E-09	33.33%	sp|Q8N257|H2B3B_HUMAN	4
Histone H2B type 3-B	VLKQVHPDTGISS(K)AMGIMNSFVNDIFER	944.4254	4+	3773.6723	79.36	0.000000081	85.08%	sp|Q8N257|H2B3B_HUMAN	3
Histone H2B type F-S	(E)IQTAVRLLLPGELAK	764.7081	3+	2291.1026	36.11	0.00041	78.07%	sp|P57053|H2BFS_HUMAN	2
Histone H2B type F-S	K(E)SYSVYVYK	602.9056	3+	1805.6949	56.56	0.000018	93.65%	sp|P57053|H2BFS_HUMAN	5
Histone H3.1	(K)PHRYRPGTVALR	523.7457	4+	2090.9538	30.94	0.0013	94.75%	sp|P68431|H31_HUMAN	1
Histone H3.1	EIAQDF(K)TDLR	516.5694	3+	1546.6864	22.6	0.034	93.80%	sp|P68431|H31_HUMAN	5
Histone H3.1	EIAQDFKTDL(R)	516.57	3+	1546.6882	35.61	0.00062	60.43%	sp|P68431|H31_HUMAN	3

Histone H3.1	FQSSAV(M)ALQE(A)CEAYLVGLFEDTNLCAIHAK	1036.6896	4+	4142.7292	81.46	0.000000023	90.49%	sp|P68431|H31_HUMAN	5
Histone H3.1	FQSSAV(M)ALQEACEAYLVG(L)FEDTNLCAIHAK	1381.9294	3+	4142.7665	58.16	0.0000057	92.32%	sp|P68431|H31_HUMAN	2
Histone H3.1	FQSSAV(M)ALQEACEAYLVG(L)FEDTNLCAIHAKR	1075.7147	4+	4298.8298	56.41	0.0000051	42.59%	sp|P68431|H31_HUMAN	1
Histone H3.1	FQSSAVMALQEAC(E)AYLVGLFEDTNLCAIHAK	1032.6923	4+	4126.7399	84.18	0.000000019	50.00%	sp|P68431|H31_HUMAN	17
Histone H3.1	FQSSAVMALQEAC(E)AYLVGLFEDTNLCAIHAKR	1071.7162	4+	4282.8356	77.99	0.000000053	88.55%	sp|P68431|H31_HUMAN	2
Histone H3.1	FQSSAVMALQEACEAYLVGLF(E)DTNLCAIHAK	1032.6993	4+	4126.7683	38.74	0.00023	33.33%	sp|P68431|H31_HUMAN	2
Histone H3.1	FQSSAVMALQEACEAYLVGLF(E)DTNLCAIHAKR	989.4654	4+	3953.8325	34.12	0.0012	92.77%	sp|P68431|H31_HUMAN	4
Histone H3.1	FQSSAVMALQEACEAYLVGLFEDTNLCAIHA(K)	1266.9143	3+	3797.7211	30.77	0.0013	25.00%	sp|P68431|H31_HUMAN	1
Histone H3.1	FQSSAVMALQEACEAYLVGLFEDTNLCAIHAK(R)	989.46	4+	3953.811	92.33	2.2E-09	20.00%	sp|P68431|H31_HUMAN	2
Histone H3.1	KPH(R)YRPGTVALR	441.4827	4+	1761.9017	25.46	0.037	75.04%	sp|P68431|H31_HUMAN	1
Histone H3.1	KPHRYRPGTVAL(R)	441.483	4+	1761.9028	24	0.0056	25.00%	sp|P68431|H31_HUMAN	2
Histone H3.1	LVREIAQDF(K)TDLR	749.0042	3+	2243.9908	34.87	0.02	74.33%	sp|P68431|H31_HUMAN	1
Histone H3.1	LVREIAQDFKTDL(R)	749.0059	3+	2243.9957	43.83	0.01	94.14%	sp|P68431|H31_HUMAN	1
Histone H3.1	RVTIMPKDIQLA(R)	584.9738	3+	1751.8996	32.02	0.0023	33.33%	sp|P68431|H31_HUMAN	1
Histone H3.1	STELLI(R)	522.2538	2+	1042.493	43.5	0.0094	50.00%	sp|P68431|H31_HUMAN	2
Histone H3.1	STELLIRKLPFQ(R)	604.9909	3+	1811.9509	41.89	0.00012	25.00%	sp|P68431|H31_HUMAN	1
Histone H3.2	FQSSAVMALQEAS(E)AYLVGLFEDTNLCAIHAK	1014.4415	4+	4053.737	96.14	1.5E-09	50.00%	sp|Q71DI3|H32_HUMAN	1
Histone H3.2	FQSSAVMALQEASEAYLVGLF(E)DTNLCAIHAK	1352.2584	3+	4053.7534	22.72	0.0074	26.36%	sp|Q71DI3|H32_HUMAN	1
Histone H3.3C	EIAQDFNTDLRFQSAAVGALQEASEAYLVGLLEDTNLCAIHAK(R)	844.252	6+	5059.4684	24.86	0.0047	14.29%	sp|Q6NXT2|H3C_HUMAN	1
Histone H3.3C	FQSAAVGALQEASEAYLVGLLEDTNLCAIHAK(R)	940.2086	4+	3756.8051	42.47	0.0001	20.00%	sp|Q6NXT2|H3C_HUMAN	1
Histone H4	(K)TVTAMDVVYALKR	602.9723	3+	1805.895	42.74	0.000098	52.30%	sp|P62805|H4_HUMAN	2
Histone H4	DAVTYT(E)HAK	559.2067	3+	1674.5982	25.75	0.0078	94.17%	sp|P62805|H4_HUMAN	7
Histone H4	DAVTYT(E)HAKR	611.2402	3+	1830.6987	20.73	0.027	93.89%	sp|P62805|H4_HUMAN	7
Histone H4	DAVTYTEHA(K)RKTVTAMDVVYALKR	682.3212	5+	3406.5695	24.38	0.0059	37.90%	sp|P62805|H4_HUMAN	1
Histone H4	DNIQGITKPAI(R)R	674.9744	3+	2021.9014	22.07	0.025	85.81%	sp|P62805|H4_HUMAN	2
Histone H4	GVL(K)VFLENVIR	643.3101	3+	1926.9085	38.35	0.012	93.17%	sp|P62805|H4_HUMAN	3
Histone H4	GVLKVFL(E)NVIRDAVTYTEHAK	761.6137	4+	3042.4257	20.58	0.014	42.54%	sp|P62805|H4_HUMAN	1
Histone H4	ISGLIY(E)ETR	861.3482	2+	1720.6819	43.03	0.00013	94.65%	sp|P62805|H4_HUMAN	17
Histone H4	ISGLIY(E)ETRGVLK	706.9858	3+	2117.9355	42.78	0.000097	94.93%	sp|P62805|H4_HUMAN	26
Histone H4	ISGLIY(E)ETRGVLKVFLENVIR	773.1323	4+	3088.5002	30.24	0.0015	69.28%	sp|P62805|H4_HUMAN	1
Histone H4	ISGLIYE(E)TR	861.341	2+	1720.6675	39.49	0.00076	84.08%	sp|P62805|H4_HUMAN	11
Histone H4	ISGLIYE(E)TRGVLK	597.3049	3+	1788.893	66.74	0.000043	77.99%	sp|P62805|H4_HUMAN	3
Histone H4	ISGLIYE(E)TRGVLKVFLENVIR	773.1356	4+	3088.5134	33.68	0.004	34.65%	sp|P62805|H4_HUMAN	1
Histone H4	ISGLIYEET(R)	696.8176	2+	1391.6206	21.26	0.026	37.13%	sp|P62805|H4_HUMAN	4
Histone H4	ISGLIYEET(R)GVLKVFLENVIR	773.1364	4+	3088.5166	24.05	0.0055	34.49%	sp|P62805|H4_HUMAN	6
Histone H4	ISGLIYEET(R)GVLKVFLENVIRDAVTYTEHAK	841.8114	5+	4204.0206	48.33	0.000029	32.76%	sp|P62805|H4_HUMAN	1
Histone H4	ISGLIYEETRGVL(K)	597.3032	3+	1788.8878	39.83	0.00066	25.00%	sp|P62805|H4_HUMAN	5
Histone H4	KTVTAMDVVYAL(K)R	602.9747	3+	1805.9022	44.95	0.00029	93.11%	sp|P62805|H4_HUMAN	2
Histone H4	R(K)TVTAMDVVYALKR	573.7684	4+	2291.0444	48.31	0.0003	50.00%	sp|P62805|H4_HUMAN	1
Histone H4	RISGLIY(E)ETR	626.5993	3+	1876.7761	39.98	0.0012	92.77%	sp|P62805|H4_HUMAN	11
Histone H4	RISGLIY(E)ETRGVLK	759.0201	3+	2274.0386	47.89	0.00013	92.28%	sp|P62805|H4_HUMAN	3
Histone H4	RISGLIYE(E)TR	516.9132	3+	1547.7178	28.6	0.022	86.93%	sp|P62805|H4_HUMAN	8
Histone H4	RISGLIYE(E)TRGVLK	759.0224	3+	2274.0454	45.81	0.00013	63.74%	sp|P62805|H4_HUMAN	5
Histone H4	RISGLIYEET(R)	939.3912	2+	1876.7679	37.66	0.03	66.27%	sp|P62805|H4_HUMAN	9
Histone H4	RISGLIYEET(R)GVLK	759.0193	3+	2274.036	41.57	0.012	52.56%	sp|P62805|H4_HUMAN	1
Histone H4	RKTVTAMDVVYALK(R)	573.7695	4+	2291.0488	27.65	0.0031	51.81%	sp|P62805|H4_HUMAN	2
Histone H4	TVTAMDVVYAL(K)R	560.2758	3+	1677.8056	41.55	0.0011	91.83%	sp|P62805|H4_HUMAN	5
Histone H4	TVTAMDVVYALK(R)	839.9075	2+	1677.8005	24.46	0.0051	50.00%	sp|P62805|H4_HUMAN	3
Histone H4	VFLENVI(R)	601.2959	2+	1200.5772	22.52	0.022	50.00%	sp|P62805|H4_HUMAN	1
Histone H4	VFLENVIRDAVTYT(E)HAK	580.0328	4+	2316.102	26.63	0.012	94.50%	sp|P62805|H4_HUMAN	2
Histone H4	VFLENVIRDAVTYTEHA(K)	882.7288	3+	2645.1646	21.54	0.036	94.65%	sp|P62805|H4_HUMAN	6
Histone H4	VFLENVIRDAVTYTEHAK(R)	619.06	4+	2472.2109	58.4	0.0000033	20.00%	sp|P62805|H4_HUMAN	1

For consideration as a Resource Article in Molecular Cell

Proteome-wide Identification of Poly(ADP-ribosyl)ation targets in different Genotoxic Stress Responses

Stephanie Jungmichel[1], Florian Rosenthal[2, 3], Michael O. Hottiger[2], and Michael L. Nielsen[1*]

[1] Department of Proteomics, The Novo Nordisk Foundation Center for Protein Research, University of Copenhagen, Faculty of Health Sciences, DK-2200 Copenhagen, Denmark
[2] Institute of Veterinary Biochemistry and Molecular Biology, University of Zurich, CH-8057 Zurich, Switzerland
[3] Life Science Zurich Graduate School, University of Zurich, CH-8057, Switzerland

* To whom correspondence should be addressed: michael.lund.nielsen@cpr.ku.dk

Summary

Poly(ADP-ribos)ylation (PARylation) is a reversible post-translational modification found in higher eukaryotes, but little is known about the acceptor proteins of PARylation. Here we describe a sensitive proteomics approach based upon quantitative mass spectrometry for identification of PARylated proteins induced under different conditions of cellular stress. Our screen identifies novel candidates not previously reported to be targets of PARylation, while confirming the majority of known PARylated proteins. *In vivo* and *in vitro* validation of novel acceptor proteins confirms that our methodology targets direct covalent PARylation. Nuclear proteins encompassing nucleic binding properties are most prominently found to be PARylated upon genotoxic stress, in agreement with the nuclear functions ascribed to ARTD1/PARP1 and ARTD2/PARP2. Distinct differences in proteins becoming PARylated upon various genotoxic insults are observed. Most significantly, proteins involved in RNA metabolism are PARylated upon oxidative and alkylation damage, demonstrating that post-transcriptional processes are controlled through specific genotoxic stress-induced PARylation.

Introduction

Mammalian cells are constantly exposed to genotoxic stress and have therefore developed sophisticated mechanisms to detect and signal the presence of damaged DNA in order to accomplish efficient DNA repair processes. Post-translational modifications (PTMs) of proteins significantly contribute to the regulation of these processes, of which phosphorylation and ubiquitylation recently have been studied extensively on a proteome-wide scale(Bennetzen et al., 2010; Bensimon et al., 2010; Matsuoka et al., 2007; Povlsen et al., 2012). Although the importance of phosphorylation and ubiquitylation in maintaining genomic integrity in the DNA damage response are indisputable, one of the earliest cellular response following exposure to genotoxic stress happens through the reversible PTM poly(ADP-ribosyl)ation (PARylation) (Altmeyer and Lukas, 2013; Lukas et al., 2011; Polo and Jackson, 2011). Activation of poly(ADP-ribose) polymerases (ARTDs, formerly PARPs) entails the rapid synthesis of long, branched poly(ADP-ribose) (PAR) chains from nicotinamide adenine dinucleotide (NAD^+) that can lead to a transient 10 to 500-fold increase of cellular PAR levels (Hassa and Hottiger, 2008). PAR polymers have been suggested to play a key role in the regulation of chromatin structure modulation, DNA repair, transcription and cell death related processes (Kraus and Hottiger, 2013; Luo and Kraus, 2012). The importance of this modification is emphasized by the fact that knockout mice for ARTD1/PARP1 or ARTD2/PARP2 are hypersensitive to DNA damaging agents and show increased genomic instability following genotoxic stress (de Murcia et al., 1997; Menissier de Murcia et al., 2003; Trucco et al., 1998). Intriguingly, double knockouts for ARTD1 and ARTD2 result in early embryonic lethality indicating that these two enzymes might functionally compensate for each other (Menissier de Murcia et al., 2003). PAR turnover is tightly controlled by the activity of PAR degrading enzymes, of which poly(ADP-ribose) glycohydrolase (PARG) accounts for the major activity in mammalian cells (Bonicalzi et al., 2005). Despite PARylation has been known for 50 years, surprisingly little is known about the molecular targets of the modification, and which processes these specifically regulate. At present, only a limited number of *in vivo* PARylated proteins (PARP substrates) is reported in the literature and public databases, primarily due to the absence of 'unbiased' technologies for detecting PARylated proteins on a global scale. Thus, proteome-wide identification of PARylated proteins would greatly expand the

number of currently known PARylated proteins. In particular, a systems-wide elucidation of PARylated proteins under various stress responses would lead to a deeper understanding of the biological mechanisms related to PARylation, especially in light of the fact that PARP inhibitors are currently tested in clinical trials to treat cancer patients (Javle and Curtin, 2011).

Mass spectrometry (MS)-based proteomics has emerged as a key technology for comprehensive identification of PTM substrates and site-specific mapping of various types of PTMs (Choudhary et al., 2009). In addition, MS is often employed in interaction studies for identification of proteins interacting with a 'bait'. In such interaction experiments a central challenge is to distinguish unspecifically binding proteins (background binders) from genuine interactors (specific binders) of the bait of interest. To alleviate this problem interaction screens can be performed in a quantitative manner, most accurately by using isotope labeling approaches such as Stable Isotope Labeling with Amino Acids in Cell culture (SILAC) (de Godoy et al., 2008; Ong et al., 2002). The use of quantitative approaches was recently described for the study of PAR-binding proteins (Gagne et al., 2012), but has until now not been employed for a systems-wide identification of PARylated proteins under genotoxic stress. Previous attempts to identify *in vivo* PARylated proteins did not utilize quantitative information, and only focused on proteins modified under basal (unstressed) cellular conditions (Dani et al., 2009). PAR formation, however, dramatically increases in response to certain genotoxic stress (Malanga and Althaus, 1994). As a consequence, only a subset of PARylated proteins was identified in previous studies, and the functional relevance of the identified PARylated proteins was not investigated.

Here, we describe a MS-based SILAC approach for assessing the extent of PARylated proteins under various types of genotoxic stress. The presented approach entails growing mammalian cells in three SILAC conditions by incorporating respectively 'light', 'medium' or 'heavy' amino acids (^{13}C and ^{15}N isotope-labeled lysines and arginines) into all cellular proteins (Ong et al., 2002). From these SILAC encoded lysates pull-down experiments are performed under stringent conditions using a PAR-binding module known to recognize covalently PARylated proteins (Karras et al., 2005) in combination with a binding-defective mutant allowing for quantitative distinction between PARylated proteins and background binders. Briefly, the binding-defective mutant is used for pull-down in 'light' SILAC lysates, while the wild-type PAR binding module is used for pull-down experiments in both

‘medium’ and ‘heavy’ SILAC lysates (Figure 1A). Protein eluates from all three pull-down conditions are combined, digested to peptides and PARylated proteins are identified by liquid chromatography tandem mass spectrometry (LC MS/MS). Collectively, this allows for identification of covalently PARylated proteins by a quantitative comparison of ‘light’ and ‘medium’ SILAC states, while concurrently allowing for investigation of stress-dependent modulations of protein PARylation in the ‘heavy’ SILAC state (Figure 1A & 1B).
Using the established approach we identify a large number of PARylated proteins induced under various types of genotoxic stress, and confirm several novel PARylated protein targets through biochemical *in vitro* and *in vivo* assays. Moreover, the presented method identifies for all four tested stresses the majority of already known modified proteins, involved in DNA metabolism, collectively demonstrating the ability of the methodology to recognize PARylated proteins and in agreement with the nuclear functions ascribed to the major PAR-inducing enzymes, ARTD1 and ARTD2. A comparison of the different types of genotoxic stress revealed that oxidative and alkylation stress induces PARylation of a large number of proteins involved in RNA metabolism. This positions PARylation as an important functional link between the DNA and RNA metabolic processes. To emphasize this connection our data reveals that pre-mRNA splicing protein THRAP3 is PARylated under oxidative damage. THRAP3 has previously been demonstrated to play a role in the DDR in a manner that parallels transcription inhibition (Beli et al., 2012). Moreover, we demonstrate that under transcriptional inhibition PARylation of THRAP3 affects its cellular localization and prevents the protein from co-localizing with splicing factors in nuclear speckles. Collectively, the presented dataset provides a clearer definition of PARylated proteins in human cells, and describes how they vary under different genotoxic stress conditions.

Results

Establishing a proteomic approach for identification of genotoxic stress-dependent protein PARylation

As an initial step we decided to evaluate the binding properties of Af1521_wt in a SILAC setup as compared to its binding-deficient counterpart Af1521 G42E. To this end, we performed a specific triple-encoded SILAC pull-down experiment, where we incubated untreated light-labeled U2OS cell lysate with unbound glutathione-sepharose beads containing no Af1521 domain. In contrast to this, a medium-labeled U2OS lysate was incubated with crosslinked GST-Af1521_mut beads while a heavy-labeled lysate was incubated with GST-Af1521_wt beads (Figure S1A). Eluates from all three SILAC states were mixed 1:1:1 and subsequently analyzed by LC-M/MS. To assess the technical reproducibility of the experimental setup a replicate 'reverse' experiment was performed, where medium and heavy SILAC labels were swapped (Figure S1B). Statistical analysis revealed that results derived from the pull-down experiments were highly consistent yielding a Pearson correlation of >0.83 when plotting corresponding SILAC ratios from the replicate experiments (Figure S1C). It should be noted that the actual ratios in SILAC-based interaction studies do not have to be identical between experiments, as they primarily serve to segregate background binders from specific interactors. However, strong correlation coefficients indicate high quantitative reproducibility between replicate experiments.

We next investigated which proteins were differentially bound between Af1521_wt and Af1521_mut pull-downs. This was achieved through a direct comparison of their SILAC ratios, which revealed a large fraction of proteins with increased abundance (stronger affinity) for Af1521_wt compared to Af1521_mut (Figure 2A). A functional Gene Ontology (GO) enrichment analysis of the regulated proteins identified these as factors primarily involved in DNA repair processes. Analyzing the same experiment by immunoblot using a PAR-antibody demonstrated a strong increase in protein PARylation for pull-down with Af1521_wt, including the known major target ARTD1 (Figure 2B). In contrast, no PARylation signal was observed for Af1521_mut.

Although our results confirm that Af1521_wt can be employed as a PAR-binding module in a SILAC-based manner, we were intrigued by the observed enrichment of PARylated proteins in the absence of genotoxic stress (Figure 2A). The basal *in vivo* activity of

ARTD1 has previously been described as low, considerably stimulated only through genotoxic stress and regulated by the opposing actions of PARG (Bonicalzi et al., 2005). However, cell lines growing in culture are usually characterized by a high proliferation status and consequently enhanced levels of genomic instability (Bartkova et al., 2005; Gorgoulis et al., 2005). This increases the risk of accumulating genotoxic byproducts from metabolic processes, which might contribute to elevated genotoxic stress response in otherwise untreated cells. Alternatively, it is well established that *in vitro* PAR formation by ARTD1 solely requires the presence of NAD^+ and DNA fragments (Altmeyer et al., 2009; Langelier et al., 2012). Thus shearing of DNA during cell lysis could also be the cause of unphysiological activation of PAR formation despite fast and gentle sample handling being employed (see methods section).

To investigate whether sample handling or endogenous cellular processes account for the activation of ARTD1 and the observed protein PARylation, we performed another SILAC screen employing PARP inhibitors during sample preparation. To this end, we set up a triple-encoded SILAC experiment using only the Af1521_wt domain as pull-down 'bait' for all three SILAC states (Figure S2A). For light and medium SILAC cells PARP inhibitor (PJ-34 or 3-aminobenzamide) was added to the lysis buffer, while heavy SILAC cells were left untreated during the entire sample handling. Additionally, light SILAC cells were pretreated with the same PARP inhibitor for 2 hours prior to cell lysis, essentially exposing them to PARP inhibitor throughout the entire experimental sample procedure (Figure S2A). Following MS analysis of the pull-downs a substantial fraction of proteins was found regulated more than 4-fold in the heavy SILAC sample (complete absence of PARP inhibitor; Figure S2B; H/L ratios). Contrary to this, very little ADP-ribosylation was detected in cells only exposed to PARP inhibitors in the lysis buffer, strongly supporting the notion that post-lysis mechanical shearing stress triggers ARTD enzymatic activity (Figure S2B) (Beneke et al., 2012). Western blot analysis of the same pull-down samples using PAR and ARTD1 antibodies further corroborated these results, with enrichment of PARylated proteins only being observed in the absence of PARP inhibitor 3-AB or PJ-34 (Figure 2C and S2C). Moreover, hierarchical clustering of the PARylated proteins affected by the sample preparation procedure (+/- PARP inhibitors) revealed, as expected, that mainly DNA repair pathways are affected by these processes (Figure 2D). On the basis of these findings we included PARP inhibitors in all sample preparations and set out to investigate

the extent of PARylation upon induction of various types of genotoxic stress. Immunoblot analysis of cells exposed to oxidative stress by hydrogen peroxide (H_2O_2) treatment showed only a relatively mild increase in PAR levels (Figure 2E), which could be related to the short half-life of PAR polymers. The steady-state levels of PAR are tightly controlled by the opposing action of PAR-degrading enzymes, of which PARG exhibits the greatest enzymatic activity (Cortes et al., 2004). As a result, the half-life of cellular PARylation has been estimated to less than a few minutes (Alvarez-Gonzalez and Althaus, 1989). Thus, in order to sustain PAR levels throughout the pull-down procedure and hereby increase the sensitivity of our system, we decided to reduce PARG activity by protein depletion via an RNAi-based approach. Figure 2E confirms that knockdown of PARG resulted in increased PAR levels in response to H_2O_2 treatment. Based on these observations, we decided to alleviate the opposing PARG activity by siRNA-dependent depletion, and include PARP and PARG inhibitors in the lysis buffer for all following experiments.

Proteomic investigation of the differential impact of various types of genotoxic stress on protein PARylation

Having established a robust SILAC-based workflow for enrichment of PARylated proteins, we next investigated the effects of genotoxic agents described to inflict various types of genotoxic stress to elicit different repair responses to these lesions. To this end, we performed four SILAC experiments respectively investigating PARylated proteins upon treatment with H_2O_2 to induce oxidative stress, methyl methane sulfonate (MMS) to induce alkylating damage, ultraviolet radiation (UV) for the formation of CPDs and 6-4 PPs, and ionizing radiation (IR) primarily for induction of double strand breaks (DSBs) (Figure 3A).

Only cells grown in heavy SILAC media were exposed to genotoxic agents, hence PARylated substrates should exhibit an increase in Heavy/Light (H/L) SILAC ratio as compared to the M/L ratios (cells not exposed to genotoxic stress). To validate this, we plotted the logarithmized M/L and H/L SILAC ratios of the quantified proteins derived from the SILAC experiment exposed to H_2O_2 insult (Figure 3B). These data showed that the distribution of SILAC ratios of quantified proteins indeed is shifted towards higher H/L SILAC ratios as compared to the M/L counterparts, demonstrating significantly increased ($p = 9.69e-35$) protein PARylation upon genotoxic stress (Figure 3B). Moreover, since light and medium SILAC conditions essentially are the same for all four SILAC experiments,

they constitute an internal control condition between pull-downs. Hence, to ensure proper comparability between the acquired SILAC experiments we compared the M/L ratios of all four datasets by Q-Q probability plots (Wilk and Gnanadesikan, 1968). All Q-Q plots followed a straight 45 degree line (y = x) for the investigated sample pairs with strong correlation coefficients (R^2>0.98), hence, the SILAC experiments can be regarded comparable (Figure S3A). As further validation of the data, box plot analysis for all M/L ratios demonstrated identical distributions across all investigated samples (Figure 3C). In contrast, box plot analysis of genotoxic stress-induced samples (H/L ratios) revealed much broader distributions confirming that PARylated proteins are induced in all applied treatments (Figure 3D). Strikingly, the degree of regulation was dependent upon the source of exogenous damage, which in the instance of H_2O_2 revealed the strongest response followed by MMS, UV and IR in a steadily decreasing manner (Figure 3D). Western blot analysis of cellular PARylation generated by the different genotoxic stress treatments revealed an identical pattern (Figure 3E), confirming the direct association between PARylated proteins and measured SILAC ratios. In support of the varying degree of PARylation caused by the different genotoxic stress treatments, a heat map clustered H_2O_2 and MMS samples together demonstrating that these chemical agents cause the greatest degree of PARylation (Figure 3F). In order to determine which proteins are significantly enriched in each pull-down experiment, we used a 'significant-outlier' strategy based upon the student t-test to establish statistical significance ($p < 0.01$) (Cox and Mann, 2008). In doing so, a total of 165 proteins could be determined as significantly upregulated in the four experiments. However, these measurements take only a normal distribution of the dataset into account, while PARylation during the H_2O_2 and MMS treatments affect a much larger proportion of proteins compared to UV or IR damage (Figure 3D and 3E). This causes an overall augmentation of the H/L ratios disproportioned to the background binders, which can lead to an underestimation of significance measurements that are based on normal distributions. As a consequence, we included PARylated substrates from the H_2O_2 and MMS experiments if they exhibited at least 2.5-fold upregulation in their H/L ratios, concomitantly assuring stringency for determining true interaction partners. Taken together, we identified 235 proteins from the four pull-down experiments as being significantly enriched under the investigated genotoxic stress conditions (Table S2).

To assess the sensitivity of our SILAC screen we compared our identified PARylome to a comprehensive proteomic study that analyzed the expression levels of >11,500 proteins from 11 different cell lines including U2OS cells, which we also used for our PARylation study (Geiger et al., 2012),. Interestingly, within this large protein expression repository five PARylated proteins identified in our screen were not found in any of the investigated cell lines. These PARylated proteins could in principle entail false-positive identifications from our screen, but considering each protein was identified with sub ppm accuracy, between 2-12 unique peptides and significant SILAC ratios renders this unlikely to be the case (Figure S3B). Instead, the detection and quantification of low abundant proteins in our pull-down experiment highlights the sensitivity of our approach, and validates that the established approach is not biased towards abundant proteins.

Investigation of the cellular distribution of the identified substrates by GO enrichment analysis revealed that 76% of the PARylated proteins belong to the nucleus (Figure 3G), signifying a strong enrichment of nuclear PARylation targets considering pull-down experiments were performed on whole cell lysates. This is in full agreement with the known nuclear localization of ARTD1 and ARTD2, which together account for the majority of genotoxic stress-induced PAR formation in cells.

Proving direct ADP-ribosylation of novel target proteins

In order to select novel candidates for further investigation of PARylation-dependent processes, we first compared our dataset to previously published PARylation targets involved in DNA repair as defined by GO annotation. We identified several of the proteins proposed to be PARylated, including ARTD1, FACT140 (SUPT16H), XRCC5, XRCC6, PCNA, RPA1, RPA2, XRCC1, TOP2 and HMGB1, further strengthening the reliability of our SILAC approach (Figure 4A). Cell-type specific protein expression or the requirement for specific genotoxic conditions could account for not identifying six previously suggested PARylated proteins. However, besides confirming the majority of known PARylated proteins involved in DNA metabolism, we additionally found 18 new PARylation targets specifically described to play a role in DNA-repair related processes (Figure 4A). Moreover, we identified several histones previously proven by mass spectrometry-based approaches to be direct targets of PARylation in vitro (Messner et al., 2010).

As a further demonstration that our established method targets PARylated proteins, we biochemically verified covalent PAR modification of purified proteins by *in vitro* PARylation assays. Recombinant protein substrates were incubated with purified ARTD1 or ARTD2 enzymes in the presence of [^{32}P]-NAD$^+$ and a DNA fragment in order to measure incorporation of NAD$^+$ radioactivity by autoradiography. Activation of ARTD1 and ARTD2 was confirmed by detection of strongly auto-modified ARTD1 or ARTD2 in the upper part of the gel lanes (Figure 4B and 4C respectively). Using ARTD1 in the assay a strong PARylation of PNKP, MPG, MECP2, NUSAP1 and POLR2E, and to a lesser degree of CETN and CDK2 could be detected. For XPC it was difficult to confirm *in vitro* PARylation as the protein runs with an almost similar size as ARTD1 (103 kDa versus 111 kDa). Consequently, PARylation signal from XPC is completely overlaid by the signal arising from auto-modified ARTD1. A similar problem arises for ARTD2, which at a mass of 64 kDa further limits the detection range. Still, MPG is validated as PARylated by ARTD2 *in vitro* (Figure 4C). Collectively, we conclude that our methodology targets covalently PARylated proteins and not proteins that non-covalently bind PAR. Several of the newly identified PARylated proteins including PNKP, MPG, NUSAP1, CETN2 and CDK2, have also previously been assigned with a functional role in DNA repair processes, indicative of PARylation influencing their mode of operation in DNA metabolism.

Notably, the derived *in vitro* results are in agreement with the fact that ARTD1 is responsible for the largest part of cellular PAR, whereas ARTD2 accounts only for up to 15% of PAR formation (Ame et al., 1999). This characteristic seems to be reflected not only in the amount of poly(ADP-ribose) formed but also the number of actual targets. In support of ARTD1 being the primary enzyme responsible for the identified PARylated substrates, siRNA-mediated knockdown of ARTD1 resulted in a strong decline of the PAR signal. In contrast, siARTD2-treated cells hardly showed any difference compared to cells treated with control siRNA (Figure 4D). Although residual PAR-signal in siARTD1-treated cells could arise from the activity of ARTD2, the incomplete knockdown of the abundantly expressed ARTD1 could equally account for low-level PAR formation (Figure 4D). Notably, we detected a reduced signal for phospho-p53 (Ser15) for all investigated genotoxic stress treatments following ARTD1 down-regulation. This in agreement with previous reports showing comprised DDR signaling for PAR-inhibited cells (Haince et al., 2007), highlighting the role of PAR as an early genotoxic stress sensory molecule.

With ARTD1 being the most active ARTD enzyme in our experiments it is not surprising that ARTD1 itself was found to be PARylated under all four genotoxic stress conditions (Figure 4E). In contrast, ARTD2 was significantly determined as being PARylated merely under H_2O_2 treatment, highlighting the stringent criteria set to ensure strong confidence in identification of PARylated substrates. Among the entire ARTD family we additionally found ARTD16/PARP8 and ARTD12/PARP12 to be PARylated under specific types of genotoxic stress (Fig. 4E). Although the functional role of these two enzymes is still largely unknown, their postulated nuclear localization could make them likely targets for ARTD1 activity, which in conjunction with the identification of genotoxic stress regulated phosphorylation sites in ARTD16 (Matsuoka et al., 2007) opens up the possibility that their functional regulation could be associated with genotoxic stress responses.

Novel targets for poly(ADP-ribosyl)ation in vivo are involved in different cellular processes

To corroborate the *in vitro* validation of PARylated substrates with *in vivo* data, we verified a number of newly *in vitro* identified PARylation targets by immunoblot analysis using specific antibodies following Af1521_wt pull-down. In response to H_2O_2-induced stress we found enrichment of MPG (MID1), PNKP, MECP2, XPC and NUSAP1, while NF-κB p65 served as a negative control (Figure 5A). Pre-treatment of the cells with PARP inhibitor PJ-34 completely abolished the signal confirming that enrichment occurs in a PARP-dependent manner.

To further demonstrate PARylation of novel targets under physiological *in vivo* conditions, we performed immunoprecipitation of stably expressed GFP-tagged proteins under the control of their endogeneous promoters (Poser et al., 2008), and blotted them with PAR-antibody. In order to cover the functional diversity of targets in our dataset best way possible, we selected proteins regulating different nuclear processes. We verified our findings for TAF15, which belongs to the TET (TLS/FUS, EWS, TAF15) protein family of RNA and DNA-binding proteins. Members of this family have been reported to modulate gene expression by controlling transcription, splicing, RNA transport and DNA repair processes (Ballarino et al., 2012; Law et al., 2006; Tan and Manley, 2009). Using GFP-TAF15 expressing HeLa cells we could confirm the results of the Af1521 pull-down by Western Blot; and similarly, GFP-TAF15 was validated to be PARylated by GFP-immunoprecipitation in a genotoxic stress- and PARP inhibitor-repressed manner (Figure

5B). Strikingly, we found all three members of the TET protein family to be PARylated proteins under genotoxic stress conditions (Table S2), suggesting a common role for PARylation in regulating the function of these proteins in response to genotoxic stress.

Another RNA-associated factor that we discovered to be PARylated in a genotoxic stress-dependent manner was THRAP3 (TRAP150), which has been shown to control mRNA-splicing and nuclear mRNA degradation and was recently assigned a role in the DDR (Beli et al., 2012; Lee et al., 2010). In support of our SILAC data, we found GFP-THRAP3 to be enriched in the Af1521 pull-down in a PARP-dependent manner by immunoblotting, and conversely, validated it to be strongly PARylated upon GFP-immunoprecipitation (Figure 5B).

The ATPase SMARCA5 (SNF2h) is a chromatin remodeler belonging to the SWI/SNF family of proteins, and has recently been linked to genotoxic stress signaling in a manner dependent on PAR formation (Smeenk et al., 2012). Despite harboring a putative PAR-binding motif, the sequence was shown to be dispensable for PAR binding *in vitro* (Gagne et al., 2008) as well as for PARP-dependent accumulation of SMARCA5 at DSBs (Smeenk et al., 2012). On the other hand, no direct *in vivo* PARylation of SMARCA5 was detected following DNA damage (Smeenk et al., 2012), which could be the consequence of the transient nature or low degree of PARylation of SMARCA5. In the background of reduced PARG activity we could effectively confirm direct *in vivo* PARylation of SMARCA5 by GFP-immunoprecipitation and Af1521 pull-down (Figure 5B). In a recent study ARTD1 was demonstrated to PARylate several components of a tandem affinity purified TIP5 complex, hereby contributing to the repression of rRNA transcription and the establishment of silent rDNA chromatin during cell division (Guetg et al., 2012). SMARCA5 was found to be part of this complex, which is also referred to as nucleolar remodeling complex NoRC, indicating that PARylation of SMARCA5 could regulate additional processes than the DDR. Interestingly, in our genotoxic stress screen we also identify H_2O_2 and MMS-dependent PARylation of UBTF/UBF1, another factor involved in regulation of nucleolar chromatin, supporting the idea of PARylation as a mean to coordinate nucleolar function in response to genotoxic stress.

Chromatin remodelers have recently been recognized as important signaling coordinators in genome stability pathways (Papamichos-Chronakis and Peterson, 2013). Compelling evidence shows that PARylation governs access and activities of some of these factors at

sites of DNA damage, as recently demonstrated for CHD1L (ALC1) and CHD4 (Ahel et al., 2009; Chou et al., 2010; Pines et al., 2012). Intriguingly, we observed a strong PARylation of CHD1L in all four genotoxic stress treatments, while CHD2 was only modified in response to H_2O_2 and MMS and CHD4 only after MMS treatment, indicating that direct PARylation of these proteins may regulate their functions (Table S2). In support of this notion, loss of CHD2 has recently been reported to result in defective genotoxic stress signaling and genomic instability (Nagarajan et al., 2009). It would therefore be of interest to study how PARylation regulates the function of CHD2 and other chromatin remodeling factors function at the chromatin level, but such investigations were out of the scope of this study.

Comparative analysis of the genotoxic stress-induced PARylome reveals distinct regulation of RNA metabolism in response to oxidative and alkylating damage

A functional GO analysis of regulated proteins from all SILAC experiments revealed, as expected, that DNA metabolic processes are significantly enriched (Figure 6A). A considerable portion of these factors are involved in DNA repair (p-value < 9e-5) including many of the previously published candidates (Figure S4A). Strikingly, more than 60% of all significantly regulated proteins also comprise nucleic acid binding activity (Figure 6B). Although the proportion of RNA binding proteins in the complete dataset was less compared to DNA binding proteins, their enrichment in relation to the total number of RNA-binding proteins in the genome was more than 2-fold higher with a concomitantly enhanced p-value. This strongly suggests that post-transcriptional processes such as splicing, polyadenylation, mRNA stability and transport, and translation are readily controlled by PARylation-induced genotoxic stress. This finding is supported by recent genome-wide siRNA screens establishing a functional intersection of RNA processing with DNA repair (Adamson et al., 2012; Paulsen et al., 2009), although very few RNA processing factors hitherto have been examined in detail for their link to the DDR (Li and Manley, 2005; Moumen et al., 2005; Ramachandran et al., 2011). Our data therefore infers that PARylation of RNA-processing factors upon genotoxic insult may provide an additional layer for the participation of RNA-binding proteins in the DDR.

In order to assess the specific functional consequences of PARylation under different types of genotoxic stress we compared the significantly regulated protein population of

each single genotoxic stress experiment to all others (Figure 6A and Suppl. Table S2). In doing so, we identified ten proteins to be PARylated in all four genotoxic stress conditions (ARTD1, RPA1, MPG, TAF15, FUS, RBMX, ALC1, DTX2, RUNX1 and ZNF384). Interestingly, dissection of the single genotoxic stress-specific datasets revealed that particularly H_2O_2 and MMS treatment affect proteins involved in RNA metabolic processes including transcription, RNA processing and RNA splicing (Figure 6C and Figure S4A). This observation is also reflected by the overrepresentation of RNA-binding proteins in H_2O_2 and MMS samples, whereas the enrichment of regulated DNA-binding proteins is equal for all genotoxic stress conditions (Figure S4B). A functional network analysis showed that a large number of PARylated substrates involved in RNA metabolic processes are interconnected (Figure 6D). The majority of proteins involved in RNA metabolic processes is hitherto unknown to be targeted for PARylation with only few proteins previously published to be modified including members of the HNRNP family and SUPT16H (FACT140) (Huang et al., 2006; Ji and Tulin, 2009). However, emerging evidence indicates that PARylation plays an important role in RNA processes during genotoxic stress. In fact, in a recent siRNA screen the RNA-binding protein RBMX was identified as positive regulator of homologues recombination and found to localize to sites of DNA damage in PARylation-dependent manner (Adamson et al., 2012). Notably, we identify RBMX as a PARylation target upon all applied genotoxic stress treatments in our SILAC screen supporting the concept of ARTD1-dependent regulation of RBMX (Table S1). To further investigate the role of PARylation in RNA metabolic processes during genotoxic stress, we decided to conduct more detailed analysis of the two proteins TAF15 and THRAP3, for which we confirmed genotoxic stress-dependent PARylation using *in vivo* assays (Figure 5B).

The biological role of THRAP3 has previously been reported to be functionally linked to its localization in nuclear speckles (Lee et al., 2010). Dynamic spatio-temporal reorganization of subnuclear structures and their constituents are important to efficiently coordinate nuclear processes and cellular stress responses. Nuclear speckles have been shown to function in storage, assembly and modification of splicing factors. Hereby, a cell-type specific basal exchange level of splicing factors occurs between speckles and nucleoplasm, which is modulated upon stress conditions such as transcriptional inhibition. In contrast to the cytoplasm, compartmentalization within the nucleus is not dependent on

diffusion barriers, such as membranes. Thus, reorganization of subnuclear structures are often regulated by protein modifications such as phosphorylation/dephosphorylation events (Lamond and Spector, 2003). As a result, we surmised that PARylation of THRAP3 could constitute another mechanism to regulate stress-dependent assembly of factors in nuclear speckles.

To investigate this in more detail, we analyzed the cellular localization of GFP-tagged THRAP3 under transcriptional inhibition of RNAP I and II using the known inhibitor Actinomycin D (ActD) (Shav-Tal et al., 2005). Incubation of THRAP3-GFP expressing cells with ActD for 3 hours hardly changed the size of THRAP3 containing speckles albeit speckles appeared to round up (Figure 7A). Additional exposure of ActD-treated cells to oxidative stress led to the formation of enlarged, rounded speckles within 2 hours of H_2O_2 treatment, possibly reflecting a more substantiated inhibition of transcription. Intriguingly, pre-incubation with PARP inhibitor PJ-34 largely prevented accumulation of THRAP3 in enlarged nuclear speckles (Figure 7A) upon oxidative stress, supporting a concept, in which the stress-related function of THRAP3 is regulated in a PARylation-dependent manner.

Another phenomenon of nuclear restructuring involves the accumulation of a specific set of proteins in perinuleolar caps (Shav-Tal 2005). Transcriptional inhibition using ActD has been shown to induce nucleolar segregation of nucleolar components resulting in the formation of nucleolar cap structures typically surrounded by a dense chromatin ring. All members of the TET family of proteins (TAF15, FUS and EWS) are known to accumulate in these caps (Joberts, EMBO Rep. 2009, Shav-Tal 2005), and we find all of them to be highly regulated in our screen for PARylated targets in response to H_2O_2, MMS and UV radiation. This led us to further investigate whether PARylation would also contribute to the regulation of nucleolar cap formation upon genotoxic stress. In agreement with previous observations we found TAF15-GFP to be enriched in cap-like structures upon transcriptional inhibition with ActD (Figure 7B) (Joberts, EMBO Rep. 2009) but not upon exposure to oxidative stress alone (Figure S5A). Interestingly, nucleolar cap formation was abrogated when ActD-treated cells were exposed for 1h to H_2O_2, indicating that oxidative stress regulates reorganization of nucleolar structures. Even more strikingly, the presence of PARP inhibitor PJ34 rescued the formation of TAF15 containing cap-like structures after H_2O_2 but also after exposure to alkylating stress using MMS (Figure 7B). Collectively, we

reason that PARylation regulates the spatio-temporal dynamics of nuclear factors THRAP3 and TAF15 thereby coordinating RNA metabolic processes in response to genotoxic stress.

Discussion

Here, we describe a SILAC-based enrichment strategy for high confidence *in vivo* detection of PARylated proteins under various types of genotoxic stress, providing the largest dataset for covalently modified ARTD substrates to date. Substantial efforts were made on establishing an optimized technical protocol including the important use of PARP inhibitors during sample preparation to circumvent artificial PARylation of proteins, which otherwise could lead to overestimation or misinterpretation of the quantitative data. In strong support of the acquired data we prove covalent PARylation of several new targets by *in vitro* and *in vivo* approaches. Intriguingly, functional analysis of the dataset establishes extensive regulation of processes related to DNA metabolism but significantly also RNA metabolism including transcription, RNA splicing and transport. We specifically uncover a novel role of PARylation for THRAP3 and TAF15 in the coordination and assembly of subnuclear structures thereby facilitating the efficient regulation of cellular responses to genotoxic stress.

The activity of ARTD1 has long been known to have an impact on base excision repair (BER) and single strand break repair (SSBR) (Dantzer et al., 2000; Fisher et al., 2007), although its specific role in these processes has remained under debate. Recent reports proposed a model in which ARTD1 activity increases the repair capacity by recurring binding to SSBs for their protection if excessive amount of DNA damage limits the immediate availability of actual repair proteins (Dianov and Hubscher, 2013; Helleday, 2011). In our screen we identified several proteins of the BER and SSBR machinery to be PARylated (ARTD1, XRCC1, MPG, LIG3, PCNA) extending the list of previously known targets by the DNA glycosylase MPG and DNA ligase LIG3 (Rouleau et al., 2007; Sedgwick et al., 2007; Simbulan-Rosenthal et al., 1996), indicating that direct PARylation of repair factors could constitute an additional level of regulating repair efficiency. Another newly identified and *in vitro* validated PARylation target, PNKP, has also been described to serve a critical role in processing broken DNA strands to allow an efficient repair process

(Weinfeld et al., 2011) indicating that PARylation might affect the enzymatic activity of its substrate proteins. Additionally, ARTD enzymes have been demonstrated to play important roles in other DNA repair pathways such as nucleotide excision repair, mismatch repair and non-homologues end joining, which is supported by our findings of regulated pathway-specific proteins such as XPC and CETN2, MSH2 and MSH6, XRCC5 and XRCC6, respectively. Whether PARylation of pathway-specific proteins either positively or negatively regulates their function, and how specific types of DNA lesions are involved in these processes, remains to be elucidated.

Besides direct PARylation of target proteins cellular responses to genotoxic stress are regulated by the recruitment of PAR-binding proteins through one of the four described PAR-binding modules (Kalisch et al., 2012). Recent proteomic studies focused on the identification and regulation of non-covalently PAR-binding proteins by employing non-denaturing affinity purification methods, which however cannot avoid co-enrichment of PARylated proteins (Gagne et al., 2012). We specifically determined the extent of covalently PARylated proteins under various types of genotoxic stress using denaturing enrichment methods. In support of our method targeting specifically PARylated substrates we did not identify PAR-binding factors such as macro H2A.1, APLF, CHFR and RNF146 which have been reported to rapidly accumulate at sites of DNA damage through their PAR-binding motifs (Grundy et al., 2013; Kang et al., 2011; Li et al., 2010; Liu et al., 2013; Timinszky et al., 2009). Nevertheless, it cannot be excluded that PAR-binding proteins also become subject to direct PARylation, which according to our dataset appears to be the case for ALC1, C6orf130 and Trip12, suggesting a complex interplay between PAR-binding activities and PARylation of substrate proteins. Macrodomain-containing protein Af1521 was recently also identified to be a mono-ADP-ribosyl hydrolase (Jankevicius et al., 2013; Rosenthal et al., 2013a). However, this activity did not interfere with our experimental setup, since all reactions were performed at 4°C and the proteins we primarily monitored were poly(ADP-ribos)ylated.

We found that PARylation affects a large number of proteins involved in RNA metabolic processes, with a significant enhancement in response to oxidative and alkylation stress as compared to UV or IR. It has only started to become apparent in recent years that PARylation seems to provide an important link between the DNA damage response (DDR) and RNA metabolism (Adamson et al., 2012; Kruhlak et al., 2007; Paulsen et al., 2009;

Shanbhag et al., 2010). Moreover, mutations in the spliceosome machinery are frequent in malignancies (Papaemmanuil et al., 2011; Yoshida et al., 2011), implying a potential role for RNA splicing factors in maintaining genome stability and protection against cancer. This connection is supported by detailed analysis of pre-mRNA splicing factor THRAP3 that we show to be PARylated *in vivo* under oxidative damage. THRAP3 has previously been demonstrated to play a role in the DDR in a manner that parallels transcription inhibition (Beli et al., 2012) and we find that under transcriptional inhibition PARylation of THRAP3 affects its cellular localization and prevents the protein from co-localizing with splicing factors in nuclear speckles. Further emphasizing the considerable enrichment of RNA-binding proteins in our dataset, we selected TAF15 for further follow-up studies thereby proving *in vivo* PARylation of TAF15 and establishing a role for PARylation in coordinating its subnuclear distribution and function. TAF15 is a member of the TET protein family, that has been described to contribute to the control of transcription, splicing, RNA transport and DNA repair processes (Ballarino et al., 2012; Law et al., 2006; Tan and Manley, 2009). The TET proteins are frequently discovered to be involved in genetic-translocations in sarcomas, where their aminoterminal transactivation domain is fused to DNA binding domains of transcription factors, hereby causing inappropriate transcriptional activation of target genes (Law et al., 2006). Furthermore, depletion of FUS or EWS leads to increased genomic instability and sensitivity to UV and ionizing radiation (Hicks et al., 2000; Kuroda et al., 2000; Li et al., 2007; Paronetto et al., 2011). In fact, recent studies have also demonstrated Ewing's sarcoma cells and xenografts, harbouring genomic fusions of EWS with specific transcription factors, to be highly sensitive towards ARTD1 inhibition (Brenner et al., 2012; Garnett et al., 2012). Suggested mechanisms for the increased sensitivity included both enforced accumulation of DNA damage and ARTD1-dependent positive feedback loops specifically of EWS-FLI1 fusion proteins for transcriptional activation (Brenner et al., 2012). Direct PARylation of EWS as well as of other TET family members, as we identify in our SILAC screen, could provide another means to regulate the function and activity of these proteins and its translocation-based fusion products.

Previously, PARylation has received much attention as a potential target in cancer therapy. PARP inhibitors showed promising results in early clinical trials with a particular focus on treatment of tumors from HR-defective BRCA-mutation carriers, for which PARP

inhibition is speculated to interfere with efficient SSB-repair resulting in synthetic lethality of tumor cells (Fong et al., 2009). Since our results confirm PARylation of proteins involved in RNA metabolic processes, further elucidation of the regulatory role of PARylation in these processes upon genotoxic stress might provide valuable information for future strategies to effectively treat specific cancer subtypes with PARP inhibitors.

Only recently, the phenomenon of PAR-dependent ubiquitylation has emerged highlighting an important regulatory crosstalk between PARylation and ubiquitylation. The E3 ligase RNF146 was recently reported to become recruited to PARylated ARTD1 through its PAR-binding WWE domain, which activates its ligase activity in order to poly-ubiquitinate specifically auto-modified ARTD1, thereby targeting ARTD1 for proteasomal degradation (Kang et al., 2011). Similarly, the E3 ligase CHFR/RNF196, comprising a PAR-binding zinc finger, has been reported to contribute to PAR-dependent ubiquitylation of PARylated ARTD1 at DSBs but also upon mitotic stress (Kashima et al., 2012; Liu et al., 2013). It is therefore likely that other PARylated proteins are substrates for PAR-dependent ubiquitylation upon induction of genotoxic stress-induced PAR formation in order to assure target-specific degradation. Additional studies using our quantitative pull-down strategy could specifically identify such targets in cells exposed to genotoxic stress or microtubule inhibitors to investigate novel regulatory PAR-dependent functions controlling the DNA damage response or the mitotic checkpoint.

In summary, our SILAC-based enrichment approach largely extends the current knowledge on PARylation substrates that become targeted under various types of genotoxic stress. The next step will be to determine specific amino acids that act as acceptor sites for PAR chains *in vivo,* preferentially using mass-spectrometry-based techniques. Advances have recently been made in identifying lysine residues as novel acceptor sites for PAR (Altmeyer et al., 2009; Chapman et al., 2013; Messner et al., 2010). However, the complexity of the PAR polymer chain raises technical challenges, and highly advanced protocols will be required for the specific enrichment of PARylated peptides and their subsequent mass spectrometric analysis. Still, future investigations most likely will center on pinpointing specific amino acids as acceptors for PARylation of proteins, as well as the detailed circumstances and effects of the occurrence of this modification.

Experimental Procedures

Cell Culture and Transfection

U2OS and HeLa cells were grown in D-MEM (Invitrogen) supplemented with 10% FCS and penicillin/ streptomycin (100U/ml) (Gibco). Stable HeLa-Kyoto cells expressing SMARCA5, TAF15 or THRAP3 tagged with C-terminal GFP under an endogenous promoter were generated by transfecting BAC transgenes and were kindly provided by Anthony Hyman (Max Planck Institute, Dresden, Germany). Selection was maintained by adding 400 µg/ml G418 to the culture medium.

For SILAC labeling U2OS cells were grown in SILAC-DMEM (Invitrogen) supplemented with 10% dialyzed FBS (Invitrogen), sodium-pyruvate, L-glutamine, penicillin/ streptomycin and either L-lysine (Lys0) and L-arginine (Arg0), L-lysine 4,4,5,5-D4 (Lys4) and L-arginine–U-13C6 (Arg6) or L-lysine–U-13C6-15N2 (Lys8) and L-arginine–U-13C6-15N4 (Arg10) (Cambridge Isotope Laboratory) as described previously (Ong et al., 2002). The siRNA oligonucleotides against endogenous proteins were purchased from Ambion for human PARG (ID: s16158 and s16159), PARP1 (ID: s1098), PARP2 (ID: s19504) and Negative Control siRNA#1. SiRNA transfections were performed using Lipofectamine RNAiMAX (Invitrogen) according to the manufacturer's protocol.

Enrichment of PARylated Proteins

Cells were exposed to the following genotoxic agents and harvested at the indicated time points unless otherwise stated: IR (10 Gy, 1h), UV (40 J/m^2, 1h), MMS (10 mM, 0.5-1h) and H_2O_2 (10 mM in PBS, 10 min). Cells were washed with PBS and lysed in 50 mM Tris pH 7.5, 400 mM NaCl, 1mM EDTA, 1% NP-40, 0.1% Na-deoxycholate, protease inhibitor cocktail (Roche) supplemented with 2 mM Na-orthovanadate, 5 mM NaF, 5 mM Glycero-2-phosphate, 1 µM ADP-HPD (Millipore) and 40 µM PJ-34 (Enzo Life Sciences) or 5 mM 3-aminobenzamide (Sigma) as appropriate. Lysates were cleared by high speed centrifugation, diluted in modified lysis buffer to final concentrations of 150 mM NaCl, 0.5% NP-40 and 0.05 % Na-dexycholate. Protein concentrations were determined using Bradford assay. Equal protein amounts were incubated with GST-Af1521 for 2h at 4°C and bound complexes were eluted in Laemmli sample buffer. Eluates were combined and resolved on 4-20% SDS-PAGE. The Coomassie-stained gel was cut into slices, reduced

with 1 mM DTT, alkylated with 5 mM chloroacetamide (Nielsen et al., 2008), digested using modified sequencing grade trypsin (Sigma) and loaded on to C18 stage tips prior to mass spectrometric analysis.

Mass spectrometric analysis

All MS experiments were performed on a nanoscale HPLC system (EASY-nLC from Proxeon Biosystems) connected to an Orbitrap Q-Exactive equipped with a nanoelectrospray source (Thermo Fisher Scientific). Each peptide fraction was auto-sampled and separated on a 15 cm analytical column (75 um inner diameter) in-house packed with 3-um C18 beads (Reprosil Pur-AQ, Dr. Maisch) with a 2 h gradient ranging from 5% to 40% acetonitrile in 0.5% acetic acid at a flow rate of 250 nl/min. The effluent from the HPLC was directly electrosprayed into the mass spectrometer. The Q Exactive mass spectrometer was operated in data-dependent acquisition mode and all samples were analyzed using previously described 'sensitive' acquisition method (Kelstrup et al., 2012).

Identification of peptides and proteins

All raw data analysis was performed with MaxQuant software suite (Cox and Mann, 2008) version 1.3.0.5 supported by the Andromeda search engine (Cox et al., 2011). Data was searched against a concatenated target/decoy (Elias and Gygi, 2007) (forward and reversed) version of UniProtKB database encompassing 71,434 protein entries. We followed the step-by-step protocol of the MaxQuant software suite to generate MS/MS peak lists that were filtered to contain at most six peaks per 100 Da interval prior to the Andromeda database search. Mass tolerance for searches was set to maximum 7 ppm for peptide masses and 20 ppm for HCD fragment ion masses. Data was searched with carbamidomethylation as a fixed modification and protein N-terminal acetylation, methionine oxidation as variable modifications. A maximum of two mis-cleavages was allowed while requiring strict trypsin specificity. Peptide assignments were statistically evaluated in a Bayesian model on the basis of sequence length and Andromeda score. Only peptides and proteins with a false discovery rate (FDR) of less than 1% were accepted, estimated on the basis of the number of accepted reverse hits. Protein sequences of common contaminants such as human keratins and proteases used were

added to the database. Statistical analysis and hierarchical clustering was performed using Perseus (Max-Planck Institute of Biochemistry, Department of Proteomics and Signal Transduction, Munich). Significantly enriched Gene Ontology terms were determined using the Functional Annotation Tool of the DAVID Bioinformatics database (Huang da et al., 2009). Protein interaction networks were analyzed using the interaction data from the STRING database (v. 9.05) (Szklarczyk et al., 2011)and visualized using Cytoscape (v. 2.8.3) (Smoot et al., 2011)

Cloning, Expression and Purification of Proteins

Recombinant proteins were generated using the Bacterial or Baculovirus Expression System with Gateway® Technology (Invitrogen). Expression clones were created by recombining entry clones from the Ultimate ORF clone library (human cDNA for PNKP, CETN2, MID1/MPG, MECP2, ANKT, POLR2E and CDK2) with destination vector pDEST™10 pDEST™10 for baculo or pDEST™17 for bacterial expression using LR Clonase™ II Enzyme Mix and transforming NEB5-α *E. coli*. Sequence-verified expression clones were transformed into MAX Efficiency® DH10Bac™ Competent *E. coli*. Recombinant bacmid DNA was isolated from cultures of restreaked white colonies, verified by PCR and sequencing reactions, and then used to transfect Sf21 insect cells using Cellfectin® II Reagent to generate baculovirus. Concentrated viral stocks were further used to infect fresh insect cells for protein expression. Recombinant proteins were purified using ProBond™ Nickel-Chelating Resin.
Expression plasmids (pGEX) for GST-tagged Af1521 wildtype and its mutant G42E were kindly provided by Maria di Girolamo (Consorzio Mario Negri Sud, Santa Maria Imbaro, Italy). Bacterial recombinant proteins were purified using Glutathione Sepharose 4B (GE Healthcare) and covalently crosslinked to the resin using dimethylpimelimidate as described in Bar-Peled M, Raikhel NV (1996). Crosslinking was stopped using ethanolamine and non-coupled proteins were washed off with glycine–HCl at pH 2.5. Resin was stored in 50 mM Tris pH 7.5, 150 mM NaCl, 1 mM DTT at 4°C prior to use.

In vitro modification of candidate proteins

The candidate proteins were modified as described earlier (Rosenthal et al., 2013b). Briefly, 20 pmol of target protein were incubated with 10 pmol HIS-ARTD1 or HIS-ARTD2

for 15 min at 30°C in reaction buffer (50 mM Tris-HCL pH 8.0, 4 mM $MgCl_2$, 250 μM DTT) in the presence of 100 nM ^{32}P-NAD^+. Reactions with HIS-ARTD1 were supplemented with 5 pmol annealed double-stranded oligomer (5`-GGAATTCC-3`). The reactions were stopped by addition of SDS-loading buffer and boiling. Proteins were separated on an SDS-gel and visualized by autoradiography.

Immunochemical methods

The following antibodies were used in this study: mouse monoclonal GFP (B-2) (Santa Cruz, sc-9996), rabbit polyclonal PARP-1/2 (H-250) (Santa Cruz), rabbit polyclonal PARP2 (Active Motif), rabbit polyclonal Poly(ADP-ribose) (Enzo Life Sciences), rabbit polyclonal Phospho-p53 (Ser15) (Cell Signaling), mouse monoclonal XPC (Abcam, ab6264), rabbit polyclonal NFκB p65 (C-20) (Santa Cruz), mouse monoclonal GAPDH (6C5) (Calbiochem) and mouse monoclonal β-Actin Clone AC-74 (Sigma). Rabbit polyclonal Prestige Antibodies for MPG (HPA006531), PNKP (HPA006782), NUSAP1 (HPA042904) and MECP2 (HPA000593) were kindly provided by Jan Mulder (SciLifeLab, Karolinska Institute, Stockholm). GFP-immunoprecipitaion was performed with GFP-Trap®_A agarose beads (Chromotek) and Western blot analysis was done using standard protocols. For immunofluorescence analysis cells were grown on coverslips, fixed in icecold methanol, additionally permeabilized in 0.25% Triton X-100/PBS, blocked in 10% FBS/PBS and incubated with primary antibody (GFP) in 5% FBS/PBS overnight at 4°C. After staining with secondary antibody Alexa Fluor 488 (Invitrogen) for 30 min at room temperature coverslips were mounted in Vectashield (Vector Laboratories) containing nuclear DAPI stain. Images were acquired on an LSM-780 confocal microscope (Carl Zeiss Microimaging) mounted on a Zeiss-Axioimager with an oil immersion objective (Plan-Apochromat 40×/1.3). Image acquisition and analysis was carried out with ZEN2012 software.

Acknowledgements

We owe special thanks to Matthias Altmeyer from NNF-CPR for sharing his profound knowledge, which greatly advanced this study. We thank members of the NNF-CPR for fruitful discussions and careful reading of the manuscript. The work carried out in this study was in part supported by the Novo Nordisk Foundation Center for Protein Research, the Lundbeck Foundation, the European Union 7th Framework Programs PRIME-XS, grant agreement number 262067, and EURAtrans, grant agreement number HEALTH-F4-2010-241504. This work was supported in part by the Swiss National Science Foundation Grant 31- 122421 and the Kanton of Zurich (both to M.O.H.). The Prestige Antibodies were a kind donation from Jan Mulder.

Figure legends.

Figure 1 – Proteome-wide identification of PARylated proteins in response to genotoxic stress using a SILAC-based quantification.

(A) Schematic representation of the SILAC-based enrichment strategy. U2OS cells were grown in 'light' (L), 'medium' (M) or 'heavy' (H) SILAC medium. Heavy-labeled cells were treated with genotoxic stress. Separate pull-downs were performed from equimolar amounts of SILAC-encoded lysates using a PAR-binding defective mutant (G42E) for light SILAC state and a PAR-binding GST-Af1521 wildtype (wt) macrodomain for medium and heavy SILAC states. Eluates were combined equally, resolved by SDS-PAGE, cut into slices and subjected to tryptic in-gel digestion. Peptide fractions were analyzed by high resolution LC-MS/MS on an Orbitrap Q-Exactive instrument and the data was further processed by bioinformatic tools.

(B) Quantitative comparison of tryptic peptide abundances. Each peptide occurs as a SILAC triplet. SILAC peptide intensity ratios of 1:1:1 between all 3 SILAC states indicate unspecific background binders, whereas proteins most abundant in heavy SILAC state correspond to PARylated proteins in response to genotoxic stress. Proteins with increased abundance in medium-isoptope encoded samples only are considered PARylated under basal conditions.

Figure 2 – Technical optimization of SILAC-strategy for specific enrichment of PARylated proteins

(A) SILAC-based enrichment of PARylated proteins in the absence of exogenous genotoxic stress (see experimental setup in Figure S1A and 1B). Logarithmized H/M SILAC ratios from the 'forward' experiment and M/H SILAC ratios from the 'reverse' experiment were plotted against each other. GO functional annotation of significantly regulated proteins in the combined dataset reveal strong enrichment of proteins involved in DNA repair processes compared to annotated GO genes across the entire human genome (indicated p-values < 0.005).

(B) Pull-downs performed on untreated U2OS cells using GST-Af1521 wt and mutant G42E were analyzed by immunoblotting using antibodies to PAR and PARP1.

(C) U2OS cell lysate preparation in the absence or presence of 5 mM PARP-inhibitor 3-AB in the lysis buffer to prevent unphysiological activation of protein PARylation (compare lane 6 and 5), and separate cells treated with 3-AB (5 mM, 1h) prior to cell lysis (lane 4). Pull-downs were performed using GST-Af1521 wt and analyzed by immunoblotting with the indicated antibodies.

(D) Hierarchical clustering of proteins derived from SILAC-based U2OS lysate pull-down (see experimental setup in Figure S2A) in the absence (-) or presence (+) of 3-AB (5 mM) or PJ-34 (40 µM) in the lysis buffer. Functional GO analysis of regulated proteins in the absence of PARP inhibitors reveals strong enrichment of PARylated proteins involved in DNA repair.

(D) U2OS cells were transfected with PARG siRNA for 72h and treated with H_2O_2 (1 mM, 10 min) as indicated and analyzed by immunoblotting with PAR antibody.

Figure 3 – Quantitative analysis of DNA damage-induced protein PARylation.

(A) Four biological SILAC experiments were performed to investigate the impact of different DNA damaging agents on protein PARylation (see also Figure 1A). In the single experiments cells were treated in heavy SILAC state with H_2O_2 (1 mM, 10 min), MMS (10 mM, 1h), UV (40 J/m^2, 1h) or IR (10 Gy, 1h) respectively. All pull-downs were performed with siPARG-treated U2OS cells and the use of 1 µM PARG inhibitor ADP-HPD and 40 µM PARP inhibitor PJ-34 in the lysis buffer.

(B) Significantly upregulated PARylated proteins in response to oxidative stress. Logarithmized M/L and H/L SILAC ratios from the H_2O_2 experiment were plotted, representing untreated and treated cells. M/L SILAC ratios cumulate around 1 and follow a normal distribution while H/L ratios are shifted upwardly corresponding to induced protein PARylation. Statistical significance was calculated using Wilcoxon rank sum test.

(C) Boxplot analysis of logarithmized M/L SILAC ratios from all four SILAC experiments (see Figure 3A). No regulation of PARylated proteins is observed in the absence of genotoxic stress.

(D) Boxplot analysis of logarithmized H/L SILAC ratios for each SILAC experiments (see Figure 3A). Significant regulation reveals strong induction of protein PARylation upon genotoxic stress.

(E) siPARG-transfected cells were treated with DNA damaging agents and analyzed by immunoblotting with the indicated antibodies. Notably, the extent of protein PARylation follows the distribution of SILAC ratios in Figure 3D.
(F) Heat map of quantified proteins from the combined pull-down experiments in the absence (-) or presence (+) of DNA damage. PARylated proteins induced by genotoxic stress are clustered together.
(G) GO term annotation enrichment for cellular distribution of significantly upregulated proteins in all four SILAC experiments.

Figure 4 – Identification and *in vitro* validation of novel protein PARylation targets.
(A) Overlap of total number of PARylated proteins identified in this study with proteins that were previously published to be PARylated and assigned with a role in DNA repair based on GO term annotation.
(B) *In vitro* PARylation of newly identified protein targets in the SILAC screen. Purified full-length human ARTD1 (left panels) and ARTD2 (right panels) were incubated with recombinantly expressed proteins in the presence of ^{32}P-NAD and double-stranded DNA oligomer. Samples were resolved by SDS-PAGE, stained with Coomassie (lower panels) and ^{32}P-incorporation was detected by autoradiography (AR) (upper panels). (*ARTD1, **ARTD2, Ctrl: Histone H1 and zinc finger 1+2 from ARTD1).
(C) ARTD1 accounts for the majority of protein PARylation in response to genotoxic stress. U2OS cells were co-transfected with PARG siRNA and either control, ARTD1 or ARTD2 siRNA. Cells were treated with DNA damaging agents as described in Figure 3A and analyzed by immunoblotting with the indicated antibodies.
(D) Logarithmized SILAC ratios of all identified PARP/ARTD family members from the individual SILAC experiments.

Figure 5 – *In vivo* PARylation of novel protein targets.
(A) SiPARG-transfected U2OS cells were incubated with PJ-34 (40 µM, 1.5h) or left untreated prior to treatment with H_2O_2 (1 mM, 10 min) as indicated. Cell lysates were pulled down with GST-Af1521 WT and analyzed by immunoblotting with the indicated antibodies to detect enriched PARylated proteins. NFκB antibody was used as negative control.

(B) HeLa cells stably expressing TAF15, THRAP3 or SMARCA5 as GFP-fusion proteins were transfected with PARG siRNA and treated with PJ-34 and H_2O_2 as in (A). Lysates were subjected to Af1521 WT pull-down or GFP-immunoprecipitation and subsequently analyzed by immunoblotting with PAR and GFP antibodies (*PARylated GFP-target protein).

Figure 6 – Functional consequences of distinct types of DNA damage treatment on protein PARylation.

(A) Protein interaction networks of significantly PARylated proteins from all SILAC experiments grouped into DNA metabolism by GO term annotation for biological process (p-value < 8e-14). Network interaction data was extracted from STRING database and visualized using Cytoscape.

(B) InterPro domain annotation associated with the molecular function of significantly regulated proteins from all SILAC experiments as compared to annotated GO genes in the entire genome (indicated p-values < 1.5e-17). Strong enrichment for RNA- and DNA-binding proteins is observed.

(C) Venn diagram demonstrating the overlap of PARylated proteins from the individual DNA damage experiments (as described in Figure 3A).

(D) GO enrichment analysis reveals specific enrichment of RNA metabolic processes in H_2O_2 and MMS experiment, while proteins involved in DNA metabolic processes are equally identified across all DNA damage experiments. Analysis was performed using GO term annotations for biological processes of significantly regulated protein sets in each DNA damage SILAC experiment (specific p-values are listed in Figure S4C).

(E) Protein interaction networks of significantly PARylated proteins from the H_2O_2 (upper panel) and MMS (lower panel) experiments grouped into RNA metabolism by GO term annotation for biological process (p-value < 2e-16).

Figure 7 – PARylation-dependent redistribution of TAF15 and THRAP3 in subnuclear structures in response to genotoxic stress.

(A) Stable THRAP3-GFP expressing HeLa cells were left untreated or pre-treated with 40 µM PJ-34 for 15 min, followed by an incubation with 5 µg/ml ActinomycinD (ActD) up to 3

h. Prior to fixation cells were exposed to 2 mM H_2O_2 for the indicated time points and immunostained with GFP antibody.

(B) Stable TAF15-GFP expressing HeLa cells were similarly left untreated or pre-treated with 40 µM PJ-34 for 15 min, followed by an incubation of 5 µg/ml ActinomycinD (ActD) up to 3 h. Prior to fixation cells were exposed to 2 mM H_2O_2 for 1h or 1 mM MMS for 2 h and immunostained with GFP antibody.

Figure S1 – SILAC experiments for comparison of binding properties for GST-Af1521 wt and the mutant G42E in the absence of exogenous genotoxic stress.

(A) In a forward experiment U2OS cell lysates grown in light SILAC condition were subjected to pull-down with Glutathione sepharose beads, while pull-down of cell lysates in medium SILAC condition was performed with mutant GST-Af1521 G42E and in heavy SILAC state with GST-Af1521 wt. Eluates were combined equally, resolved by SDS-PAGE, cut into slices and subjected to tryptic in-gel digestion. Peptide fractions were analyzed by high resolution LC-MS/MS.

(B) A reverse SILAC experiment was carried out in exactly the same manner as in (A) except for a SILAC label swap between the medium and heavy SILAC condition for pull-down with GST-Af1521 wt and G42E.

(C) High reproducibility between forward and reverse SILAC experiments for GST-AF1521 pull-downs. For analysis of GST-Af1521 G42E pull-down efficiency logarithmized M/L SILAC ratios of the forward experiment and H/L ratios of the reverse experiment were plotted against each other. Similarly, logarithmized H/L SILAC ratios of the forward experiment and M/L ratios of the reverse experiment were plotted against each other for analysis of GST-Af1521 wt pull-down efficiency. Pearson correlation coefficient was calculated for each plotted dataset.

Figure S2 – SILAC experiments showing the indispensability of PARP inhibitors during sample preparation.

(A) U2OS cells grown in light SILAC condition were pre-treated with PARP inhibitors in two different SILAC experiments (experiment A: 5 mM 3-AB, 2 h; experiment B: 40 µM PJ-34, 2 h). Cell lysates for light and medium SILAC condition additionally contained 40 µM PJ-34 or 5 mM 3-AB, respectively, in the lysis buffer. Equal protein amounts from cell lysates of all 3 SILAC conditions were subjected to pull-down with GST-Af1521 wt. Eluates were combined, resolved by SDS-PAGE, cut into slices and subjected to tryptic in-gel digestion. Peptide fractions were analyzed by high resolution LC-MS/MS.

(B) Summed peptide intensities were plotted against logarithmized SILAC ratios in the presence or absence of PJ-34 or 3-AB as indicated. Upregulation of SILAC ratios for PARylated proteins occured only in the absence of PARP inhibitors in the lysis buffer

(H/L), while inclusion of PARP inhibitors in the lysis buffer did not result in enrichment of PARylated proteins with increased M/L SILAC ratios.
(C) U2OS cell lysate preparation excluded or involved 40 µM PARP-inhibitor PJ-34 in the lysis buffer (LB) to prevent unphysiological activation of protein PARylation (compare lane 6 and 5), or cells were additionally treated with PJ-34 (40 µM, 1h) prior to lysis (lane 4). Pull-downs were performed using GST-Af1521 wt and analyzed by immunoblotting with the indicated antibodies.

Figure S3 – Reproducibility and sensitivity of different DNA damage SILAC experiments.
(A) Q-Q probability plots show correlation of logarithmized M/L ratios from the single DNA damage SILAC experiments as indicated.
(B) Overlap of previously published dataset for in-depth proteome analysis of the U2OS cell line (Geiger et al., 2012) with significantly regulated proteins identified with at least 2 peptides and indicated sequence coverage in the DNA damage SILAC experiments.

Figure S4 – Functional consequences of distinct types of DNA damage treatment on protein PARylation.
(A) Protein interaction networks of significantly PARylated proteins from each SILAC experiment grouped into DNA repair by GO term annotation for biological process (p-value < 8e-5). Network interaction data was extracted from the STRING database and visualized using Cytoscape.
(B) Fold enrichment of GO term annotations of significantly upregulated proteins with RNA binding and DNA binding activities in each DNA damage SILAC experiment.
(C) P-values for the specific enrichment of the listed GO term annotated biological processes for significantly upregulated proteins in each DNA damage SILAC experiment (graphical representation of GO term enrichment in Figure 6C).

Figure S5 – Control samples for analysis of PARylation-dependent redistribution of TAF15 and THRAP3 in subnuclear structures in response to genotoxic stress.
(A) Stable THRAP3-GFP expressing HeLa cells were left untreated or pre-treated with 40 µM PJ-34 for up to 3 h. Prior to fixation cells were exposed to 2 mM H_2O_2 for the indicated time points, fixed and immunostained with GFP antibody.

(B) Stable TAF15-GFP expressing HeLa cells were pre-treated with 40 µM PJ-34 for 15 min, followed by an incubation of 5 µg/ml ActinomycinD (ActD) up to 3 h where indicated, fixed and immunostained with GFP antibody.

Table S1 – List of identified proteins in total for the SILAC experiment comparing the binding properties for GST-Af1521 wt and the mutant G42E in the absence of exogenous genotoxic stress (related to Figure 2 and S1).

Table S2 – List of identified proteins for the SILAC experiments comparing different types of genotoxic stress (related to Figure 1, 3, 4A, 6, S3 and S4).

(A) Proteins that were found to be significantly regulated in response to a specific type of genotoxic stress as indicated.
(B) Total list of proteins identified in the SILAC experiments comparing different genotoxic stress conditions.

References

Adamson, B., Smogorzewska, A., Sigoillot, F.D., King, R.W., and Elledge, S.J. (2012). A genome-wide homologous recombination screen identifies the RNA-binding protein RBMX as a component of the DNA-damage response. Nat Cell Biol *14*, 318-328.

Ahel, D., Horejsi, Z., Wiechens, N., Polo, S.E., Garcia-Wilson, E., Ahel, I., Flynn, H., Skehel, M., West, S.C., Jackson, S.P.*, et al.* (2009). Poly(ADP-ribose)-dependent regulation of DNA repair by the chromatin remodeling enzyme ALC1. Science *325*, 1240-1243.

Altmeyer, M., and Lukas, J. (2013). To spread or not to spread-chromatin modifications in response to DNA damage. Curr Opin Genet Dev.

Altmeyer, M., Messner, S., Hassa, P.O., Fey, M., and Hottiger, M.O. (2009). Molecular mechanism of poly(ADP-ribosyl)ation by PARP1 and identification of lysine residues as ADP-ribose acceptor sites. Nucleic Acids Res *37*, 3723-3738.

Alvarez-Gonzalez, R., and Althaus, F.R. (1989). Poly(ADP-ribose) catabolism in mammalian cells exposed to DNA-damaging agents. Mutat Res *218*, 67-74.

Ame, J.C., Rolli, V., Schreiber, V., Niedergang, C., Apiou, F., Decker, P., Muller, S., Hoger, T., Menissier-de Murcia, J., and de Murcia, G. (1999). PARP-2, A novel mammalian DNA damage-dependent poly(ADP-ribose) polymerase. J Biol Chem *274*, 17860-17868.

Ballarino, M., Jobert, L., Dembele, D., de la Grange, P., Auboeuf, D., and Tora, L. (2012). TAF15 is important for cellular proliferation and regulates the expression of a subset of cell cycle genes through miRNAs. Oncogene.

Bartkova, J., Horejsi, Z., Koed, K., Kramer, A., Tort, F., Zieger, K., Guldberg, P., Sehested, M., Nesland, J.M., Lukas, C.*, et al.* (2005). DNA damage response as a candidate anti-cancer barrier in early human tumorigenesis. Nature *434*, 864-870.

Beli, P., Lukashchuk, N., Wagner, S.A., Weinert, B.T., Olsen, J.V., Baskcomb, L., Mann, M., Jackson, S.P., and Choudhary, C. (2012). Proteomic investigations reveal a role for RNA processing factor THRAP3 in the DNA damage response. Mol Cell *46*, 212-225.

Beneke, S., Meyer, K., Holtz, A., Huttner, K., and Burkle, A. (2012). Chromatin composition is changed by poly(ADP-ribosyl)ation during chromatin immunoprecipitation. PLoS One *7*, e32914.

Bennetzen, M.V., Larsen, D.H., Bunkenborg, J., Bartek, J., Lukas, J., and Andersen, J.S. (2010). Site-specific phosphorylation dynamics of the nuclear proteome during the DNA damage response. Mol Cell Proteomics *9*, 1314-1323.

Bensimon, A., Schmidt, A., Ziv, Y., Elkon, R., Wang, S.Y., Chen, D.J., Aebersold, R., and Shiloh, Y. (2010). ATM-dependent and -independent dynamics of the nuclear phosphoproteome after DNA damage. Sci Signal *3*, rs3.

Bonicalzi, M.E., Haince, J.F., Droit, A., and Poirier, G.G. (2005). Regulation of poly(ADP-ribose) metabolism by poly(ADP-ribose) glycohydrolase: where and when? Cell Mol Life Sci *62*, 739-750.

Brenner, J.C., Feng, F.Y., Han, S., Patel, S., Goyal, S.V., Bou-Maroun, L.M., Liu, M., Lonigro, R., Prensner, J.R., Tomlins, S.A.*, et al.* (2012). PARP-1 inhibition as a targeted strategy to treat Ewing's sarcoma. Cancer Res *72*, 1608-1613.

Chapman, J.D., Gagne, J.P., Poirier, G.G., and Goodlett, D.R. (2013). Mapping PARP-1 Auto-ADP-ribosylation Sites by Liquid Chromatography-Tandem Mass Spectrometry. J Proteome Res.

Chou, D.M., Adamson, B., Dephoure, N.E., Tan, X., Nottke, A.C., Hurov, K.E., Gygi, S.P., Colaiacovo, M.P., and Elledge, S.J. (2010). A chromatin localization screen reveals poly (ADP ribose)-regulated recruitment of the repressive polycomb and NuRD complexes to sites of DNA damage. Proc Natl Acad Sci U S A *107*, 18475-18480.

Choudhary, C., Kumar, C., Gnad, F., Nielsen, M.L., Rehman, M., Walther, T.C., Olsen, J.V., and Mann, M. (2009). Lysine acetylation targets protein complexes and co-regulates major cellular functions. Science *325*, 834-840.

Cortes, U., Tong, W.M., Coyle, D.L., Meyer-Ficca, M.L., Meyer, R.G., Petrilli, V., Herceg, Z., Jacobson, E.L., Jacobson, M.K., and Wang, Z.Q. (2004). Depletion of the 110-kilodalton isoform of poly(ADP-ribose) glycohydrolase increases sensitivity to genotoxic and endotoxic stress in mice. Mol Cell Biol *24*, 7163-7178.
Cox, J., and Mann, M. (2008). MaxQuant enables high peptide identification rates, individualized p.p.b.-range mass accuracies and proteome-wide protein quantification. Nat Biotechnol *26*, 1367-1372.
Cox, J., Neuhauser, N., Michalski, A., Scheltema, R.A., Olsen, J.V., and Mann, M. (2011). Andromeda: a peptide search engine integrated into the MaxQuant environment. J Proteome Res *10*, 1794-1805.
Dani, N., Stilla, A., Marchegiani, A., Tamburro, A., Till, S., Ladurner, A.G., Corda, D., and Di Girolamo, M. (2009). Combining affinity purification by ADP-ribose-binding macro domains with mass spectrometry to define the mammalian ADP-ribosyl proteome. Proc Natl Acad Sci U S A *106*, 4243-4248.
Dantzer, F., de La Rubia, G., Menissier-De Murcia, J., Hostomsky, Z., de Murcia, G., and Schreiber, V. (2000). Base excision repair is impaired in mammalian cells lacking Poly(ADP-ribose) polymerase-1. Biochemistry *39*, 7559-7569.
de Godoy, L.M., Olsen, J.V., Cox, J., Nielsen, M.L., Hubner, N.C., Frohlich, F., Walther, T.C., and Mann, M. (2008). Comprehensive mass-spectrometry-based proteome quantification of haploid versus diploid yeast. Nature *455*, 1251-1254.
de Murcia, J.M., Niedergang, C., Trucco, C., Ricoul, M., Dutrillaux, B., Mark, M., Oliver, F.J., Masson, M., Dierich, A., LeMeur, M.*, et al.* (1997). Requirement of poly(ADP-ribose) polymerase in recovery from DNA damage in mice and in cells. Proc Natl Acad Sci U S A *94*, 7303-7307.
Dianov, G.L., and Hubscher, U. (2013). Mammalian base excision repair: the forgotten archangel. Nucleic Acids Res *41*, 3483-3490.
Elias, J.E., and Gygi, S.P. (2007). Target-decoy search strategy for increased confidence in large-scale protein identifications by mass spectrometry. Nat Methods *4*, 207-214.
Fisher, A.E., Hochegger, H., Takeda, S., and Caldecott, K.W. (2007). Poly(ADP-ribose) polymerase 1 accelerates single-strand break repair in concert with poly(ADP-ribose) glycohydrolase. Mol Cell Biol *27*, 5597-5605.
Fong, P.C., Boss, D.S., Yap, T.A., Tutt, A., Wu, P., Mergui-Roelvink, M., Mortimer, P., Swaisland, H., Lau, A., O'Connor, M.J.*, et al.* (2009). Inhibition of poly(ADP-ribose) polymerase in tumors from BRCA mutation carriers. N Engl J Med *361*, 123-134.
Gagne, J.P., Isabelle, M., Lo, K.S., Bourassa, S., Hendzel, M.J., Dawson, V.L., Dawson, T.M., and Poirier, G.G. (2008). Proteome-wide identification of poly(ADP-ribose) binding proteins and poly(ADP-ribose)-associated protein complexes. Nucleic Acids Res *36*, 6959-6976.
Gagne, J.P., Pic, E., Isabelle, M., Krietsch, J., Ethier, C., Paquet, E., Kelly, I., Boutin, M., Moon, K.M., Foster, L.J.*, et al.* (2012). Quantitative proteomics profiling of the poly(ADP-ribose)-related response to genotoxic stress. Nucleic Acids Res.
Garnett, M.J., Edelman, E.J., Heidorn, S.J., Greenman, C.D., Dastur, A., Lau, K.W., Greninger, P., Thompson, I.R., Luo, X., Soares, J.*, et al.* (2012). Systematic identification of genomic markers of drug sensitivity in cancer cells. Nature *483*, 570-575.
Geiger, T., Wehner, A., Schaab, C., Cox, J., and Mann, M. (2012). Comparative proteomic analysis of eleven common cell lines reveals ubiquitous but varying expression of most proteins. Mol Cell Proteomics *11*, M111 014050.
Gorgoulis, V.G., Vassiliou, L.V., Karakaidos, P., Zacharatos, P., Kotsinas, A., Liloglou, T., Venere, M., Ditullio, R.A., Jr., Kastrinakis, N.G., Levy, B.*, et al.* (2005). Activation of the DNA damage checkpoint and genomic instability in human precancerous lesions. Nature *434*, 907-913.
Grundy, G.J., Rulten, S.L., Zeng, Z., Arribas-Bosacoma, R., Iles, N., Manley, K., Oliver, A., and Caldecott, K.W. (2013). APLF promotes the assembly and activity of non-homologous end joining protein complexes. EMBO J *32*, 112-125.
Guetg, C., Scheifele, F., Rosenthal, F., Hottiger, M.O., and Santoro, R. (2012). Inheritance of silent rDNA chromatin is mediated by PARP1 via noncoding RNA. Mol Cell *45*, 790-800.

Haince, J.F., Kozlov, S., Dawson, V.L., Dawson, T.M., Hendzel, M.J., Lavin, M.F., and Poirier, G.G. (2007). Ataxia telangiectasia mutated (ATM) signaling network is modulated by a novel poly(ADP-ribose)-dependent pathway in the early response to DNA-damaging agents. J Biol Chem *282*, 16441-16453.
Hassa, P.O., and Hottiger, M.O. (2008). The diverse biological roles of mammalian PARPS, a small but powerful family of poly-ADP-ribose polymerases. Front Biosci *13*, 3046-3082.
Helleday, T. (2011). The underlying mechanism for the PARP and BRCA synthetic lethality: clearing up the misunderstandings. Mol Oncol *5*, 387-393.
Hicks, G.G., Singh, N., Nashabi, A., Mai, S., Bozek, G., Klewes, L., Arapovic, D., White, E.K., Koury, M.J., Oltz, E.M*., et al.* (2000). Fus deficiency in mice results in defective B-lymphocyte development and activation, high levels of chromosomal instability and perinatal death. Nat Genet *24*, 175-179.
Huang da, W., Sherman, B.T., and Lempicki, R.A. (2009). Bioinformatics enrichment tools: paths toward the comprehensive functional analysis of large gene lists. Nucleic Acids Res *37*, 1-13.
Huang, J.Y., Chen, W.H., Chang, Y.L., Wang, H.T., Chuang, W.T., and Lee, S.C. (2006). Modulation of nucleosome-binding activity of FACT by poly(ADP-ribosyl)ation. Nucleic Acids Res *34*, 2398-2407.
Jankevicius, G., Hassler, M., Golia, B., Rybin, V., Zacharias, M., Timinszky, G., and Ladurner, A.G. (2013). A family of macrodomain proteins reverses cellular mono-ADP-ribosylation. Nat Struct Mol Biol *20*, 508-514.
Javle, M., and Curtin, N.J. (2011). The potential for poly (ADP-ribose) polymerase inhibitors in cancer therapy. Ther Adv Med Oncol *3*, 257-267.
Ji, Y., and Tulin, A.V. (2009). Poly(ADP-ribosyl)ation of heterogeneous nuclear ribonucleoproteins modulates splicing. Nucleic Acids Res *37*, 3501-3513.
Kalisch, T., Ame, J.C., Dantzer, F., and Schreiber, V. (2012). New readers and interpretations of poly(ADP-ribosyl)ation. Trends Biochem Sci *37*, 381-390.
Kang, H.C., Lee, Y.I., Shin, J.H., Andrabi, S.A., Chi, Z., Gagne, J.P., Lee, Y., Ko, H.S., Lee, B.D., Poirier, G.G*., et al.* (2011). Iduna is a poly(ADP-ribose) (PAR)-dependent E3 ubiquitin ligase that regulates DNA damage. Proc Natl Acad Sci U S A *108*, 14103-14108.
Karras, G.I., Kustatscher, G., Buhecha, H.R., Allen, M.D., Pugieux, C., Sait, F., Bycroft, M., and Ladurner, A.G. (2005). The macro domain is an ADP-ribose binding module. EMBO J *24*, 1911-1920.
Kashima, L., Idogawa, M., Mita, H., Shitashige, M., Yamada, T., Ogi, K., Suzuki, H., Toyota, M., Ariga, H., Sasaki, Y*., et al.* (2012). CHFR protein regulates mitotic checkpoint by targeting PARP-1 protein for ubiquitination and degradation. J Biol Chem *287*, 12975-12984.
Kelstrup, C.D., Young, C., Lavallee, R., Nielsen, M.L., and Olsen, J.V. (2012). Optimized Fast and Sensitive Acquisition Methods for Shotgun Proteomics on a Quadrupole Orbitrap Mass Spectrometer. J Proteome Res.
Kraus, W.L., and Hottiger, M.O. (2013). PARP-1 and gene regulation: Progress and puzzles. Mol Aspects Med.
Kruhlak, M., Crouch, E.E., Orlov, M., Montano, C., Gorski, S.A., Nussenzweig, A., Misteli, T., Phair, R.D., and Casellas, R. (2007). The ATM repair pathway inhibits RNA polymerase I transcription in response to chromosome breaks. Nature *447*, 730-734.
Kuroda, M., Sok, J., Webb, L., Baechtold, H., Urano, F., Yin, Y., Chung, P., de Rooij, D.G., Akhmedov, A., Ashley, T*., et al.* (2000). Male sterility and enhanced radiation sensitivity in TLS(-/-) mice. EMBO J *19*, 453-462.
Lamond, A.I., and Spector, D.L. (2003). Nuclear speckles: a model for nuclear organelles. Nat Rev Mol Cell Biol *4*, 605-612.
Langelier, M.F., Planck, J.L., Roy, S., and Pascal, J.M. (2012). Structural basis for DNA damage-dependent poly(ADP-ribosyl)ation by human PARP-1. Science *336*, 728-732.
Law, W.J., Cann, K.L., and Hicks, G.G. (2006). TLS, EWS and TAF15: a model for transcriptional integration of gene expression. Brief Funct Genomic Proteomic *5*, 8-14.
Lee, K.M., Hsu Ia, W., and Tarn, W.Y. (2010). TRAP150 activates pre-mRNA splicing and promotes nuclear mRNA degradation. Nucleic Acids Res *38*, 3340-3350.

Li, G.Y., McCulloch, R.D., Fenton, A.L., Cheung, M., Meng, L., Ikura, M., and Koch, C.A. (2010). Structure and identification of ADP-ribose recognition motifs of APLF and role in the DNA damage response. Proc Natl Acad Sci U S A *107*, 9129-9134.
Li, H., Watford, W., Li, C., Parmelee, A., Bryant, M.A., Deng, C., O'Shea, J., and Lee, S.B. (2007). Ewing sarcoma gene EWS is essential for meiosis and B lymphocyte development. J Clin Invest *117*, 1314-1323.
Li, X., and Manley, J.L. (2005). Inactivation of the SR protein splicing factor ASF/SF2 results in genomic instability. Cell *122*, 365-378.
Liu, C., Wu, J., Paudyal, S.C., You, Z., and Yu, X. (2013). CHFR is important for the first wave of ubiquitination at DNA damage sites. Nucleic Acids Res *41*, 1698-1710.
Lukas, J., Lukas, C., and Bartek, J. (2011). More than just a focus: The chromatin response to DNA damage and its role in genome integrity maintenance. Nat Cell Biol *13*, 1161-1169.
Luo, X., and Kraus, W.L. (2012). On PAR with PARP: cellular stress signaling through poly(ADP-ribose) and PARP-1. Genes Dev *26*, 417-432.
Malanga, M., and Althaus, F.R. (1994). Poly(ADP-ribose) molecules formed during DNA repair in vivo. J Biol Chem *269*, 17691-17696.
Matsuoka, S., Ballif, B.A., Smogorzewska, A., McDonald, E.R., 3rd, Hurov, K.E., Luo, J., Bakalarski, C.E., Zhao, Z., Solimini, N., Lerenthal, Y.*, et al.* (2007). ATM and ATR substrate analysis reveals extensive protein networks responsive to DNA damage. Science *316*, 1160-1166.
Menissier de Murcia, J., Ricoul, M., Tartier, L., Niedergang, C., Huber, A., Dantzer, F., Schreiber, V., Ame, J.C., Dierich, A., LeMeur, M.*, et al.* (2003). Functional interaction between PARP-1 and PARP-2 in chromosome stability and embryonic development in mouse. EMBO J *22*, 2255-2263.
Messner, S., Altmeyer, M., Zhao, H., Pozivil, A., Roschitzki, B., Gehrig, P., Rutishauser, D., Huang, D., Caflisch, A., and Hottiger, M.O. (2010). PARP1 ADP-ribosylates lysine residues of the core histone tails. Nucleic Acids Res *38*, 6350-6362.
Moumen, A., Masterson, P., O'Connor, M.J., and Jackson, S.P. (2005). hnRNP K: an HDM2 target and transcriptional coactivator of p53 in response to DNA damage. Cell *123*, 1065-1078.
Nagarajan, P., Onami, T.M., Rajagopalan, S., Kania, S., Donnell, R., and Venkatachalam, S. (2009). Role of chromodomain helicase DNA-binding protein 2 in DNA damage response signaling and tumorigenesis. Oncogene *28*, 1053-1062.
Nielsen, M.L., Vermeulen, M., Bonaldi, T., Cox, J., Moroder, L., and Mann, M. (2008). Iodoacetamide-induced artifact mimics ubiquitination in mass spectrometry. Nat Methods *5*, 459-460.
Ong, S.E., Blagoev, B., Kratchmarova, I., Kristensen, D.B., Steen, H., Pandey, A., and Mann, M. (2002). Stable isotope labeling by amino acids in cell culture, SILAC, as a simple and accurate approach to expression proteomics. Mol Cell Proteomics *1*, 376-386.
Papaemmanuil, E., Cazzola, M., Boultwood, J., Malcovati, L., Vyas, P., Bowen, D., Pellagatti, A., Wainscoat, J.S., Hellstrom-Lindberg, E., Gambacorti-Passerini, C.*, et al.* (2011). Somatic SF3B1 mutation in myelodysplasia with ring sideroblasts. N Engl J Med *365*, 1384-1395.
Papamichos-Chronakis, M., and Peterson, C.L. (2013). Chromatin and the genome integrity network. Nat Rev Genet *14*, 62-75.
Paronetto, M.P., Minana, B., and Valcarcel, J. (2011). The Ewing sarcoma protein regulates DNA damage-induced alternative splicing. Mol Cell *43*, 353-368.
Paulsen, R.D., Soni, D.V., Wollman, R., Hahn, A.T., Yee, M.C., Guan, A., Hesley, J.A., Miller, S.C., Cromwell, E.F., Solow-Cordero, D.E.*, et al.* (2009). A genome-wide siRNA screen reveals diverse cellular processes and pathways that mediate genome stability. Mol Cell *35*, 228-239.
Pines, A., Vrouwe, M.G., Marteijn, J.A., Typas, D., Luijsterburg, M.S., Cansoy, M., Hensbergen, P., Deelder, A., de Groot, A., Matsumoto, S.*, et al.* (2012). PARP1 promotes nucleotide excision repair through DDB2 stabilization and recruitment of ALC1. J Cell Biol *199*, 235-249.
Polo, S.E., and Jackson, S.P. (2011). Dynamics of DNA damage response proteins at DNA breaks: a focus on protein modifications. Genes Dev *25*, 409-433.

Poser, I., Sarov, M., Hutchins, J.R., Heriche, J.K., Toyoda, Y., Pozniakovsky, A., Weigl, D., Nitzsche, A., Hegemann, B., Bird, A.W*., et al.* (2008). BAC TransgeneOmics: a high-throughput method for exploration of protein function in mammals. Nat Methods *5*, 409-415.
Povlsen, L.K., Beli, P., Wagner, S.A., Poulsen, S.L., Sylvestersen, K.B., Poulsen, J.W., Nielsen, M.L., Bekker-Jensen, S., Mailand, N., and Choudhary, C. (2012). Systems-wide analysis of ubiquitylation dynamics reveals a key role for PAF15 ubiquitylation in DNA-damage bypass. Nat Cell Biol *14*, 1089-1098.
Ramachandran, S., Tran, D.D., Klebba-Faerber, S., Kardinal, C., Whetton, A.D., and Tamura, T. (2011). An ataxia-telangiectasia-mutated (ATM) kinase mediated response to DNA damage down-regulates the mRNA-binding potential of THOC5. RNA *17*, 1957-1966.
Rosenthal, F., Feijs, K.L., Frugier, E., Bonalli, M., Forst, A.H., Imhof, R., Winkler, H.C., Fischer, D., Caflisch, A., Hassa, P.O*., et al.* (2013a). Macrodomain-containing proteins are new mono-ADP-ribosylhydrolases. Nat Struct Mol Biol *20*, 502-507.
Rosenthal, F., Feijs, K.L.H., Frugier, E., Bonalli, M., Forst, A.H., Imhof, R., Winkler, H.C., Fischer, D., Caflisch, A., Hassa, P.O*., et al.* (2013b). Macrodomain-containing proteins are novel mono-ADP-ribosylhydrolases. Nat Struct Mol Biol, accepted for publication.
Rouleau, M., McDonald, D., Gagne, P., Ouellet, M.E., Droit, A., Hunter, J.M., Dutertre, S., Prigent, C., Hendzel, M.J., and Poirier, G.G. (2007). PARP-3 associates with polycomb group bodies and with components of the DNA damage repair machinery. J Cell Biochem *100*, 385-401.
Sedgwick, B., Bates, P.A., Paik, J., Jacobs, S.C., and Lindahl, T. (2007). Repair of alkylated DNA: recent advances. DNA Repair (Amst) *6*, 429-442.
Shanbhag, N.M., Rafalska-Metcalf, I.U., Balane-Bolivar, C., Janicki, S.M., and Greenberg, R.A. (2010). ATM-dependent chromatin changes silence transcription in cis to DNA double-strand breaks. Cell *141*, 970-981.
Shav-Tal, Y., Blechman, J., Darzacq, X., Montagna, C., Dye, B.T., Patton, J.G., Singer, R.H., and Zipori, D. (2005). Dynamic sorting of nuclear components into distinct nucleolar caps during transcriptional inhibition. Mol Biol Cell *16*, 2395-2413.
Simbulan-Rosenthal, C.M., Rosenthal, D.S., Hilz, H., Hickey, R., Malkas, L., Applegren, N., Wu, Y., Bers, G., and Smulson, M.E. (1996). The expression of poly(ADP-ribose) polymerase during differentiation-linked DNA replication reveals that it is a component of the multiprotein DNA replication complex. Biochemistry *35*, 11622-11633.
Smeenk, G., Wiegant, W.W., Marteijn, J.A., Luijsterburg, M.S., Sroczynski, N., Costelloe, T., Romeijn, R.J., Pastink, A., Mailand, N., Vermeulen, W*., et al.* (2012). Poly(ADP-ribosyl)ation links the chromatin remodeler SMARCA5/SNF2H to RNF168-dependent DNA damage signaling. J Cell Sci.
Smoot, M.E., Ono, K., Ruscheinski, J., Wang, P.L., and Ideker, T. (2011). Cytoscape 2.8: new features for data integration and network visualization. Bioinformatics *27*, 431-432.
Szklarczyk, D., Franceschini, A., Kuhn, M., Simonovic, M., Roth, A., Minguez, P., Doerks, T., Stark, M., Muller, J., Bork, P*., et al.* (2011). The STRING database in 2011: functional interaction networks of proteins, globally integrated and scored. Nucleic Acids Res *39*, D561-568.
Tan, A.Y., and Manley, J.L. (2009). The TET family of proteins: functions and roles in disease. J Mol Cell Biol *1*, 82-92.
Timinszky, G., Till, S., Hassa, P.O., Hothorn, M., Kustatscher, G., Nijmeijer, B., Colombelli, J., Altmeyer, M., Stelzer, E.H., Scheffzek, K*., et al.* (2009). A macrodomain-containing histone rearranges chromatin upon sensing PARP1 activation. Nat Struct Mol Biol *16*, 923-929.
Trucco, C., Oliver, F.J., de Murcia, G., and Menissier-de Murcia, J. (1998). DNA repair defect in poly(ADP-ribose) polymerase-deficient cell lines. Nucleic Acids Res *26*, 2644-2649.
Weinfeld, M., Mani, R.S., Abdou, I., Aceytuno, R.D., and Glover, J.N. (2011). Tidying up loose ends: the role of polynucleotide kinase/phosphatase in DNA strand break repair. Trends Biochem Sci *36*, 262-271.
Wilk, M.B., and Gnanadesikan, R. (1968). Probability plotting methods for the analysis of data. Biometrika *55*, 1-17.

Yoshida, K., Sanada, M., Shiraishi, Y., Nowak, D., Nagata, Y., Yamamoto, R., Sato, Y., Sato-Otsubo, A., Kon, A., Nagasaki, M.*, et al.* (2011). Frequent pathway mutations of splicing machinery in myelodysplasia. Nature *478*, 64-69.

Figure 1

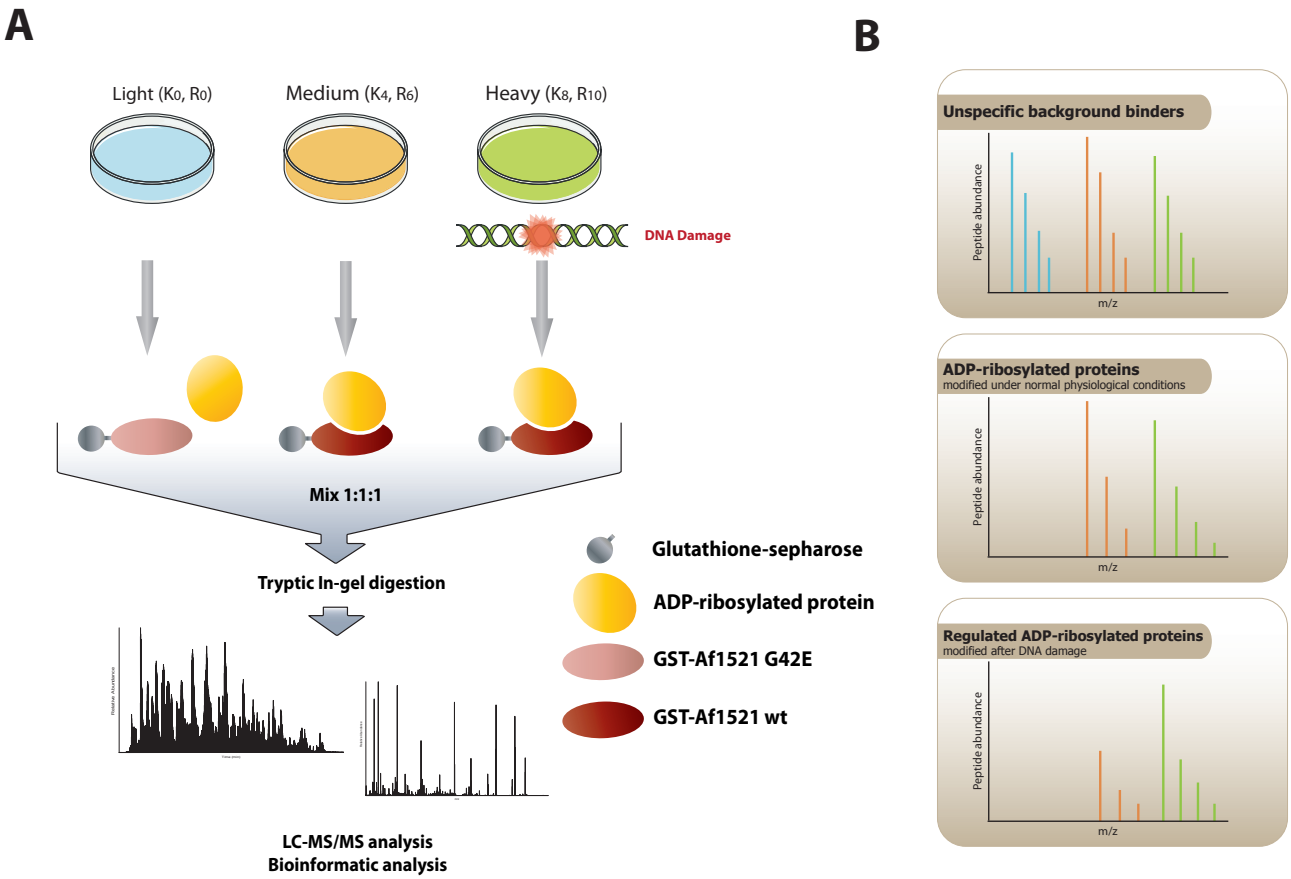
A
Light (K0, R0)
Medium (K4, R6)
Heavy (K8, R10)
DNA Damage
Mix 1:1:1
Tryptic In-gel digestion
LC-MS/MS analysis
Bioinformatic analysis
Glutathione-sepharose
ADP-ribosylated protein
GST-Af1521 G42E
GST-Af1521 wt
B
Unspecific background binders
Peptide abundance
m/z
ADP-ribosylated proteins
modified under normal physiological conditions
Peptide abundance
m/z
Regulated ADP-ribosylated proteins
modified after DNA damage
Peptide abundance
m/z

Figure 2

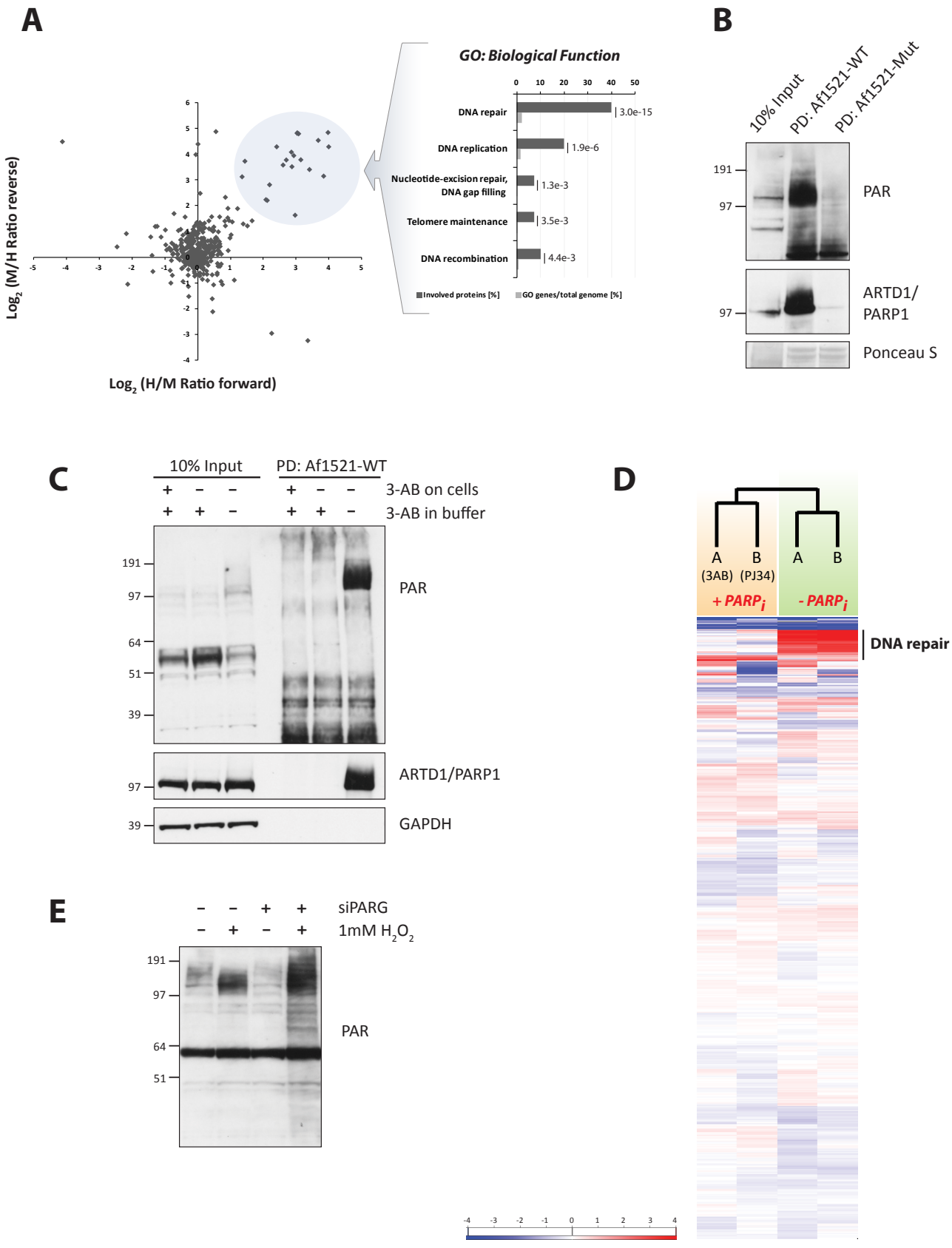
A
Log2 (M/H Ratio reverse)
Log2 (H/M Ratio forward)
GO: Biological Function
DNA repair
3.0e-15
DNA replication
1.9e-6
Nucleotide-excision repair, DNA gap filling
1.3e-3
Telomere maintenance
3.5e-3
DNA recombination
4.4e-3
Involved proteins [%]
GO genes/total genome [%]
B
10% Input
PD: Af1521-WT
PD: Af1521-Mut
191
97
PAR
97
ARTD1/ PARP1
Ponceau S
C
10% Input
PD: Af1521-WT
3-AB on cells
3-AB in buffer
191
97
64
51
39
PAR
97
ARTD1/PARP1
39
GAPDH
D
A (3AB)
B (PJ34)
A
B
+ PARPi
- PARPi
DNA repair
E
siPARG
1mM H2O2
191
97
64
51
PAR

Figure 3

A

	SILAC-Experiment	Treatment	Light (L)	Medium (M)	Heavy (H)
+ siPARG + PJ-34 (in lysis buffer) + ADP-HPD (in lysis buffer)	1	H_2O_2	Af1521-mut	Af1521-wt	Af1521-wt + H_2O_2
	2	MMS	Af1521-mut	Af1521-wt	Af1521-wt + MMS
	3	UV	Af1521-mut	Af1521-wt	Af1521-wt + UV
	4	IR	Af1521-mut	Af1521-wt	Af1521-wt + IR

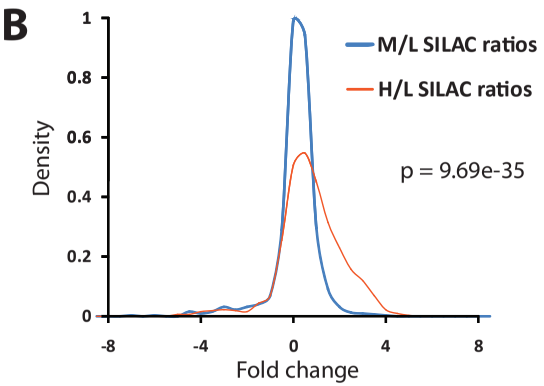

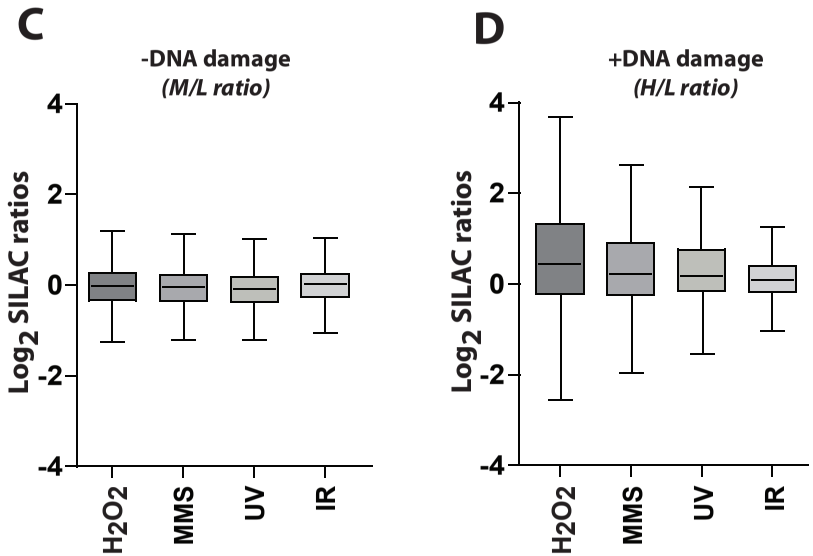

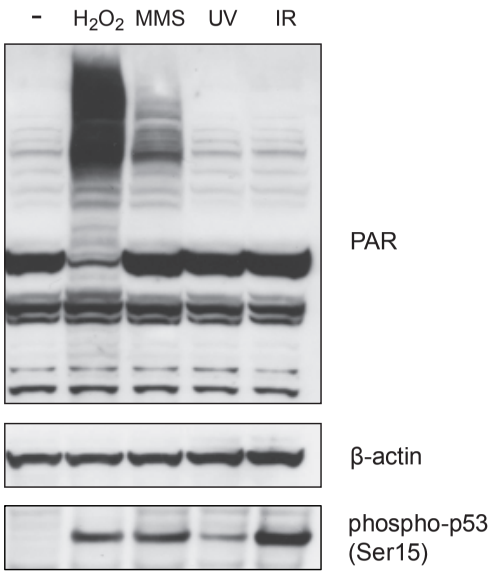

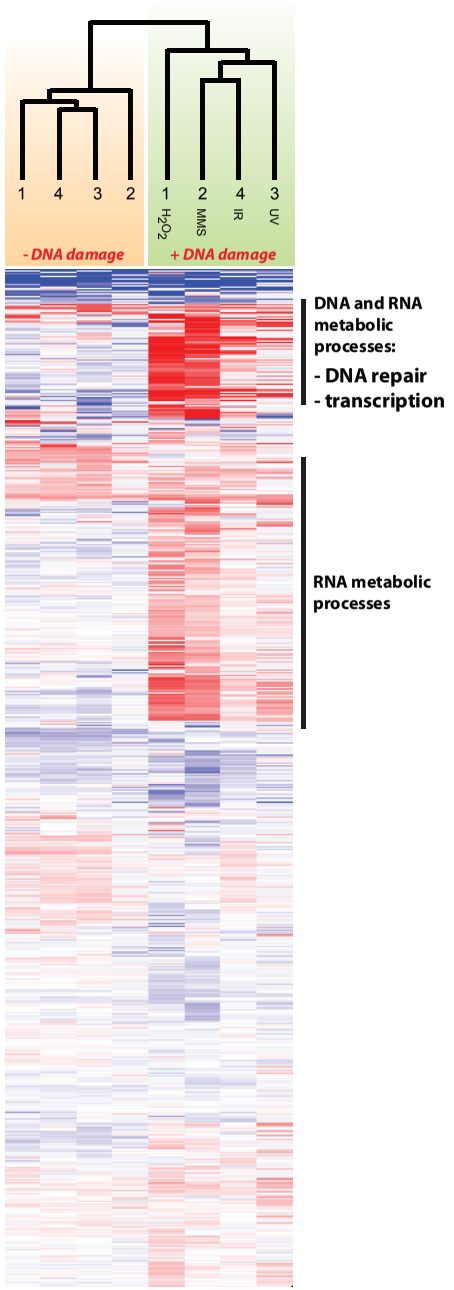

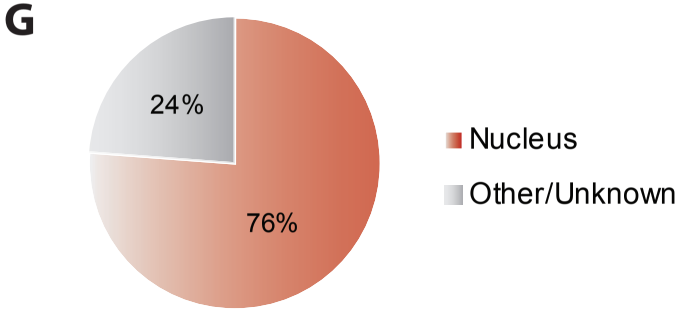

Figure 4

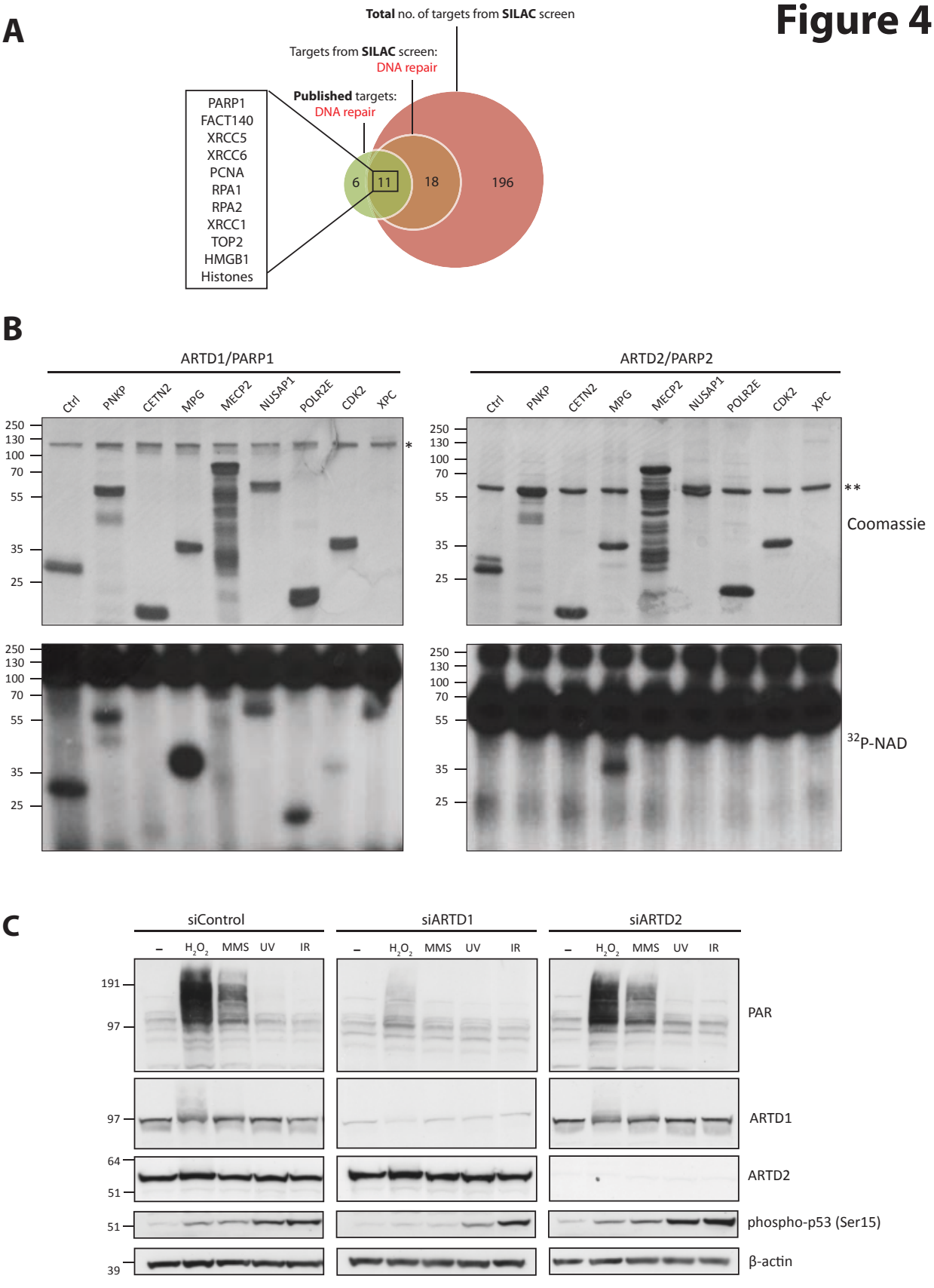

D

	H_2O_2 log_2 (H/L)	MMS log_2 (H/L)	UV log_2 (H/L)	IR log_2 (H/L)	PAR-binding domain	Automodification
PARP1/ARTD1	3.65	3.18	2.66	3.42	+	+
PARP2/ARTD2	2.20	-	-	-	+	+
PARP8/ARTD16	-	-	2.08	-	+	ND
PARP12/ARTD12	2.46	-	-	-	WWE	ND

Figure 5

Figure 5

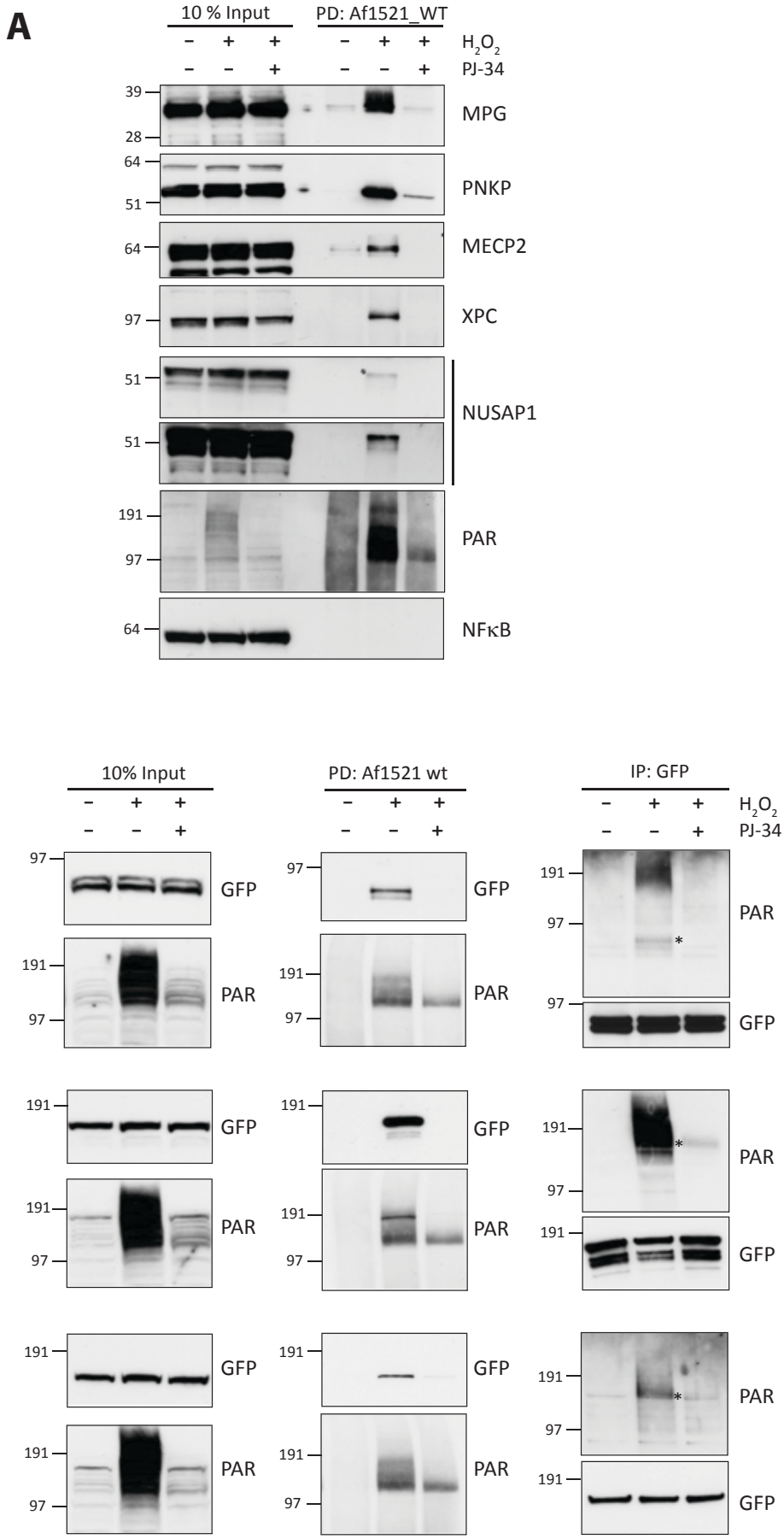

Figure 6

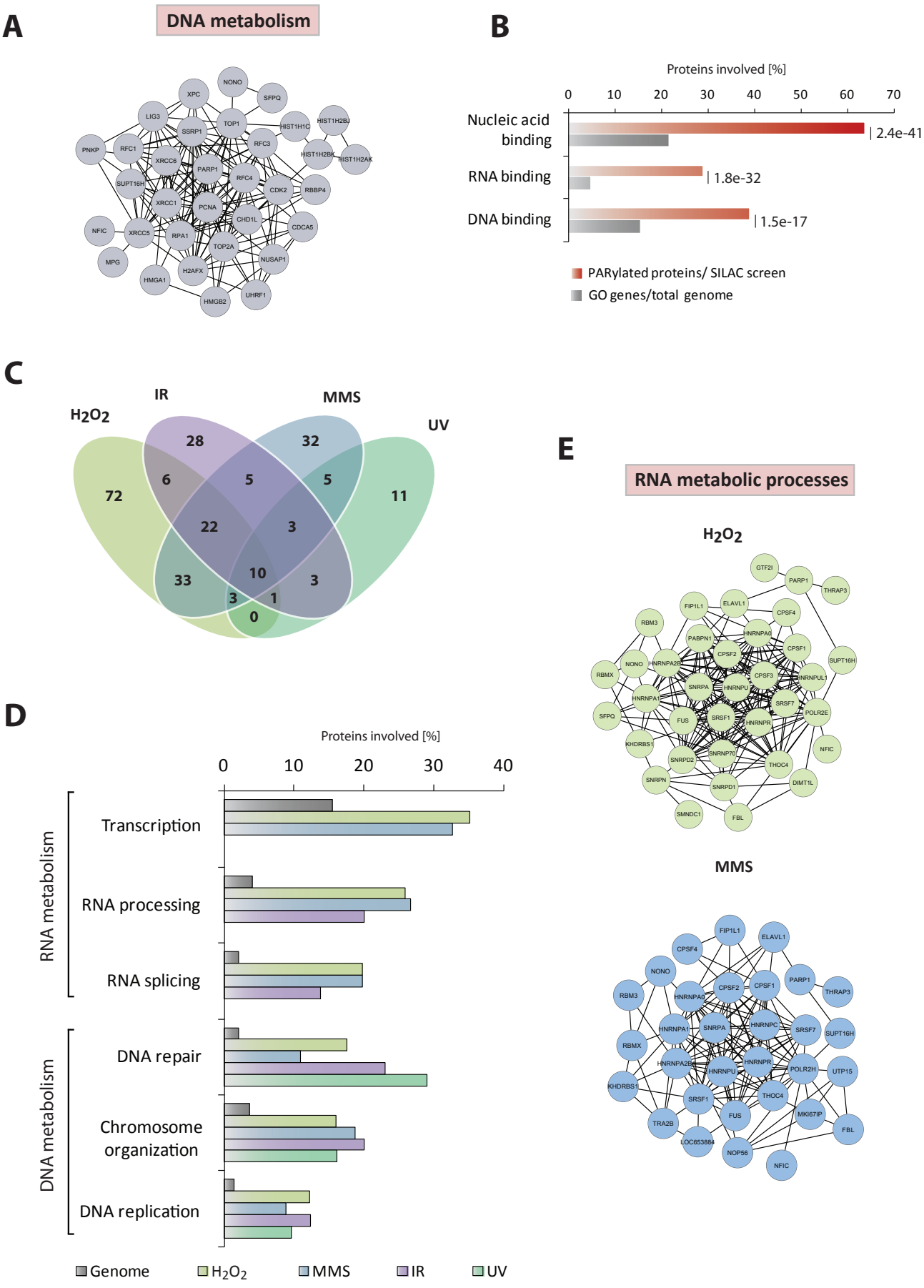
A
DNA metabolism
XPC
NONO
SFPQ
LIG3
TOP1
HIST1H1C
HIST1H2BJ
SSRP1
RFC3
PNKP
RFC1
XRCC6
HIST1H2BK
HIST1H2AK
PARP1
RFC4
SUPT16H
CDK2
RBBP4
XRCC1
PCNA
CHD1L
NFIC
XRCC5
RPA1
CDCA5
TOP2A
MPG
NUSAP1
H2AFX
HMGA1
UHRF1
HMGB2
B
Proteins involved [%]
0
10
20
30
40
50
60
70
Nucleic acid binding
2.4e-41
RNA binding
1.8e-32
DNA binding
1.5e-17
PARylated proteins/ SILAC screen
GO genes/total genome
C
H2O2
IR
MMS
UV
28
32
6
5
5
72
11
22
3
33
10
3
3
1
0
D
Proteins involved [%]
0
10
20
30
40
RNA metabolism
Transcription
RNA processing
RNA splicing
DNA metabolism
DNA repair
Chromosome organization
DNA replication
Genome
H2O2
MMS
IR
UV
E
RNA metabolic processes
H2O2
GTF2I
PARP1
THRAP3
FIP1L1
ELAVL1
CPSF4
RBM3
HNRNPA0
PABPN1
CPSF1
CPSF2
NONO
HNRNPA2B
SUPT16H
RBMX
CPSF3
HNRNPUL1
SNRPA
HNRNPU
HNRNPA1
SRSF7
SFPQ
FUS
SRSF1
POLR2E
HNRNPR
KHDRBS1
NFIC
SNRPD2
SNRNP70
THOC4
SNRPN
DIMT1L
SNRPD1
SMNDC1
FBL
MMS
FIP1L1
ELAVL1
CPSF4
NONO
PARP1
THRAP3
RBM3
CPSF2
CPSF1
HNRNPA0
SRSF7
HNRNPA1
SNRPA
HNRNPC
SUPT16H
RBMX
HNRNPA2B1
HNRNPR
POLR2H
UTP15
HNRNPU
KHDRBS1
THOC4
SRSF1
MKI67IP
FUS
TRA2B
FBL
LOC653884
NOP56
NFIC

Figure 7

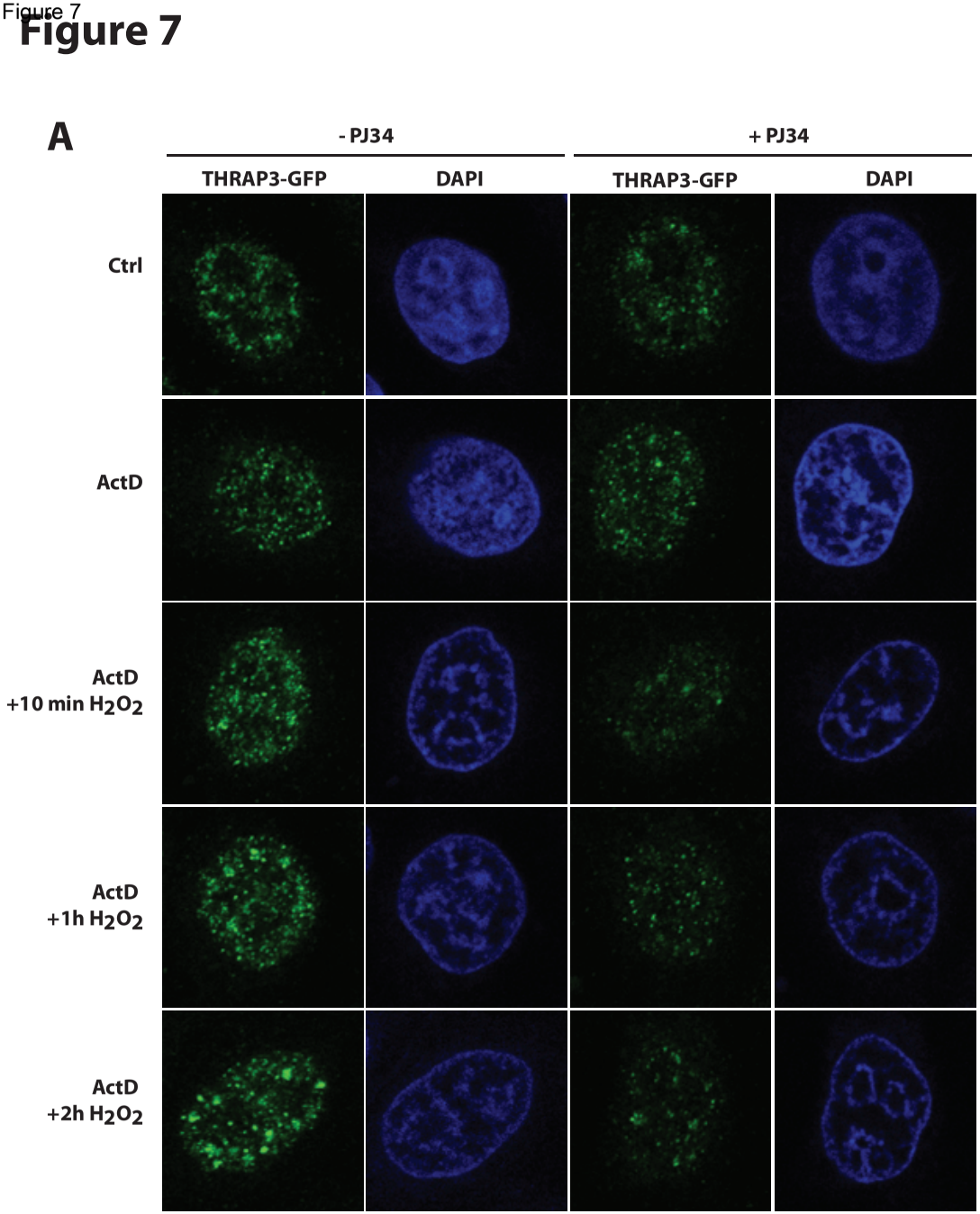
A
- PJ34
+ PJ34
THRAP3-GFP
DAPI
THRAP3-GFP
DAPI
Ctrl
ActD
ActD +10 min H2O2
ActD +1h H2O2
ActD +2h H2O2

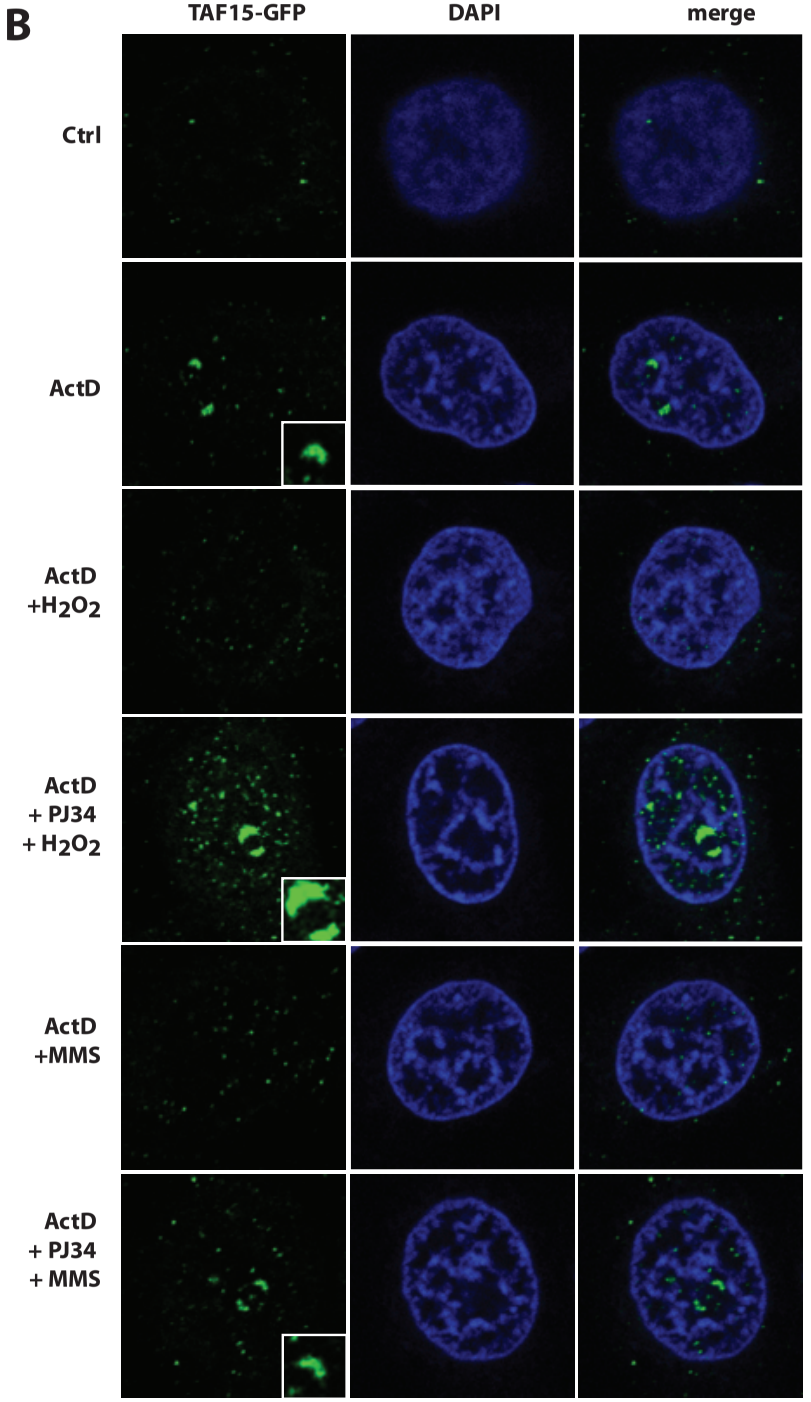
B
TAF15-GFP
DAPI
merge
Ctrl
ActD
ActD +H2O2
ActD + PJ34 + H2O2
ActD +MMS
ActD + PJ34 + MMS

Supplementary Figure 1

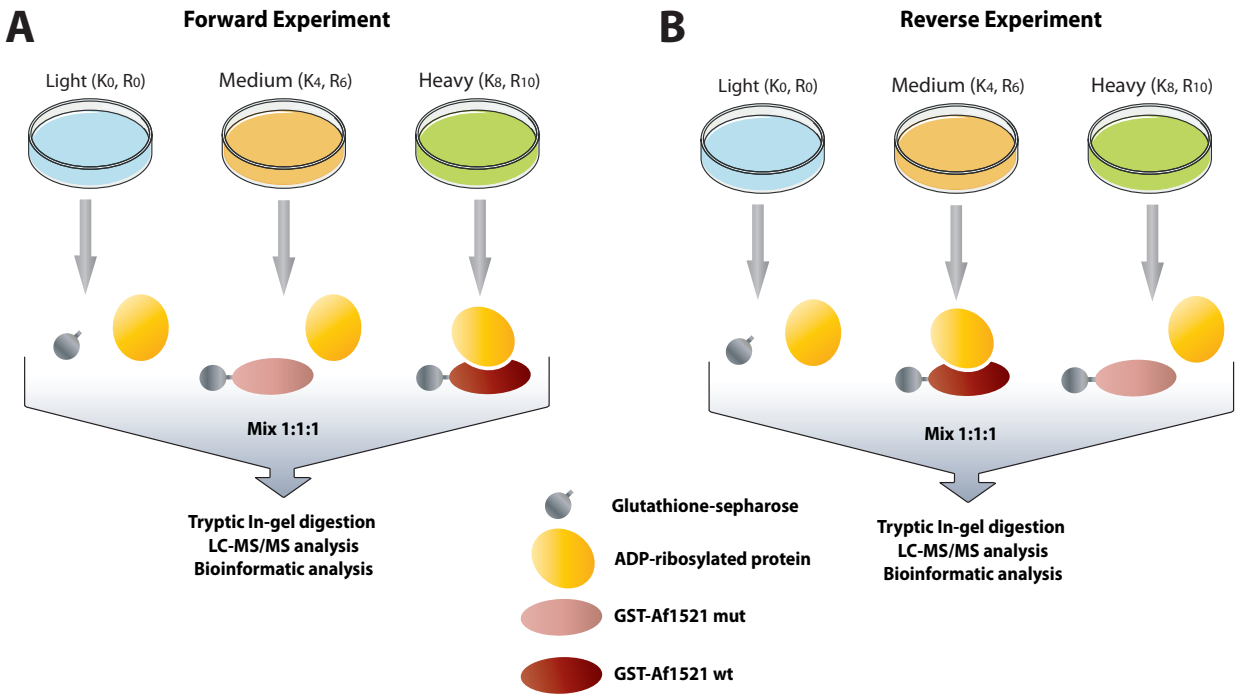

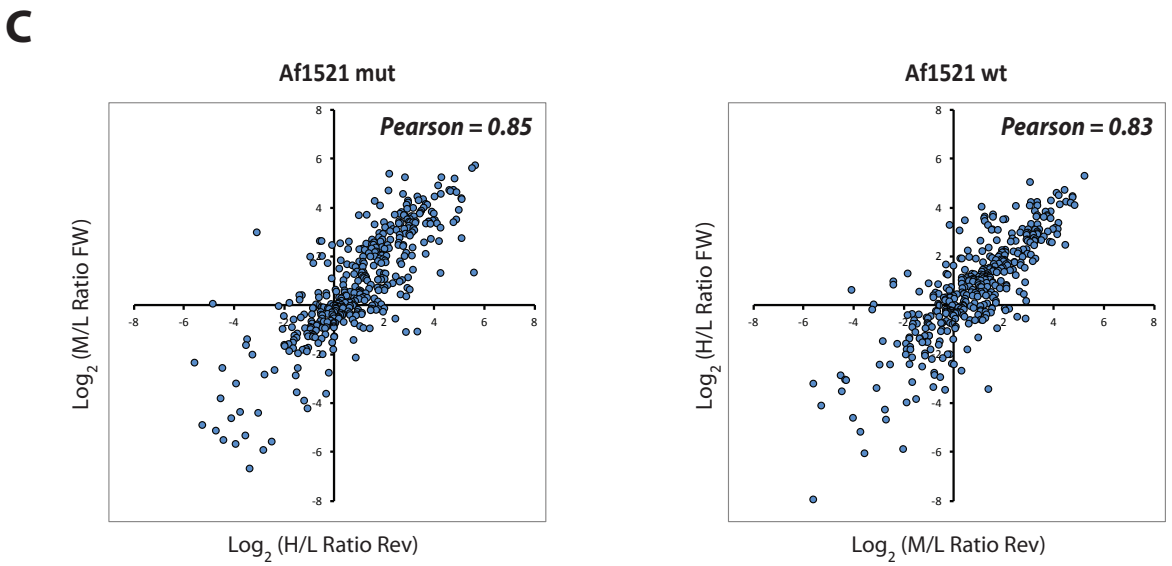

Supplementary Figure 2

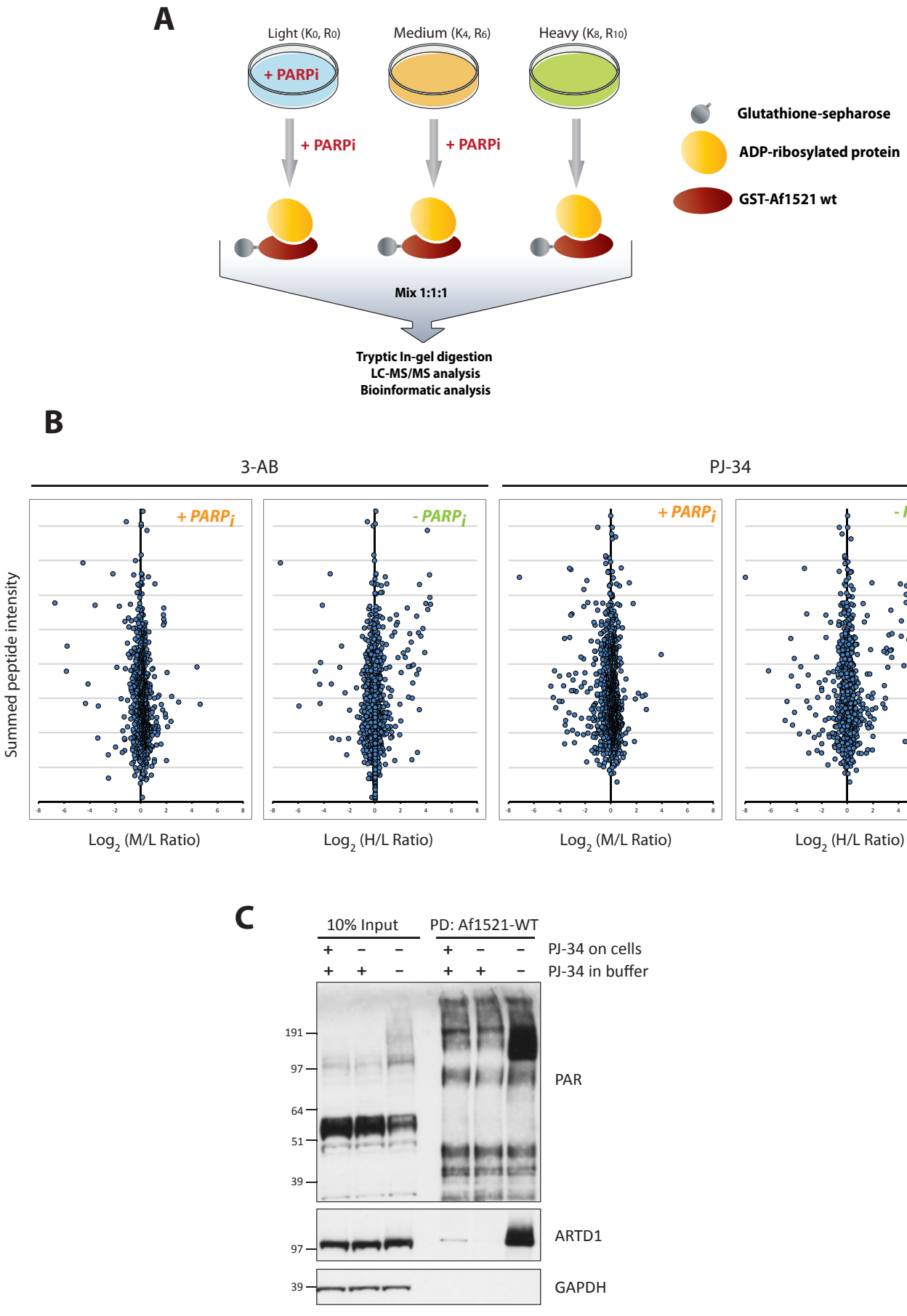

Supplementary Figure 3

A

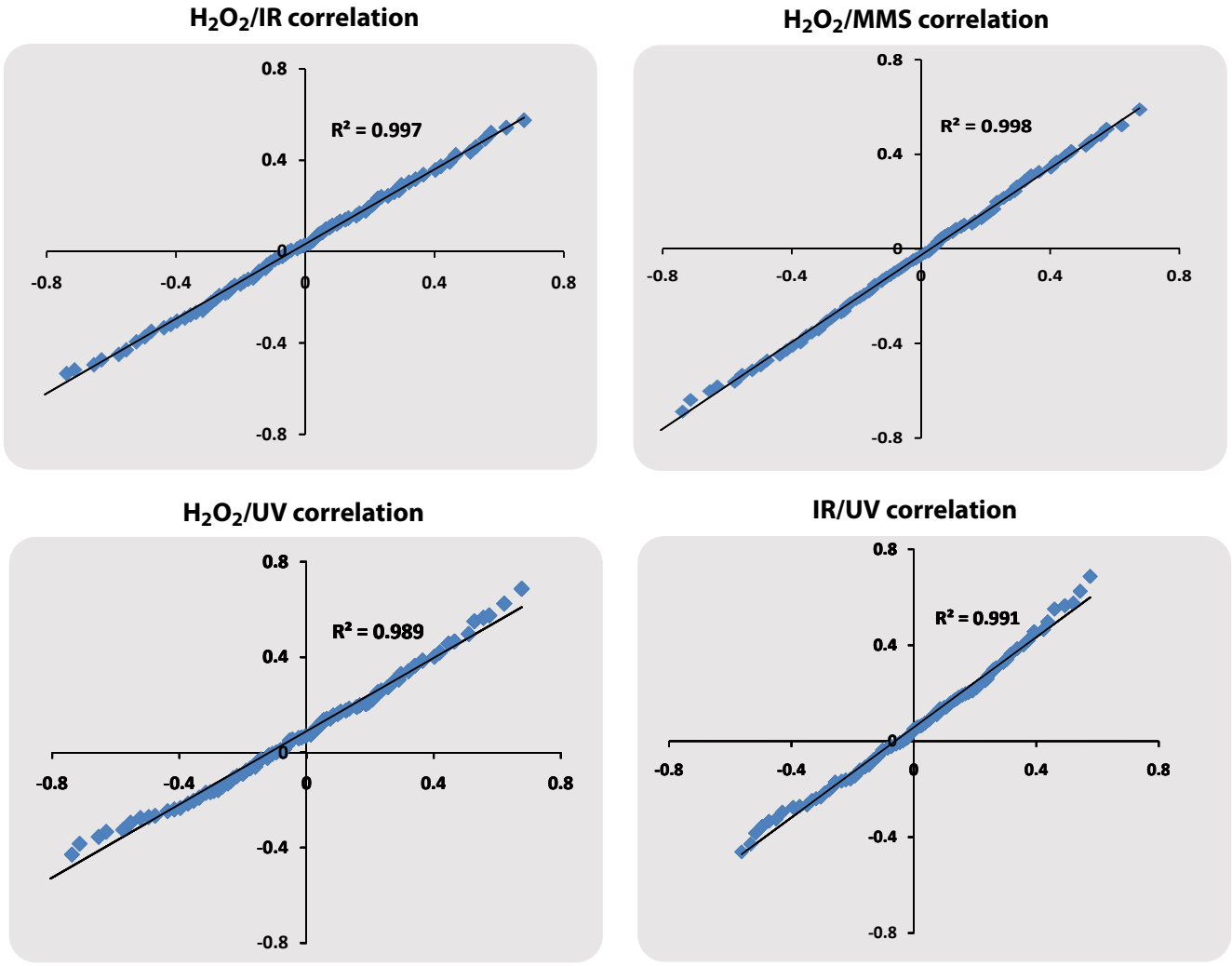

B

Genes	Pep.	Seq.Cov.
ENC1	12	21.70%
HOXB9	4	20.00%
BEND7	7	17.70%
ZNF697	4	7.30%
C9orf84	2	1.40%

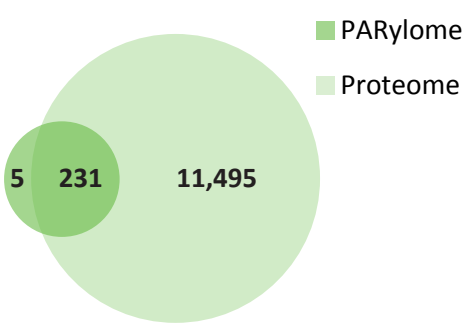

Supplementary Figure 4

A

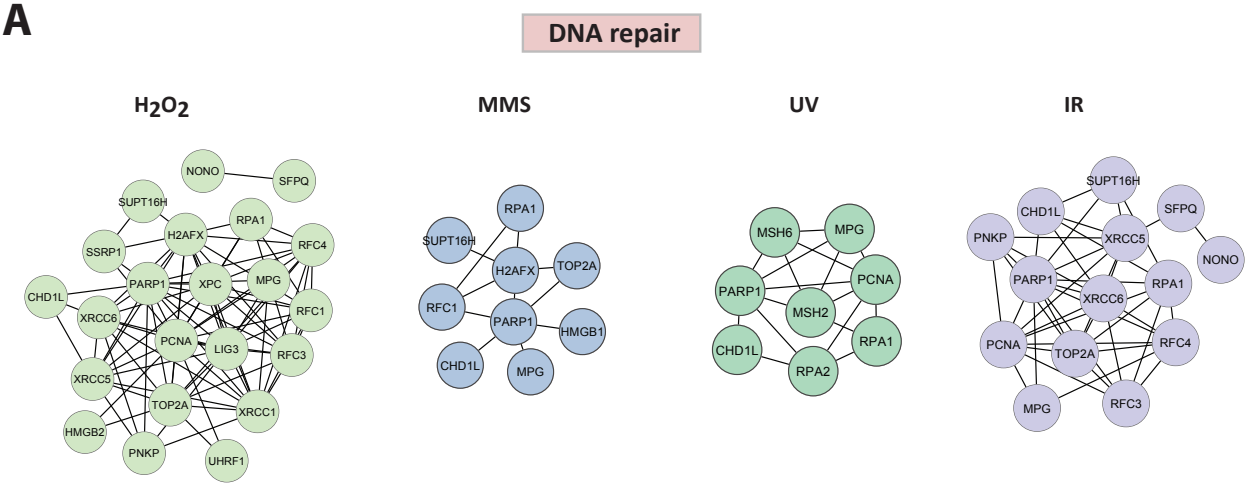

B

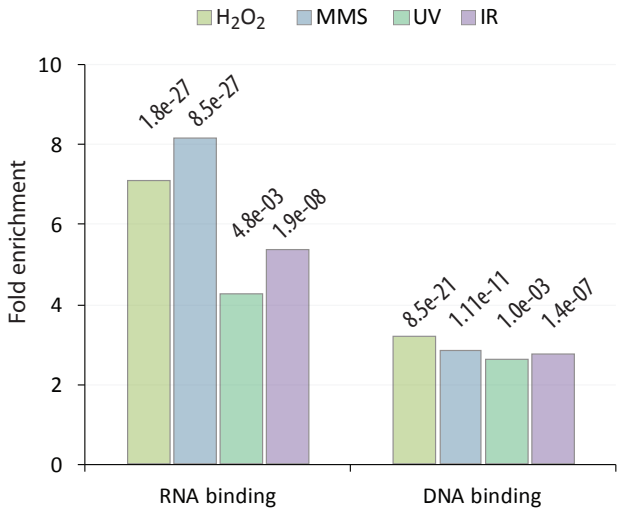

C

	- Log_2 (p-value)			
	H_2O_2	MMS	IR	UV
Transcription	24.06	15.09		
RNA processing	56.94	46.01	16.91	
RNA splicing	55.51	42.13	14.16	
DNA repair	44.88	14.4	34.40	22.80
Chromosome organization	24.73	26.08	18.69	5.55
DNA replication	31.27	13.60	15.00	3.92

Supplementary Figure 5

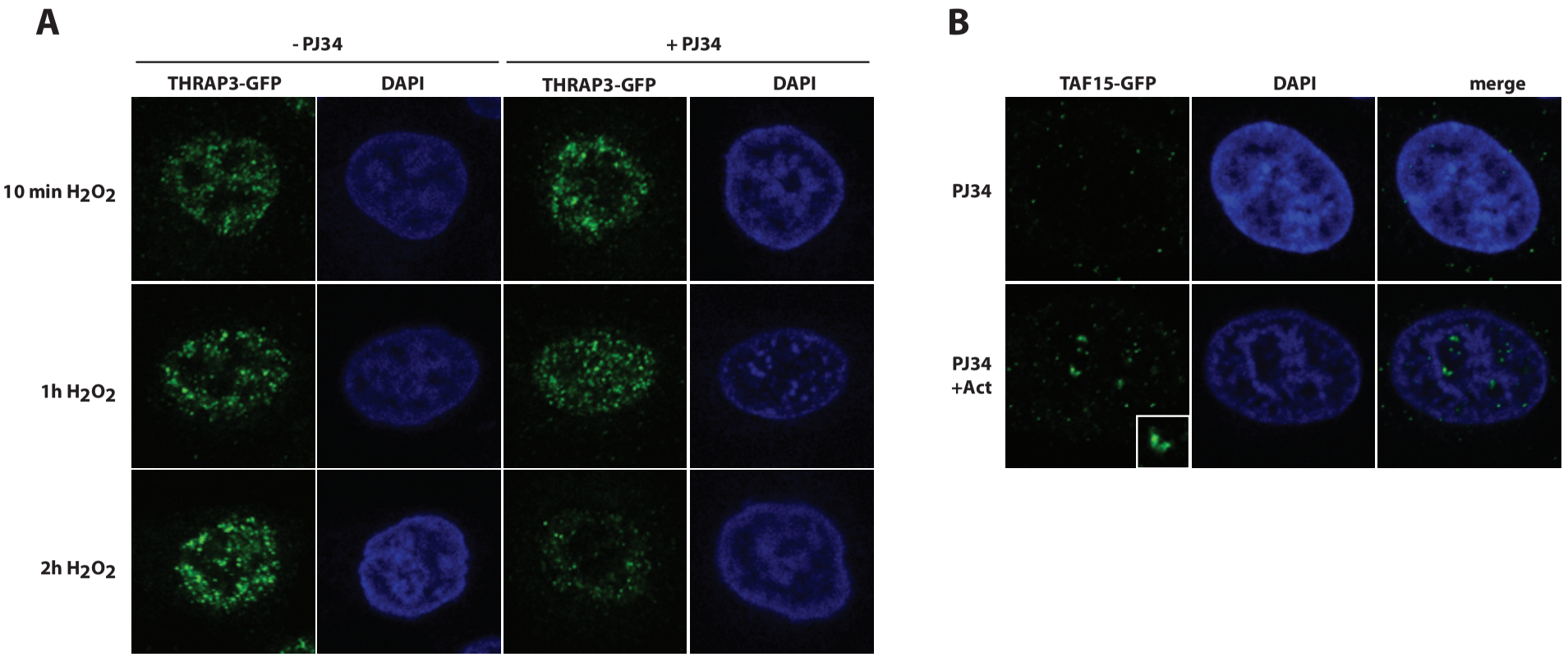

3.3 Unpublished results

3.3.1.1 ADPRibase-Mn hydrolyzes the pyrophosphate of mono/poly-ADP-ribose bound to proteins

ADP-ribose and especially branched PAR chains represent a challenge for mass spectrometric analysis because they are unstable and complex structures without defined mass. Previously, PARG was shown to enzymatically degrade PAR to the last protein-bound moiety (47). This step obviously reduces the complexity of the samples and simplifies the MS/MS analysis, resulting in increased ADP-ribose identifications (139). To further simplify and standardize sample preparation, phosphodiesterase 1 PDE1 was used to cleave the pyrophosphate bond within ADP-ribose units (148). Unfortunately, PDE1 purified from snake venom was very unstable, difficult to store and thus very costly (data not shown). As an alternative method, the application of Mn_2^+-dependent ADP-ribose/CDP-alcohol pyrophosphatase (ADPRibase-Mn) from rat liver was investigated. ADPRibase-Mn belongs to a metallophospho-esterase superfamily, which efficiently hydrolyzes free ADP-ribose and PAR comparable to nudix hydrolases (149). Incubation of *in vitro* poly-ADP-ribosylated ARTD1 with recombinant ADPRibase-Mn massively decreased the signal of radioactive labeled auto-modified ARTD1 (Figure 7A). The loss of radioactive ADP-ribose was even stronger when compared to treatment of ARTD1 by PARG, indicating that less than one ADP-ribose moiety (possibly a phospho-ribose) remained attached on ARTD1 after ADPRibase-Mn treatment. Further MS-analysis of the ADPRibase-Mn treated samples indeed confirmed the cleavage of the pyrophosphate bond, which results in a defined phospho-ribose moiety that is easily detectable by mass spectrometry (Figure 7B). Taken together, recombinant ADPRibase-Mn could be confirmed as a pyrophosphate hydrolase that is able to cleave human ARTD1 bound ADP-ribose, resulting in a phospho-ribose moiety, which is readily detectable by mass spectrometry.

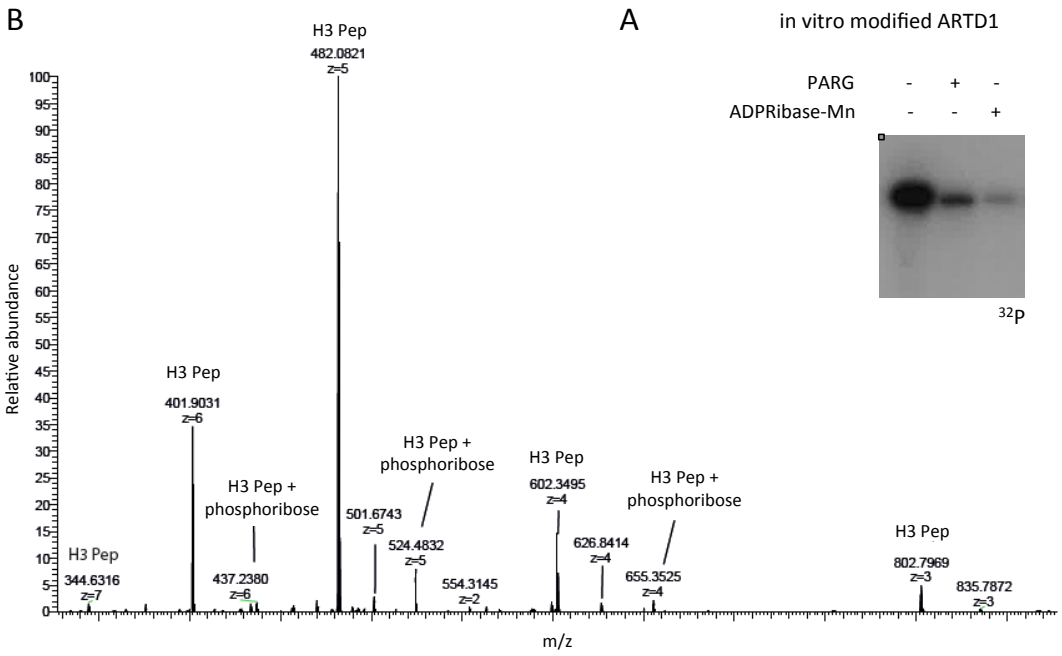

Figure 7: ADPRibase-Mn cleaves protein-bound PAR. A. ARTD1 was poly-ADP-ribosylated in the presence of radioactively labeled ^{32}P-NAD^{+} and subsequently treated with PARG or ADPRibase-Mn. The reactions were separated on a SDS-PAGE and visualized by autoradiography. B. HCD spectrum of the ADP-ribosylated biotin-KAARKSAPATGGVKKPHRYR H3-peptide after ADPRibase-Mn treatment. The different charge states of the unmodified and the phospho-ribose modified peptide can be observed.

3.3.2 Phospho-ribose can be used in Mascot to identify a modified standard peptide

To further investigate the eligibility of the ADPRibase-Mn treatment for sample preparations and the subsequent identification of ADP-ribosylated peptides, the phospho-ribose modification was included as a variable modification to the Mascot software. First, we tested the procedure with a biotinylated standard peptide with the sequence KAARKSAPATGGVKKPHRYR, representing a part of the histone H3 unstructured N-terminal tail (139). The peptide was either *in vitro* modified with ARTD1 or with the catalytic domain of ARTD10 (ARTD10 (818-1025)), resulting in a poly- or mono-ADP-ribosylated peptide, respectively. The modified peptide was subsequently treated with ADPRibase-Mn or PARG (for ARTD1) or only with ADPRibase-Mn (for ARTD10 modified peptide) and subsequently analyzed with the different fragmentation techniques or combinations thereof, as described (139) (Figure 8). The HCD fragmentation of the phospho-ribose modification attached to the standard peptide generated no indicative ions, thus not allowing a product dependent

or two-stage HCD-ETD analysis (data not shown). Therefore, samples treated with ADPRibase-Mn were only analyzed by one-stage analysis with HCD, ETD or a combination of both fragmentation techniques without analyzing the indicative ions of the ADP-ribose (139).

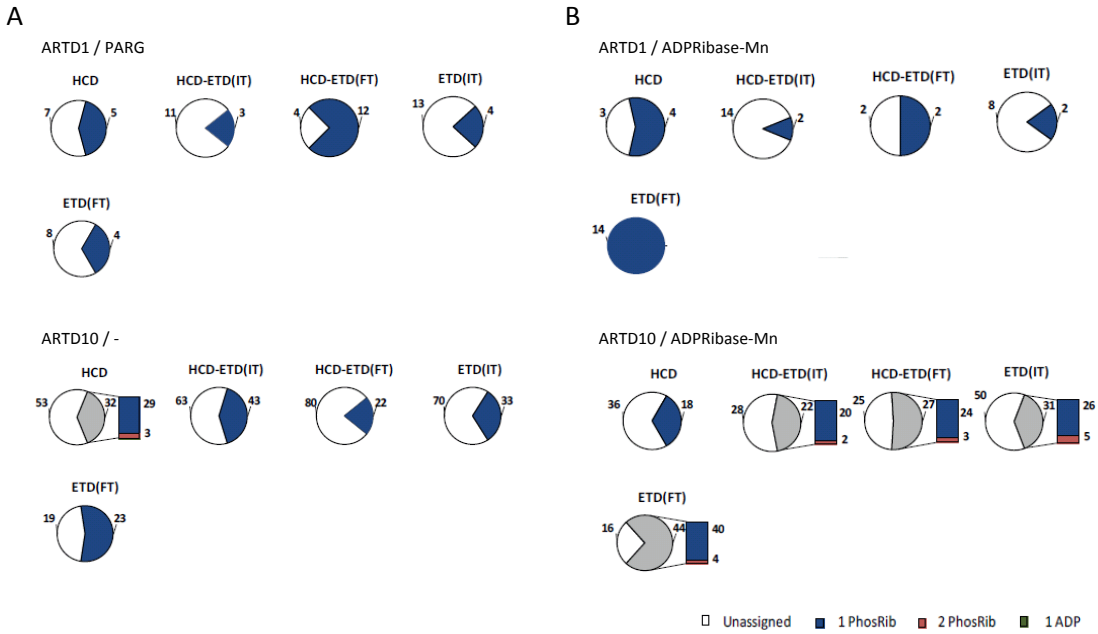

Figure 8: Analysis of the ADPRibase-Mn treated H3 peptide by HCD and ETD fragmentation. Every pie-chart shows for each combination of HCD and ETD fragmentation the number of unassigned spectra (white) and those assigned to ADP-ribosylated or phospho-ribose modified peptides (colored). A. Results obtained by the analysis of the peptide treated with ARTD1/PARG and ARTD10. The bars report the number of spectra identified as peptides carrying 1 (blue) or 2 (red) modifications. B. Results for the peptide treated with ARTD1/ADPRibase-Mn and ART10/ADPRibase-Mn

Surprisingly, these MS measurements revealed that ADPRibase-Mn treatment did in general not improve the identification of the modification acceptor site, when compared to untreated (for ARTD10 modified peptide) or PARG treated samples (for ARTD1 modified peptide) (compare Figure 8A and B). The only benefit of the ADPRibase-Mn treatment was observed when modified samples were analyzed by high accuracy ETD (FT) data analysis. Although, the phospho-ribose was expected to provide a more stable and defined moiety for the MS analysis, this seemed, for unknown reasons, not to be the case for the tested standard peptide.

3.3.3 Phospho-ribose can be used to identify a modified peptides in complex mixtures

To investigate whether the enzymatically-generated phospho-ribose would provide advantages in more complex samples, a heterogeneous mixture of all four core histones and the linker histone H1 was modified by ARTD10 (818-1025) *in vitro*. After trypsin digestion and subsequent ADPRibase-Mn treatment, samples were analyzed by HCD, ETD(IT), ETD(FT) or a HCD-ETD(IT) combination. As observed with the standard peptide, the overall number of ADP-ribosylated peptides as well as the number of differentially modified peptides were comparable between ADPRibase-Mn treated and untreated samples. Modification sites with a probability of ≥ 95% were considered as accurately identified, whereas all other hits were defined as modified peptides without accurately defined modification site. In general, no benefit for the ADPRibase-Mn treatment was observed when samples were analyzed by HCD. The number of modified peptides with an accuracy of <95% even decreased after ADPRibase-Mn treatment. Only for the analysis of samples with ETD(IT) and (FT), the ADPRibase-Mn treated samples allowed the identification of a higher number of modified peptides (Fig. 9 A-C). Therefore, ADPRibase-Mn treatment might be advantageous in samples containing mainly long and highly charged peptides, which fragment better in ETD. In addition, the ADPRibase-Mn treatment could potentially be used as an elution step in enrichment protocols for ADP-ribosylated peptides with binding modules (macro domains) or resins (boronic acid). Moreover, it could be used as a pre-treatment for phospho-enrichment protocols as recently introduced for PDE1 (136).

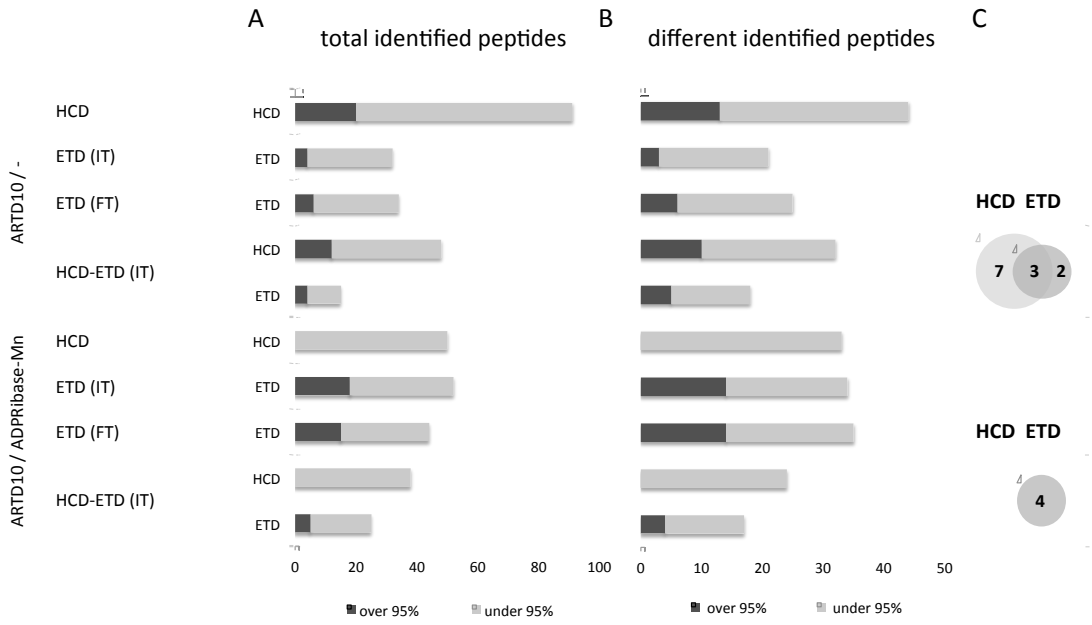

Figure 9: Analysis of histones modified *in vitro* by ARTD10 and treated with ADPRibase-Mn. Histones modified *in vitro* by ARTD10 and treated with ADPRibase-Mn were analyzed by MS/MS using four different combinations of HCD and/or ETD fragmentation techniques. Both, ADP-ribosylated peptides where the site localization confidence score was higher than 95% (black bars) and lower than 95% (grey bar) are plotted. A. Number of spectra assigned to ADP-ribosylated peptides. B. Number of different ADP-ribosylated peptides identifications (different modification sites on the same peptide are considered as different peptides). C. Venn diagrams showing the differences and overlaps between HCD and ETD identifications. The diagrams refer only to the peptides having a site localization score higher than 95%.

3.3.4 Methods to unpublished results

ADPRibase-Mn purification

The bacterial GST-expression vector for rADPRibase-Mn was kindly provided by José Carlos Cameselle (149). GST-tagged proteins were expressed in BL21 bacteria and purified with Glutathione Sepharose 4 Fast Flow (GE Healthcare, Uppsala, Sweden) as described (41).

ADPRibase-Mn treatment

To hydrolyze ADP-ribose polymers, *in vitro* modified GST-ARTD10 (818-1025) or HIS-ARTD1 with histones or peptides were used in a buffer consisting of 50 mM Tris-HCL pH 8.0, 10 mM $MgCl_2$, 50 mM NaCl, 250 μM and 100 nM $MnCl_2$, 5 pmol GST-ADPRibase-Mn were added, and the reaction was incubated for 1h at 30°C.

4 DISCUSSION AND PERSPECTIVES

4.1 Summary of the results

One aim of this thesis was to identify ADP-ribosylated peptides from cells and to localize the modification site(s) by mass spectrometry. To gain more insight into the ADP-ribosylome and ADP-ribose acceptor sites, we first established an optimized mass spectrometry based protocol allowing the specific enrichment of ADP-ribosylated proteins and peptides with phenylboronic acid resins to subsequently map their ADP-ribosylation sites by ETD mass spectrometry (150). Although we could provide evidence that the ETD fragmentation results in the stabilization of ADP-ribosylation (compared to HCD), the method nevertheless revealed other weaknesses. First, long and highly charged peptides are required for the efficient analysis by ETD. Second, even in cases when the peptides are sufficiently long, the number of gained ions is often very low and a mapping of the ADP-ribosylation site with a good confidence (>95%) is difficult to reach. The MS-based data analysis methods had thus to be further improved (139). Along this line, HCD was identified as the method of choice for the analysis of ADP-ribosylated peptides, since it generates indicative ions of ADP-ribose, which allows the detection of modified peptides and their modification site(s) with high accuracy. When combining with ETD in a product dependent or two-stage approach, the advantages of both methods could be combined and the quality of data further improved (139). Applying this improved protocol to a not-enriched lysate of H_2O_2 treated cells, we could, for the first time, identify several ADP-ribosylation sites of proteins, opening new possibilities for the further characterization of the ADP-ribosylome (see below).

We furthermore identified human macrodomain MacroD1, MacroD2 and C6orf130, as well as Af1521 from archaebacteria, as a novel class of enzymes able to hydrolyze mono-ADP-ribosylated glutamic-acid residues (151). Structural modeling and mutagenesis of the macrodomains suggested a common enzymatic mechanism requiring Asp102 and His106 for the catalytic reaction. Macrodomain containing proteins were able to fully de-ADP-ribosylate *in vitro* modified ARTD10. Furthermore, mono-ADP-ribosylation of glycogen synthase 3β (GSK3β) by ARTD10 inhibited its kinase activity, which could be reversed by MacroD2 *in vivo*. Together, we established mono-ADP-ribosylation of acidic residues by ARTD10 as a dynamic modification that

can be reversed by macrodomain containing proteins and thus identified a missing link in the ADP-ribosylation cycle (151).

4.2 Towards identifying ADP-ribose acceptor sites

The identification of the ADP-ribosylation sites on different ARTDs as well as on their target proteins is, due to the complexity and heterogeneous nature of PAR, which has been an obstacle for more than 30 years. The first insights were obtained by studying the stability of protein-attached ADP-ribose to treatment with different chemical compounds (114,152). Based on the chemical sensitivity of the modification (1.4 and Table 1), glutamic acid residues on ARTD1, histone H2B and H1 were suggested to be ADP-ribosylated. As these studies were never confirmed by site directed mutagenesis analyses and performed with chemically and not enzymatically ADP-ribosylated peptides and proteins, the identified sites remained under dispute (35). More recent work, utilizing site directed mutagenesis, provided evidence for a strong reduction of ARTD1 auto-ADP-ribosylation *in vitro* when specific lysine residues in the ARTD1 auto-modification domain were mutated to arginines (119). These studies indicated that lysine residues might serve as ADP-ribose acceptor sites. But since the mutagenesis of amino acids could also disrupt the protein structure, the identification of the ADP-ribose acceptor site(s) was still not resolved and, because of the strong recent medical interest, urgently sought.

Only the recent advances in mass spectrometry with more advanced instrumentation and new possibilities to map labile PTMs such as ADP-ribose, opened novel perspectives for the ADP-ribosylation research. The newly invented fragmentation technique ETD stabilizes labile post-translational modifications on peptides and was recently successfully used to analyze ADP-ribosylated peptides (153). When ETD was applied to histone peptides modified *in vitro* by ARTD1, lysine residues could be identified as acceptor amino acids (41). Beside our own published ETD study, two studies aimed to identify the automodification sites of ARTD1 by conventional CID fragmentation (135,136). The first group analyzed the auto-modification sites of the E988Q ARTD1 mutant, which hampers PAR formation and also strongly reduces the ability to catalyze mono-ADP-ribosylation, and identified the acidic amino acids D387, E488 and E491 as ADP-ribose acceptor sites (135). Since mutating the catalytically important glutamic acid residue E988 of ARTD1 might change the chemical reaction as well as the modification specificity, and also because

of the very high NAD^+ concentrations (500µM) that were used for the automodification, these data do not necessarily reflect the physiological situation. A second group used PDE1 to reduce PAR of *in vitro* auto-modified ARTD1 to generate a single phospho-ribose moiety (136). The terminal phosphate of the remaining protein bound phospho-ribose was subsequently used to enrich the modified peptides with a phospho-enrichment resin. Subsequent CID-based MS/MS analysis revealed that both, glutamic acid and lysine residues are serving as acceptor sites. The CID approach was, however, not able to accurately assign the acceptor sites when glutamic acid and lysine residues were found in close proximity, underlining the problems to precisely pinpoint ADP-ribosylation to a certain amino acid and leaving the question open, which amino acids serve as acceptor site. These initial studies clearly reveal that further experimental efforts are required to clarify and confirm these findings and that ADP-ribosylation sites should be preferentially identified with proteins extracted from cells in order to determine whether the above described *in vitro* findings indeed represent the *in vivo* situation.

4.3 Combining different MS technologies for the accurate identification of ADP-ribosylation acceptor sites

The optimization of HCD fragmentation with stepped collision energies allowed the reliable detection of ADP-ribose specific ions, providing an additional indication for the existence of ADP-ribosylation on fragmented peptides (139,153). When these ions were implemented in the Mascot search engine as neutral losses, ADP-ribosylation sites could be reproducibly identified. This result was surprising since HCD was expected to completely remove the ADP-ribose from its acceptor amino acid. As this was not the case, HCD became a promising tool for the identification of ADP-ribose acceptor sites and was further combined with the previously applied ETD technique to combine the advantages of both fragmentation techniques in one MS/MS analysis. As a result, different proteins and their ADP-ribosylation sites could be identified for the first time with high confidence and reliability, demonstrating the advantages of the newly established protocol. Interestingly, glutamic acid, lysine and arginine residues on histone proteins were detected as ADP-ribose acceptor sites under the tested conditions. This finally confirms that more than one type of amino acid can indeed serve as *in vivo* ADP-ribose acceptor sites in cells. Several of the identified sites are located within histone proteins, which were reported to be targets of other PTMs. This

provides evidence that the mapped sites are accessible *in vivo* and in generally regulated by PTMs. Moreover, a functional crosstalk of ADP-ribosylation with other PTMs can be foreseen.

Applying the HCD-ETD mass spectrometry approach to other treated lysates will help to shed more light on this topic and will help us to understand, which amino acids are ADP-ribosylated under which conditions and which ARTD is responsible for the modification of specific acceptor sites. Additional experiments should help to answer which ADP-ribosylation patterns are induced under basal or cellular stress conditions, such as oxidative stress, DNA-damage or inflammation. The cellular ADP-ribosylation reactions might thus be divided into a basal "maintenance" ADP-ribosylation and a "stress induced" ADP-ribose modification.

4.4 Modification of different amino acids by the same ARTD

The identification of different modified ADP-ribosylated amino acids *in vivo* challenges the existing views and invites the research community to review the dogma that all ARTDs in the mammalian cell catalyze the same biochemical raction and thus modify the same amino acid residue (15). Different ARTD family members might thus modify different amino acids or one ARTD might alternatively be able to modify several different types of amino acids, depending on whether the modification is catalyzed *in cis* or *in trans*. In this scenario, even the auto-modification of an ARTD might lead to targeting of different acceptor sites, depending on the molecular concentration and the experimental conditions (favoring the formation of monomers and modification *in cis* or formation of dimers and the modification *in trans*). Consequently, modification of a target protein would always be catalyzed *in trans* and should thus reveal the same acceptor site. Moreover, it needs to be further investigated whether ADP-ribosylation is only regulated by a directed enzymatic reaction or if non-enzymatic chemical reactions are involved in the transfer of the modification to adjacent amino acids. Knocking down defined ARTDs or using ARTD knockout cells, combined with the new MS/MS workflow, will now make it possible to address several of these points and will provide valuable insight into the cellular ADP-ribosylation reactions. Such information will also help to further characterize the family of ARTDs and open the possibility to raise antibodies against specific ADP-ribosylated proteins. Obtaining antibodies would allow applying many standard and state of the art techniques, such as western blot, immunofluorescence, chromatin

immunoprecipitation (ChIP) and ChIP-sequencing, that cold so far not be applied in the ADP-ribosylation research.

Finally, as the new MS approach is potentially applicable to other PTMs, which produce indicative ions upon HCD fragmentation, it could help to characterize other labile PTMs such as phosphorylated or glycosylated serine and threonine and nitrosylated cysteine (154,155).

4.5 Cell lysis-dependent induction of ADP-ribosylation

Some ARTDs (e.g., ARTD1/2) can be activated by DNA *in vitro* (119) and might thus also be activated by DNA fragments generated during protein extraction or fixation of cells (156), leading to ADP-ribosylation that does not reflect the physiological situation in the cell (157). To prevent false positive identifications, lysis-induced ADP-ribosylation has to be inhibited by including PARP inhibitors in all buffers during extraction. This prevents overestimation and misinterpretation of mass spectrometric results and helps to identify the physiologically relevant ADP-ribosylome (157).

As ADP-ribosylation is a transient PTM and quickly degraded by the cellular PARG enzymes, experiments are also performed under conditions of PARG inhibition or depletion (158). This generally facilitates the analysis of modified proteins, as PARylation is enhanced, and increases the number of modified proteins. Whether proteins identified under such conditions are indeed modified *in vivo* under untreated conditions needs to be further addressed.

4.6 Functional aspects of ADP-ribosylated lysine acceptor sites.

Modification of proteins by ADP-ribosylation often alters their structure or binding properties of other proteins or DNA (38,39). As indicated, enzymes with de-ADP-ribosylating activities towards modified arginines and glutamates could be identified, proving that mono-ADP-ribosylation of these residues is revertible ((57), and this thesis). The fact that PARG and MacroD2 can only reverse some ARTD1 auto-modifications further strengthens the point that additional amino acids of ARTD1 are modified (e.g., lysine residues) and points at the need for additional hydrolase(s) with activity towards other amino acids (e.g., lysine residues). Identifying a lysine-specific hydrolase would be of great interest, especially because lysine histone modifications could be identified and their ADP-ribosylation cycle might be of great importance for the histone code (41,139,159). A potential hydrolase that was reported to remove

mono-ADP-ribose from glutamic acid or lysine residues was purified over 30 years ago (62,63). This enzyme was already postulated to be the lysine specific ADP-ribose hydrolase (121) but was unfortunately never fully characterized and is unknown until today. An alternative scenario foresees that lysine mono-ADP-ribosylation is a permanent (non-hydrolysable) modification, which cannot be reversed by any enzyme and therefore marks proteins for a final destiny. This would imply that in order to remove the accompanied signal, the lysine-ADP-ribosylated protein would need to be degraded, otherwise removed or shielded.

4.7 Macrodomains are glutamic acid specific mono-ADP-ribosylhydrolases

Poly- and mono-ADP-ribosylation are dynamic modifications and defects in their synthesis and turnover are implicated in various diseases (13,34,69). Therefore, both mechanisms have to be tightly regulated by enzymes catalyzing specific enzymatic reactions in the ADP-ribose metabolism. Up to now, two enzymes (PARG and ARH3) where identified that hydrolyze PAR, but both are unable to remove the protein-proximal ADP-ribose moiety (47,55). This might be due to different types of linkages within PAR on the one side and the protein proximal ADP-ribose linkage to the amino acid on the other side. Alternatively, steric hindrance could interfere with the removal of the last ADP-ribose (160). As a result of these PAR-hydrolyzing activities and the activity of mono-ADP-ribosyltransferases such as ARTD10 a massive pool of mono-ADP-ribosylated proteins in the cell could potentially be generated. In order to reverse mono-ADP-ribosylated proteins into their unmodified state, enzymes with activities towards mono-ADP-ribose are expected to exist. This is especially valid for ADP-ribosylation on lysines, arginines and glutamic acid residues, which were detected in human cells (139). So far, ARH1 is the only *in vitro* characterized enzyme with activity against mono-ADP-ribosylated arginine (55,57). This enzyme stands in contrast to the huge family of ARTDs and ARTCs, which also underlines the substantial lack of knowledge in the field of mono-ADP-ribosylhydrolases.

Up to now, over 300 proteins, including 14 human proteins, with macrodomains were identified (87). Macrodomains are found in histone proteins, ARTDs and other proteins involved in chromatin metabolism (88,90) and bind mono- and/or poly-ADP-ribose and OAADPr (96,100). In addition, human MacroD1, MacroD2 and C6orf130 contain C2- or C3-specific OAADPr deacetylase activity as well as weak C1-specific phosphatase activity towards ADP-ribose-1″-phosphate

(103,104). A subgroup of macrodomain containing proteins was identified in this thesis work to be able to reverse mono-ADP-ribosylation catalyzed by ARTD10 *in vitro* (151). This new class of enzymes could be furthermore shown to de-ADP-ribosylate glutamic acid residues and to release intact ADP-ribose and thus completely reverses ADP-ribosylation. Hence, macrodomain-containing proteins represent a missing link in the mono-ADP-ribosylation cycle and the first characterized family of enzymes able to revert glutamic acid mono-ADP-ribosylation. In parallel to our study, others have also identified MacroD1, MacroD2 and Af1521 as mono-ADP-ribosylhydrolases towards ARTD10 catalyzed modifications (161). In addition, Poa1p from yeast could be identified as member of the mono-ADP-ribosylhydrolase family, underlining that this new mechanism is conserved throughout many kingdoms of life. Interestingly, MacroD2 was also able to remove a sub-fraction of ADP-ribose modifications of ARTD1, which was mono-ADP-ribosylated under low NAD^+ conditions (161).

In a third publication, C6orf130 was not only observed to hydrolyze mono-ADP-ribose, but in addition also released whole polymers from automodified ARTD1 (162). In contrast to PARG, which hydrolyzes the glycosidic linkages within PAR and thus generates free mono-ADP-ribose, C6orf130 was described to release the intact polymer, which can potentially act as a signaling molecule for mitochondria to trigger apoptosis (163). As the release of a complete PAR chain could not be observed for MacroD1 or MacroD2 by us and others (151,161), C6orf130 might catalyze a different enzymatic reaction or structural differences might enable C6orf130 to access the protein-attachment site of PAR in a different manner. The other macrodomain-containing proteins, in contrast, might thus not be able to reach this bond due to steric hindrance or other structural interferences. Clearly, further studies will have to address this question in order to characterize and sort the different macrodomain containing proteins and to identify additional members of the relevant protein families. This knowledge will help to understand the ADP-ribose metabolism, the involved players and its regulation.

4.8 Functionality of the ribose C-atom bound to glutamic acids in ADP-ribosylation

An additional important aspect to be considered for protein ADP-ribosylation is, which C-atom of the ribose moiety is linked to the modified acceptor residue. The

exact type of linkage affects the position of the ribose, but also influences the stability of the modification. Theoretically, the ribose could be linked through the C1, C2 or C3 atom to glutamic acidic residues, while only a C1 linkage has been proposed for basic amino acids such as lysines (124). Consecutively, this linkages might furthermore be converted into a ketoamine bond (124). The ability of macrodomain containing proteins to hydrolyze OAADPr and molecular modeling suggest that they are able to hydrolyze a C2 or C3 linkage and experimental evidence from others also suggests that C1 linkages can be hydrolyzed by MacroD2 (161). Whether only one type or different kinds of linkages are synthesized and the potential specificity of hydrolases for a particular type of linkage has yet to be defined. To provide further evidence, the activity of the so far identified hydrolases towards synthesized standard peptides that are ADP-ribosylated via a C1, C2 or C3 linkages and NMR studies would be of great value. Very recently, progress in this direction was made and could in the near future provide tools to address this issue (164).

4.9 Reversal of mono-ADP-ribosylation is important for cellular functions

The kinase GSK3β is involved in various signaling pathways and defects are linked to diseases like cancer, Alzheimer and type II diabetes (165). It was previously shown that the mono-ADP-ribosylation of GSK3β leads to the inhibition of its kinase activity (126) and excitingly, we could show in this work that the inhibitory effect of GSK3β ADP-ribosylation can be reversed by MacroD2, thus making mono-ADP-ribosylation of GSK3β a reversible PTM that regulates GSK3β enzymatic activity (151). This important finding opens a variety of research possibilities and raises interesting questions, especially about the specificity of macrodomain containing proteins and the regulation of the hydrolysis reaction, for example by other PTMs or the recruitment through other factors. In addition, it is important to investigate whether certain ADP-ribosylhydrolases can be linked to specific mechanisms in the cell, such as signal transduction, inflammation or transcriptional regulation, which are all influenced by ADP-ribosylation (10,22).

4.10 Medical relevance of macrodomains and ADP-ribosylation

A very recent study identified a homozygous mutation in C6orf130 to be the cause of a neurodegenerative disorder in an extended consanguineous family over two generations (162). This mutation leads to a dramatic loss in hydrolysis activity,

confirming that a defect in the de-ADP-ribosylation activity of the mutant C6orf130 was indeed the cause for the observed disease phenotype. Unfortunately, no substrates for C6orf130 in cells have been identified so far. Therefore, the authors speculate that the defect in hydrolysis leads to perturbations in the DNA damage response, proliferation and senescence, which subsequently lead to cell death and neurodegeneration, but additional efforts are required in order to understand the molecular background of this observations.

Taken together, the above mentioned results clearly emphasize the importance of mono-ADP-ribose hydrolysis by macrodomain-containing proteins and the need to further characterize and identify how the mono-ADP-ribosylation cycle influences cellular functions. In addition, the disease-relevance of macrodomain-containing proteins sets the stage for the evaluation of macrodomains as potential therapeutic targets. Especially the availability of structural information about the three identified human macrodomains will help to accelerate this process. Recent findings, defining roles for macrodomain containing proteins in diseases such as breast cancer, Kabuki syndrome and neuroblastoma, could lead to interesting new results and applications for ADP-ribosylhydrolase inhibitors (95,96).

5 ABBREVIATIONS

3-AB	3-aminobenzamide
^{32}P	phosphorus-32
ADP	Adenosine diphosphate
ADPr	ADP-ribose
ADPRibase-Mn	Mn_2^+-dependent ADP-ribose/CDP-alcohol pyrophosphatase
ALC1	Amplified in liver cancer protein 1
AMP	Adenosine monophosphate
APLF	Aprataxin and PNK-like factor
ARH	ADP-ribosylhydrolase
ART	ADP-ribosyltransferase
ARTC	ART cholera toxin like
ARTD	ART diphteria toxin like
Asp	Aspartic acid
ATM	Ataxia telangiectasia mutated
ATP	Adenosine triphosphate
BAL	B-aggressive lymphoma
BRCA	Breast cancer type susceptibility protein homolog
C	cysteine
C6orf130	O-acetyl-ADP-ribose deacetylase 1
CHFR	Checkpoint with forkhead and RING finger domains protein
ChIP	Chromatin immunoprecipitation
CID	Collision induced dissociation
D	Aspartate
DDH2	DDHD domain-containing protein 2
DNA	Desoxyribonucleic acid
DNA-PK	DNA-dependent protein kinase
Dph	Diphtamide
E	Glutamate / glutamic acid
ECD	Electron capture dissociation
ETD	Electron transfer dissociation
FT	Fourier transform
GDAP2	Ganglioside-induced differentiation-associated protein 2
GDH1	Glutamate dehydrogenase 1
GHD1	Glucose 1-dehydrogenase 1
GSK3β	Glycogen synthase kinase 3 beta
GST	Glutathione S-transferase
H	Histidine
HCD	Higher energy collisional dissociation
HEV	Hepatitis E virus
His	Histidine
HPLC	High performance liquid chromatography
HR	Homologous recombination
IT	Ion trap
K	Lysine
kDa	Kilodalton
Ku70/86	Lupus Ku autoantigen protein p70/p86
LC	Liquid chromatography

MacroD1	MACRO domain-containing protein 1
MacroD2	MACRO domain-containing protein 2
$MgCl_2$	Magnesium chloride
Mn	Manganese
MnCl2	Manganese(II) chloride
MNNG	N-methyl-N' -nitro-N'-nitro- soguanidine
MRE11	Meiotic recombination 11 homolog 1
MS	Mass spectrometry
N	Asparagine
NaCl	Sodium chloride
NAD+	Nicotinamide adenine dinucleotide
NH_2OH	Hydroxylamine
NMR	Nuclear magnetic resonance
Nudix	Nucleoside diphosphate linked to X
NUDT	Nucleoside diphosphate-linked moiety X motif
OAADPr	O-acetyl-ADP-ribose
p53	Cellular tumor antigen p53
PAR	Poly-ADP-ribose
PARG	Poly-ADP-ribose glycohydrolase
PARP	Poly-ADP-ribose polymerase
PBM	PAR-binding motif
PBZ	PAR-binding zinc-finger
PDE1	Phosphodiesterase 1
PNK	Polynucleotide kinase
pS	Phospho-serine
PTEN	Phosphatase and tensin homolog
PTM	Post-translational modification
Q	Glutamine
R	Arginine
rDNA	Ribosomal DNA
RhoA	Transforming protein RhoA
RING	Really interesting new gene
RNA	Ribonucleic acid
RNF146	RING finger protein 146
S	Serine
SARS-CoV	Severe acute respiratory syndrome coronavirus
SDS	Sodium dodecyl sulfate
SET7/9	SET domain-containing protein 7
SFV	Simian foamy virus
SILAC	Stable isotope labeling by amino acids in cell
Snf2	Transcription regulatory protein
SUMO	Small ubiquitin-like modifier
Trip12	Thyroid receptor-interacting protein 12
UV	Ultraviolet
W	Tryptophane
XRCC1	X-ray repair cross-complementing protein 1
Y	Tyrosine

6 REFERENCES

1. Prabakaran, S., Lippens, G., Steen, H. and Gunawardena, J. (2012) Post-translational modification: nature's escape from genetic imprisonment and the basis for dynamic information encoding. *Wiley Interdiscip Rev Syst Biol Med*, **4**, 565-583.
2. Jensen, O.N. (2006) Interpreting the protein language using proteomics. *Nat Rev Mol Cell Biol*, **7**, 391-403.
3. Khoury, G.A., Baliban, R.C. and Floudas, C.A. (2011) Proteome-wide post-translational modification statistics: frequency analysis and curation of the swiss-prot database. *Sci Rep*, **1**.
4. Vosseller, K., Wells, L. and Hart, G.W. (2001) Nucleocytoplasmic O-glycosylation: O-GlcNAc and functional proteomics. *Biochimie*, **83**, 575-581.
5. Yang, X.J. (2005) Multisite protein modification and intramolecular signaling. *Oncogene*, **24**, 1653-1662.
6. Cosgrove, M.S., Boeke, J.D. and Wolberger, C. (2004) Regulated nucleosome mobility and the histone code. *Nature structural & molecular biology*, **11**, 1037-1043.
7. Schwartz, D.C. and Hochstrasser, M. (2003) A superfamily of protein tags: ubiquitin, SUMO and related modifiers. *Trends in biochemical sciences*, **28**, 321-328.
8. Gyorgy, B., Toth, E., Tarcsa, E., Falus, A. and Buzas, E.I. (2006) Citrullination: a posttranslational modification in health and disease. *Int J Biochem Cell Biol*, **38**, 1662-1677.
9. Creighton, T.E. (1993) *Proteins: Structures and Molecular Properties*. W H Freeman & Co. ISBN 0-7167-2317-4.
10. Kraus, W.L. and Hottiger, M.O. (2013) PARP-1 and gene regulation: Progress and puzzles. *Molecular aspects of medicine*.
11. Chambon, P., Weill, J.D. and Mandel, P. (1963) Nicotinamide mononucleotide activation of new DNA-dependent polyadenylic acid synthesizing nuclear enzyme. *Biochem Biophys Res Commun*, **11**, 39-43.
12. Hottiger, M.O., Hassa, P.O., Lüscher, B., Schüler, H. and Koch-Nolte, F. (2010) Toward a unified nomenclature for mammalian ADP-ribosyltransferases. *Trends Biochem Sci*, **35**, 208-219.
13. Hassa, P.O., Haenni, S., Elser, M. and Hottiger, M.O. (2006) Nuclear ADP-ribosylation reactions in mammalian cells: where are we today and where are we going? *Microbiol Mol Biol Rev*, **70**, 789-829.
14. Bredehorst, R., Wielckens, K., Gartemann, A., Lengyel, H., Klapproth, K. and Hilz, H. (1978) Two different types of bonds linking single ADP-ribose residues covalently to proteins. Quantification in eukaryotic cells. *Eur J Biochem*, **92**, 129-135.
15. Hakme, A., Wong, H.K., Dantzer, F. and Schreiber, V. (2008) The expanding field of poly(ADP-ribosyl)ation reactions. 'Protein Modifications: Beyond the Usual Suspects' Review Series. *EMBO Rep*, **9**, 1094-1100.
16. Alvarez-Gonzalez, R. and Mendoza-Alvarez, H. (1995) Dissection of ADP-ribose polymer synthesis into individual steps of initiation, elongation, and branching. *Biochimie*, **77**, 403-407.
17. Alvarez-Gonzalez, R. and Jacobson, M.K. (1987) Characterization of polymers of adenosine diphosphate ribose generated in vitro and in vivo. *Biochemistry*, **26**, 3218-3224.
18. Kim, M.Y., Zhang, T. and Kraus, W.L. (2005) Poly(ADP-ribosyl)ation by PARP-1: 'PAR-laying' NAD+ into a nuclear signal. *Genes & development*, **19**, 1951-1967.
19. Fieldhouse, R.J. and Merrill, A.R. (2008) Needle in the haystack: structure-based toxin discovery. *Trends in biochemical sciences*, **33**, 546-556.
20. Deng, Q. and Barbieri, J.T. (2008) Molecular mechanisms of the cytotoxicity of ADP-ribosylating toxins. *Annu Rev Microbiol*, **62**, 271-288.
21. Shimizu, Y., Hasegawa, S., Fujimura, S. and Sugimura, T. (1967) Solubilization of enzyme forming ADPR polymer from NAD. *Biochem Biophys Res Commun*, **29**, 80-83.
22. Hassa, P.O. and Hottiger, M.O. (2008) The diverse biological roles of mammalian PARPs, a small but powerful family of poly-ADP-ribose polymerases. *Front Biosci*, **13**, 3046-3082.
23. Loseva, O., Jemth, A.S., Bryant, H.E., Schuler, H., Lehtio, L., Karlberg, T. and Helleday, T. (2010) PARP-3 is a mono-ADP-ribosylase that activates PARP-1 in the absence of DNA. *The Journal of biological chemistry*, **285**, 8054-8060.
24. Shieh, W.M., Ame, J.C., Wilson, M.V., Wang, Z.Q., Koh, D.W., Jacobson, M.K. and Jacobson, E.L. (1998) Poly(ADP-ribose) polymerase null mouse cells synthesize ADP-ribose polymers. *The Journal of biological chemistry*, **273**, 30069-30072.

25. Ame, J.C., Rolli, V., Schreiber, V., Niedergang, C., Apiou, F., Decker, P., Muller, S., Hoger, T., Menissier-de Murcia, J. and de Murcia, G. (1999) PARP-2, A novel mammalian DNA damage-dependent poly(ADP-ribose) polymerase. *The Journal of biological chemistry*, **274**, 17860-17868.
26. Rulten, S.L., Fisher, A.E., Robert, I., Zuma, M.C., Rouleau, M., Ju, L., Poirier, G., Reina-San-Martin, B. and Caldecott, K.W. (2011) PARP-3 and APLF function together to accelerate nonhomologous end-joining. *Molecular cell*, **41**, 33-45.
27. Rippmann, J.F., Damm, K. and Schnapp, A. (2002) Functional characterization of the poly(ADP-ribose) polymerase activity of tankyrase 1, a potential regulator of telomere length. *J Mol Biol*, **323**, 217-224.
28. Cook, B.D., Dynek, J.N., Chang, W., Shostak, G. and Smith, S. (2002) Role for the related poly(ADP-Ribose) polymerases tankyrase 1 and 2 at human telomeres. *Mol Cell Biol*, **22**, 332-342.
29. Kleine, H., Poreba, E., Lesniewicz, K., Hassa, P.O., Hottiger, M.O., Litchfield, D.W., Shilton, B.H. and Luscher, B. (2008) Substrate-assisted catalysis by PARP10 limits its activity to mono-ADP-ribosylation. *Molecular cell*, **32**, 57-69.
30. Aguiar, R.C., Takeyama, K., He, C., Kreinbrink, K. and Shipp, M.A. (2005) B-aggressive lymphoma family proteins have unique domains that modulate transcription and exhibit poly(ADP-ribose) polymerase activity. *The Journal of biological chemistry*, **280**, 33756-33765.
31. Bianchi, M.E. (2007) DAMPs, PAMPs and alarmins: all we need to know about danger. *J Leukoc Biol*, **81**, 1-5.
32. Newton, K. and Dixit, V.M. (2012) Signaling in innate immunity and inflammation. *Cold Spring Harb Perspect Biol*, **4**.
33. Zhang, Q., Raoof, M., Chen, Y., Sumi, Y., Sursal, T., Junger, W., Brohi, K., Itagaki, K. and Hauser, C.J. (2010) Circulating mitochondrial DAMPs cause inflammatory responses to injury. *Nature*, **464**, 104-107.
34. Schreiber, V., Dantzer, F., Ame, J.C. and de Murcia, G. (2006) Poly(ADP-ribose): novel functions for an old molecule. *Nat Rev Mol Cell Biol*, **7**, 517-528.
35. Hottiger, M.O. (2011) ADP-ribosylation of histones by ARTD1: An additional module of the histone code? *FEBS Lett*, **585**, 1595-1599.
36. Riffell, J.L., Lord, C.J. and Ashworth, A. (2012) Tankyrase-targeted therapeutics: expanding opportunities in the PARP family. *Nat Rev Drug Discov*, **11**, 923-936.
37. Gibson, B.A. and Kraus, W.L. (2012) New insights into the molecular and cellular functions of poly(ADP-ribose) and PARPs. *Nat Rev Mol Cell Biol*, **13**, 411-424.
38. Krishnakumar, R. and Kraus, W.L. (2010) PARP-1 regulates chromatin structure and transcription through a KDM5B-dependent pathway. *Molecular cell*, **39**, 736-749.
39. Asher, G., Reinke, H., Altmeyer, M., Gutierrez-Arcelus, M., Hottiger, M.O. and Schibler, U. (2010) Poly(ADP-ribose) polymerase 1 participates in the phase entrainment of circadian clocks to feeding. *Cell*, **142**, 943-953.
40. Wang, Z., Michaud, G.A., Cheng, Z., Zhang, Y., Hinds, T.R., Fan, E., Cong, F. and Xu, W. (2012) Recognition of the iso-ADP-ribose moiety in poly(ADP-ribose) by WWE domains suggests a general mechanism for poly(ADP-ribosyl)ation-dependent ubiquitination. *Genes & development*, **26**, 235-240.
41. Messner, S., Altmeyer, M., Zhao, H., Pozivil, A., Roschitzki, B., Gehrig, P., Rutishauser, D., Huang, D., Caflisch, A. and Hottiger, M.O. (2010) PARP1 ADP-ribosylates lysine residues of the core histone tails. *Nucleic Acids Res*, **38**, 6350-6362.
42. Moss, J., Yost, D.A. and Stanley, S.J. (1983) Amino acid-specific ADP-ribosylation. *The Journal of biological chemistry*, **258**, 6466-6470.
43. Adamietz, P. and Hilz, H. (1976) Poly(adenosine diphosphate ribose) is covalently linked to nuclear proteins by two types of bonds. *Hoppe Seylers Z Physiol Chem*, **357**, 527-534.
44. Brochu, G., Shah, G.M. and Poirier, G.G. (1994) Purification of poly(ADP-ribose) glycohydrolase and detection of its isoforms by a zymogram following one- or two-dimensional electrophoresis. *Anal Biochem*, **218**, 265-272.
45. Meyer-Ficca, M.L., Meyer, R.G., Coyle, D.L., Jacobson, E.L. and Jacobson, M.K. (2004) Human poly(ADP-ribose) glycohydrolase is expressed in alternative splice variants yielding isoforms that localize to different cell compartments. *Exp Cell Res*, **297**, 521-532.
46. Min, W. and Wang, Z.Q. (2009) Poly (ADP-ribose) glycohydrolase (PARG) and its therapeutic potential. *Frontiers in bioscience : a journal and virtual library*, **14**, 1619-1626.

47. Slade, D., Dunstan, M.S., Barkauskaite, E., Weston, R., Lafite, P., Dixon, N., Ahel, M., Leys, D. and Ahel, I. (2011) The structure and catalytic mechanism of a poly(ADP-ribose) glycohydrolase. *Nature*, **477**, 616-620.
48. Patel, C.N., Koh, D.W., Jacobson, M.K. and Oliveira, M.A. (2005) Identification of three critical acidic residues of poly(ADP-ribose) glycohydrolase involved in catalysis: determining the PARG catalytic domain. *Biochem J*, **388**, 493-500.
49. Wang, Z.Q., Auer, B., Stingl, L., Berghammer, H., Haidacher, D., Schweiger, M. and Wagner, E.F. (1995) Mice lacking ADPRT and poly(ADP-ribosyl)ation develop normally but are susceptible to skin disease. *Genes & development*, **9**, 509-520.
50. Koh, D.W., Lawler, A.M., Poitras, M.F., Sasaki, M., Wattler, S., Nehls, M.C., Stoger, T., Poirier, G.G., Dawson, V.L. and Dawson, T.M. (2004) Failure to degrade poly(ADP-ribose) causes increased sensitivity to cytotoxicity and early embryonic lethality. *Proc Natl Acad Sci U S A*, **101**, 17699-17704.
51. Erdelyi, K., Bai, P., Kovacs, I., Szabo, E., Mocsar, G., Kakuk, A., Szabo, C., Gergely, P. and Virag, L. (2009) Dual role of poly(ADP-ribose) glycohydrolase in the regulation of cell death in oxidatively stressed A549 cells. *Faseb J*, **23**, 3553-3563.
52. Fisher, A.E., Hochegger, H., Takeda, S. and Caldecott, K.W. (2007) Poly(ADP-ribose) polymerase 1 accelerates single-strand break repair in concert with poly(ADP-ribose) glycohydrolase. *Mol Cell Biol*, **27**, 5597-5605.
53. Cortes, U., Tong, W.M., Coyle, D.L., Meyer-Ficca, M.L., Meyer, R.G., Petrilli, V., Herceg, Z., Jacobson, E.L., Jacobson, M.K. and Wang, Z.Q. (2004) Depletion of the 110-kilodalton isoform of poly(ADP-ribose) glycohydrolase increases sensitivity to genotoxic and endotoxic stress in mice. *Mol Cell Biol*, **24**, 7163-7178.
54. Fathers, C., Drayton, R.M., Solovieva, S. and Bryant, H.E. (2012) Inhibition of poly(ADP-ribose) glycohydrolase (PARG) specifically kills BRCA2-deficient tumor cells. *Cell Cycle*, **11**, 990-997.
55. Moss, J., Stanley, S.J., Nightingale, M.S., Murtagh, J.J., Jr., Monaco, L., Mishima, K., Chen, H.C., Williamson, K.C. and Tsai, S.C. (1992) Molecular and immunological characterization of ADP-ribosylarginine hydrolases. *The Journal of biological chemistry*, **267**, 10481-10488.
56. Glowacki, G., Braren, R., Firner, K., Nissen, M., Kuhl, M., Reche, P., Bazan, F., Cetkovic-Cvrlje, M., Leiter, E., Haag, F. *et al.* (2002) The family of toxin-related ecto-ADP-ribosyltransferases in humans and the mouse. *Protein Sci*, **11**, 1657-1670.
57. Oka, S., Kato, J. and Moss, J. (2006) Identification and characterization of a mammalian 39-kDa poly(ADP-ribose) glycohydrolase. *The Journal of biological chemistry*, **281**, 705-713.
58. Mueller-Dieckmann, C., Kernstock, S., Lisurek, M., von Kries, J.P., Haag, F., Weiss, M.S. and Koch-Nolte, F. (2006) The structure of human ADP-ribosylhydrolase 3 (ARH3) provides insights into the reversibility of protein ADP-ribosylation. *Proc Natl Acad Sci U S A*, **103**, 15026-15031.
59. Okazaki, I.J., Zolkiewska, A., Nightingale, M.S. and Moss, J. (1994) Immunological and structural conservation of mammalian skeletal muscle glycosylphosphatidylinositol-linked ADP-ribosyltransferases. *Biochemistry*, **33**, 12828-12836.
60. Braren, R., Glowacki, G., Nissen, M., Haag, F. and Koch-Nolte, F. (1998) Molecular characterization and expression of the gene for mouse NAD+:arginine ecto-mono(ADP-ribosyl)transferase, Art1. *Biochem J*, **336 (Pt 3)**, 561-568.
61. Kato, J., Zhu, J., Liu, C., Stylianou, M., Hoffmann, V., Lizak, M.J., Glasgow, C.G. and Moss, J. (2011) ADP-ribosylarginine hydrolase regulates cell proliferation and tumorigenesis. *Cancer Res*, **71**, 5327-5335.
62. Okayama, H., Honda, M. and Hayaishi, O. (1978) Novel enzyme from rat liver that cleaves an ADP-ribosyl histone linkage. *Proc Natl Acad Sci U S A*, **75**, 2254-2257.
63. Oka, J., Ueda, K., Hayaishi, O., Komura, H. and Nakanishi, K. (1984) ADP-ribosyl protein lyase. Purification, properties, and identification of the product. *The Journal of biological chemistry*, **259**, 986-995.
64. McLennan, A.G. (2006) The Nudix hydrolase superfamily. *Cell Mol Life Sci*, **63**, 123-143.
65. Kraszewska, E. (2008) The plant Nudix hydrolase family. *Acta Biochim Pol*, **55**, 663-671.
66. Gasmi, L., Cartwright, J.L. and McLennan, A.G. (1999) Cloning, expression and characterization of YSA1H, a human adenosine 5'-diphosphosugar pyrophosphatase possessing a MutT motif. *Biochem J*, **344 Pt 2**, 331-337.
67. Lin, S., Gasmi, L., Xie, Y., Ying, K., Gu, S., Wang, Z., Jin, H., Chao, Y., Wu, C., Zhou, Z. *et al.* (2002) Cloning, expression and characterisation of a human Nudix hydrolase specific for adenosine 5'-diphosphoribose (ADP-ribose). *Biochim Biophys Acta*, **1594**, 127-135.

68. Carloto, A., Costas, M.J., Cameselle, J.C., McLennan, A.G. and Ribeiro, J.M. (2006) The specific, submicromolar-Km ADP-ribose pyrophosphatase purified from human placenta is enzymically indistinguishable from recombinant NUDT9 protein, including a selectivity for Mn2+ as activating cation and increase in Km for ADP-ribose, both elicited by H2O2. *Biochim Biophys Acta*, **1760**, 1545-1551.
69. De Vos, M., Schreiber, V. and Dantzer, F. (2012) The diverse roles and clinical relevance of PARPs in DNA damage repair: current state of the art. *Biochem Pharmacol*, **84**, 137-146.
70. Curtin, N.J. (2005) PARP inhibitors for cancer therapy. *Expert Rev Mol Med*, **7**, 1-20.
71. Helleday, T. (2011) The underlying mechanism for the PARP and BRCA synthetic lethality: clearing up the misunderstandings. *Mol Oncol*, **5**, 387-393.
72. Rouleau, M., Patel, A., Hendzel, M.J., Kaufmann, S.H. and Poirier, G.G. (2010) PARP inhibition: PARP1 and beyond. *Nat Rev Cancer*, **10**, 293-301.
73. Javle, M. and Curtin, N.J. (2011) The role of PARP in DNA repair and its therapeutic exploitation. *Br J Cancer*, **105**, 1114-1122.
74. Helleday, T., Bryant, H.E. and Schultz, N. (2005) Poly(ADP-ribose) polymerase (PARP-1) in homologous recombination and as a target for cancer therapy. *Cell Cycle*, **4**, 1176-1178.
75. Farmer, H., McCabe, N., Lord, C.J., Tutt, A.N., Johnson, D.A., Richardson, T.B., Santarosa, M., Dillon, K.J., Hickson, I., Knights, C. *et al.* (2005) Targeting the DNA repair defect in BRCA mutant cells as a therapeutic strategy. *Nature*, **434**, 917-921.
76. Basu, B., Sandhu, S.K. and de Bono, J.S. (2012) PARP inhibitors: mechanism of action and their potential role in the prevention and treatment of cancer. *Drugs*, **72**, 1579-1590.
77. Dedes, K.J., Wetterskog, D., Mendes-Pereira, A.M., Natrajan, R., Lambros, M.B., Geyer, F.C., Vatcheva, R., Savage, K., Mackay, A., Lord, C.J. *et al.* (2010) PTEN deficiency in endometrioid endometrial adenocarcinomas predicts sensitivity to PARP inhibitors. *Sci Transl Med*, **2**, 53ra75.
78. Audeh, M.W., Carmichael, J., Penson, R.T., Friedlander, M., Powell, B., Bell-McGuinn, K.M., Scott, C., Weitzel, J.N., Oaknin, A., Loman, N. *et al.* (2010) Oral poly(ADP-ribose) polymerase inhibitor olaparib in patients with BRCA1 or BRCA2 mutations and recurrent ovarian cancer: a proof-of-concept trial. *Lancet*, **376**, 245-251.
79. Tutt, A., Robson, M., Garber, J.E., Domchek, S.M., Audeh, M.W., Weitzel, J.N., Friedlander, M., Arun, B., Loman, N., Schmutzler, R.K. *et al.* (2010) Oral poly(ADP-ribose) polymerase inhibitor olaparib in patients with BRCA1 or BRCA2 mutations and advanced breast cancer: a proof-of-concept trial. *Lancet*, **376**, 235-244.
80. Chan, S.L. and Mok, T. (2010) PARP inhibition in BRCA-mutated breast and ovarian cancers. *Lancet*, **376**, 211-213.
81. Kleine, H. and Luscher, B. (2009) Learning how to read ADP-ribosylation. *Cell*, **139**, 17-19.
82. Oberoi, J., Richards, M.W., Crumpler, S., Brown, N., Blagg, J. and Bayliss, R. (2010) Structural basis of poly(ADP-ribose) recognition by the multizinc binding domain of checkpoint with forkhead-associated and RING Domains (CHFR). *The Journal of biological chemistry*, **285**, 39348-39358.
83. Eustermann, S., Brockmann, C., Mehrotra, P.V., Yang, J.C., Loakes, D., West, S.C., Ahel, I. and Neuhaus, D. (2010) Solution structures of the two PBZ domains from human APLF and their interaction with poly(ADP-ribose). *Nature structural & molecular biology*, **17**, 241-243.
84. Ahel, I., Ahel, D., Matsusaka, T., Clark, A.J., Pines, J., Boulton, S.J. and West, S.C. (2008) Poly(ADP-ribose)-binding zinc finger motifs in DNA repair/checkpoint proteins. *Nature*, **451**, 81-85.
85. Allen, M.D., Buckle, A.M., Cordell, S.C., Lowe, J. and Bycroft, M. (2003) The crystal structure of AF1521 a protein from Archaeoglobus fulgidus with homology to the non-histone domain of macroH2A. *J Mol Biol*, **330**, 503-511.
86. Pehrson, J.R. and Fried, V.A. (1992) MacroH2A, a core histone containing a large nonhistone region. *Science*, **257**, 1398-1400.
87. Kalisch, T., Ame, J.C., Dantzer, F. and Schreiber, V. (2012) New readers and interpretations of poly(ADP-ribosyl)ation. *Trends in biochemical sciences*, **37**, 381-390.
88. Gamble, M.J. (2013) Expanding the functional repertoire of macrodomains. *Nature structural & molecular biology*, **20**, 407-408.
89. Kraus, W.L. (2009) New functions for an ancient domain. *Nature structural & molecular biology*, **16**, 904-907.

90. Timinszky, G., Till, S., Hassa, P.O., Hothorn, M., Kustatscher, G., Nijmeijer, B., Colombelli, J., Altmeyer, M., Stelzer, E.H., Scheffzek, K. *et al.* (2009) A macrodomain-containing histone rearranges chromatin upon sensing PARP1 activation. *Nature structural & molecular biology*, **16**, 923-929.
91. Pehrson, J.R. and Fuji, R.N. (1998) Evolutionary conservation of histone macroH2A subtypes and domains. *Nucleic acids research*, **26**, 2837-2842.
92. Ehrlich, M.E. and Gandy, S. (2011) Chromatin plasticity and the pathogenesis of Huntington disease. *Proc Natl Acad Sci U S A*, **108**, 16867-16868.
93. Kapoor, A., Goldberg, M.S., Cumberland, L.K., Ratnakumar, K., Segura, M.F., Emanuel, P.O., Menendez, S., Vardabasso, C., Leroy, G., Vidal, C.I. *et al.* (2010) The histone variant macroH2A suppresses melanoma progression through regulation of CDK8. *Nature*, **468**, 1105-1109.
94. Ahel, D., Horejsi, Z., Wiechens, N., Polo, S.E., Garcia-Wilson, E., Ahel, I., Flynn, H., Skehel, M., West, S.C., Jackson, S.P. *et al.* (2009) Poly(ADP-ribose)-dependent regulation of DNA repair by the chromatin remodeling enzyme ALC1. *Science*, **325**, 1240-1243.
95. Zhao, Y.L., Han, W.D., Li, Q., Mu, Y.M., Lu, X.C., Yu, L., Song, H.J., Li, X., Lu, J.M. and Pan, C.Y. (2005) Mechanism of transcriptional regulation of LRP16 gene expression by 17-beta estradiol in MCF-7 human breast cancer cells. *J Mol Endocrinol*, **34**, 77-89.
96. Neuvonen, M. and Ahola, T. (2009) Differential activities of cellular and viral macro domain proteins in binding of ADP-ribose metabolites. *J Mol Biol*, **385**, 212-225.
97. Cho, S.H., Ahn, A.K., Bhargava, P., Lee, C.H., Eischen, C.M., McGuinness, O. and Boothby, M. (2011) Glycolytic rate and lymphomagenesis depend on PARP14, an ADP ribosyltransferase of the B aggressive lymphoma (BAL) family. *Proc Natl Acad Sci U S A*, **108**, 15972-15977.
98. Camicia, R., Bachmann, S.B., Winkler, H.C., Beer, M., Tinguely, M., Haralambieva, E. and Hassa, P.O. (2013) BAL1/ARTD9 represses the anti-proliferative and pro-apoptotic IFNgamma-STAT1-IRF1-53 axes in diffuse large B-cell lymphoma. *J Cell Sci*.
99. Forst, A.H., Karlberg, T., Herzog, N., Thorsell, A.G., Gross, A., Feijs, K.L., Verheugd, P., Kursula, P., Nijmeijer, B., Kremmer, E. *et al.* (2013) Recognition of mono-ADP-ribosylated ARTD10 substrates by ARTD8 macrodomains. *Structure*, **21**, 462-475.
100. Karras, G.I., Kustatscher, G., Buhecha, H.R., Allen, M.D., Pugieux, C., Sait, F., Bycroft, M. and Ladurner, A.G. (2005) The macro domain is an ADP-ribose binding module. *Embo J*, **24**, 1911-1920.
101. Egloff, M.P., Malet, H., Putics, A., Heinonen, M., Dutartre, H., Frangeul, A., Gruez, A., Campanacci, V., Cambillau, C., Ziebuhr, J. *et al.* (2006) Structural and functional basis for ADP-ribose and poly(ADP-ribose) binding by viral macro domains. *J Virol*, **80**, 8493-8502.
102. Till, S. and Ladurner, A.G. (2009) Sensing NAD metabolites through macro domains. *Frontiers in bioscience : a journal and virtual library*, **14**, 3246-3258.
103. Peterson, F.C., Chen, D., Lytle, B.L., Rossi, M.N., Ahel, I., Denu, J.M. and Volkman, B.F. (2011) Orphan macrodomain protein (human C6orf130) is an O-acyl-ADP-ribose deacylase: solution structure and catalytic properties. *The Journal of biological chemistry*, **286**, 35955-35965.
104. Chen, D., Vollmar, M., Rossi, M.N., Phillips, C., Kraehenbuehl, R., Slade, D., Mehrotra, P.V., von Delft, F., Crosthwaite, S.K., Gileadi, O. *et al.* (2011) Identification of macrodomain proteins as novel O-acetyl-ADP-ribose deacetylases. *The Journal of biological chemistry*, **286**, 13261-13271.
105. Tanner, K.G., Landry, J., Sternglanz, R. and Denu, J.M. (2000) Silent information regulator 2 family of NAD- dependent histone/protein deacetylases generates a unique product, 1-O-acetyl-ADP-ribose. *Proc Natl Acad Sci U S A*, **97**, 14178-14182.
106. Aravind, L. (2001) The WWE domain: a common interaction module in protein ubiquitination and ADP ribosylation. *Trends in biochemical sciences*, **26**, 273-275.
107. He, F., Tsuda, K., Takahashi, M., Kuwasako, K., Terada, T., Shirouzu, M., Watanabe, S., Kigawa, T., Kobayashi, N., Guntert, P. *et al.* (2012) Structural insight into the interaction of ADP-ribose with the PARP WWE domains. *FEBS letters*, **586**, 3858-3864.
108. Pleschke, J.M., Kleczkowska, H.E., Strohm, M. and Althaus, F.R. (2000) Poly(ADP-ribose) binds to specific domains in DNA damage checkpoint proteins. *The Journal of biological chemistry*, **275**, 40974-40980.
109. Gagne, J.P., Isabelle, M., Lo, K.S., Bourassa, S., Hendzel, M.J., Dawson, V.L., Dawson, T.M. and Poirier, G.G. (2008) Proteome-wide identification of poly(ADP-ribose) binding proteins and poly(ADP-ribose)-associated protein complexes. *Nucleic acids research*, **36**, 6959-6976.

110. Simpson, L.L. (1984) Molecular basis for the pharmacological actions of Clostridium botulinum type C2 toxin. *J Pharmacol Exp Ther*, **230**, 665-669.
111. West, R.E., Jr., Moss, J., Vaughan, M., Liu, T. and Liu, T.Y. (1985) Pertussis toxin-catalyzed ADP-ribosylation of transducin. Cysteine 347 is the ADP-ribose acceptor site. *The Journal of biological chemistry*, **260**, 14428-14430.
112. Vandekerckhove, J., Schering, B., Barmann, M. and Aktories, K. (1988) Botulinum C2 toxin ADP-ribosylates cytoplasmic beta/gamma-actin in arginine 177. *The Journal of biological chemistry*, **263**, 696-700.
113. Lang, A.E., Schmidt, G., Schlosser, A., Hey, T.D., Larrinua, I.M., Sheets, J.J., Mannherz, H.G. and Aktories, K. (2010) Photorhabdus luminescens toxins ADP-ribosylate actin and RhoA to force actin clustering. *Science*, **327**, 1139-1142.
114. Ogata, N., Ueda, K., Kagamiyama, H. and Hayaishi, O. (1980) ADP-ribosylation of histone H1. Identification of glutamic acid residues 2, 14, and the COOH-terminal lysine residue as modification sites. *J Biol Chem*, **255**, 7616-7620.
115. Kawaichi, M., Ueda, K. and Hayaishi, O. (1981) Multiple autopoly(ADP-ribosyl)ation of rat liver poly(ADP-ribose) synthetase. Mode of modification and properties of automodified synthetase. *The Journal of biological chemistry*, **256**, 9483-9489.
116. Ueda, K. and Hayaishi, O. (1985) ADP-ribosylation. *Annu Rev Biochem*, **54**, 73-100.
117. Moss, J. and Vaughan, M. (1978) Isolation of an avian erythrocyte protein possessing ADP-ribosyltransferase activity and capable of activating adenylate cyclase. *Proc Natl Acad Sci U S A*, **75**, 3621-3624.
118. Yost, D.A. and Moss, J. (1983) Amino acid-specific ADP-ribosylation. Evidence for two distinct NAD:arginine ADP-ribosyltransferases in turkey erythrocytes. *The Journal of biological chemistry*, **258**, 4926-4929.
119. Altmeyer, M., Messner, S., Hassa, P.O., Fey, M. and Hottiger, M.O. (2009) Molecular mechanism of poly(ADP-ribosyl)ation by PARP1 and identification of lysine residues as ADP-ribose acceptor sites. *Nucleic Acids Res*, **37**, 3723-3738.
120. Oppenheimer, N.J. (1978) Structural determination and stereospecificity of the choleragen-catalyzed reaction of NAD+ with guanidines. *The Journal of biological chemistry*, **253**, 4907-4910.
121. Cervantes-Laurean, D., Jacobson, E.L. and Jacobson, M.K. (1996) Glycation and glycoxidation of histones by ADP-ribose. *The Journal of biological chemistry*, **271**, 10461-10469.
122. Kun, E., Chang, A.C., Sharma, M.L., Ferro, A.M. and Nitecki, D. (1976) Covalent modification of proteins by metabolites of NAD+. *Proc Natl Acad Sci U S A*, **73**, 3131-3135.
123. Cervantes-Laurean, D., Loflin, P.T., Minter, D.E., Jacobson, E.L. and Jacobson, M.K. (1995) Protein modification by ADP-ribose via acid-labile linkages. *The Journal of biological chemistry*, **270**, 7929-7936.
124. Cervantes-Laurean, D., Minter, D.E., Jacobson, E.L. and Jacobson, M.K. (1993) Protein glycation by ADP-ribose: studies of model conjugates. *Biochemistry*, **32**, 1528-1534.
125. Meng, L., Michaud, G.A., Merkel, J.S., Zhou, F., Huang, J., Mattoon, D.R. and Schweitzer, B. (2008) Protein kinase substrate identification on functional protein arrays. *BMC Biotechnol*, **8**, 22.
126. Feijs, K.L., Kleine, H., Braczynski, A., Forst, A.H., Herzog, N., Verheugd, P., Linzen, U., Kremmer, E. and Luscher, B. (2013) ARTD10 substrate identification on protein microarrays: regulation of GSK3beta by mono-ADP-ribosylation. *Cell Commun Signal*, **11**, 5.
127. Troiani, S., Lupi, R., Perego, R., Depaolini, S.R., Thieffine, S., Bosotti, R. and Rusconi, L. (2011) Identification of candidate substrates for poly(ADP-ribose) polymerase-2 (PARP2) in the absence of DNA damage using high-density protein microarrays. *Febs J*, **278**, 3676-3687.
128. Fila, J. and Honys, D. (2012) Enrichment techniques employed in phosphoproteomics. *Amino Acids*, **43**, 1025-1047.
129. Bodenmiller, B. and Aebersold, R. (2010) Quantitative analysis of protein phosphorylation on a system-wide scale by mass spectrometry-based proteomics. *Methods Enzymol*, **470**, 317-334.
130. Dani, N., Stilla, A., Marchegiani, A., Tamburro, A., Till, S., Ladurner, A.G., Corda, D. and Di Girolamo, M. (2009) Combining affinity purification by ADP-ribose-binding macro domains with mass spectrometry to define the mammalian ADP-ribosyl proteome. *Proc Natl Acad Sci U S A*, **106**, 4243-4248.
131. Jiang, H., Kim, J.H., Frizzell, K.M., Kraus, W.L. and Lin, H. (2010) Clickable NAD analogues for labeling substrate proteins of poly(ADP-ribose) polymerases. *Journal of the American Chemical Society*, **132**, 9363-9372.

132. Kawamitsu, H., Hoshino, H., Okada, H., Miwa, M., Momoi, H. and Sugimura, T. (1984) Monoclonal antibodies to poly(adenosine diphosphate ribose) recognize different structures. *Biochemistry*, **23**, 3771-3777.
133. Rolli, V., O'Farrell, M., Menissier-de Murcia, J. and de Murcia, G. (1997) Random mutagenesis of the poly(ADP-ribose) polymerase catalytic domain reveals amino acids involved in polymer branching. *Biochemistry*, **36**, 12147-12154.
134. Marsischky, G.T., Wilson, B.A. and Collier, R.J. (1995) Role of glutamic acid 988 of human poly-ADP-ribose polymerase in polymer formation. Evidence for active site similarities to the ADP-ribosylating toxins. *The Journal of biological chemistry*, **270**, 3247-3254.
135. Tao, Z., Gao, P. and Liu, H. (2009) Identification of the ADP-ribosylation sites in the PARP-1 automodification domain: analysis and implications. *J Am Chem Soc*, **131**, 14258-14260.
136. Chapman, J.D., Gagne, J.P., Poirier, G.G. and Goodlett, D.R. (2013) Mapping PARP-1 Auto-ADP-ribosylation Sites by Liquid Chromatography-Tandem Mass Spectrometry. *Journal of proteome research*.
137. Margarit, S.M., Davidson, W., Frego, L. and Stebbins, C.E. (2006) A steric antagonism of actin polymerization by a salmonella virulence protein. *Structure*, **14**, 1219-1229.
138. Hengel, S.M., Shaffer, S.A., Nunn, B.L. and Goodlett, D.R. (2009) Tandem mass spectrometry investigation of ADP-ribosylated kemptide. *Journal of the American Society for Mass Spectrometry*, **20**, 477-483.
139. Rosenthal, F.N., P.; Barkow-Oesterreicher, S.; Hottiger, M.O. (2013) Identification of ADP-ribosylation sites in cell extracts by higher energy collisional dissociation (HCD)-based mass spectrometry. *manuscript submitted*.
140. Bakhtiar, R. and Guan, Z. (2006) Electron capture dissociation mass spectrometry in characterization of peptides and proteins. *Biotechnol Lett*, **28**, 1047-1059.
141. Breuker, K., Oh, H., Lin, C., Carpenter, B.K. and McLafferty, F.W. (2004) Nonergodic and conformational control of the electron capture dissociation of protein cations. *Proc Natl Acad Sci U S A*, **101**, 14011-14016.
142. Mikesh, L.M., Ueberheide, B., Chi, A., Coon, J.J., Syka, J.E., Shabanowitz, J. and Hunt, D.F. (2006) The utility of ETD mass spectrometry in proteomic analysis. *Biochim Biophys Acta*, **1764**, 1811-1822.
143. Zee, B.M. and Garcia, B.A. (2010) Electron transfer dissociation facilitates sequencing of adenosine diphosphate-ribosylated peptides. *Anal Chem*, **82**, 28-31.
144. Fedorova, M., Frolov, A. and Hoffmann, R. (2010) Fragmentation behavior of Amadori-peptides obtained by non-enzymatic glycosylation of lysine residues with ADP-ribose in tandem mass spectrometry. *J Mass Spectrom*, **45**, 664-669.
145. Olsen, J.V., Macek, B., Lange, O., Makarov, A., Horning, S. and Mann, M. (2007) Higher-energy C-trap dissociation for peptide modification analysis. *Nat Methods*, **4**, 709-712.
146. Mann, M. and Kelleher, N.L. (2008) Precision proteomics: the case for high resolution and high mass accuracy. *Proc Natl Acad Sci U S A*, **105**, 18132-18138.
147. Jedrychowski, M.P., Huttlin, E.L., Haas, W., Sowa, M.E., Rad, R. and Gygi, S.P. (2011) Evaluation of HCD- and CID-type fragmentation within their respective detection platforms for murine phosphoproteomics. *Mol Cell Proteomics*, **10**, M111 009910.
148. Hayaishi, O. and Ueda, K. (1977) Poly(ADP-ribose) and ADP-ribosylation of proteins. *Annu Rev Biochem*, **46**, 95-116.
149. Canales, J., Fernandez, A., Ribeiro, J.M., Cabezas, A., Rodrigues, J.R., Cameselle, J.C. and Costas, M.J. (2008) Mn2+-dependent ADP-ribose/CDP-alcohol pyrophosphatase: a novel metallophosphoesterase family preferentially expressed in rodent immune cells. *Biochem J*, **413**, 103-113.
150. Rosenthal, F., Messner, S., Roschitzki, B., Gehrig, P., Nanni, P. and Hottiger, M.O. (2011) Identification of distinct amino acids as ADP-ribose acceptor sites by mass spectrometry. *Methods Mol Biol*, **780**, 57-66.
151. Rosenthal, F., Feijs, K.L., Frugier, E., Bonalli, M., Forst, A.H., Imhof, R., Winkler, H.C., Fischer, D., Caflisch, A., Hassa, P.O. *et al.* (2013) Macrodomain-containing proteins are new mono-ADP-ribosylhydrolases. *Nature structural & molecular biology*, **20**, 502-507.
152. Ogata, N., Ueda, K. and Hayaishi, O. (1980) ADP-ribosylation of histone H2B. Identification of glutamic acid residue 2 as the modification site. *J Biol Chem*, **255**, 7610-7615.
153. Hengel, S.M. and Goodlett, D.R. (2012) A Review of Tandem Mass Spectrometry Characterization of Adenosine Diphosphate-Ribosylated Peptides. *Int J Mass Spectrom*, **312**, 114-121.

154. Witze, E.S., Old, W.M., Resing, K.A. and Ahn, N.G. (2007) Mapping protein post-translational modifications with mass spectrometry. *Nat Methods*, **4**, 798-806.
155. Carapito, C., Klemm, C., Aebersold, R. and Domon, B. (2009) Systematic LC-MS analysis of labile post-translational modifications in complex mixtures. *Journal of proteome research*, **8**, 2608-2614.
156. Beneke, S., Meyer, K., Holtz, A., Huttner, K. and Burkle, A. (2012) Chromatin composition is changed by poly(ADP-ribosyl)ation during chromatin immunoprecipitation. *PLoS One*, **7**, e32914.
157. Jungmichel, S.R., F.; Hottiger, M.O.; Nielsen, M.L. (2013) Proteome-wide Identification of Poly(ADP-ribosyl)ation targets in different Genotoxic Stress Responses. *manuscript submitted*.
158. Alvarez-Gonzalez, R. and Althaus, F.R. (1989) Poly(ADP-ribose) catabolism in mammalian cells exposed to DNA-damaging agents. *Mutat Res*, **218**, 67-74.
159. Messner, S. and Hottiger, M.O. (2011) Histone ADP-ribosylation in DNA repair, replication and transcription. *Trends Cell Biol*, **21**, 534-542.
160. Dunstan, M.S., Barkauskaite, E., Lafite, P., Knezevic, C.E., Brassington, A., Ahel, M., Hergenrother, P.J., Leys, D. and Ahel, I. (2012) Structure and mechanism of a canonical poly(ADP-ribose) glycohydrolase. *Nat Commun*, **3**, 878.
161. Jankevicius, G., Hassler, M., Golia, B., Rybin, V., Zacharias, M., Timinszky, G. and Ladurner, A.G. (2013) A family of macrodomain proteins reverses cellular mono-ADP-ribosylation. *Nature structural & molecular biology*, **20**, 508-514.
162. Sharifi, R., Morra, R., Denise Appel, C., Tallis, M., Chioza, B., Jankevicius, G., Simpson, M.A., Matic, I., Ozkan, E., Golia, B. *et al.* (2013) Deficiency of terminal ADP-ribose protein glycohydrolase TARG1/C6orf130 in neurodegenerative disease. *Embo J*, **32**, 1225-1237.
163. Andrabi, S.A., Kim, N.S., Yu, S.W., Wang, H., Koh, D.W., Sasaki, M., Klaus, J.A., Otsuka, T., Zhang, Z., Koehler, R.C. *et al.* (2006) Poly(ADP-ribose) (PAR) polymer is a death signal. *Proc Natl Acad Sci U S A*, **103**, 18308-18313.
164. Kistemaker, H.A., van der Heden van Noort, G.J., Overkleeft, H.S., van der Marel, G.A. and Filippov, D.V. (2013) Stereoselective ribosylation of amino acids. *Org Lett*, **15**, 2306-2309.
165. Wu, D. and Pan, W. (2010) GSK3: a multifaceted kinase in Wnt signaling. *Trends in biochemical sciences*, **35**, 161-168.

7 CURRICULUM VITAE

PERSONAL INFORMATION

Name	**Florian Nils Rosenthal**
Address	Gasometerstrasse 26, CH-8005 Zürich
Email	florian.rosenthal@uzh.ch
Date of birth	July 21, 1982
Place of birth	Kirchen (Sieg), Germany

EDUCATION

Nov 2009 - present	University of Zürich (Switzerland), PhD Program in Molecular Life Sciences, Life Science Zürich Graduate School
Oct 2003 – Mar 2009	Philips University Marburg (Germany), Diploma studies in Biology
Jul 2002 – May 2003	Stiftung Diakonissenhaus Friedenshort Freudenberg (Germany), Civilian Service
Mar 2002	Freiherr-vom-Stein Gymnasium, Betzdorf (Germany), Abitur

PROFESSIONAL EXPERIENCE

Nov 2009 - present	University of Zürich (Switzerland), Institute of Veterinary Biochemistry and Molecular Biology, PhD thesis in the laboratory of Prof. Dr. Dr. Michael O. Hottiger, "Targeting histone ADP-ribosylation by Mass spectrometry"
Sep 2011	Selected student for the Spetses Summer School, Spetses Island (Greece), Chromatin and Systems Biology

May 2008 – Mar 2009	Philips University Marburg (Germany), Institute of Genetics, Diploma thesis in the laboratory of Prof. Dr. Michael Bölker, "The role of Intersectin during infection of *Ustilago maydis"*
Sep 2007 – Dec 2007	University of Oxford (England), Department of Biochemistry, Research internship in the laboratory of Dr. Garry Brown, "Insights into genetic defects of mitochondrial biogenesis"

PUBLICATIONS

Rosenthal F*, Feijs KLH*, Frugier E, Bonalli M, Forst AH, Imhof R, Winkler HC, Fischer D, Caflisch A, Hassa PO, Lüscher B and Hottiger MO. Macrodomain-containing proteins are novel mono-ADP-ribosylhydrolases, *Nat Struct Mol Biol* 20(4):502-7 (2013)

Kassner I, Barandun M, Fey M, **Rosenthal F** and Hottiger MO. Crosstalk between SET7/9-dependent methylation and ARTD1-mediated ADP-ribosylation of histone H1.4, *Epigenetics & Chromatin* 6(1):1 (2013)

Guetg C, Scheifele F, **Rosenthal F**, Hottiger MO and Santoro R. Inheritance of silent rDNA chromatin is mediated by PARP1 via noncoding RNA, *Mol Cell* 45(6):790-800 (2012)

Rosenthal F, Messner S, Roschitzki B, Gehrig P, Nanni P and Hottiger MO. Identification of distinct amino acids as ADP-ribose acceptor sites by mass spectrometry, *Methods Mol Biol* 780:57-66 (2011)

* equal contribution

8 ACKNOWLEDGEMENTS

First of all I want to thank my supervisor Prof. Dr. Dr. Michael O. Hottiger for the possibility to do my PhD thesis in his lab. I professionally and personally learned a lot during the last 3 ½ years and I am thankful for a constant input, discussions and very nice group trips. Additionally I would like to thank my thesis committee members, Prof. Dr. Konrad Basler, Prof. Dr. Ruedi Aebersold and Prof. Dr. Robert Schneider for their time and suggestions as well as the input during my committee meetings. Furthermore, I would like to thank Prof. Dr. Myron K. Jacobson for agreeing to review this thesis and Dr. Florian Freimoser for his work and input on this thesis and other manuscripts.

A big thank you goes to our collaborators for all their help and input. Especially Dr. Paolo Nanni from the Functional Genomics Center Zürich (FGZC) for his patience with me, having a bad influence on all reachable machines and for the help and work he invested into my project. I also want to thank Dr. Bernd Roschitzki, Dr. Peter Gehrig, Dr. Asa Wahlander from the FGCZ for their technical and social support. Additionally I would like to thank Dr. Birgit Dreyer and Prof. Dr. Andreas Plückthun.

I am very thankful for the great working surrounding, which was generated by the former and present members of the IVBMB and CABMM. I really enjoyed the time here, especially the lot of fun, the very nice Apéros, the sunny after work beers and the scientific input and technical help from many people. A great thank goes to Mareike and Anneli who had to sat next to me for most of the time and therefore had to cope with most of my annoyingness, which they did very well ☺.

Outside the lab I am most thankful for my family and friends. Especially my parents for their constant support and for being a save port I can always go to and relax. Last but definitively not least I would like to thank Michèle for making me happy!